DISSERTATION

CHARACTERIZATION AND QUANTIFICATION OF URINARY METABOLIC BIOMARKERS FOR EARLY RESPONSE TO ANTI-TUBERCULOSIS TREATMENT

Submitted by

Bryna Fitzgerald

Department of Microbiology, Immunology and Pathology

In partial fulfillment of the requirements

For the Degree of Doctor of Philosophy

Colorado State University

Fort Collins, Colorado

Fall 2016

Doctoral Committee:

Advisor: John Belisle

Dean Crick
Karen Dobos
Robert Cohen

ABSTRACT

CHARACTERIZATION AND QUANTIFICATION OF URINARY METABOLIC BIOMARKERS FOR EARLY RESPONSE TO ANTI-TUBERCULOSIS TREATMENT

Development of new anti-tuberculosis (TB) therapies remains a major priority to combat this infectious disease and to prevent continued transmission of the causative agent *Mycobacterium tuberculosis* (*Mtb*). However, newly developed therapies require large, lengthy clinical trials to determine the number of treatment failures and relapses for evaluation of treatment efficacy. Biomarkers for the prediction of treatment outcome in TB patients at early time points would facilitate movement of new therapies through clinical trials. Previously, liquid chromatography-mass spectrometry (LC-MS) based metabolomics experiments identified potential biomarkers for early response to anti-TB treatment. The research presented in this dissertation involves experiments needed for the progression of these compounds towards a clinically useful biosignature.

A major impediment to metabolomics-based biomarker discovery is metabolite identification, as approximately 50% of detectable products do not match structures in existing databases. In concordance with this, several of the potential small molecule biomarkers of anti-TB treatment response lacked structural identification. This research resulted in the structural characterization of three of these compounds as a core 1 *O*-glycosylated SerLeu peptide, *N*-acetylisoputreanine, and N^1, N^{12}-diacetylspermine. Both the core 1 *O*-glycosylated SerLeu peptide and *N*-acetylisoputreanine are novel compounds that had not been previously detected in

human urine. Characterization of these compounds indicated a potential alteration of polyamine catabolism and the complement and coagulation pathways during anti-TB treatment.

Another key aspect in biomarker discovery is defining the processes involved in formation of potential biomarkers. In order to determine whether these compounds were formed by processes upregulated during active disease, the abundances of these compounds were assessed in active TB patients and household contacts as well as in *Mtb* infected and uninfected Balb/c mice. The core 1 *O*-glycosylated SerLeu peptide and N^1, N^{12}-diacetylspermine were increased in the urine of index patients demonstrating a potential link between *Mtb* infection, associated disease pathology, and the formation of these compounds. *N*-acetylisoputreanine, however, was not increased in TB patient urine or infected mouse tissue indicating that this compound may be formed due to off target drug interactions. These experiments not only provided insights into the mechanisms behind alteration of these compounds during anti-TB treatment, but also highlighted those compounds that may be better biomarkers for anti-TB treatment response.

Assessment of these compounds using an independent set of patient samples is needed to validate them as biomarkers for early anti-TB treatment response. Unlike the untargeted experiments used for discovery of potential biomarkers, validation typically employs targeted assays. This research describes the development of a targeted multiple reaction monitoring (MRM) assay which enabled accurate and precise quantitation of compounds previously detected in an untargeted metabolomics experiment. This targeted assay will be used for validation of these compounds in a larger set of patient samples representing a variety of different treatment outcomes.

Overall these experiments confirmed the identity of three metabolites that decrease with anti-TB treatment response. Two of these metabolites are novel compounds and their characterization adds to metabolite databases expanding the number of metabolites available to other metabolomics researchers. Assessment of these compounds in samples representative of active TB disease confirmed two of them as promising biomarkers for anti-TB treatment response and highlighted another as a potential result of unintended drug effects. The development of a MRM assay for the quantification of these compounds enables their validation and confirmation as biomarkers of anti-TB treatment response. The work presented in this dissertation describes the advancement of metabolites identified during biomarker discovery towards application in clinical trials.

ACKNOWLEDGEMENTS

I would like to thank my advisor Dr. John Belisle for challenging, motivating, and believing in me throughout my graduate career. I have learned so much from him. I am truly grateful for his willingness to explain difficult concepts and help me work through challenges encountered in my research. I would also like to thank my committee for teaching me to question my data and providing stimulating discussion and useful feedback. I would also like to thank past and present members of the Belisle lab for their guidance, support and friendship. I am fortunate to have been a part of a lab with many wonderful people. I would like to thank my amazing friends for allowing me to complain about my struggles whenever I needed to and for providing some much needed humor and fun when things were tough. I would like to thank my family, especially my mom and dad for being wonderful and loving parents. Their constant support and encouragement helped me to make it through. Finally, a special thank you to my grandma Kathy for stimulating my interest in science. I am sad that she could not see me achieve this accomplishment, but I know that she would be proud of me.

TABLE OF CONTENTS

LIST OF TABLES

LIST OF FIGURES

CHAPTER 1: LITERATURE REVIEW

1.1 Tuberculosis

Tuberculosis (TB) has afflicted humans since at least the sixth century BC. DNA and lipid biomarker analysis revealed *Mycobacterium tuberculosis* specific DNA and cell-wall mycolic acids in the remains of mummified woman from 600 BC [2]. In 1882, the causative agent of TB, *Mycobacterium tuberculosis* (*Mtb*), was identified by Robert Koch [3]. This was a pivotal point in tuberculosis control. Prior to this knowledge, the cause of the different manifestations of TB were thought to be hereditary, due to a contagious agent, or overwork and malnutrition [4]. Discovery that *Mtb*, a bacterium, caused TB enabled the development of additional diagnostics, vaccines and therapeutics targeting this pathogen [5]. Despite these advances, TB is still a problem worldwide with 9.6 million new cases reported in 2014. New treatments and diagnostics are needed to help end the TB epidemic [6].

Numerous manifestations of TB exist including pulmonary TB, Pott's disease, TB meningitis, scrofula, and miliary TB [4]. This broad tissue tropism along with the longstanding interaction between *Mtb* and humans demonstrate the success of *Mtb* as a human pathogen. Upon infection with *Mtb*, a patient can progress to active disease, contain the bacteria and maintain a latent infection or completely eradicate the bacteria [7]. The outcome of infection is determined by a delicate interplay between the host's immune system and the bacteria. An understanding of these host control mechanisms and how the *Mtb* counteracts and overcomes this control is needed to design new diagnostics, therapeutics and vaccines.

1.2 Pathogenesis: Host-Pathogen interactions leading to disease

The general succession of TB disease involves early events in which infection is established followed by development of active disease during later stages [4,8]. *Mtb* enters the alveoli through inhalation of aerosolized droplets [5]. In the alveoli, *Mtb* produces ligands for various cellular receptors allowing recognition by macrophages, dendritic cells and pneumocytes. *Mtb* produces lipoproteins and lipoglycans such as LpqH, lipomannan and phosphatidylinositol mannoside that are recognized by toll like receptors (TLRs) [9-12]. Opsonization of *Mtb* with complement component C3 results in complement receptor (CR) recognition [13,14]. The terminal mannose residues of lipoarabinomannan (ManLam) expressed by virulent *Mtb* strains are recognized by mannose receptors (MR) [15]. MR and CR mediated recognition of *Mtb* is thought to facilitate its survival in macrophages after phagocytosis [16,17]. TLR2 recognition of LpqH lead to decreased class II MHC expression limiting detection of *Mtb* by adaptive immune cells [18]. In modulating its proteins and cell wall lipids, *Mtb* can target host defense pathways that are beneficial for the bacterium.

After recognition, macrophages and dendritic cells (DCs) internalize *Mtb* to remove the bacterial threat and alert the adaptive immune response. The widely accepted mechanism for internalization of *Mtb* is phagocytosis. After phagocytosis, phagosomes fuse with lysosomes resulting in the acidification of the vacuole and the activation of degradative enzymes enabling killing of ingested bacteria and production of antigens for presentation to T-cells [4,19,20]. *Mtb* has evolved mechanisms to prevent phagolysosomal fusion enabling its growth and replication within the macrophage. Acidification is prevented by *Mtb* protein tyrosine phosphatase, PtpA, mediated exclusion of the v-ATPase from the phagosomal membrane [21]. Specific *Mtb* products; ManLam, PknG and SapM, inhibit the generation of phosphatidylinositol-3-phosphate and

subsequent recruitment of early endosomal antigen-1 preventing phagosomal maturation [22-25]. The *Mtb* PE-PGRS proteins belong to family of 61 proteins with a conserved N-terminal domain containing Pro-Glu motifs and a similar C-terminal domain with polymorphic repetitive sequences [26]. The function of these proteins remains unclear, however, they do contain a Ca^{2+}-binding motif which could potentially control host cell calcium signaling, a critical component in phagosome maturation [27]. Additionally, if phagolysosomal fusion does occur, *Mtb* has developed mechanisms to survive these harsh conditions. *Mtb* can escape from the phagolysosome to the cytosol through ESX-1 mediated permeablization of the membrane [28-30]. Induction of the acid and phagosome regulated (*aprABC*) locus helps the bacterium respond to acid stress encountered in the phagolysosome [31]. Modulation of α and β integrin subunit expression in *Mtb* infected DCs can impair DC migration to the lymph node delaying the onset of the adaptive immune response [32]. After phagocytosis, *Mtb* modulates host cell processes to permit survival, replication and evasion of the adaptive immune response.

The recognition and phagocytosis of *Mtb* results in production of the cytokines, TNF-α, IL-1, -6, and -12 and the chemokines, CCL2 and CXCL10, which recruit neutrophils, lymphocytes, and monocytes to the site of infection [4,33]. Continued expression of TNF-α results in continued inflammatory cell recruitment and formation of the granulomatous lesion [4,33]. The production of interferon-γ (IFN-γ), mainly by lymphocytes, activates the infected macrophages resulting in more effective killing of intracellular *Mtb* [34]. Of the people infected with *Mtb*, 90-95% of people have an effective cellular immune response resulting in development of a latent, asymptomatic infection or eradication of *Mtb* [4]. However, in the other 5-10%, there is uncontrolled *Mtb* replication leading to necrosis of infected macrophages and the development of

a necrotic, caseous center within the granuloma [4]. Formation of cavities promotes the spread of *Mtb* within the host as well as transmission to other hosts through coughing [4].

The granuloma is a host defense mechanism meant to contain and prevent the spread of *Mtb*, however, *Mtb* can survive and persist in this hypoxic environment. Transitioning into a non-replicative state allows *Mtb* to survive within the granuloma until conditions are favorable for replication. In response to hypoxia, *Mtb* induces the DosR regulon enabling expression of genes required for maintenance of ATP levels and NAD-to-NADH ratios, and for adaptation to anaerobic metabolism which allows for persistence of the bacterium[35,36]. During persistence, bacilli switch from aerobic respiration to anaerobic dormancy [37]. Additionally, the presence of mycolic acids stimulates the accumulation of host lipids and generation of foamy macrophages, which make this environment more tolerable for *Mtb* survival as *Mtb* can metabolize host lipid substrates in the absence of other carbon sources [38].

1.3 Diagnosis

There are symptoms commonly associated with pulmonary tuberculosis such as prolonged cough, hemoptysis, chest pain, and weight loss. These symptoms can be used for TB diagnosis, however, this diagnosis must be confirmed with further testing as these symptoms can be caused by other diseases. One of the most common and simple diagnostic tests is the Mantoux tuberculin skin test (TST). Following injection of a small amount of purified protein derivative (PPD) immune cells migrate to the injection site causing a measurable induration [39-41]. However, the TST cannot distinguish between infection with *Mtb*, environmental mycobacteria or vaccination with Bacillus Calmette-Guérin (BCG) and can give false-negative results in immunocompromised individuals [40]. Due to the drawbacks of TST, blood tests measuring the release of IFN-γ are increasingly used in high-income countries [40]. IFN-γ release assays (IGRA)

including the QuantiFERON-TB Gold In-tube test and the T-SPOT.TB test measure the release of IFN-γ either from white blood cells or peripheral blood mononuclear cells (PBMCs) incubated with synthetic *Mtb* peptides (ESAT-6, CFP-10, and TB7.7) [40]. IGRAs are more specific for *Mtb* infection, however, like the TST, they measure an immunological response and may not be effective in immunocompromised individuals [40]. Both of these tests are indicative of exposure to *Mtb* and cannot be used for definitive diagnosis of active or latent disease.[40].

Definitive diagnosis of active disease requires direct detection of *Mtb* in patient specimens [40]. Culturing of *Mtb* is the gold standard technique due to its high sensitivity and accuracy [40]. However, the results cannot be acquired for 2-4 weeks (liquid media) or 4-8 weeks (solid media) due to the slow growth of the bacilli [40]. This slow turnaround time prompted the development of more rapid *Mtb* detection strategies. Sputum smear microscopy allows for quick and accurate detection of acid fast bacilli, but has low sensitivity and the absence of bacilli is not always indicative of a negative result [40]. The nucleic acid amplification (NAA) tests, including GeneXpert, are rapid, specific and much more sensitive than sputum smear microscopy [40]. In addition to being able to detect the presence of *Mtb*, these tests can also identify rifampicin drug resistant strains [40,42]. It can be argued that NAA tests are not amenable to low-resource settings due to the high costs and electricity requirements, however, the GeneXpert Omni which can be used without constant electricity demonstrating that advanced instruments can be developed for use as a point of care test in resource limited settings [40,43].

1.4 Treatment

1.4.1 Current TB Treatment

The current treatment regimen for drug susceptible tuberculosis involves an intensive phase lasting two months which includes isoniazid, pyrazinamide, rifampicin, and ethambutol

followed by a four month continuation phase of isoniazid and rifampicin. The intensive phase kills the majority of the bacilli, and the continuation phase is required to achieve a non-relapsing cure. This drug regimen was developed in the 1970s based on short course chemotherapy studies in Singapore utilizing drugs that were discovered in the 1950s and 60s [44,45].

During the synthesis of two other anti-tubercular agents, β- and γ-pyridylaldehyde thiosemicarbazone, a synthetic intermediate, isonicotinic acid hydrazide (INH), was found to have *in vivo* anti-tubercular activity superior to any other agents available at the time [46]. INH, discovered in 1952, is still a main component of anti-tuberculosis treatment and is responsible for the early bactericidal activity [46,47]. Early experiments revealed that exposure of *Mtb* to INH interferes with cell envelope lipid biosynthesis, resulting in loss of acid-fastness and viability [48]. Later experiments expanded upon this by demonstrating that INH is oxidized by the *Mtb* catalase/peroxidase enzyme, KatG, to form a number of highly reactive intermediates including the isonicotinoyl radical, all of which can have several effects on *Mtb* cellular processes [49,50]. The isonicotinoyl radical can form an adduct with NAD, which inhibits the function of the mycobacterial NADH-dependent enoyl-acyl carrier protein reductase, InhA, and interferes with mycolic acid biosynthesis, resulting in cell death [47,48]. Other additional INH targets have been proposed, such as KasA and AcpM which are also involved in mycolic acid biosynthesis [50,51]. Resistance to INH is achieved either by mutations in *katG* inhibiting activation of INH and increased expression or modification of InhA which inhibits interactions with INH-NAD adduct [47].

Rifampicin (RIF), rifapentine, and rifabutin are semisynthetic derivatives of the natural product Rifamycin B produced by *Amycolatopsis (Nocardia) mediterranei* [47,52,53]. Its synthesis and the discovery of its *in vivo* activity against a variety of bacteria in the mid-1960s quickly

resulted in its clinical use [52]. RIF is critical to sterilization and its addition to the treatment regimen in the 1970s enabled a decrease in treatment duration from 12 to 9 months [53]. RIF inhibits the β-subunit of the bacterial DNA dependent RNA polymerase (RNAP) in a highly specific manner [54]. This inhibition results in decreased RNA synthesis at the chain initiation step [54]. Resistance to RIF arises from mutations in *rpoB* preventing RIF from binding to RNAP [47].

Pyrazinamide (PZA) is a nicotinamide analog that is critical for sterilizing activity against persistent *Mtb* [47]. PZA is also a prodrug that is converted to pyrazinoic acid by the *Mtb* enzyme pyrazinamidase, PncA [47]. Pyrazinoic acid's mode of action is unconfirmed, but there is evidence that it might interfere with *Mtb* trans-translation and/or disrupt *Mtb* membrane potential [47,55]. Resistance to PZA arises in *Mtb* due to a mutation in *pncA* which affects pyrazinamidase mediated conversion of PZA and in *rpsA* potentially preventing PZA mediated interference of trans-translation [47].

Ethambutol is a bacteriostatic drug and is only effective against actively dividing cells. It's mode of action has not been fully elucidated, however, the *Mtb* arabinosyltransferases are one molecular target. Ethambutol inhibits the polymerization of arabinan and causes intracellular accumulation of mycolic acids.

Despite the success of this treatment regimen, there are considerable drawbacks including the six month duration and adverse side effects. These drawbacks contribute to poor treatment adherence and the emergence of drug resistant *Mtb* strains. Currently, there are *Mtb* strains resistant to all first-line drugs and 480,000 people were estimated to have drug resistant TB in 2014 [6]. Though there are available treatments for drug resistant TB, these treatments have more harmful side effects and require up to two years for treatment completion which perpetuates the

cycle of poor treatment adherence and increasing drug resistance. There is an urgent need for new therapeutics to treat drug susceptible and drug resistant TB patients.

1.4.2 New TB Treatments

Currently, new or repurposed drugs and new therapeutic regimens being assessed in phase 2 and 3 trials [56]. Recently, two new drugs, bedaquiline and delamanid, were approved for treatment of multidrug resistant TB cases [56,57]. Unfortunately, *Mtb* strains resistant to both of these drugs have already been detected [57,58]. Approval of the other drugs and therapeutic regimens is crucial for controlling this epidemic.

The approval of a new drug is a lengthy and expensive process [59]. The approval process for bedaquiline and delamanid took at least six and eight years, respectively, and this was with accelerated approval [60-62]. Contributing to the duration and cost of this process are the clinical trial phases [59]. Phase I typically involves 20 to 80 patients in which the reduction in viable bacilli in sputum is assessed at 0-2 and 2-14 days [44,59]. During Phase II, drug efficacy is assessed in 48 to 300 patients who are monitored for time to sputum culture conversion and culture negative sputa after two months [44,59]. Phase III requires two to three treatment groups with 300-1000 people in each and these patients are monitored for the whole 6 month course of treatment and for 12-18 months following treatment completion to assess for relapse [44]. One proposal for improvement of this process is replacement of phase III trials with smaller clinical trials consisting of only drug resistant infections as phase III trials require large patient populations to capture highly resistant infections and relapses [56]. If a new treatment regimen is successful in MDR patients, then most likely it will be successful in drug sensitive patients.

Another solution is the use of biomarkers that can serve as surrogates for drug efficacy. Currently, sputum culture status at two months of treatment is used as a prognostic for drug

efficacy [44,56]. However, there are considerable drawbacks to this method: it is based on the presence or absence of bacteria which does not provide information about the extent of the response; sputum is not always easily obtained from all patients including children and those responding successfully to treatment; *Mtb* growth is slow which delays acquisition of results [44]. Other biomarkers that are being evaluated for more rapid assessment of treatment efficacy are PET-CT scans, whole-blood bactericidal activity, and gene expression profiles [56]. Whole blood bactericidal activity correlated with sputum culture conversion and aided in accelerating development of sutezolid and bedaquiline [56]. A recent study identified and validated two gene expression signatures that are predictive of progression to active disease and may be useful in evaluating drug efficacy and predicting relapse [63]. Discovery of other biomarkers predictive of patient treatment outcome at time points earlier than two months will greatly accelerate phase II and III clinical trials. The use of high-throughput techniques to identify other potential biomarkers is discussed in the next section.

1.5 Biomarker Discovery

1.5.1 Biomarker Background

The FDA-NIH Biomarker Working Group defines a biomarker as a "defined characteristic that is measured as an indicator of normal biological processes, pathogenic processes, or responses to an exposure or intervention, including therapeutic interventions" [64]. There are three main types of biomarkers, those that indicate disease or extent of disease (diagnostic), those that indicate the likely clinical outcome of a disease independent of therapy administered (prognostic) and those that indicate the effectiveness of a treatment against that disease (predictive) [65-68]. Utilization of biomarkers as surrogate endpoints for lengthy and

adverse clinical outcomes would greatly improve the evaluation of treatments and therapies during clinical trials.

Development of a robust and clinically useful biosignature is an involved process beginning with the discovery of candidate biomarkers through unbiased analyses of samples representing different parameters of interest, such as untreated vs. treated [69]. The discovery of these candidate biomarkers might be indicative of a true biological change or unwanted method variation, making it important to confirm them with additional, independent analyses during biomarker qualification [69]. Initial biomarker qualification is important for determining whether or not a candidate biomarker should be pursued and requires a different analytical method and/or a different set of patient samples [69]. Following confirmation that these candidate biomarkers are indicative of biological processes and not due to unexpected analytical discrepancy, the behavior of the candidate biomarker is assessed in an even wider range of samples [69]. The final stage of the biomarker qualification process is comprised of the analysis of this biomarker alongside conventional methodology [69].

During biomarker qualification, statistical evaluation is extremely important for identifying biomarkers that are truly indicative of the parameters of interest. Diagnostic biomarkers are used to classify patient's disease status, such as having TB or not having TB. For example in Figure 1.1A, the variable D designates disease status with 0 equating to no disease and 1 equating to disease and the variable Y designates diagnostic biomarker values with 0 equating to negative value and 1 equating to positive value [67]. Diagnostic biomarkers are evaluated mainly using sensitivity and specificity, however, additional calculations including the positive and negative predictive values (PPV and NPV), correct classification rate, and likelihood ratios are also important [1,67,70]. Examples of these calculations are depicted in Figure

1.1B. In evaluating a diagnostic biomarker for TB, a sensitivity value close to one indicates that most patients with TB have a biomarker positive value and a specificity value close to one indicates that most patients without TB have a biomarker negative value [1,67,70,71]. Additionally, a PPV close to one demonstrates that the majority of the positive biomarker values are from true

A.

	D = 0	D = 1	Total
Y = 0	a	b	a + b
Y = 1	c	d	c + d
Total	a + c	b + d	a + b + c + d

B.

Measure	Calculation
Prevalence	(d + b)/(a + b + c + d)
Overall diagnostic power	(c + a)/(a + b + c + d)
Correct classification rate	(d + a)/(a + b + c + d)
Sensitivity	d/(d + b)
Specificity	a/(c + a)
False positive rate	c/(c + a)
False negative rate	b/(b + d)
Positive predictive value	d/(d + c)
Negative predictive value	a/(a + b)
Misclassification rate	(c + b)/(a + b + c + d)
Odds-ratio	(da)/(cb)
Likelihood Ratio	[d/(d + b)]/[c/(c + a)]

Figure 1.1
(A) Confusion matrix displaying predicted and observed outcomes from classification models. The variable Y denotes predicted outcomes (0 or 1) based on biomarker values and the variable D denotes observed outcomes (0 or 1) based on actual patient data. (B) Useful calculations for understanding data from confusion matrix. Adapted from Broadhurst et al.[1]. a, b, c, and d refer to numbers of patients.

TB patients and a NPV close to one demonstrates the majority of biomarker negative values are from true non-TB patients [1,67,70,71]. If the correct classification rate is equal to one, then there were no false positives or false negatives and is indicative of a highly accurate test [1]. However, unless the prevalence is 50%, the correct classification rate is more indicative of either specificity or sensitivity than of diagnostic accuracy [72]. A likelihood ratio greater than one indicates that a biomarker positive value is more likely in a person with TB than a person without TB [67].

Prognostic biomarkers are indicative of a specific clinical outcome such as successful anti-TB treatment (good outcome) or failed anti-TB treatment (poor outcome). Using Figure 1.1A, the variable D can now designate clinical outcome with 0 equating to successful treatment and 1 equating to failed treatment and the variable Y can now designate prognostic biomarker values with 0 equating to negative value and 1 equating to positive value [67]. Similar to evaluation of a diagnostic, prognostic biomarkers are mainly evaluated with the odds ratio or hazards ratio, sensitivity and specificity, PPV and NPV, and receiver operating curves (ROC) [67,68,73]. An odds ratio greater than one demonstrates an association between the biomarker value and the clinical outcome, however, this test is inadequate on its own to demonstrate that a biomarker is prognostic [73,74]. A sensitivity close to one indicates that most of the patients who failed treatment have a positive biomarker value and a specificity close to one indicates that most of the patients with successful treatment have a negative biomarker value [67,71,73]. A PPV close to one indicates that a majority of patients with a positive biomarker truly failed treatment and a NPV close to one indicates that most patients with a biomarker negative value truly had successful treatment [67,73]. However, the PPV and NPV are affected by the prevalence of the clinical outcome, thus a low value may be the result of a low prevalence rather than a poor prognostic marker [67,73]. A ROC curve is useful for determining the cut-off level during evaluation of a continuous biomarker [67,73]. The cut-off level that gives the highest sensitivity and specificity is desired [67,73].

Discovery of a diagnostic and prognostic biomarker that meets all of the above criteria is unlikely, thus it is important to determine which criteria need to be satisfied on a case by case basis by evaluating the associated costs. For example in the case of TB diagnosis, it is more important to have a high sensitivity, ensuring detection of all TB patients and prevention of

disease transmission, than a high specificity. A low specificity is acceptable due to infection control measures, such as separation and face masks, that will not cause harm to non-TB patients misclassified as having TB. A high sensitivity is also desired in assessment of a prognostic biomarker for treatment outcome as it is important to detect all treatment failures in order to prevent patient death and disease transmission. Misclassification of some patients as treatment failures due to a low specificity could subject these patients to adverse treatment side effects and longer treatment durations, however, this will still result in curing of the disease.

Unlike diagnostic and prognostic biomarkers for which an association with a disease or clinical outcome is important, evaluation of predictive biomarkers requires a large randomized trial to demonstrate a correlation between biomarker changes over time and treatment effect on clinical endpoint [68,73,75]. This is typically achieved through interaction tests, however, these tests require large clinical trials including patients with both high and low biomarker levels to achieve adequate power, thus validation of predictive biomarkers is uncommon [68,75].

Both prognostic and predictive biomarkers can be further validated and utilized as surrogate markers for clinical endpoints. The statistical validation of surrogate markers has evolved throughout the years and though there is not a standardized method for statistical validation, a general consensus has been achieved [68,75,76]. In 1989, Prentice proposed three criteria for defining surrogates of clinical endpoints: the surrogate should be associated with the true clinical endpoint, treatment should impact the surrogate as well as the clinical endpoint, and the surrogate should capture the full effect of treatment on the clinical endpoint[73,75,77]. However, these criteria have been criticized due to the stringency of the third criterion and thus alternate approaches were developed [75,78,79]. In 1992, Freedman *et al.* proposed the proportion of treatment effect explained (PTE) as an improvement on Prentice's last criterion [80]. Two further measures,

relative effect and adjusted association, were introduced to replace PTE by Buyse and Molenberghs in 1998 [81]. A drawback for all of these methods is their reliance on single trials to determine surrogacy, thus a meta-analytic approach was proposed which combined data from multiple trials [82-85]. Currently, the preferred approach for validation of surrogate markers is based on either a fixed-effects model or a mixed-effects model described by Buyse *et al*. in 2000 [85]. These models enable evaluation of "individual-level surrogacy", correlation of surrogate with final clinical outcome, and "trial-level surrogacy", correlation of surrogate with effect of treatment on final clinical outcome [85]. Additionally, surrogate threshold effect (STE), a concept introduced by Burzykowski *et al.* in 2006, improves interpretation of surrogacy for clinicians supporting practical use of the surrogate [86].

Recently, this preferred approach was used to evaluate disease-free survival (DFS) and progression-free survival (PFS) as surrogates for overall survival (OS) in gastric cancer patients [87]. Buyse *et al*. define DFS as "the time from randomization to a cancer recurrence, second cancer or death from any cause" and PFS as "the time from randomization to the time of progression or death from any cause" [87]. Using the meta-analytic approaches, the individual-level surrogacy for DFS and PFS was 0.935 (95% CI [0.924, 0.938]) and 0.859 (95% CI [0.842, 0.862]) respectively, which demonstrates a correlation between each surrogate and the clinical endpoint [87]. The trial-level surrogacy for DFS and PFS was 0.969 (95% CI [0.879, 0.991]) and 0.61(95% CI [0.04, 1.00]) respectively, which demonstrates a tight correlation between treatment effects on DFS and a moderate correlation between treatment effects on PFS and on OS [87]. A STE of 0.92 and 0.56 was determined for DFS and PFS respectively [87]. This indicates that a treatment that demonstrates at least an 8% reduction in risk of tumor recurrence or a 44% reduction in risk of tumor progression would be expected to yield a benefit on overall survival

[75,87]. Thus it was determined that DFS was a good surrogate for OS in gastric cancer patients, while PFS was not [87].

TB research would benefit from the discovery of new biomarkers for diagnosis and anti-TB treatment response evaluation. The current mechanisms for diagnosis of tuberculosis are lengthy and cannot always discriminate between infection and exposure [88]. Sputum culture at month two of anti-TB treatment, which is currently used as a prognostic marker for treatment outcome, still requires a lengthy amount of time and is not feasible in some patients [56,89]. Additionally, both sputum smear and culture at two months of anti-TB treatment had low sensitivities and PPVs for predicting relapse and failure indicating that sputum smear and culture are poor prognostic markers for anti-TB treatment outcome [90]. However, as noted earlier, the PPV is affected by prevalence and the low PPVs observed may be due to the low prevalence of treatment failure and relapse [67]. Perhaps assessment of the prognostic capabilities of sputum smear and culture for poor outcome, including both failures and relapses, would yield better PPVs.

The long doubling time of *Mtb* is a major impediment in tuberculosis control and biomarkers demonstrating *Mtb* infection or killing at time points earlier than culture based methods would be extremely useful. For instance, a biosignature that can immediately differentiate between exposure and an active versus latent infection would enable earlier implementation of infection control measures such as separation of tuberculosis patients and commencement of antibiotic treatment which would limit the exposure and spread of the bacteria [91,92]. Furthermore, a prognostic biosignature for treatment outcomes in TB patients that can be measured at diagnosis or soon after the start of treatment would permit earlier identification of patients with the potential for a poor treatment outcome. Ultimately, a surrogate marker

predicting anti-TB treatment outcome would enable prompter drug efficacy decisions, decrease the duration and number of people needed during clinical trials and aid in the design of personalized treatment regimens [56]. The discovery of biomarkers leading to development of biosignatures such as those described above would aid in the control and prevention of TB.

High-throughput "omics" techniques including metabolomics, transcriptomics and proteomics are often used in biomarker discovery [88]. A recent review by Haas *et al.* discusses the use of these techniques in the development of diagnostic markers for active TB [93]. Many of the studies discussed by Haas *et al.* are covered in the following sections, thus the reader is referred to Tables 1, 2, and 3 from their review [93]. These "omics" techniques are advantageous in their ability to detect a multitude of biomarkers quickly, promoting development of a multi-component biosignature. Although these techniques have not yet yielded a clinically useful biosignature for the TB field, immense progress has been made. The following sections discuss the basics of these techniques, findings made and challenges that have arisen.

1.5.2 Proteomics

Proteomics aims to describe all proteins present in biological samples. In biomarker discovery, this typically involves separation followed by MS based detection of proteins and endogenous peptides that are differentially regulated. Prior to MS analysis, proteins can be enriched or fractionated using column or chip chromatography or with gel electrophoresis [94]. The MS detection methods used can be either direct analysis of endogenous peptides and proteins from a biological sample with MALDI or SELDI-TOF MS or enzymatic digestion of proteins and peptides followed by ESI-MS/MS analysis [94]. More precise quantification of peptides can be achieved with the use of special labeling reagents such as isobaric tags for relative and absolute quantification (iTRAQ) [94]. Alternatively, aptamers, artificial nucleic acid ligands, have been used

to detect differentially regulated proteins in biological samples [95]. While this is not an MS based technique it allows for high-throughput discovery of protein biomarkers. The use of these different techniques for tuberculosis biomarker discovery has resulted in potential host and bacterial protein biomarkers for the diagnosis and evaluation of treatment response.

Proteomics Identification of Host Biomarkers

Tuberculosis patient serum and plasma are the main biofluids utilized for detection of protein abundance changes. Adewole *et al.* was the first group to look for biomarkers of active TB using the proteomic profile of eccrine sweat [96]. Multiple groups have detected immune-related proteins that could be potential biomarkers. Several complement components including C-reactive protein and immunoglobulin chains were detected exclusively in the sweat of TB patients [96]. Protein markers of pulmonary inflammation, tissue damage, and leukocyte homing and infiltration (CD14, SEPP1, SELL and LUM) distinguished active TB patients from those with other respiratory diseases [97]. CD5L, a scavenger receptor important in innate immune responses, was demonstrated to be significantly increased in active TB patients compared with healthy controls [98]. Two groups detected an increased abundance of the acute phase protein, serum amyloid A (SAA) in active TB patients [96,99]. Altered levels of coagulation related proteins in TB patients were reported by several groups as well [98,100-104]. Despite this overlap of detected proteins involved in similar mechanisms, a consistent proteomic profile has not been established.

There are two studies that analyzed the serum proteomic profile during anti-TB treatment. Both studies employed the same 39 patients and the use of SOMAmers for protein detection [105,106]. De Groote *et al.* identified biomarkers of disease severity and successful treatment response, while Nahid *et al.* identified biomarkers that were predictive of successful treatment response and correlated with sputum culture status at 2 months and time to conversion.

While proteins involved in similar pathways were detected in both studies, there was only one common protein, SAA. One would expect that proteins indicative of successful treatment would also correlate with the current prognostic biomarker for successful treatment outcome.

It is encouraging that similar pathways are being identified, however, impeding progress towards a clinically useful biomarker is the fact that the same proteins are not being detected by multiple groups. Perhaps, instead of focusing on a select few, researchers should combine all significant proteins identified that belong to the same pathways for validation.

Proteomics Identification of Mtb Specific Proteins

While, the discovery of host protein biomarkers is important, discovery of *Mtb* protein biomarkers would provide added specificity to a tuberculosis related biosignature. Using pulmonary TB patient urine, Kashino *et al.* identified four unique peptides that corresponded to four *Mtb* proteins [107]. One of the identified proteins, Rv1681, is only present in *Mtb* complex members, making it a possible biomarker for specific diagnosis of tuberculosis [107]. Additionally, the four proteins are involved in synthesis of molecules required for active growth and thus may be potentially useful in distinguishing between latent and active disease [107]. Confirmation that these proteins are produced *in vivo* in TB patients was achieved by probing electroblotted purified, recombinant proteins with TB patient sera [107]. Additionally, the antigenicity of these proteins makes them suitable candidates for an antigen-detection-based diagnostic assay [107]. A follow-up validation study using capture ELISA detected Rv1681 in the urine of 11/25 pulmonary TB patients, 1/21 TB suspects and in none of the other non-TB control samples [108]. While this demonstrates a high specificity in diagnosing TB, the addition of other *Mtb* proteins like Rv3341, which was more antigenic than Rv1681 in the previous study, might improve sensitivity [107]. Kruh-Garcia *et al.* developed a MRM assay targeting *Mtb* proteins detected in

exosomes of *Mtb* infected macrophages and animal models [109]. Using this MRM assay, 20 of the 33 proteins were detected in isolated exosomes from pulmonary TB patient sera [109]. A diagnostic assay based on detection of these 20 proteins could potentially differentiate between latent and active TB as well as diagnose immunocompromised patients with TB, both an improvement on the current diagnostic techniques [109]. Another studying using TB patient urine identified 10 *Mtb* proteins found exclusively in active TB patients and six *Mtb* proteins found exclusively in latent TB patients [110]. Interestingly, there was no overlap with the *Mtb* proteins detected by Kashino *et al.* though both used TB patient urine. These studies demonstrate the feasibility of using *Mtb* proteins in diagnosing active disease. Though not yet evaluated, *Mtb* proteins detected in TB patients also have the potential to be effective in monitoring treatment response and should be evaluated in further validation studies.

A major challenge in targeting *Mtb* proteins is their low abundance compared with host proteins. The above studies addressed this issue using different methods. Kashino *et al.* reduced the number of interfering proteins by separating proteins in the urine with gel electrophoresis and then analyzing individual protein bands [107]. Kruh-Garcia *et al.* increased the ratio of bacterial to host components by purifying exosomes from the serum which eliminated many of the abundant host serum proteins [109]. Additionally, Kruh-Garcia *et al*. used a MRM assay for targeted analysis of *Mtb* proteins [109]. Young *et al.* increased the signal of lower abundant proteins by filtering the urine through 50kDa molecular weight cut-off filters prior to analysis [110].

Challenges Associated with Proteomics

Determination of the peptide sequence is extremely important. Liu *et al.* identified 30 peptides that discriminated between TB and non-TB patients, the abundance of three of these could successfully diagnose TB patients [111]. Unfortunately, none of these peptides were

sequenced impeding the comparison and validation of these results by other groups. Different groups may detect different peptides from the same protein and sequencing of these peptides will allow for identification of this common protein.

1.5.3 Transcriptomics

A larger volume of work has been done regarding the identification of biomarkers using transcriptomics. Transcriptomics involves the detection of mRNA transcripts to derive gene expression profiles under various biological conditions. These transcripts are detected using techniques such as microarray, mRNA sequencing, and dual-color reverse-transcriptase multiplex ligation-dependent probe amplification (dcRT-MLPA). While mRNA sequencing is unbiased and ideal for identifying novel biomarkers, this technique is costly and produces a large amount of data. Microarrays can be relatively unbiased based on the set of probes used, but are limited to known transcripts. Both mRNA sequencing and microarrays are technically challenging and require complex data analyses [112]. The dcRT-MLPA technique is also limited to known transcripts like microarrays, but can only analyze a smaller number of genes at a time (~ 90-100 genes). However, this technique is cheaper and has simpler data analyses [112]. Typically, whole blood is the source of the mRNA, though isolated blood cells and bronchoalveolar lavage (BAL) fluid have also been used for RNA extraction.

Transcriptomics Identification of Host Biomarkers

Common host blood gene expression profiles associated with *Mtb* infection have arisen though the analysis of different patient populations at different time points along the disease spectrum. Berry *et al.* reported a 393-transcript signature which described the upregulation of genes involved in both Type I and II IFN signaling during active TB disease [113]. Transcripts corresponding to these genes have been repeatedly observed and inclusion of transcripts from

this signature consistently distinguishes active TB patients [113-118]. Additionally, genes from this IFN inducible transcriptional signature are also successful at predicting progression to disease and successful treatment [63,118,119]. Continual identification of these transcripts demonstrates the importance of both Type II IFN-γ and Type I IFNαβ signaling during tuberculosis. Increased abundance of FC γ receptor I (FCγRI) transcripts is highly associated with active TB disease regardless of age or HIV status, highlighting the importance of antibodies and/or FC receptor mediated persistent activation of the immune system during tuberculosis [114-118,120-123]. Expression of these genes can also be predictive of disease development or successful treatment [63,116,118]. The complement system is a key player in the innate immune response to *Mtb* infection. Coinciding with this, altered expression of complement system genes has been observed during response to anti-TB treatment, progression to disease as well as active TB [63,115-118,124]. Dysregulation of apoptosis has also been described as being a predictor of disease progression [116,121,125,126]. Lower expression levels of *Bcl2*, an anti-apoptotic factor, was associated with progression to disease, however, patients with active disease had higher expression levels of *Bcl2* than patients with latent disease. These common expression profiles are encouraging for development of biosignatures for all components of the TB disease spectrum.

However, Maertzdorf *et al.* argue that these expression profiles are just general markers of chronic activation of the immune system and that their commonality with sarcoidosis, a lung disease with similar pathology, diminishes their capability of being a differential diagnostic for tuberculosis [117]. This group went on to identify TB specific gene patterns which included genes involved in response to reactive oxygen species, specifically *KLF2* and *HIF-1α* [117]. Though, Maertzdorf *et al.* claim to have identified transcripts specific to TB, the only comparison made was with sarcoidosis. The original IFN inducible gene signature described by Berry *et al.*

maintained a high sensitivity and specificity when compared with five other bacterial and inflammatory diseases including SLE and Still's disease, however, sarcoidosis was not compared in this study [113]. Though comparison with other diseases exhibiting similar pathology or tropism is important, it is impossible to evaluate prospective biosignatures in all diseases. Shared transcriptional biosignatures amongst different diseases is inevitable, however, the expression levels of these shared genes may be different. Despite the common transcriptional signatures between TB and sarcoidosis observed by several groups, the expression levels of these shared genes were significantly different and enabled division of TB and sarcoidosis patients [114,117,127]. The only way to obtain a true TB specific biosignature would be to include *Mtb* specific transcripts.

Transcriptomics Identification of Mtb Specific Biomarkers

Contrasting to the large volume of research identifying host transcriptomic biomarkers for tuberculosis, relatively few studies have focused on *Mtb* transcripts. In the transcriptomics experiments that have been conducted, patient sputum was utilized for detection of *Mtb* transcripts [128-130]. Sputum is routinely used to culture *Mtb* bacilli for diagnosis or assessment of treatment response, thus it is an ideal sample for ensuring detection of *Mtb* mRNA. *Mtb* transcripts could be detected in patient sputum samples even when the samples were culture negative establishing an increased sensitivity of mRNA detection compared to that of standard culturing methods [129]. The presence of *Mtb* mRNA in these samples can be an indicator of live *Mtb* bacilli as mRNA is not detected from dead bacilli [131]. Additionally, treatment resulted in a similar biphasic decline to that seen using culture based methods, with a rapid decline in mRNA abundance early on and a slower decline until the end of treatment [129]. All three studies identified similar *Mtb* transcriptional profiles representing a "fat and lazy persister" phenotype including

dysregulation of *icl1, hspX, narK2, tgs1, nuoB, qcrC*, and *ctaD* [128-130]. These transcriptional profiles represent a mixture of mycobacterial subpopulations and alterations during treatment indicate a shift in those subpopulations rather than altered transcriptional regulation by *Mtb* in response to treatment. Reflective of patient and bacterial heterogeneity, *Mtb* transcriptional signatures differed amongst patients during treatment and these patient specific signatures correlated with their clinical and microbiological parameters; bacterial load, time-to-positivity values and chest x-ray scores [130]. Encouragingly, *Mtb* transcriptional signatures were identified that correctly predicted disease severity and treatment response [130]. Though the main goal of these studies was not to identify biomarkers, they demonstrate the applicability of *Mtb* mRNA as biomarkers for TB diagnosis and prediction of treatment response.

microRNAs

In addition to profiling mRNA expression, the differential expression profiles of microRNAs have also been examined in relation to tuberculosis. MicroRNAs (miRNAs) are small RNAs, approximately 23 nucleotides in length, that bind to target mRNAs and regulate their expression through translational repression and/or mRNA destabilization [132]. Unlike the mRNA transcriptional studies which mainly used whole blood or PBMCs as an mRNA source, miRNA profiling was conducted using serum, sputum and PBMCs. Certain groups reasoned that the stability of miRNAs in serum and sputum made these biofluids more amenable to miRNA detection than other sources such as PBMCs [133]. Despite the use of serum and the stability of miRNAs in serum, few detected miRNAs were shared amongst groups and none of the miRNAs that distinguished active TB patients were shared [103,117,133-136]. So far, only one group has studied differential expression of miRNAs in sputum and aside from miR-29a, these results were inconsistent with the serum results [137]. MiRNA expression profiles from PBMCs had more in

common, though the trends observed differed [138-142]. Three separate groups detected significant upregulations of miR-424 in active TB patients [103,138,141]. Two studies found that levels of miR-365 were higher in active TB patients compared to healthy controls, however, Spinelli *et al.* saw no significant difference between active TB patients and healthy controls [138,141,142]. Using PBMCs from children with TB, Zhou *et al.* describe a miRNA profile that both validates and disproves previous results from both serum and PBMCs [139]. Though altered miRNA expression profiles could be used as biomarkers for TB, there are inconsistencies between studies which hinders development of a miRNA expression signature for diagnosis of TB. Contributing to these inconsistencies is an incomplete knowledge of mRNA targets. Perhaps directed analysis of miRNAs that are known to target mRNAs with altered abundances during tuberculosis would be more fruitful.

1.5.4 Metabolomics

Metabolomics is measurement of small molecules formed during metabolic processes of an organism [143]. Lipidomics, a subset of metabolomics, involves the detection of lipid species produced by an organism [144]. Both techniques can reveal an organism's active biochemical processes during specific times and conditions. For example, cholesteryl esters accumulate during prostate cancer indicating altered cholesterol metabolism [145]. Additionally, L-carnitine decreases during emphysema progression indicating altered fatty acid metabolism [146]. Alterations in polyamine metabolites and thus polyamine metabolism have been associated with many different cancers [147-151]. Dysregulated metabolism results in altered levels of metabolites which can be detected and used as biomarkers for disease conditions.

A typical metabolomics experiment begins with the extraction of metabolites from biological samples using different techniques that are dependent on the type of sample (tissue vs.

serum) or experiment being done (targeted vs. untargeted) [143]. Prior to detection, these complex mixtures can be separated using liquid-chromatography (LC) or gas-chromatography (GC) [143]. Detection of the metabolites is achieved with either mass spectrometry (MS) or nuclear magnetic resonance (NMR), and these data are analyzed to identify the metabolites present and determine if any are significantly altered in different sample groups [143]. The differential metabolites are then qualified using targeted assays to confirm them as candidate biomarkers for a particular physiology or pathology [152].

Pertaining to tuberculosis biomarker discovery, these metabolomics techniques have been utilized in the detection of metabolic alterations in both the host and the bacteria. Biological fluid and tissue samples from both human patients and animal models have been analyzed using different techniques including ^{1}H-NMR, LC-MS or GC-MS. A benefit and a hindrance to these different experiments is the range of sample sources and analysis platforms. The benefit is the ability to detect many different classes of metabolites, however, it is difficult to combine and compare data from the different experiments.

Metabolomics Identification of Host Biomarkers

The biological samples most commonly used for detection of metabolites in humans are serum/plasma, sputum and urine. Each has its own advantages and disadvantages. Sputum is more representative of metabolic alterations at the site of infection, while urine is easy to obtain and requires minimal sample processing. Serum metabolite levels are more regulated making it easier to normalize than sputum and urine [153].

Despite the different samples and analysis platforms used, common metabolites and pathways have been detected. The analysis of tuberculosis patient serum using LC and GC-MS by two separate groups revealed altered tryptophan metabolism with tryptophan being lower in

TB patients and downstream metabolites, kynurenine and quinolinic acid, being higher in TB patients [154,155]. Additionally, a decrease in tryptophan was also detected in infected *Mtb* infected guinea pigs [156]. Downstream tryptophan metabolites, quinolinic acid and trigonelline, decreased in the urine of TB patients undergoing anti-TB treatment (S. Mahapatra, unpublished data).

Alterations in phenylalanine and tyrosine metabolism were detected in five different studies. Analysis of human serum with either GC-MS or NMR identified an increase in phenylalanine in TB patients [155,157]. In concordance with this finding, analysis of tissue and biofluids from *Mtb* infected mice detected an increase in tyrosine and phenylalanine in infected animals [158]. Analysis of the TB patient urine using GC-MS detected increased levels of downstream tyrosine and phenylalanine metabolites; 4-hydroxybenzoic acid, 4-hydroxyhippuric acid, hydroquinone, gentisic acid, and norepinephrine, in patients with active disease [159]. Tyrosine and phenylalanine levels were also decreased during anti-TB treatment (S. Mahapatra, unpublished data).

It is encouraging that common pathways have been identified using a range of biological samples and analysis platforms, however, some incongruities have arisen amongst the different experiments. In contrast to the results above, Che *et al.* detected decreased levels of phenylalanine in TB patients [160]. Three separate studies detected increased levels of lactate in TB patients, however, Somashekar *et al.* detected decreased lactate levels in *Mtb* infected guinea pigs [156-158,161]. There are additional discrepancies amongst metabolites involved in the glutathione and glutamate metabolism [155-158,160-162]. These incongruities highlight the importance in validation of these metabolic biomarkers as well as understanding the mechanisms behind these metabolic alterations.

Another level of complexity arises from experiments using techniques targeted towards specific classes of metabolites, such as volatile organic compounds (VOCs). While detected VOCs might be the basis of a biosignature, the origin of these compounds is ambiguous [163-165]. This ambiguity hinders discovery of common altered pathways and comparison with data from other studies.

Metabolomics Identification of Mtb Biomarkers

The majority of changes observed in host metabolites are associated with a general host response to infection rather than a specific response to *Mtb* infection. Detection of *Mtb* metabolites would confirm infection with *Mtb* and could be used for diagnosis as well as monitoring disease progression and response to treatment.

The unique mycobacterial cell wall contains a multitude of lipids, some of which are species specific [166-168]. These *Mtb* specific lipids can be targeted to differentiate *Mtb* infection from infection with nontuberculous mycobacteria (NTM) or other bacteria. Additionally, *Mtb* lipids might correlate well with sputum smear and culture. Using TB patient sputum, two groups developed biosignatures capable of determining the presence of *Mtb*. Both of these biosignatures rely on the presence of mycocerosates, which are relevant markers of the *Mtb* complex [169]. Initially, Kaal *et al.* used tuberculostearic acid (TBSA) and hexacosanoic acid (HCA) to detect *Mtb* in the sputum of TB patients, however, these were not specific enough for *Mtb* as they are present in other mycobacteria [170]. Then, a biosignature containing 20 *Mtb* specific compounds was developed which included TBSA, HCA, along with more specific *Mtb* metabolites such as mycocerosates [169,171]. To further differentiate sputum from healthy controls, TB patients, and NTM patients, a decision tree containing six metabolites, TBSA, HCA, and C29, C30 and C32 mycocerosates was developed [172]. The use of this decision tree along with a more improved

analytical method for the analysis sputum samples resulted in a sensitivity of 89% and specificity of 100% [172]. The second group also had success with a mycocerosate containing biosignature [173]. O'Sullivan *et al.* monitored three mycocerosates (C29, C30 and C32) which are characteristic of *Mtb* and result in a reproducible doublet peak due to racemization during alkaline hydrolysis[173]. Using these markers, they achieved a specificity of 76.3% and sensitivity of 64.9% [173]. These *Mtb* biosignatures from both groups perform adequately, however, they both suffer from the presence of contaminating host molecules, and required further optimization of extraction and detection techniques [172,174]. The addition of a normal phase solid phase extraction (SPE) step was capable of removing interfering lipids such as cholesterol while also maintaining recovery of the mycocerosate targets which enabled more accurate and sensitive detection of mycobacterial lipids [172,174]. Aside from *Mtb* specific lipids, other *Mtb* specific compounds have been targeted as biomarkers for TB diagnosis. Pan *et al.* were able to detect two *Mtb* secreted molecules, mycobactin and tuberculosinyladenosine (TbAd), in the sputum of TB patients [175]. As sputum contains bacteria and originates near the site of infection, it is the best specimen for detecting *Mtb*. However, production of sputum is not always possible for some patients including children and those at later stages of successful anti-TB treatment. Thus, it would be advantageous to assess other biological fluids for *Mtb* specific biomarkers.

Mtb generates unique volatiles when grown in culture. Based on *in vitro* studies, volatile organic compounds (VOCs) unique to mycobacteria could be detected [176,177]. Four of these *Mtb* volatiles (methyl phenylacetate, methyl p-anisate, methyl nicotinate, and *o*-phenylanisole) can be detected in patient breath and one, methyl nicotinate, is highly specific for *Mtb* and can differentiate between TB and non-smoking healthy controls [178]. Two separate groups have tried to optimize the collection, concentration and detection of these four compounds [179,180]. The

optimized parameters developed by Scott-Thomas *et al.* rely on GC-MS detection in anticipation of the development of a portable GC-MS [179]. As an alternative to GC-MS, Metters *et al.* used electrochemical sensors to detect *Mtb* volatiles, however, they were only able to detect two of the four compounds, methyl nicotinate and *o*-phenylanisole, as only these two were electrochemically active [180]. Both of these optimized methods hold promise in being useful point-of-care tests for diagnosing TB, however, they need to be need to be further validated with additional patient samples. Phillips *et al.* analyzed the breath of TB patients and identified breath VOC biomarkers that originate either from the host, *Mtb*, or both [181-183]. Unlike, Syhre *et al.* which targeted VOCs identified from *Mtb* cultures, these VOC biomarkers were identified by using an unbiased analysis of TB patient breath and most likely picked up on the most abundant compounds that differed as opposed to *Mtb* specific compounds. Thus, it is not surprising that the four VOCs previously discussed were not detected by Phillips *et al.*. Perhaps a combination of the VOCs detected by both groups would result in a more robust breath test. The fact that breath VOCs are capable of distinguishing between TB and non-TB patients is promising for the development of a rapid diagnostic tool. Evaluation of these VOCs during anti-TB treatment could also generate a prognostic biomarker of anti-TB treatment response.

Mtb produces and secretes unique metabolites when grown *in vitro* and while these might not be an accurate representation of what is produced *in vivo*, they provide *Mtb* specific metabolites that can be targeted in clinical samples. Development of methods targeted towards these metabolites increases the likelihood of detecting these molecules amongst the abundant host metabolites. Further investigation into *Mtb* specific biomarkers is needed as these could be combined with host biomarkers to create a test indicative of host alterations due to *Mtb* infection.

Challenges in Metabolomics Based Biomarker Discovery

A major impediment to the discovery of metabolic based biomarkers is the challenge associated with metabolite identification [184]. A significant portion of detected metabolic features remain structurally uncharacterized. Almost 50% of the compounds detected in four separate studies could not be identified [155,159,160,185]. Though some metabolites match with compounds in known databases, few groups actually go on to verify the structural identity of significant metabolites. Though putative identities could be determined for all 12 metabolites described by Feng *et al.*, none of these identities were confirmed with commercial standards [154]. While these uncharacterized metabolic features can still be useful biomarkers, their lack of characterization impedes discovery of the metabolic pathways involved and the reasons for observed alterations.

Another challenge encountered is the lack of validation of detected metabolites. Validation requires the use of more targeted methods and larger and more diverse patient sets [152]. This step is important for demonstrating that the detected metabolite alterations are due to specific biological processes and not due to analytical or nonspecific biological processes. A more targeted method confirms that the metabolite alterations were not due to technical variation and can include selective extraction techniques, chromatographic conditions, and/or detection methods. For instance, if a significantly altered metabolite identified during biomarker discovery is chemically confirmed as cotinine, an extraction technique optimized for nicotine metabolites can be used to enrich for the target metabolite, cotinine [186,187]. Additionally, previously optimized and validated methods targeted towards the analysis of cotinine can be used such as GC-MS or ELISA assays [187,188]. The use of larger and more diverse patient sets aids in confirmation that metabolite alteration is due to specific biological processes. If cotinine had significantly increased abundances in active tuberculosis in patients from South Africa relative to healthy controls, analysis of cotinine abundances in active tuberculosis patients from other countries or

with pulmonary diseases that display similar symptoms to tuberculosis could help to determine if this metabolite is truly a biomarker for active tuberculosis or whether it is a biomarker for exposure to cigarettes. Additionally, if cotinine was significantly decreased in TB patients during successful, standard anti-TB treatment, evaluation of cotinine abundances in patients with different treatment outcomes or on different treatment regimens could help determine if this metabolite is a true biomarker of anti-TB treatment response or if standard anti-TB treatment affects metabolism of nicotine and is unrelated to disease resolution. Validation provides more confidence in the alteration of these significantly different metabolites and confirms them as robust predictors of particular biological processes.

As seen above, there were conflicting results about the levels of detected metabolites in TB patients. This highlights the importance of both structural confirmation and validation as these discrepancies might be due to improper identification or may be resolved through targeted validation.

1.5.5 Lipoarabinomannan (LAM)

As stated in the previous sections, an *Mtb* specific biomarker that can be detected in the absence of culture-based methods would be ideal for demonstrating infection with *Mtb* for diagnosis and killing of *Mtb* for treatment response. LAM is a lipoglycan associated with the mycobacterial cell wall which consists of three main structural components; the phosphoinositol anchor, the mannan core and the terminal arabinan branches [167,189,190]. Though LAM is common to all mycobacteria, variations in LAM endcapping, branching, size, and acylation can aid in distinguishing mycobacterial species, such as the terminal mannose caps which are characteristic of *Mtb* and other pathogenic, slow growing mycobacterial species [189-191]. The specificity of this molecule for mycobacteria and its potential to discriminate between mycobacterial species made

LAM a perfect candidate for a TB diagnostic biomarker. Adding to this was its immunogenicity and its postulated release from actively growing mycobacteria as well as from *Mtb* infected macrophages during TB[192-195].

In 2001, Hamasur *et al.* reported the detection of LAM in the urine of TB infected patients using both an ELISA and dipstick test and the diagnostic accuracy of the ELISA was subsequently evaluated the subsequent evaluation at an Ethiopian tuberculosis center [195,196]. Based on the high specificity and moderate sensitivity reported by these early studies, Chemogen Inc. (Portland, ME, USA) produced a LAM ELISA test which was eventually developed into the commercial Clearview TB ELISA by Alere Inc. (Waltham, MA, USA) [197]. A systematic review by Minion *et al.* evaluated the diagnostic accuracy of urinary LAM antigen detection in seven studies and determined variable sensitivity ranging from 13 – 93% and more consistent specificity ranges from 87 – 99% [198]. A meta-analysis including all seven studies decreased the overall sensitivity, however, there was an increased sensitivity in HIV positive patients relative to HIV negative patients, which is important since sputum smear and culture sensitivity is low in HIV patients [198,199]. Another more recent assessment of the Determine TB LAM test as a diagnostic for HIV positive TB patients was performed by Peter *et al.* and demonstrated that administration of anti-TB treatment on the basis of a positive LAM result reduced the risk of mortality by 17% [200]. Additionally, the Determine TB LAM test (Alere Inc., Waltham, MA, USA) was used to monitor LAM from the urine of TB patients undergoing anti-TB treatment in HIV endemic regions to determine its prognostic capabilities [201]. The number of LAM positive patients decreased during treatment from 32% at baseline to 10% at six months and patients with a grade of $\geq$ 2+ (on a scale of 1+ to 5+) had an increased risk of mortality [201]. Though LAM test

had moderate sensitivity, a positive test after 2 months of treatment served to denote those patients that required further clinical evaluations thus reducing their risk of mortality [201].

In order to improve the sensitivity of these antibody-based detection methods, Hamasur *et al.* developed a magnetic immunoassay platform, which uses magnetic nanoparticles and anti-LAM monoclonal antibodies [197]. In addition to making sample processing more amenable to development of a point of care test, this improved method resulted in a sensitivity of 100% and a specificity of 82% [197]. Though the pilot study had a small sample size (17 TB patients, 22 healthy controls), this improved sensitivity, especially in HIV negative patients, is quite promising. Other groups have used antibody independent methods such as GC-MS and capillary electrophoresis (CE) to detect LAM [202,203]. Derivatization and GC-MS analysis of D-arabinose released from purified, urinary LAM purified yielded a sensitivity of 98% and a specificity of 63% [202]. Importantly, the samples evaluated consisted of both HIV positive and negative patients and the range of LAM concentrations were similar amongst the two groups.

The moderate and variable sensitivities associated with the urinary LAM ELISA tests sparked some debate about how LAM enters the urine [194]. The first proposed mechanism is that LAM released by *Mtb* into circulation binds to LAM specific antibodies which prevents passage through the normal kidney and excretion in the urine, resulting in a negative LAM test [194]. The second proposed mechanism is that LAM released by *Mtb* into circulation passes through the normal kidney and is excreted in the urine, resulting in a positive LAM test [194]. The third proposed mechanism is that LAM is released by *Mtb* in the renal tract giving rise to a positive LAM test as well as *Mtb* in the urine [194]. Wood *et al.* detected *Mtb* in the urine of almost half of the LAM positive patients, which provided evidence, but did not confirm, the third proposed mechanism [194]. Cox *et al.* also demonstrated that a majority of the patients with positive LAM

tests also had renal TB, providing more evidence for the third proposed mechanism [204]. These two studies propose that a disseminated infection due to a compromised immune system can lead to renal TB and the presence of LAM in the urine, however, this does not explain the presence of LAM in the urine of HIV negative patients and patients without *Mtb* in their urine. Presently, it is unclear whether the variable sensitivity of the LAM tests is due to the detection methods used or to a lack of understanding of the mechanisms behind the presence of LAM in the urine.

1.5.6 Conclusions

Many biomarkers have been discovered using high-throughput "omics" techniques. The challenge now is to move on to structural characterization and validation of these newly discovered biomarkers. A comprehensive TB biomarker database that contains the different transcripts, proteins, and metabolites discovered as well as the different host processes that they are involved in would be highly beneficial. Researchers could conveniently compare their list of discovered biomarkers with other transcripts, proteins or metabolites identified and find out whether any other biomarkers in a pathway of interest have been detected. This could aid in the development of a biosignature that contains a combination of metabolites, transcripts and proteins, which might prove to be more robust.

Any biosignature that is developed should include *Mtb* specific molecules to enhance its specificity. Many of the host molecules that have been discovered are related to general infection processes. While they are robust when comparing active vs. healthy patients, they lose their robustness when comparing patients with other pulmonary diseases. By including *Mtb* specific biomarkers, the developed biosignature would be more specific when comparing TB to other pulmonary diseases.

Though each of these high-throughput "omics" techniques has advantages and has yielded potential biomarkers for the tuberculosis field, this dissertation will focus on the use of metabolomics in TB biomarker discovery. While transcriptomics and proteomics can detect changes in transcript and protein abundances, these levels might not be a true representation of what is happening in an organism as post-transcriptional and post-translational modifications exist which can affect cellular processes [143]. Metabolomics, on the other hand measures intermediates and end-products of cellular processes that have already occurred in the cell providing a more accurate representation of an organism's physiology [143,205]. Based on this attribute, metabolomics was chosen as the analytical platform for this dissertation. This platform enabled identification of biomarkers for successful anti-TB treatment response and provided novel insights into host metabolic pathways that are altered during anti-TB treatment. However, a combination of all three "omics" techniques would provide a more comprehensive understanding of host physiology during anti-TB treatment.

1.6 Research Rationale and Summary of Aims

The long duration of standard therapy and the increasing prevalence of drug resistant TB cases require the development and approval of new anti-TB treatments and regimens. A significant impediment to their approval, however, is the evaluation of treatment efficacy during phase II and III clinical trials. Development of a biosignature that can predict a patient's response to treatment at early time points during treatment would accelerate clinical trials. Initial steps by Mahapatra *et al.* towards development of a biosignature involved metabolomics analyses of pulmonary TB patients undergoing standard therapy [185]. These metabolomics experiments resulted in the definition of a TB-early treatment response biosignature consisting of 12

metabolites (1-12 in Table 1.1) as well as 13 additional metabolites that decreased during anti-TB therapy (13-25 in Table 1.1) [185].

The 12 metabolite TB-early treatment response biosignature had statistically significant changes in abundance between baseline and all time points during treatment (M1, M2, and M6) [185]. Six of these metabolites were identified by logistic regression analysis to be able to classify D0 and M1 patients with an 11.8% error rate [185]. Additionally, the thirteen metabolites demonstrated consistent decreased abundance during anti-TB treatment (S. Mahapatra, unpublished data, CSU). These studies provided proof that urinary metabolites are altered during anti-TB treatment and that these alterations could be detected as early as one month during treatment [185]. This provides evidence that these metabolites could potentially be prognostic biomarkers or surrogate endpoints for successful anti-TB treatment response. This led to the hypothesis that structural characterization and quantification of the metabolites detected during biomarker discovery will determine those that are suitable for a robust, clinically useful biosignature and rule out those that are not.

The following specific aims were developed to address this hypothesis and continue advancement of these metabolites towards a clinically applied biosignature.

I. Structurally identify significant, yet uncharacterized metabolites belonging to TB-early treatment response biosignature (Chapters 2 and 3)

II. Determine if structurally identified metabolites are altered during active TB disease (Chapter 4)

III. To validate identified metabolites as biomarkers of anti-TB treatment response (Chapter 5)

Table 1.1 List of Urinary Metabolites

List of urinary metabolites detected during untargeted metabolomics analysis of pulmonary TB patients undergoing standard anti-TB therapy.

	Mass	Predicted Formula	DB Match	Confirmed Structure
1	137.0484	C7H7NO2	p-Aminobenzoic acid[#]	No
2	167.0591	C8H9NO3	Pyridoxal/isopyridoxal[#]	No
3	174.0636	C6H10N2O4[*]	Formimino-L-glutamic acid[#]	No
4	202.1326	C9H18N2O3	Leu Ala[#]	No
5	231.1831	C12H25NO3	None	No
6	246.0865	C9H14N2O6[*]	L-alpha-Aspartyl-L-hydroxyproline[#]	No
7	263.1124	C9H17N3O6[*]	Thr Gly Ser[#]	No
8	286.2374	C14H30N4O2	N1, N12-Diacetylspermine[#]	No
9	421.2051	C19H27N5O6[*]	None	No
10	496.2014	C25H28N4O7[*]	None	No
11	566.2683	C29H48N2O2P2S2[*]	None	No
12	874.3547	C36H65N2O16P3[*]	None	No
13	131.0582	C5H9NO3	1-Hydroxyproline	Yes
14	175.0481	C6H9NO5	N-Acetyl-L-aspartic acid	Yes
15	202.1430	C8H18N4O2	Dimethyl-L-arginine	Yes
16	174.0641	C6H10N2O4	N-Acetylasparagine	Yes
17	169.0851	C7H11N3O2	1-Methylhistidine	Yes
18	165.0790	C9H11NO2	L-Phenylalanine	Yes
19	129.0426	C5H7NO3	Pyroglutamic acid	Yes
20	163.0303	C5H9NO3S	Acetylcysteine	Yes
21	137.0477	C7H7NO2	Trigonelline	Yes
22	384.1216	C14H20N6O5S	S-Adenosylhomocysteine	Yes
23	181.0739	C9H11NO4	L-Tyrosine	Yes
24	161.0688	C6H11NO4	alpha-Amino adipic acid	Yes
25	167.0219	C7H5NO4	Quinolinic Acid	Yes

[*]other alternate chemical formulas exist

[#]other alternate structures exist

REFERENCES

1. Broadhurst DI, Kell DB. Statistical strategies for avoiding false discoveries in metabolomics and related experiments. Metabolomics 2006;2(4):171-196.
2. Donoghue HD, Lee OY, Minnikin DE, Besra GS, Taylor JH, Spigelman M. Tuberculosis in Dr Granville's mummy: a molecular re-examination of the earliest known Egyptian mummy to be scientifically examined and given a medical diagnosis. Proc Biol Sci 2010;277(1678):51-6.
3. Koch R. THE ETIOLOGY OF TUBERCULOSIS. Reviews of Infectious Diseases 1982;4(6):1270-1274.
4. Smith I. Mycobacterium tuberculosis pathogenesis and molecular determinants of virulence. Clin Microbiol Rev 2003;16(3):463-96.
5. Kaufmann SHE. Immunopathology of mycobacterial diseases INTRODUCTION. Seminars in Immunopathology 2016;38(2):135-138.
6. Organization WH. Global tuberculosis report 2015. Geneva: WHO; 2015.
7. Gengenbacher M, Kaufmann SH. Mycobacterium tuberculosis: success through dormancy. FEMS Microbiol Rev 2012;36(3):514-32.
8. Ernst JD. The immunological life cycle of tuberculosis. Nature Reviews Immunology 2012;12(8):581-591.
9. Brightbill HD, Libraty DH, Krutzik SR, Yang RB, Belisle JT, Bleharski JR, Maitland M, Norgard MV, Plevy SE, Smale ST and others. Host defense mechanisms triggered by microbial lipoproteins through toll-like receptors. Science 1999;285(5428):732-736.
10. Quesniaux VJ, Nicolle DM, Torres D, Kremer L, Guerardel Y, Nigou J, Puzo G, Erard FO, Ryffel B. Toll-like receptor 2 (TLR2)-dependent-positive and TLR2-independent-negative regulation of proinflammatory cytokines by mycobacterial lipomannans. Journal of Immunology 2004;172(7):4425-4434.
11. Thoma-Uszynski S, Stenger S, Takeuchi O, Ochoa MT, Engele M, Sieling PA, Barnes PF, Rollinghoff M, Bolcskei PL, Wagner M and others. Induction of direct antimicrobial activity through mammalian toll-like receptors. Science 2001;291(5508):1544-1547.
12. Gilleron M, Himoudi N, Adam O, Constant P, Venisse A, Riviere M, Puzo G. Mycobacterium smegmatis phosphoinositols-glyceroarabinomannans - Structure and localization of alkali-labile and alkali-stable phosphoinositides. Journal of Biological Chemistry 1997;272(1):117-124.
13. Ferguson JS, Weis JJ, Martin JL, Schlesinger LS. Complement protein c3 binding to Mycobacterium tuberculosis is initiated by the classical pathway in human bronchoalveolar lavage fluid. Infection and Immunity 2004;72(5):2564-2573.
14. Schlesinger LS, Bellingerkawahara CG, Payne NR, Horwitz MA. PHAGOCYTOSIS OF MYCOBACTERIUM-TUBERCULOSIS IS MEDIATED BY HUMAN MONOCYTE COMPLEMENT RECEPTORS AND COMPLEMENT COMPONENT-C3. Journal of Immunology 1990;144(7):2771-2780.
15. Schlesinger LS, Kaufman TM, Iyer S, Hull SR, Marchiando LK. Differences in mannose receptor-mediated uptake of lipoarabinomannan from virulent and attenuated strains of Mycobacterium tuberculosis by human macrophages. Journal of Immunology 1996;157(10):4568-4575.

16. Kang PB, Azad AK, Torrelles JB, Kaufman TM, Beharka A, Tibesar E, DesJardin LE, Schlesinger LS. The human macrophage mannose receptor directs Mycobacterium tuberculosis lipoarabinomannan-mediated phagosome biogenesis. Journal of Experimental Medicine 2005;202(7):987-999.
17. Sweet L, Singh PP, Azad AK, Rajaram MVS, Schlesinger LS, Schorey JS. Mannose Receptor-Dependent Delay in Phagosome Maturation by Mycobacterium avium Glycopeptidolipids. Infection and Immunity 2010;78(1):518-526.
18. Pennini ME, Pai RK, Schultz DC, Boom WH, Harding CV. Mycobacterium tuberculosis 19-kDa lipoprotein inhibits IFN-gamma-induced chromatin remodeling of MHC2TA by TLR2 and MAPK signaling. Journal of Immunology 2006;176(7):4323-4330.
19. Fenton MJ, Vermeulen MW. Immunopathology of tuberculosis: Roles of macrophages and monocytes. Infection and Immunity 1996;64(3):683-690.
20. Mellman I, Steinman RM. Dendritic cells: specialized and regulated antigen processing machines. Cell 2001;106(3):255-8.
21. Wong D, Bach H, Sun J, Hmama Z, Av-Gay Y. Mycobacterium tuberculosis protein tyrosine phosphatase (PtpA) excludes host vacuolar-H+-ATPase to inhibit phagosome acidification. Proceedings of the National Academy of Sciences of the United States of America 2011;108(48):19371-19376.
22. Vergne I, Chua J, Deretic V. Tuberculosis toxin blocking phagosome maturation inhibits a novel Ca2+/calmodulin-PI3K hVPS34 cascade. Journal of Experimental Medicine 2003;198(4):653-659.
23. Vergne I, Chua J, Lee HH, Lucas M, Belisle J, Deretic V. Mechanism of phagolysosome biogenesis block by viable Mycobacterium tuberculosis. Proceedings of the National Academy of Sciences of the United States of America 2005;102(11):4033-4038.
24. Fratti RA, Chua J, Vergne I, Deretic V. Mycobacterium tuberculosis glycosylated phosphatidylinositol causes phagosome maturation arrest. Proceedings of the National Academy of Sciences of the United States of America 2003;100(9):5437-5442.
25. Walburger A, Koul A, Ferrari G, Nguyen L, Prescianotto-Baschong C, Huygen K, Klebl B, Thompson C, Bacher G, Pieters J. Protein kinase G from pathogenic mycobacteria promotes survival within macrophages. Science 2004;304(5678):1800-1804.
26. Cole ST, Brosch R, Parkhill J, Garnier T, Churcher C, Harris D, Gordon SV, Eiglmeier K, Gas S, Barry CE and others. Deciphering the biology of Mycobacterium tuberculosis from the complete genome sequence. Nature 1998;393(6685):537-+.
27. Goldberg MF, Saini NK, Porcelli SA. Evasion of Innate and Adaptive Immunity by Mycobacterium tuberculosis. Microbiol Spectr 2014;2(5).
28. van der Wel N, Hava D, Houben D, Fluitsma D, van Zon M, Pierson J, Brenner M, Peters PJ. M-tuberculosis and M-leprae translocate from the phagolysosome to the cytosol in myeloid cells. Cell 2007;129(7):1287-1298.
29. Gao LY, Guo S, McLaughlin B, Morisaki H, Engel JN, Brown EJ. A mycobacterial virulence gene cluster extending RD1 is required for cytolysis, bacterial spreading and ESAT-6 secretion. Molecular Microbiology 2004;53(6):1677-1693.
30. Houben D, Demangel C, van Ingen J, Perez J, Baldeon L, Abdallah AM, Caleechurn L, Bottai D, van Zon M, de Punder K and others. ESX-1-mediated translocation to the cytosol controls virulence of mycobacteria. Cellular Microbiology 2012;14(8):1287-1298.

31. Abramovitch RB, Rohde KH, Hsu FF, Russell DG. aprABC: a Mycobacterium tuberculosis complex-specific locus that modulates pH-driven adaptation to the macrophage phagosome. Molecular Microbiology 2011;80(3):678-694.
32. Roberts LL, Robinson CM. Mycobacterium tuberculosis infection of human dendritic cells decreases integrin expression, adhesion and migration to chemokines. Immunology 2014;141(1):39-51.
33. Russell DG. Who puts the tubercle in tuberculosis? Nature Reviews Microbiology 2007;5(1):39-47.
34. Lee J, Kornfeld H. Interferon-γ Regulates the Death of M. tuberculosis-Infected Macrophages. J Cell Death 2010;3:1-11.
35. Mehra S, Foreman TW, Didier PJ, Ahsan MH, Hudock TA, Kissee R, Golden NA, Gautam US, Johnson AM, Alvarez X and others. The DosR Regulon Modulates Adaptive Immunity and Is Essential for Mycobacterium tuberculosis Persistence. Am J Respir Crit Care Med 2015;191(10):1185-96.
36. Leistikow RL, Morton RA, Bartek IL, Frimpong I, Wagner K, Voskuil MI. The Mycobacterium tuberculosis DosR Regulon Assists in Metabolic Homeostasis and Enables Rapid Recovery from Nonrespiring Dormancy. Journal of Bacteriology 2010;192(6):1662-1670.
37. Wayne LG, Lin KY. GLYOXYLATE METABOLISM AND ADAPTATION OF MYCOBACTERIUM-TUBERCULOSIS TO SURVIVAL UNDER ANAEROBIC CONDITIONS. Infection and Immunity 1982;37(3):1042-1049.
38. Peyron P, Vaubourgeix J, Poquet Y, Levillain F, Botanch C, Bardou F, Daffe M, Emile JF, Marchou B, Cardona PJ and others. Foamy Macrophages from Tuberculous Patients' Granulomas Constitute a Nutrient-Rich Reservoir for M-tuberculosis Persistence. Plos Pathogens 2008;4(11):14.
39. Cheon SA, Cho HH, Kim J, Lee J, Kim HJ, Park TJ. Recent tuberculosis diagnosis toward the end TB strategy. J Microbiol Methods 2016;123:51-61.
40. Caminero Luna JA. Update on the diagnosis and treatment of pulmonary tuberculosis. Rev Clin Esp 2016;216(2):76-84.
41. Black CA. Delayed type hypersensitivity: current theories with an historic perspective. Dermatol Online J 1999;5(1):7.
42. Zeka AN, Tasbakan S, Cavusoglu C. Evaluation of the GeneXpert MTB/RIF Assay for Rapid Diagnosis of Tuberculosis and Detection of Rifampin Resistance in Pulmonary and Extrapulmonary Specimens. Journal of Clinical Microbiology 2011;49(12):4138-4141.
43. Niemz A, Boyle DS. Nucleic acid testing for tuberculosis at the point-of-care in high-burden countries. Expert Review of Molecular Diagnostics 2012;12(7):687-701.
44. Zumla A, Nahid P, Cole ST. Advances in the development of new tuberculosis drugs and treatment regimens. Nat Rev Drug Discov 2013;12(5):388-404.
45. Fox W, Ellard GA, Mitchison DA. Studies on the treatment of tuberculosis undertaken by the British Medical Research Council tuberculosis units, 1946-1986, with relevant subsequent publications. Int J Tuberc Lung Dis 1999;3(10 Suppl 2):S231-79.
46. FOX HH. The chemical approach to the control of tuberculosis. Science 1952;116(3006):129-34.
47. Cohen KA, Bishai WR, Pym AS. Molecular Basis of Drug Resistance in Mycobacterium tuberculosis. Microbiol Spectr 2014;2(3).

48. Takayama K, Wang L, David HL. Effect of isoniazid on the in vivo mycolic acid synthesis, cell growth, and viability of Mycobacterium tuberculosis. Antimicrob Agents Chemother 1972;2(1):29-35.
49. Lei B, Wei CJ, Tu SC. Action mechanism of antitubercular isoniazid. Activation by Mycobacterium tuberculosis KatG, isolation, and characterization of inha inhibitor. J Biol Chem 2000;275(4):2520-6.
50. Slayden RA, Barry CE. The genetics and biochemistry of isoniazid resistance in Mycobacterium tuberculosis. Microbes and Infection 2000;2(6):659-669.
51. Mdluli K, Slayden RA, Zhu YQ, Ramaswamy S, Pan X, Mead D, Crane DD, Musser JM, Barry CE. Inhibition of a Mycobacterium tuberculosis beta-ketoacyl ACP synthase by isoniazid. Science 1998;280(5369):1607-1610.
52. Sensi P. History of the development of rifampin. Rev Infect Dis 1983;5 Suppl 3:S402-6.
53. Riva MA. From milk to rifampicin and back again: history of failures and successes in the treatment for tuberculosis. J Antibiot (Tokyo) 2014;67(9):661-5.
54. Wehrli W, Staehelin M. Actions of the rifamycins. Bacteriol Rev 1971;35(3):290-309.
55. Zhang Y, Wade MM, Scorpio A, Zhang H, Sun ZH. Mode of action of pyrazinamide: disruption of Mycobacterium tuberculosis membrane transport and energetics by pyrazinoic acid. Journal of Antimicrobial Chemotherapy 2003;52(5):790-795.
56. Wallis RS, Maeurer M, Mwaba P, Chakaya J, Rustomjee R, Migliori GB, Marais B, Schito M, Churchyard G, Swaminathan S and others. Tuberculosis-advances in development of new drugs, treatment regimens, host-directed therapies, and biomarkers. Lancet Infect Dis 2016;16(4):e34-46.
57. Blair HA, Scott LJ. Delamanid: A Review of Its Use in Patients with Multidrug-Resistant Tuberculosis. Drugs 2015;75(1):91-100.
58. Field SK. Bedaquiline for the treatment of multidrug-resistant tuberculosis: great promise or disappointment? Ther Adv Chronic Dis 2015;6(4):170-84.
59. Administration UFaD. The FDA's Drug Review Process: Ensuring Drugs are Safe and Effective. 2014.
60. Cox E, Laessig K. FDA approval of bedaquiline--the benefit-risk balance for drug-resistant tuberculosis. N Engl J Med 2014;371(8):689-91.
61. de Jonge MR, Koymans LH, Guillemont JE, Koul A, Andries K. A computational model of the inhibition of Mycobacterium tuberculosis ATPase by a new drug candidate R207910. Proteins 2007;67(4):971-80.
62. Matsumoto M, Hashizume H, Tomishige T, Kawasaki M, Tsubouchi H, Sasaki H, Shimokawa Y, Komatsu M. OPC-67683, a nitro-dihydro-imidazooxazole derivative with promising action against tuberculosis in vitro and in mice. PLoS Med 2006;3(11):e466.
63. Zak DE, Penn-Nicholson A, Scriba TJ, Thompson E, Suliman S, Amon LM, Mahomed H, Erasmus M, Whatney W, Hussey GD and others. A blood RNA signature for tuberculosis disease risk: a prospective cohort study. Lancet 2016;387(10035):2312-22.
64. FDA-NIH Biomarker Working Group. BEST (Biomarkers, EndpointS, and other Tools) Resource. Silver Spring, MD Bethesda, MD: Food and Drug Administration National Institutes of Health; 2016.
65. Brody T. Chapter 19 - Biomarkers. Clinical Trials (Second Edition). Boston: Academic Press; 2016. p 377-419.
66. Winter JM, Yeo CJ, Brody JR. Diagnostic, prognostic, and predictive biomarkers in pancreatic cancer. J Surg Oncol 2013;107(1):15-22.

67. Pepe MS. The statistical evaluation of medical tests for classification and prediction. USA: Oxford University Press; 2003.
68. Buyse M. Towards validation of statistically reliable biomarkers. Ejc Supplements 2007;5(5):89-95.
69. Koulman A, Lane GA, Harrison SJ, Volmer DA. From differentiating metabolites to biomarkers. Anal Bioanal Chem 2009;394(3):663-70.
70. Banoo S, Bell D, Bossuyt P, Herring A, Mabey D, Poole F, Smith PG, Sriram N, Wongsrichanalai C, Linke R and others. Evaluation of diagnostic tests for infectious diseases: general principles. Nat Rev Microbiol 2008;6(11 Suppl):S16-26.
71. Florkowski CM. Sensitivity, specificity, receiver-operating characteristic (ROC) curves and likelihood ratios: communicating the performance of diagnostic tests. Clin Biochem Rev 2008;29 Suppl 1:S83-7.
72. Alberg AJ, Park JW, Hager BW, Brock MV, Diener-West M. The use of "overall accuracy" to evaluate the validity of screening or diagnostic tests. Journal of General Internal Medicine 2004;19(5):460-465.
73. Phillips PPJ. Prognostic and Surrogate Markers for Outcome in the Treatment of Pulmonary Tuberculosis: London School of Hygiene and Tropical Medicine, University of London; 2009.
74. Pepe MS, Janes H, Longton G, Leisenring W, Newcomb P. Limitations of the odds ratio in gauging the performance of a diagnostic, prognostic, or screening marker. American Journal of Epidemiology 2004;159(9):882-890.
75. Buyse M, Sargent DJ, Grothey A, Matheson A, de Gramont A. Biomarkers and surrogate end points--the challenge of statistical validation. Nat Rev Clin Oncol 2010;7(6):309-17.
76. The evaluation of surrogate endpoints. In: Molenberghs G, Buyse ME, Burzykowski T, editors. New York: Springer; 2005. p 1 online resource (xxiii, 408 pages) :.
77. Prentice RL. Surrogate endpoints in clinical trials: definition and operational criteria. Stat Med 1989;8(4):431-40.
78. Lassere MN. The Biomarker-Surrogacy Evaluation Schema: a review of the biomarker-surrogate literature and a proposal for a criterion-based, quantitative, multidimensional hierarchical levels of evidence schema for evaluating the status of biomarkers as surrogate endpoints. Stat Methods Med Res 2008;17(3):303-40.
79. Molenberghs G, Buyse M, Geys H, Renard D, Burzykowski T, Alonso A. Statistical challenges in the evaluation of surrogate endpoints in randomized trials. Controlled Clinical Trials 2002;23(6):607-625.
80. Freedman LS, Graubard BI, Schatzkin A. STATISTICAL VALIDATION OF INTERMEDIATE END-POINTS FOR CHRONIC DISEASES. Statistics in Medicine 1992;11(2):167-178.
81. Buyse M, Molenberghs G. Criteria for the validation of surrogate endpoints in randomized experiments. Biometrics 1998;54(3):1014-1029.
82. Daniels MJ, Hughes MD. Meta-analysis for the evaluation of potential surrogate markers. Stat Med 1997;16(17):1965-82.
83. Albert JM, Ioannidis JPA, Reichelderfer P, Conway B, Coombs RW, Crane L, Demasi R, Dixon DO, Flandre P, Hughes MD and others. Statistical issues for HIV surrogate endpoints: Point/counterpoint. Statistics in Medicine 1998;17(21):2435-2462.
84. Gail MH, Pfeiffer R, Van Houwelingen HC, Carroll RJ. On meta-analytic assessment of surrogate outcomes. Biostatistics 2000;1(3):231-46.

85. Buyse M, Molenberghs G, Burzykowski T, Renard D, Geys H. The validation of surrogate endpoints in meta-analyses of randomized experiments. Biostatistics 2000;1(1):49-67.
86. Burzykowski T, Buyse M. Surrogate threshold effect: an alternative measure for meta-analytic surrogate endpoint validation. Pharm Stat 2006;5(3):173-86.
87. Buyse M, Molenberghs G, Paoletti X, Oba K, Alonso A, Van der Elst W, Burzykowski T. Statistical evaluation of surrogate endpoints with examples from cancer clinical trials. Biom J 2016;58(1):104-32.
88. Maertzdorf J, Kaufmann SH, Weiner J. Molecular signatures for vaccine development. Vaccine 2015;33(40):5256-61.
89. Kurbatova EV, Cegielski JP, Lienhardt C, Akksilp R, Bayona J, Becerra MC, Caoili J, Contreras C, Dalton T, Danilovits M and others. Sputum culture conversion as a prognostic marker for end-of-treatment outcome in patients with multidrug-resistant tuberculosis: a secondary analysis of data from two observational cohort studies. Lancet Respiratory Medicine 2015;3(3):201-209.
90. Horne DJ, Royce SE, Gooze L, Narita M, Hopewell PC, Nahid P, Steingart KR. Sputum monitoring during tuberculosis treatment for predicting outcome: systematic review and meta-analysis. Lancet Infectious Diseases 2010;10(6):387-394.
91. Malangu N, Mngomezulu M. Evaluation of tuberculosis infection control measures implemented at primary health care facilities in Kwazulu-Natal province of South Africa. BMC Infect Dis 2015;15:117.
92. Claassens MM, Van Schalkwyk C, du Toit E, Roest E, Lombard CJ, Enarson DA, Beyers N, Borgdorff MW. Tuberculosis in Healthcare Workers and Infection Control Measures at Primary Healthcare Facilities in South Africa. Plos One 2013;8(10):8.
93. Haas CT, Roe JK, Pollara G, Mehta M, Noursadeghi M. Diagnostic 'omics' for active tuberculosis. BMC Med 2016;14:37.
94. Savino R, Paduano S, Preianò M, Terracciano R. The proteomics big challenge for biomarkers and new drug-targets discovery. Int J Mol Sci 2012;13(11):13926-48.
95. Mairal T, Ozalp VC, Lozano Sánchez P, Mir M, Katakis I, O'Sullivan CK. Aptamers: molecular tools for analytical applications. Anal Bioanal Chem 2008;390(4):989-1007.
96. Adewole OO, Erhabor GE, Adewole TO, Ojo AO, Oshokoya H, Wolfe LM, Prenni JE. Proteomic profiling of eccrine sweat reveals its potential as a diagnostic biofluid for active tuberculosis. Proteomics Clin Appl 2016;10(5):547-53.
97. Achkar JM, Cortes L, Croteau P, Yanofsky C, Mentinova M, Rajotte I, Schirm M, Zhou Y, Junqueira-Kipnis AP, Kasprowicz VO and others. Host Protein Biomarkers Identify Active Tuberculosis in HIV Uninfected and Co-infected Individuals. EBioMedicine 2015;2(9):1160-8.
98. Xu DD, Deng DF, Li X, Wei LL, Li YY, Yang XY, Yu W, Wang C, Jiang TT, Li ZJ and others. Discovery and identification of serum potential biomarkers for pulmonary tuberculosis using iTRAQ-coupled two-dimensional LC-MS/MS. Proteomics 2014;14(2-3):322-31.
99. Agranoff D, Fernandez-Reyes D, Papadopoulos MC, Rojas SA, Herbster M, Loosemore A, Tarelli E, Sheldon J, Schwenk A, Pollok R and others. Identification of diagnostic markers for tuberculosis by proteomic fingerprinting of serum. Lancet 2006;368(9540):1012-21.

100. Liu J, Jiang T, Wei L, Yang X, Wang C, Zhang X, Xu D, Chen Z, Yang F, Li JC. The discovery and identification of a candidate proteomic biomarker of active tuberculosis. BMC Infect Dis 2013;13:506.
101. Zhang X, Liu F, Li Q, Jia H, Pan L, Xing A, Xu S, Zhang Z. A proteomics approach to the identification of plasma biomarkers for latent tuberculosis infection. Diagn Microbiol Infect Dis 2014;79(4):432-7.
102. Xu D, Li Y, Li X, Wei LL, Pan Z, Jiang TT, Chen ZL, Wang C, Cao WM, Zhang X and others. Serum protein S100A9, SOD3, and MMP9 as new diagnostic biomarkers for pulmonary tuberculosis by iTRAQ-coupled two-dimensional LC-MS/MS. Proteomics 2015;15(1):58-67.
103. Wang C, Liu CM, Wei LL, Shi LY, Pan ZF, Mao LG, Wan XC, Ping ZP, Jiang TT, Chen ZL and others. A Group of Novel Serum Diagnostic Biomarkers for Multidrug-Resistant Tuberculosis by iTRAQ-2D LC-MS/MS and Solexa Sequencing. Int J Biol Sci 2016;12(2):246-56.
104. Tanaka T, Sakurada S, Kano K, Takahashi E, Yasuda K, Hirano H, Kaburagi Y, Kobayashi N, Hang NT, Lien LT and others. Identification of tuberculosis-associated proteins in whole blood supernatant. BMC Infect Dis 2011;11:71.
105. Nahid P, Bliven-Sizemore E, Jarlsberg LG, De Groote MA, Johnson JL, Muzanyi G, Engle M, Weiner M, Janjic N, Sterling DG and others. Aptamer-based proteomic signature of intensive phase treatment response in pulmonary tuberculosis. Tuberculosis (Edinb) 2014;94(3):187-96.
106. De Groote MA, Nahid P, Jarlsberg L, Johnson JL, Weiner M, Muzanyi G, Janjic N, Sterling DG, Ochsner UA. Elucidating novel serum biomarkers associated with pulmonary tuberculosis treatment. PLoS One 2013;8(4):e61002.
107. Kashino SS, Pollock N, Napolitano DR, Rodrigues V, Campos-Neto A. Identification and characterization of Mycobacterium tuberculosis antigens in urine of patients with active pulmonary tuberculosis: an innovative and alternative approach of antigen discovery of useful microbial molecules. Clin Exp Immunol 2008;153(1):56-62.
108. Pollock NR, Macovei L, Kanunfre K, Dhiman R, Restrepo BI, Zarate I, Pino PA, Mora-Guzman F, Fujiwara RT, Michel G and others. Validation of Mycobacterium tuberculosis Rv1681 Protein as a Diagnostic Marker of Active Pulmonary Tuberculosis. Journal of Clinical Microbiology 2013;51(5):1367-1373.
109. Kruh-Garcia NA, Wolfe LM, Chaisson LH, Worodria WO, Nahid P, Schorey JS, Davis JL, Dobos KM. Detection of Mycobacterium tuberculosis peptides in the exosomes of patients with active and latent M. tuberculosis infection using MRM-MS. PLoS One 2014;9(7):e103811.
110. Young BL, Mlamla Z, Gqamana PP, Smit S, Roberts T, Peter J, Theron G, Govender U, Dheda K, Blackburn J. The identification of tuberculosis biomarkers in human urine samples. Eur Respir J 2014;43(6):1719-29.
111. Liu JY, Jin L, Zhao MY, Zhang X, Liu CB, Zhang YX, Li FJ, Zhou JM, Wang HJ, Li JC. New serum biomarkers for detection of tuberculosis using surface-enhanced laser desorption/ionization time-of-flight mass spectrometry. Clin Chem Lab Med 2011;49(10):1727-33.
112. Haks MC, Goeman JJ, Magis-Escurra C, Ottenhoff TH. Focused human gene expression profiling using dual-color reverse transcriptase multiplex ligation-dependent probe amplification. Vaccine 2015;33(40):5282-8.

113. Berry MP, Graham CM, McNab FW, Xu Z, Bloch SA, Oni T, Wilkinson KA, Banchereau R, Skinner J, Wilkinson RJ and others. An interferon-inducible neutrophil-driven blood transcriptional signature in human tuberculosis. Nature 2010;466(7309):973-7.
114. Bloom CI, Graham CM, Berry MP, Rozakeas F, Redford PS, Wang Y, Xu Z, Wilkinson KA, Wilkinson RJ, Kendrick Y and others. Transcriptional blood signatures distinguish pulmonary tuberculosis, pulmonary sarcoidosis, pneumonias and lung cancers. PLoS One 2013;8(8):e70630.
115. Maertzdorf J, Ota M, Repsilber D, Mollenkopf HJ, Weiner J, Hill PC, Kaufmann SH. Functional correlations of pathogenesis-driven gene expression signatures in tuberculosis. PLoS One 2011;6(10):e26938.
116. Maertzdorf J, Repsilber D, Parida SK, Stanley K, Roberts T, Black G, Walzl G, Kaufmann SH. Human gene expression profiles of susceptibility and resistance in tuberculosis. Genes Immun 2011;12(1):15-22.
117. Maertzdorf J, Weiner J, Mollenkopf HJ, Bauer T, Prasse A, Müller-Quernheim J, Kaufmann SH, Network T. Common patterns and disease-related signatures in tuberculosis and sarcoidosis. Proc Natl Acad Sci U S A 2012;109(20):7853-8.
118. Bloom CI, Graham CM, Berry MP, Wilkinson KA, Oni T, Rozakeas F, Xu Z, Rossello-Urgell J, Chaussabel D, Banchereau J and others. Detectable changes in the blood transcriptome are present after two weeks of antituberculosis therapy. PLoS One 2012;7(10):e46191.
119. Sloot R, Schim van der Loeff MF, van Zwet EW, Haks MC, Keizer ST, Scholing M, Ottenhoff TH, Borgdorff MW, Joosten SA. Biomarkers Can Identify Pulmonary Tuberculosis in HIV-infected Drug Users Months Prior to Clinical Diagnosis. EBioMedicine 2015;2(2):172-9.
120. Jenum S, Dhanasekaran S, Lodha R, Mukherjee A, Kumar Saini D, Singh S, Singh V, Medigeshi G, Haks MC, Ottenhoff TH and others. Approaching a diagnostic point-of-care test for pediatric tuberculosis through evaluation of immune biomarkers across the clinical disease spectrum. Sci Rep 2016;6:18520.
121. Mihret A, Loxton AG, Bekele Y, Kaufmann SH, Kidd M, Haks MC, Ottenhoff TH, Aseffa A, Howe R, Walzl G. Combination of gene expression patterns in whole blood discriminate between tuberculosis infection states. BMC Infect Dis 2014;14:257.
122. Sutherland JS, Loxton AG, Haks MC, Kassa D, Ambrose L, Lee JS, Ran L, van Baarle D, Maertzdorf J, Howe R and others. Differential gene expression of activating Fcγ receptor classifies active tuberculosis regardless of human immunodeficiency virus status or ethnicity. Clin Microbiol Infect 2014;20(4):O230-8.
123. Joosten SA, Goeman JJ, Sutherland JS, Opmeer L, de Boer KG, Jacobsen M, Kaufmann SH, Finos L, Magis-Escurra C, Ota MO and others. Identification of biomarkers for tuberculosis disease using a novel dual-color RT-MLPA assay. Genes Immun 2012;13(1):71-82.
124. Cliff JM, Lee JS, Constantinou N, Cho JE, Clark TG, Ronacher K, King EC, Lukey PT, Duncan K, Van Helden PD and others. Distinct phases of blood gene expression pattern through tuberculosis treatment reflect modulation of the humoral immune response. J Infect Dis 2013;207(1):18-29.

125. Elliott TO, Owolabi O, Donkor S, Kampmann B, Hill PC, Ottenhoff TH, Haks MC, Kaufmann SH, Maertzdorf J, Sutherland JS. Dysregulation of Apoptosis Is a Risk Factor for Tuberculosis Disease Progression. J Infect Dis 2015;212(9):1469-79.
126. Sutherland JS, Hill PC, Adetifa IM, de Jong BC, Donkor S, Joosten SA, Opmeer L, Haks MC, Ottenhoff TH, Adegbola RA and others. Identification of probable early-onset biomarkers for tuberculosis disease progression. PLoS One 2011;6(9):e25230.
127. Koth LL, Solberg OD, Peng JC, Bhakta NR, Nguyen CP, Woodruff PG. Sarcoidosis blood transcriptome reflects lung inflammation and overlaps with tuberculosis. Am J Respir Crit Care Med 2011;184(10):1153-63.
128. Garton NJ, Waddell SJ, Sherratt AL, Lee SM, Smith RJ, Senner C, Hinds J, Rajakumar K, Adegbola RA, Besra GS and others. Cytological and transcript analyses reveal fat and lazy persister-like bacilli in tuberculous sputum. PLoS Med 2008;5(4):e75.
129. Walter ND, Dolganov GM, Garcia BJ, Worodria W, Andama A, Musisi E, Ayakaka I, Van TT, Voskuil MI, de Jong BC and others. Transcriptional Adaptation of Drug-tolerant Mycobacterium tuberculosis During Treatment of Human Tuberculosis. J Infect Dis 2015;212(6):990-8.
130. Honeyborne I, McHugh TD, Kuittinen I, Cichonska A, Evangelopoulos D, Ronacher K, van Helden PD, Gillespie SH, Fernandez-Reyes D, Walzl G and others. Profiling persistent tubercule bacilli from patient sputa during therapy predicts early drug efficacy. BMC Med 2016;14(1):68.
131. Hu Y, Mangan JA, Dhillon J, Sole KM, Mitchison DA, Butcher PD, Coates AR. Detection of mRNA transcripts and active transcription in persistent Mycobacterium tuberculosis induced by exposure to rifampin or pyrazinamide. J Bacteriol 2000;182(22):6358-65.
132. Bartel DP. MicroRNAs: target recognition and regulatory functions. Cell 2009;136(2):215-33.
133. Zhang X, Guo J, Fan S, Li Y, Wei L, Yang X, Jiang T, Chen Z, Wang C, Liu J and others. Screening and identification of six serum microRNAs as novel potential combination biomarkers for pulmonary tuberculosis diagnosis. PLoS One 2013;8(12):e81076.
134. Fu Y, Yi Z, Wu X, Li J, Xu F. Circulating microRNAs in patients with active pulmonary tuberculosis. J Clin Microbiol 2011;49(12):4246-51.
135. Qi Y, Cui L, Ge Y, Shi Z, Zhao K, Guo X, Yang D, Yu H, Shan Y, Zhou M and others. Altered serum microRNAs as biomarkers for the early diagnosis of pulmonary tuberculosis infection. BMC Infect Dis 2012;12:384.
136. Abd-El-Fattah AA, Sadik NA, Shaker OG, Aboulftouh ML. Differential microRNAs expression in serum of patients with lung cancer, pulmonary tuberculosis, and pneumonia. Cell Biochem Biophys 2013;67(3):875-84.
137. Yi Z, Fu Y, Ji R, Li R, Guan Z. Altered microRNA signatures in sputum of patients with active pulmonary tuberculosis. PLoS One 2012;7(8):e43184.
138. Spinelli SV, Diaz A, D'Attilio L, Marchesini MM, Bogue C, Bay ML, Bottasso OA. Altered microRNA expression levels in mononuclear cells of patients with pulmonary and pleural tuberculosis and their relation with components of the immune response. Mol Immunol 2013;53(3):265-9.

139. Zhou M, Yu G, Yang X, Zhu C, Zhang Z, Zhan X. Circulating microRNAs as biomarkers for the early diagnosis of childhood tuberculosis infection. Mol Med Rep 2016;13(6):4620-6.
140. Wu J, Lu C, Diao N, Zhang S, Wang S, Wang F, Gao Y, Chen J, Shao L, Lu J and others. Analysis of microRNA expression profiling identifies miR-155 and miR-155* as potential diagnostic markers for active tuberculosis: a preliminary study. Hum Immunol 2012;73(1):31-7.
141. Wang C, Yang S, Sun G, Tang X, Lu S, Neyrolles O, Gao Q. Comparative miRNA expression profiles in individuals with latent and active tuberculosis. PLoS One 2011;6(10):e25832.
142. Liu Y, Wang X, Jiang J, Cao Z, Yang B, Cheng X. Modulation of T cell cytokine production by miR-144* with elevated expression in patients with pulmonary tuberculosis. Mol Immunol 2011;48(9-10):1084-90.
143. Patti GJ, Yanes O, Siuzdak G. Metabolomics: the apogee of the omics trilogy. Nature Reviews Molecular Cell Biology 2012;13(4):263-269.
144. Shevchenko A, Simons K. Lipidomics: coming to grips with lipid diversity. Nature Reviews Molecular Cell Biology 2010;11(8):593-598.
145. Li J, Ren S, Piao HL, Wang F, Yin P, Xu C, Lu X, Ye G, Shao Y, Yan M and others. Integration of lipidomics and transcriptomics unravels aberrant lipid metabolism and defines cholesteryl oleate as potential biomarker of prostate cancer. Sci Rep 2016;6:20984.
146. Conlon TM, Bartel J, Ballweg K, Günter S, Prehn C, Krumsiek J, Meiners S, Theis FJ, Adamski J, Eickelberg O and others. Metabolomics screening identifies reduced L-carnitine to be associated with progressive emphysema. Clin Sci (Lond) 2016;130(4):273-87.
147. Huang W, Eickhoff JC, Mehraein-Ghomi F, Church DR, Wilding G, Basu HS. Expression of spermidine/spermine N(1) -acetyl transferase (SSAT) in human prostate tissues is related to prostate cancer progression and metastasis. Prostate 2015;75(11):1150-9.
148. Manni A, Grove R, Kunselman S, Aldaz M. INVOLVEMENT OF THE POLYAMINE PATHWAY IN BREAST-CANCER PROGRESSION. Cancer Letters 1995;92(1):49-57.
149. Gilmour SK. Polyamines and nonmelanoma skin cancer. Toxicology and Applied Pharmacology 2007;224(3):249-256.
150. Russell D, Snyder SH. AMINE SYNTHESIS IN RAPIDLY GROWING TISSUES - ORNITHINE DECARBOXYLASE ACTIVITY IN REGENERATING RAT LIVER CHICK EMBRYO AND VARIOUS TUMORS. Proceedings of the National Academy of Sciences of the United States of America 1968;60(4):1420-&.
151. Upp JR, Saydjari R, Townsend CM, Singh P, Barranco SC, Thompson JC. POLYAMINE LEVELS AND GASTRIN RECEPTORS IN COLON CANCERS. Annals of Surgery 1988;207(6):662-669.
152. Kitteringham NR, Jenkins RE, Lane CS, Elliott VL, Park BK. Multiple reaction monitoring for quantitative biomarker analysis in proteomics and metabolomics. J Chromatogr B Analyt Technol Biomed Life Sci 2009;877(13):1229-39.
153. Alvarez-Sanchez B, Priego-Capote F, de Castro MDL. Metabolomics analysis I. Selection of biological samples and practical aspects preceding sample preparation. Trac-Trends in Analytical Chemistry 2010;29(2):111-119.

154. Feng S, Du YQ, Zhang L, Feng RR, Liu SY. Analysis of serum metabolic profile by ultra-performance liquid chromatography-mass spectrometry for biomarkers discovery: application in a pilot study to discriminate patients with tuberculosis. Chin Med J (Engl) 2015;128(2):159-68.
155. Weiner J, Parida SK, Maertzdorf J, Black GF, Repsilber D, Telaar A, Mohney RP, Arndt-Sullivan C, Ganoza CA, Faé KC and others. Biomarkers of inflammation, immunosuppression and stress with active disease are revealed by metabolomic profiling of tuberculosis patients. PLoS One 2012;7(7):e40221.
156. Somashekar BS, Amin AG, Tripathi P, MacKinnon N, Rithner CD, Shanley CA, Basaraba R, Henao-Tamayo M, Kato-Maeda M, Ramamoorthy A and others. Metabolomic signatures in guinea pigs infected with epidemic-associated W-Beijing strains of Mycobacterium tuberculosis. J Proteome Res 2012;11(10):4873-84.
157. Zhou A, Ni J, Xu Z, Wang Y, Lu S, Sha W, Karakousis PC, Yao YF. Application of (1)h NMR spectroscopy-based metabolomics to sera of tuberculosis patients. J Proteome Res 2013;12(10):4642-9.
158. Shin JH, Yang JY, Jeon BY, Yoon YJ, Cho SN, Kang YH, Ryu DH, Hwang GS. (1)H NMR-based metabolomic profiling in mice infected with Mycobacterium tuberculosis. J Proteome Res 2011;10(5):2238-47.
159. Das MK, Bishwal SC, Das A, Dabral D, Badireddy VK, Pandit B, Varghese GM, Nanda RK. Deregulated tyrosine-phenylalanine metabolism in pulmonary tuberculosis patients. J Proteome Res 2015;14(4):1947-56.
160. Che N, Cheng J, Li H, Zhang Z, Zhang X, Ding Z, Dong F, Li C. Decreased serum 5-oxoproline in TB patients is associated with pathological damage of the lung. Clin Chim Acta 2013;423:5-9.
161. Somashekar BS, Amin AG, Rithner CD, Troudt J, Basaraba R, Izzo A, Crick DC, Chatterjee D. Metabolic profiling of lung granuloma in Mycobacterium tuberculosis infected guinea pigs: ex vivo 1H magic angle spinning NMR studies. J Proteome Res 2011;10(9):4186-95.
162. Frediani JK, Jones DP, Tukvadze N, Uppal K, Sanikidze E, Kipiani M, Tran VT, Hebbar G, Walker DI, Kempker RR and others. Plasma metabolomics in human pulmonary tuberculosis disease: a pilot study. PLoS One 2014;9(10):e108854.
163. Banday KM, Pasikanti KK, Chan EC, Singla R, Rao KV, Chauhan VS, Nanda RK. Use of urine volatile organic compounds to discriminate tuberculosis patients from healthy subjects. Anal Chem 2011;83(14):5526-34.
164. Silva CL, Passos M, Câmara JS. Solid phase microextraction, mass spectrometry and metabolomic approaches for detection of potential urinary cancer biomarkers--a powerful strategy for breast cancer diagnosis. Talanta 2012;89:360-8.
165. Mochalski P, Unterkofler K. Quantification of selected volatile organic compounds in human urine by gas chromatography selective reagent ionization time of flight mass spectrometry (GC-SRI-TOF-MS) coupled with head-space solid-phase microextraction (HS-SPME). Analyst 2016.
166. Jankute M, Cox JAG, Harrison J, Besra GS. Assembly of the Mycobacterial Cell Wall. In: Gottesman S, editor. Annual Review of Microbiology, Vol 69. Volume 69, Annual Review of Microbiology. Palo Alto: Annual Reviews; 2015. p 405-423.
167. Brennan PJ. Structure, function, and biogenesis of the cell wall of Mycobacterium tuberculosis. Tuberculosis 2003;83(1-3):91-97.

168. OrtaloMagne A, Lemassu A, Laneelle MA, Bardou F, Silve G, Gounon P, Marchal G, Daffe M. Identification of the surface-exposed lipids on the cell envelopes of Mycobacterium tuberculosis and other mycobacterial species. Journal of Bacteriology 1996;178(2):456-461.
169. Dang NA, Kuijper S, Walters E, Claassens M, van Soolingen D, Vivo-Truyols G, Janssen HG, Kolk AHJ. Validation of Biomarkers for Distinguishing Mycobacterium tuberculosis from Non-Tuberculous Mycobacteria Using Gas Chromatography-Mass Spectrometry and Chemometrics. Plos One 2013;8(10):10.
170. Kaal E, Kolk AHJ, Kuijper S, Janssen HG. A fast method for the identification of Mycobacterium tuberculosis in sputum and cultures based on thermally assisted hydrolysis and methylation followed by gas chromatography-mass spectrometry. Journal of Chromatography A 2009;1216(35):6319-6325.
171. Dang NA, Kolk AHJ, Kuijper S, Janssen HG, Vivo-Truyols G. The identification of biomarkers differentiating Mycobacterium tuberculosis and non-tuberculous mycobacteria via thermally assisted hydrolysis and methylation gas chromatography-mass spectrometry and chemometrics. Metabolomics 2013;9(6):1274-1285.
172. Dang NA, Mourao M, Kuijper S, Walters E, Janssen HG, Kolk AHJ. Direct detection of Mycobacterium tuberculosis in sputum using combined solid phase extraction-gas chromatography-mass spectrometry. Journal of Chromatography B-Analytical Technologies in the Biomedical and Life Sciences 2015;986:115-122.
173. O'Sullivan DM, Nicoara SC, Mutetwa R, Mungofa S, Lee OYC, Minnikin DE, Bardwell MW, Corbett EL, McNerney R, Morgan GH. Detection of Mycobacterium tuberculosis in Sputum by Gas Chromatography-Mass Spectrometry of Methyl Mycocerosates Released by Thermochemolysis. Plos One 2012;7(3):8.
174. Nicoara SC, Turner NW, Minnikin DE, Lee OYC, O'Sullivan DM, McNerney R, Mutetwa R, Corbett LE, Morgan GH. Development of sample clean up methods for the analysis of Mycobacterium tuberculosis methyl mycocerosate biomarkers in sputum extracts by gas chromatography-mass spectrometry. Journal of Chromatography B-Analytical Technologies in the Biomedical and Life Sciences 2015;986:135-142.
175. Pan SJ, Tapley A, Adamson J, Little T, Urbanowski M, Cohen K, Pym A, Almeida D, Dorasamy A, Layre E and others. Biomarkers for Tuberculosis Based on Secreted, Species-Specific, Bacterial Small Molecules. Journal of Infectious Diseases 2015;212(11):1827-1834.
176. Syhre M, Chambers ST. The scent of Mycobacterium tuberculosis. Tuberculosis 2008;88(4):317-323.
177. Nawrath T, Mgode GF, Weetjens B, Kaufmann SHE, Schulz S. The volatiles of pathogenic and nonpathogenic mycobacteria and related bacteria. Beilstein Journal of Organic Chemistry 2012;8:290-299.
178. Syhre M, Manning L, Phuanukoonnon S, Harino P, Chambers ST. The scent of Mycobacterium tuberculosis - Part II breath. Tuberculosis 2009;89(4):263-266.
179. Scott-Thomas A, Epton M, Chambers S. Validating a breath collection and analysis system for the new tuberculosis breath test. Journal of Breath Research 2013;7(3):7.
180. Metters JP, Kampouris DK, Banks CE. Fingerprinting Breath: Electrochemical Monitoring of Markers Indicative of Bacteria Mycobacterium tuberculosis Infection. Journal of the Brazilian Chemical Society 2014;25(9):1667-1672.

181. Phillips M, Basa-Dalay V, Bothamley G, Cataneo RN, Lam PK, Natividad MPR, Schmitt P, Wai J. Breath biomarkers of active pulmonary tuberculosis. Tuberculosis 2010;90(2):145-151.
182. Phillips M, Basa-Dalay V, Blais J, Bothamley G, Chaturvedi A, Modi KD, Pandya M, Natividad MPR, Patel U, Ramraje NN and others. Point-of-care breath test for biomarkers of active pulmonary tuberculosis. Tuberculosis 2012;92(4):314-320.
183. Phillips M, Cataneo RN, Condos R, Erickson GAR, Greenberg J, La Bombardi V, Munawar MI, Tietje O. Volatile biomarkers of pulmonary tuberculosis in the breath. Tuberculosis 2007;87(1):44-52.
184. Dunn WB, Erban A, Weber RJM, Creek DJ, Brown M, Breitling R, Hankemeier T, Goodacre R, Neumann S, Kopka J and others. Mass appeal: metabolite identification in mass spectrometry-focused untargeted metabolomics. Metabolomics 2013;9(1):S44-S66.
185. Mahapatra S, Hess AM, Johnson JL, Eisenach KD, DeGroote MA, Gitta P, Joloba ML, Kaplan G, Walzl G, Boom WH and others. A metabolic biosignature of early response to anti-tuberculosis treatment. BMC Infect Dis 2014;14:53.
186. Zuccaro P, Altieri I, Rosa M, Passa AR, Pichini S, Pacifici R. Solid-phase extraction of nicotine and its metabolites for high-performance liquid chromatographic determination in urine. J Chromatogr B Biomed Appl 1995;668(1):187-8.
187. Matsumoto A, Ino T, Ohta M, Otani T, Hanada S, Sakuraoka A, Ichiba M, Hara M. Enzyme-linked immunosorbent assay of nicotine metabolites. Environ Health Prev Med 2010;15(4):211-6.
188. Man CN, Gam LH, Ismail S, Lajis R, Awang R. Simple, rapid and sensitive assay method for simultaneous quantification of urinary nicotine and cotinine using gas chromatography-mass spectrometry. J Chromatogr B Analyt Technol Biomed Life Sci 2006;844(2):322-7.
189. Hunter SW, Gaylord H, Brennan PJ. STRUCTURE AND ANTIGENICITY OF THE PHOSPHORYLATED LIPOPOLYSACCHARIDE ANTIGENS FROM THE LEPROSY AND TUBERCLE-BACILLI. Journal of Biological Chemistry 1986;261(26):2345-2351.
190. Chatterjee D, Khoo KH. Mycobacterial lipoarabinomannan: an extraordinary lipoheteroglycan with profound physiological effects. Glycobiology 1998;8(2):113-120.
191. Gilleron M, Bala L, Brando T, Vercellone A, Puzo G. Mycobacterium tuberculosis H37Rv parietal and cellular lipoarabinomannans - Characterization of the acyl- and glyco-forms. Journal of Biological Chemistry 2000;275(1):677-684.
192. Beatty WL, Rhoades ER, Ullrich HJ, Chatterjee D, Heuser JE, Russell DG. Trafficking and release of mycobacterial lipids from infected macrophages. Traffic 2000;1(3):235-247.
193. Boehme C, Molokova E, Minja F, Geis S, Loscher T, Maboko L, Koulchin V, Hoelscher M. Detection of mycobacterial lipoarabinomannan with an antigen-capture ELISA in unprocessed urine of Tanzanian patients with suspected tuberculosis. Transactions of the Royal Society of Tropical Medicine and Hygiene 2005;99(12):893-900.
194. Wood R, Racow K, Bekker LG, Middelkoop K, Vogt M, Kreiswirth BN, Lawn SD. Lipoarabinomannan in urine during tuberculosis treatment: association with host and pathogen factors and mycobacteriuria. Bmc Infectious Diseases 2012;12:11.
195. Tessema TA, Hamasur B, Bjune G, Svenson S, Bjorvatn B. Diagnostic evaluation of urinary lipoarabinomannan at an Ethiopian tuberculosis centre. Scandinavian Journal of Infectious Diseases 2001;33(4):279-284.

196. Hamasur B, Bruchfeld J, Haile M, Pawlowski A, Bjorvan B, Kallenius G, Svenson SB. Rapid diagnosis of tuberculosis by detection of mycobacterial lipoarabinomannan in urine. Journal of Microbiological Methods 2001;45(1):41-52.
197. Hamasur B, Bruchfeld J, van Helden P, Kallenius G, Svenson S. A Sensitive Urinary Lipoarabinomannan Test for Tuberculosis. PLoS One 2015;10(4):11.
198. Minion J, Leung E, Talbot E, Dheda K, Pai M, Menzies D. Diagnosing tuberculosis with urine lipoarabinomannan: systematic review and meta-analysis. European Respiratory Journal 2011;38(6):1398-1405.
199. Reither K, Saathoff E, Jung J, Minja LT, Kroidl I, Saad E, Huggett JF, Ntinginya EN, Maganga L, Maboko L and others. Low sensitivity of a urine LAM-ELISA in the diagnosis of pulmonary tuberculosis. Bmc Infectious Diseases 2009;9:10.
200. Peter JG, Zijenah LS, Chanda D, Clowes P, Lesosky M, Gina P, Mehta N, Calligaro G, Lombard CJ, Kadzirange G and others. Effect on mortality of point-of-care, urine-based lipoarabinomannan testing to guide tuberculosis treatment initiation in HIV-positive hospital inpatients: a pragmatic, parallel-group, multicountry, open-label, randomised controlled trial. Lancet 2016;387(10024):1187-1197.
201. Drain PK, Gounder L, Grobler A, Sahid F, Bassett IV, Moosa MYS. Urine lipoarabinomannan to monitor antituberculosis therapy response and predict mortality in an HIV-endemic region: a prospective cohort study. Bmj Open 2015;5(4):8.
202. De P, Amin AG, Valli E, Perkins MD, McNeil M, Chatterjee D. Estimation of D-Arabinose by Gas Chromatography/Mass Spectrometry as Surrogate for Mycobacterial Lipoarabinomannan in Human Urine. Plos One 2015;10(12):17.
203. Sirén H, Savolainen LE, Tuuminen T. Capillary electrophoresis as a method to determine underivatized urinary lipoarabinomannans, a biomarker of active tuberculosis caused by Mycobacterium tuberculosis. J Sep Sci 2016;39(14):2853-61.
204. Cox JA, Lukande RL, Kalungi S, Van Marck E, Van de Vijver K, Kambugu A, Nelson AM, Colebunders R, Manabe YC. Is Urinary Lipoarabinomannan the Result of Renal Tuberculosis? Assessment of the Renal Histology in an Autopsy Cohort of Ugandan HIV-Infected Adults. PLoS One 2015;10(4):e0123323.
205. Bouatra S, Aziat F, Mandal R, Guo AC, Wilson MR, Knox C, Bjorndahl TC, Krishnamurthy R, Saleem F, Liu P and others. The human urine metabolome. PLoS One 2013;8(9):e73076.

CHAPTER 2: STRUCTURAL CHARACTERIZATION OF *M/Z* 875.36 METABOLITE

2.1 Introduction

Globally, drug resistant tuberculosis cases are still a problem with an estimated 480,000 new MDR-TB cases in 2014 [1]. Although treatments are available, only about half of patients have successful outcomes [1]. Contributing to this low success rate is the high toxicity and increased treatment duration associated with second-line antibiotics [2]. New anti-TB therapies without these adverse effects are urgently needed for TB patients with drug resistant and drug susceptible infections.

Eight new or repurposed compounds are in the later phases of the TB antimicrobial drug pipeline [3]. However, a main hindrance in making these compounds available to patients is the time needed to assess compound efficacy. A biosignature that can accurately predict patient treatment outcome at early time points would expedite this process. We hypothesize that a robust metabolite based biosignature can be achieved by characterizing the specific host metabolic alterations that occur during anti-TB treatment.

Development of a clinically useful metabolite based biosignature is feasible because alterations in host metabolic profiles during anti-TB treatment are distinct. Das *et al.* demonstrate a separation between patients at diagnosis and patients at different stages of treatment (2,4, and 6 months), with some overlap between healthy controls and clinically cured patients [4]. Mahapatra *et al.* detected 12 metabolic features that were consistently altered during treatment, six of these could accurately classify patients at day zero and month one of treatment [5]. Che *et al.* detected 20 metabolites that were altered in TB patients before and after treatment [6]. Thus, these studies

demonstrate the potential utility of metabolite quantification in monitoring anti-TB treatment, and provide support for our hypothesis.

Unfortunately, a remaining hindrance to the development of a metabolite based biosignature is the large proportion of uncharacterized or putatively identified metabolites in the existing or future biosignatures. Out of the 20 metabolites detected by Che *et al.*, 11 of them remain uncharacterized. Seven of the twelve metabolic features detected by Mahapatra *et al.* have putative, yet unconfirmed, identifications and the rest are uncharacterized. This is not surprising as a majority of detected metabolites do not match with known compounds in available databases and chemical characterization is labor intensive [7,8]. Unlike proteins and transcripts which have a defined, relatively consistent linkages, a single metabolite can have an exponentially higher number of potential structural arrangements and linkages [8]. Providing structural identification for these uncharacterized metabolites will add to the available databases and aid in the development of robust and clinically useful biosignatures. Specifically, such efforts will enable elucidation of host metabolic alterations potentially leading to additional biomarkers, and allow for determination of those metabolites that result from off-target responses due to the therapeutic agents.

This chapter describes the structural characterization of one metabolite detected by Mahapatra *et al.* [9]. Using liquid chromatography and tandem mass spectrometry (LC-MS/MS), along with an enzymatic assay and pure synthetic standards, the *m/z* 875.36 metabolite was identified as being a core-1 *O*-glycosylated serine leucine peptide (Table 1.1). By determining the structure of this novel metabolite, this research added to the list of known metabolites that are available to researchers, enabled identification of host metabolic pathways involved in

production of this metabolite, and progressed development of a host biosignature for anti-TB treatment response.

2.2 Materials and Methods

Chemicals

N-acetylneuraminic acid was obtained from Sigma Aldrich (St. Louis, MO, USA). Serine-Leucine peptide standard was obtained from Peptide 2.0 Inc. (Chantilly, VA, USA). LC-MS grade water, methanol were from Honeywell Burdick & Jackson (Muskegon, MI, USA). Formic Acid was from Fischer Scientific (Pittsburgh, PA, USA). Human urine used as a control was obtained from Gemini Bio-Products (West Sacramento, CA, USA).

Clinical Samples

Patient urine for metabolite identification was from a subset of the samples used for metabolite discovery in the previously published study by Mahapatra *et al.* [5]. This subset of samples was obtained from the tuberculosis research unit (TBRU) NAA2m study (DMID 08-0023) conducted in Uganda.

LC-MS and LC-MS/MS Analysis

Chromatography was based on a previously described method using an Agilent 1200 series high-performance liquid chromatography system (Agilent Technologies, Palo Alto, CA, USA) coupled with an Atlantis T3 reverse-phase C_{18} 3.5µm column (2.1 by 150mm; Waters Corp., Milford, MA) [9]. Elution of metabolites was achieved using a 0-90% nonlinear gradient of methanol in 0.1% formic acid at a constant flow rate of 0.25ml/min. Mass spectrometry was performed using an Agilent 6510 quadrupole time of flight (Q-TOF) LC/MS instrument equipped with an Agilent electrospray ionization source that was operated in positive ionization mode. The operating conditions for the mass spectrometer were: gas temperature, 300˚C; drying

gas, 8 L/min; nebulizer 45 lb/in^2; capillary voltage, 2,000 V; fragmentation energy for MS and MS/MS, 120 V; skimmer, 60V; and octapole RF setting, 750 V. Specified ions were isolated for MS/MS fragmentation (isolation width of 1.3 Da) by collision induced dissociation at set collision energies (5-40V). Data were collected in profile and centroid mode at a scan rate of 2.0 spectra/sec and scan range of *m/*z 50 – 1,700 using the Agilent MassHunter Data Acquisition software.

HPLC Isolation of m/z 875.36 metabolites

The metabolite was isolated from human urine with the same chromatography that was used for metabolite identification: an Agilent 1200 series high-performance liquid chromatography system (Agilent Technologies, Palo Alto, CA, USA) coupled with an Atlantis T3 reverse-phase C_{18} 3.5µm column (2.1 by 150mm; Waters Corp., Milford, MA). Elution of metabolites was achieved using a 0-90% nonlinear gradient of methanol in 0.1% formic acid at a constant flow rate of 0.25ml/min. MS was utilized to confirm presence of metabolite in fractions obtained from HPLC separation. Metabolite containing fractions were dried using a Savant SpeedVac and the dried material was stored at -20˚C.

Deglycosylation of m/z 875.36 metabolite

Isolated metabolite was incubated with Neuraminidase and O-glycosidase (New England Biolabs Inc., Ipswich, MA, USA) at 37˚C for two hours according to manufacturer's instructions.

Data Analyses

The LC-MS/MS spectra were manually interrogated against available MS/MS spectra in the METLIN metabolite database, the Human Metabolome Database (HMDB), and the National Institutes of Standards and Technology commercial library (NIST) [10-12]. Theoretical fragments

were obtained using ACD/MS Fragmenter (Advanced Chemistry Development, Inc., Toronto, On, Canada)

2.3 Results

Development of Hypothesized Structure for Unknown Metabolite

Information pertaining to the structure of the *m/z* 875.36 metabolite was obtained by targeting this metabolite for LC-MS/MS fragmentation at different collision energies in six

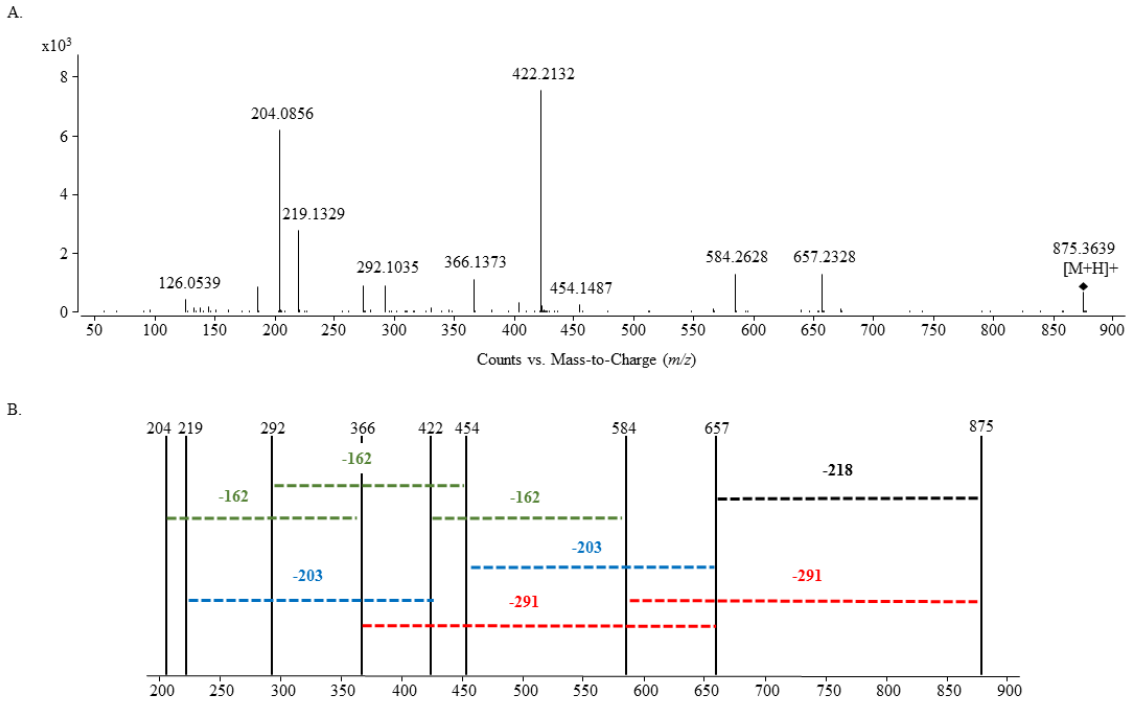

Figure 3.1 MS/MS of *m/z* 875.36 metabolite.
Representative MS/MS spectrum for m/z 875.36 in TB patient urine at 20V CE (A). Diagram depicting neutral losses of N-acetylneuraminic acid (291) in red, hexose (162) in green, N-acetylhexosamine (203) in blue, and unknown fragment (219) in black within the MS/MS spectrum (B).

patient urine samples. A representative MS/MS spectrum of the unknown metabolite from one patient's urine at a collision energy (CE) of 20V is shown in Figure 2.1A. Manual interrogation of the MS/MS spectra revealed diagnostic fragments for *N*-acetylhexosamine (*m/z* 204.0856) and *N*-acetylneuraminic acid (*m/z* 292.1035). Further inspection of the spectra revealed that the fragments ions *m/z* 584.2628, *m/z* 422.2132 and *m/z* 219.1329 equated to sequential neutral losses of *N*-acetylneuraminic acid (291), hexose (162), and *N*-acetylhexosamine (203) respectively (Fig 2.1). Starting with the parent ion *m/z* 875.36, sequential losses of each of these sugar moieties resulted in an unknown fragment ion (*m/z* 219.1329). Additionally, the difference between the parent ion and the fragment ion (*m/z* 657.2328) is 218, which could correspond to the unknown fragment ion (Figure 2.1B). The information gathered from the MS/MS spectra resulted in the hypothesis that the unknown metabolite was a glycoconjugate containing *N*-

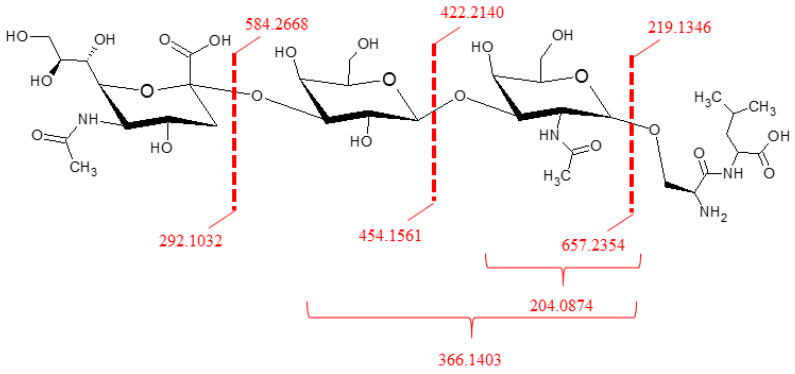

Figure 2.2 Structure of *m/z* 875.36 Metabolite
Neu5Ac(α 2 → 3,6,8) Gal(α 1 → 3) GalNAc(α 1 → O) SerLeu, proposed structure of m/z 875.36 metabolite. Theoretical fragmentation (depicted in red) demonstrates the origin of the fragment ions seen in MS/MS spectrum. 204.0874 corresponds to GalNAc and 366.1403 corresponds to Gal(α 1 → 3) GalNAc in the depicted structure.

acetylhexosamine, hexose and *N*-acetylneuraminic acid attached to an unknown molecule (*m/z* 219.1329).

This unknown molecule with an *m/z* of 219.1329 did not match with the lipid moiety of any known glycolipids. Thus, its structure was initially hypothesized to be a peptide. In humans, glycosylation typically occurs on asparagine residues (N-linked) and serine or threonine residues (O-linked). Different amino acid combinations containing either asparagine, serine or threonine were assessed to see which combinations matched with the unknown fragment mass (*m/z* 219.1329). This resulted in six possible amino acid combinations: serine-leucine, serine-isoleucine, leucine-serine, isoleucine-serine, threonine-valine, and valine-threonine. This information was used to develop a hypothesized structure containing the different peptides. A representative structure with serine-leucine is depicted in Figure 2.2. Theoretical fragmentation of these hypothesized structures results in the fragment ions present in the experimental spectra seen in Figure 2.1.

Defining Glycosyl Moiety

The *O*-linked glycosylation was confirmed by enzymatic digestion of the HPLC purified metabolite with neuraminidase and *O*-glycosidase. Neuraminidase is an enzyme with acetyl-neuraminyl hydrolase activity and a specificity for α2-3, α 2-6 and α 2-8 linked *N*-acetylneuraminic acid residues [13]. LC-MS analysis after treatment of the HPLC purified metabolite with neuraminidase revealed the presence of *N*-acetylneuraminic acid (*m/z* 310.1130) and the disappearance of the intact metabolite (*m/z* 875.36), confirming the presence of a terminal α 2-3,6,8 linked *N*-acetylneuraminic acid (data not shown). *O*-glycosidase is an enzyme with Endo-α-*N*-acetylgalactosaminidase activity and specificity for Core 1 and Core 3 *O*-linked disaccharides which are common core glycans of longer, more complex glycan structures found on glycoproteins and mucins [13-15]. The HPLC purified metabolite was treated with this enzyme subsequent to digestion with neuraminidase and analyzed by LC-MS. This resulted in the

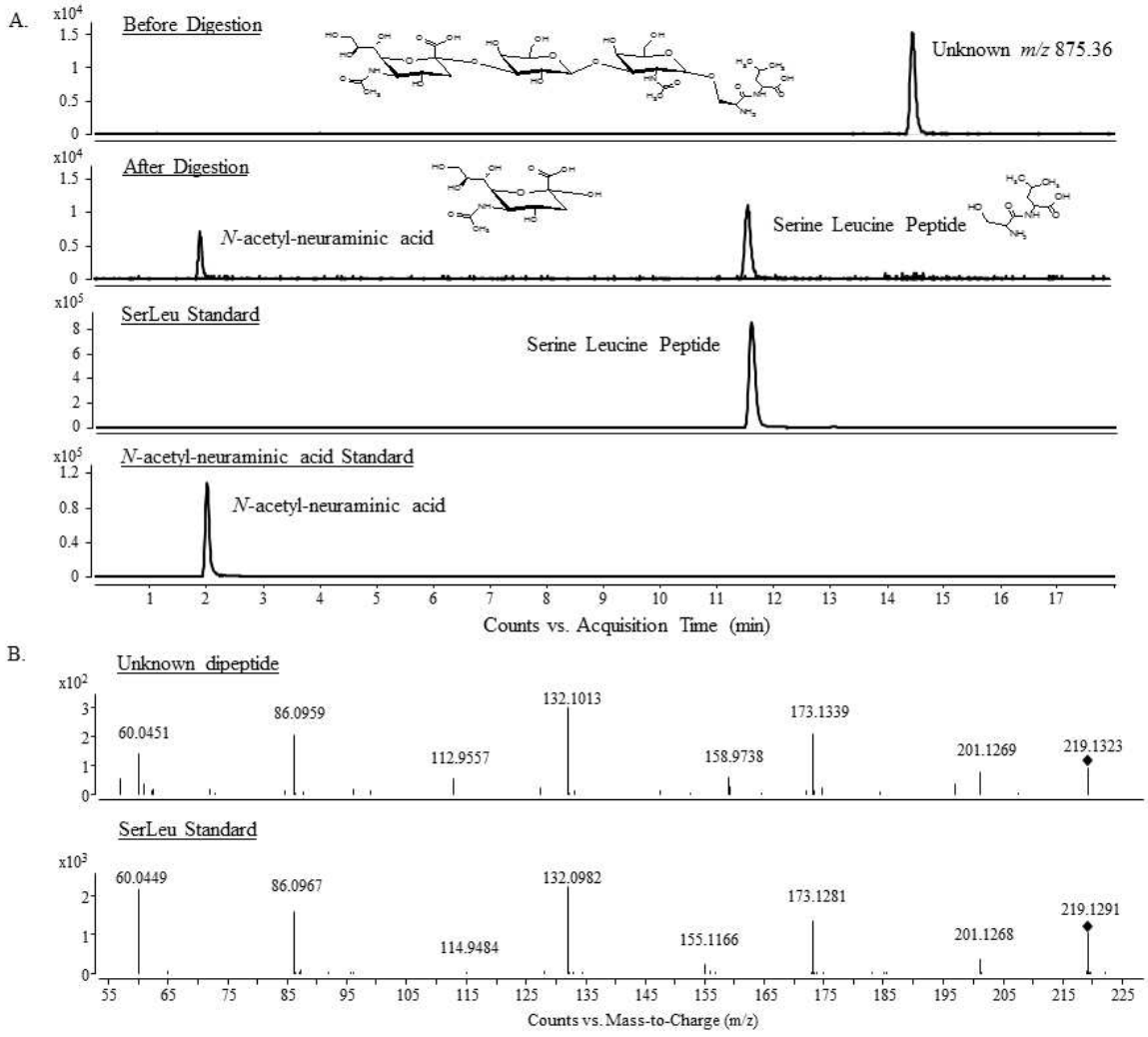

Figure 2.3 Structure Confirmation

Confirmation of Structure with Neuraminidase and O-glycosidase digestion. The extracted ion chromatograms (EIC) show intact m/z 875.36 metabolite before digestion and the appearance of two peaks after digestion with both enzymes. These peaks matched in retention time to N-acetylneuraminic acid and the serine-leucine peptide standards (A). The MS/MS spectra of the peptide after digestion and the serine-leucine peptide standard have matching fragmentation patterns.

disappearance of the intact metabolite (*m/z* 875.36) and the appearance of *N*-acetylneuraminic acid (*m/z* 310.1130) and the putative dipeptide (*m/z* 219.1329) as seen in Figure 2.3B. This confirmed that our unknown metabolite contained either a Core 1 or Core 3 *O*-linked disaccharide with a terminal α 2-3,6,8 *N*-acetylneuraminic acid. Core 1 disaccharides consist of

one *N*-acetylgalactosamine linked to one galactose, which does fit with the proposed glycosyl structure (Figure 2.2). Alternatively, core 3 disaccharides consist of one *N*-acetylgalactosamine linked to one *N*-acetylglucosamine which does not fit with the MS/MS spectra (Figure 2.1). Thus, the glycosylation structure of the *m/z* 875.36 metabolite was confirmed as Neu5Ac(α 2 → 3,6,8) Gal(α 1 → 3) GalNAc.

Defining Peptide Moiety

The structure of the unknown dipeptide was elucidated by LC-MS/MS comparison of the enzymatically digested *m/z* 875.36 metabolite with synthetic dipeptide standards. The unknown dipeptide matched both the retention time and MS/MS spectra of the serine-leucine standard and failed to match one or both of these parameters in the other dipeptide standards (Figure 2.3). This confirmed that the entire structure of the *m/z* 875.36 metabolite was Neu5Ac(α 2 → 3,6,8) Gal(α 1 → 3) GalNAc(α 1 → O) SerLeu as depicted in Figure 2.2. Querying the UniProt database for all known and documented glycosylated proteins resulted in a list of 4508 proteins. This list was examined for proteins that contained an *O*-glycosylation motif on a serine residue with a leucine in the +1 position and yielded nine proteins. Further investigation of the available literature on these proteins regarding the specific glycan structures at those sites narrowed the list to seven proteins. Table 2.1 contains a list of the seven possible proteins containing a core 1 *O*-glycosylated serine-leucine that could be the origin of the *m/z* 875.36 glycosylated dipeptide.

This list was compared with whole blood RNAseq data from TB patients during the course of treatment to determine whether any correlation existed between the transcripts of these proteins and the *m/z* 875.36 glycosylated dipeptide. The transcript belonging to plasma protease C1 inhibitor followed the same trend as the glycosylated dipeptide and decreased approximately

four fold during treatment (Table 2.1). Based on these results, plasma protease C1 inhibitor is a plausible precursor protein of the glycosylated dipeptide.

Table 2.1 Potential Source Proteins
RNAseq expression data for seven proteins containing core-1 O-glycosylated Ser-Leu. Manual interrogation of the glycosylated proteins in the UniProt database resulted in these proteins. Their gene names were used to search RNAseq data from Stellenbosch University.

Protein Name	Slope*	Average Expression
Odontogenic ameloblast-associated protein (Apin)	N/A	N/A
Small cell adhesion glycoprotein	0.02366	2.91205
Plasma protease C1 inhibitor	-2.16818	7.05464
Glycophorin-C	-0.34009	9.33026
SPARC-like protein 1	N/A	N/A
Amyloid beta A4 protein	-0.07873	6.07801
Asporin	N/A	N/A
Natriuretic peptides B	N/A	N/A
Kallikrein-1	-0.10329	-1.32285

*Slope was obtained from the line of best fit for expression data plotted over time. A negative value indicates a decrease in abundance during treatment
#Average expression is calculated using expression data from all time points
N/A indicates that the transcript was not detected

2.4 Discussion

This chapter described the structural identification of a naturally occurring urinary core 1 *O*-glycosylated serine leucine peptide. By revealing this metabolite's structure, this research enables the design of more targeted quantification methods for validating this metabolite as a true biomarker of anti-TB treatment response. The source of this glycopeptide, however, was not conclusively determined. Although plasma protease C1 inhibitor (C1INH) is a plausible precursor, the actual source of this glycopeptide needs to be elucidated before concrete

conclusions can be made about host pathogen interactions during tuberculosis and anti-TB therapy.

Structural characterization of this metabolite enables utilization of specific structural components for targeted quantification. For example, chromatographic conditions optimized for separation of glycosylated peptides can be used to develop a multiple reaction monitoring (MRM) assay and a standard for MRM assay development can now be obtained through chemical synthesis. Additionally, antibodies against this peptide can be generated for development of an ELISA based quantification method. While quantification is important in the advancement of this metabolite as a biomarker of anti-TB treatment response, the source of this glycopeptide remains unknown concealing the biological significance of observed alterations.

Naturally occurring urinary peptides, like the glycopeptide identified in this chapter, are common in the urine of healthy individuals due to normal protein turnover in the body or normal enzymatic activity in the urine [16]. These peptides, ranging from 800 to 4500 Da, are mainly a product of proteolytic degradation in the body representing normal physiologic turnover and altered levels may correspond to changes in protease activity or protein level [16-18]. The major urinary peptide constituents are those originating from collagen and highly abundant serum proteins including α-1-antitrypsin and fibrinogen [16]. Additionally, normal proteolytic activity in the urine can originate from the serum, renal tubular cells, epithelial cells, and glandular secretions of the urogenital tract and altered levels of urinary peptides can arise from changes in normal enzyme levels or the presence of entirely new enzymes in the urine [19]. Some serum enzymes such as amylase which are less than 80,000 Da are regularly secreted into the urine [19]. Permeation of the renal tubular cell membrane can lead to the presence of enzymes such as alkaline phosphatase and amino acid arylamidase in the urine [19]. Acid phosphatase, one of the

enzymes found in the enzymatically active secretions of the urogenital glands can also be found in the urine [19]. Altered levels of these naturally occurring peptides have been associated with different diseases such as diabetes, chronic kidney disease, rheumatoid arthritis and even ageing [16,17,20-22].

Based on the RNAseq data, C1INH is a plausible precursor protein for the glycosylated peptide identified in this chapter (Table 2.1). C1INH, a regulator of the complement and coagulation cascades, is an abundant, heavily glycosylated serum protein supporting the hypothesis that it is the source of the glycopeptide [23-26]. It contains seven *O*-glycosylation sites determined by Edman degradation, one of which is Ser-42 with leucine in the +1 position, and the *O*-linked oligosaccharide sequences described for C1INH match that of the identified glycopeptide, Neu5Ac(α 2 → 3,6,8) Gal(α 1 → 3) GalNAc [23-25]. Further support for C1INH being the source is the similar trends between the glycopeptide and C1INH transcript levels during anti-TB treatment [27]. Additionally, other studies detected naturally occurring C1INH peptides in the urine, though the peptides detected did not contain the identified glycopeptide sequence [28,29]. Expression levels of C1INH are also increased during active tuberculosis disease and progression to disease indicating an importance of this protein during infection with *Mtb* [30-33]. Increased expression of C1INH during active TB could lead to increased glycopeptide levels in the urine that return to normal as the infection resolves with anti-TB treatment. While this scenario is practical, without concrete evidence linking C1INH and the glycopeptide, other possible source proteins cannot be ruled out.

Fibrinogen is also a highly abundant serum protein and could be the source of the glycopeptide. Naturally occurring urinary fibrinogen peptides have been detected in numerous studies [17,20-22,29,34-37]. One study detected two glycopeptides, one that matched the *m/z* and

fragmentation patterns of the glycopeptide identified in this chapter, and the other was confirmed as isoform 2 fibrinogen α C terminal peptide [37]. Due to the similarities between these two glycopeptides, it was proposed that the smaller, uncharacterized glycopeptide also originated from fibrinogen [37]. In addition to isoform 2 of the fibrinogen α chain, the fibrinogen β chain also contains a core 1 *O*-glycosylated serine leucine, providing another possible source for the glycopeptide [22,29,34,36]. The glycopeptide identified in this chapter is present in normal patient urine, thus the fibrinogen β chain seems a more likely source, as it is present in normal circulating fibrinogen. In contrast, isoform 2 of the fibrinogen α chain is not present in normal circulating fibrinogen [36,37]. Similar to C1INH, increased levels of fibrinogen have been detected in active TB patients, further corroborating fibrinogen as the source of the glycopeptide [38-43].

A limitation of this study is the reliance on the specificity of the *O*-glycosidase enzyme for determination of the glycan structure. Though, *O*-glycosidase specificity is for core 1 glycans which are the most common O-GalNAc glycan, mammalian proteins can also contain O-linked mannose, fucose, glucose and even *N*-acetylglucosamine [44]. The enzymatic specificity of *O*-glycosidase has been comprehensively characterized against 18 other possible glycan structures that were fluorescently labeled and no activity was observed using thin layer chromatography (NEB, COA for P0733S). While this provides strong evidence for the specificity of the enzyme as well as the confirmed structure of the glycopeptide, without comparing the retention time of the digested material with a Gal(α 1 → 3) GalNAc disaccharide standard, there is still some uncertainty associated with the confirmed glycopeptide structure. An alternative method to confirm the sugar composition of the disaccharide would be to generate trimethylsilyl (TMS) sugar derivatives from the digested material and standards [45]. Analysis of these TMS derivatives with GC-MS would enable confirmation of the sugar moieties present in the disaccharide [45].

Though there is strong evidence for the glycopeptide being a core 1 *O*-glycosylated serine leucine, further analyses can be performed to confirm this structure.

Conclusive determination of the origin of this glycopeptide is needed to determine host metabolic pathways that are altered during *Mtb* infection. This will be challenging; out of the documented glycosylated proteins, nine contain the core 1 *O*-glycosylated serine leucine motif. Additionally, there is the potential that additional proteins with this glycosylation motif exist but have not been documented. This glycopeptide could also arise from the enzymatic degradation of several proteins with this motif and the altered glycopeptide levels could be due to changes in abundance or activity of a specific unknown enzyme. However, C1INH and fibrinogen are likely candidates and further evaluation of these proteins as the origin of the glycopeptide can be achieved. If one of these is the source protein, lower levels of the glycopeptide would be expected in the urine from either patients deficient in C1INH (hereditary angioedema Type 1) or fibrinogen (afibrinogenemia, hypofibrogenemia) [26,46]. Additionally, the generation of this glycopeptide after lysosomal, proteolytic, or urinary degradation of C1INH or fibrinogen would provide evidence of the glycopeptide's origin, however, this analysis would need to be performed with all potential sources to rule them out [47,48]

REFERENCES

1. Organization WH. Global tuberculosis report 2015. Geneva: WHO; 2015.
2. Ramachandran G, Swaminathan S. Safety and tolerability profile of second-line anti-tuberculosis medications. Drug Saf 2015;38(3):253-69.
3. Wallis RS, Maeurer M, Mwaba P, Chakaya J, Rustomjee R, Migliori GB, Marais B, Schito M, Churchyard G, Swaminathan S and others. Tuberculosis-advances in development of new drugs, treatment regimens, host-directed therapies, and biomarkers. Lancet Infect Dis 2016;16(4):e34-46.
4. Das MK, Bishwal SC, Das A, Dabral D, Badireddy VK, Pandit B, Varghese GM, Nanda RK. Deregulated tyrosine-phenylalanine metabolism in pulmonary tuberculosis patients. J Proteome Res 2015;14(4):1947-56.
5. Mahapatra S, Hess AM, Johnson JL, Eisenach KD, DeGroote MA, Gitta P, Joloba ML, Kaplan G, Walzl G, Boom WH and others. A metabolic biosignature of early response to anti-tuberculosis treatment. BMC Infect Dis 2014;14:53.
6. Che N, Cheng J, Li H, Zhang Z, Zhang X, Ding Z, Dong F, Li C. Decreased serum 5-oxoproline in TB patients is associated with pathological damage of the lung. Clin Chim Acta 2013;423:5-9.
7. Zamboni N, Saghatelian A, Patti GJ. Defining the metabolome: size, flux, and regulation. Mol Cell 2015;58(4):699-706.
8. Dunn WB, Erban A, Weber RJM, Creek DJ, Brown M, Breitling R, Hankemeier T, Goodacre R, Neumann S, Kopka J and others. Mass appeal: metabolite identification in mass spectrometry-focused untargeted metabolomics. Metabolomics 2013;9(1):S44-S66.
9. Mahapatra S, Hess AM, Johnson JL, Eisenach KD, DeGroote MA, Gitta P, Joloba ML, Kaplan G, Walzl G, Boom WH and others. A metabolic biosignature of early response to anti-tuberculosis treatment. BMC Infectious Diseases 2014 14(1):53.
10. Wishart DS, Jewison T, Guo AC, Wilson M, Knox C, Liu Y, Djoumbou Y, Mandal R, Aziat F, Dong E and others. HMDB 3.0 - The Human Metabolome Database in 2013. Nucleic Acids Research 2013;41 (Database Issue):D801-D807.
11. Smith CA, O'Maille G, Want EJ, Qin C, Trauger SA, Brandon TR, Custodio DE, Abagyan R, Siuzdak G. METLIN: A Metabolite Mass Spectral Database. Therapeutic Drug Monitoring 2005;27(6):747-751.
12. Simon-Manso Y, Lowenthal MS, Kilpatrick LE, Sampson ML, Telu KH, Rudnick PA, Mallard WG, II DWB, II TBS, Tchekhovskoi DV and others. Metabolite Profiling of a NIST Standard Reference Material for Human Plasma (SRM 1950): GC-MS, LC-MS, NMR, and Clinical Laboratory Analyses, Libraries, and Web-Based Resources. Analytical Chemistry 2013;85(24):11725-11731.
13. Kobata A. Use of endo- and exoglycosidases for structural studies of glycoconjugates. Anal Biochem 1979;100(1):1-14.
14. Winterhalter PR, Lommel M, Ruppert T, Strahl S. O-glycosylation of the non-canonical T-cadherin from rabbit skeletal muscle by single mannose residues. FEBS Lett 2013;587(22):3715-21.

15. I B, H S, P S. O-GalNAc Glycans. In: A V, RD C, JD E, editors. Essentials of Glycobiology. 2 ed. Cold Spring Harbor (NY): Cold Spring Harbor Laboratory Press; 2009.
16. Siwy J, Mullen W, Golovko I, Franke J, Zürbig P. Human urinary peptide database for multiple disease biomarker discovery. Proteomics Clin Appl 2011;5(5-6):367-74.
17. Good DM, Zürbig P, Argilés A, Bauer HW, Behrens G, Coon JJ, Dakna M, Decramer S, Delles C, Dominiczak AF and others. Naturally occurring human urinary peptides for use in diagnosis of chronic kidney disease. Mol Cell Proteomics 2010;9(11):2424-37.
18. Candiano G, Musante L, Bruschi M, Petretto A, Santucci L, Del Boccio P, Pavone B, Perfumo F, Urbani A, Scolari F and others. Repetitive fragmentation products of albumin and alpha 1-antitrypsin in glomerular diseases associated with nephrotic syndrome. Journal of the American Society of Nephrology 2006;17(11):3139-3148.
19. Raab WP. DIAGNOSTIC VALUE OF URINARY ENZYME DETERMINATIONS. Clinical Chemistry 1972;18(1):5-&.
20. Zhang M, Fu G, Lei T. Two urinary peptides associated closely with type 2 diabetes mellitus. PLoS One 2015;10(4):e0122950.
21. Stalmach A, Johnsson H, McInnes IB, Husi H, Klein J, Dakna M, Mullen W, Mischak H, Porter D. Identification of urinary peptide biomarkers associated with rheumatoid arthritis. PLoS One 2014;9(8):e104625.
22. Nkuipou-Kenfack E, Bhat A, Klein J, Jankowski V, Mullen W, Vlahou A, Dakna M, Koeck T, Schanstra JP, Zürbig P and others. Identification of ageing-associated naturally occurring peptides in human urine. Oncotarget 2015;6(33):34106-17.
23. Bock SC, Skriver K, Nielsen E, Thogersen HC, Wiman B, Donaldson VH, Eddy RL, Marrinan J, Radziejewska E, Huber R and others. HUMAN C1BAR INHIBITOR - PRIMARY STRUCTURE, CDNA CLONING, AND CHROMOSOMAL LOCALIZATION. Biochemistry 1986;25(15):4292-4301.
24. Strecker G, Ollierhartmann MP, Vanhalbeek H, Friederik J, Vliegenthart G, Montreuil J, Hartmann L. PRIMARY STRUCTURE ELUCIDATION OF CARBOHYDRATE CHAINS OF NORMAL C1-ESTERASE INHIBITOR (C1-INH) BY 400-MHZ H-1-NMR STUDY. Comptes Rendus De L Academie Des Sciences Serie Iii-Sciences De La Vie-Life Sciences 1985;301(11):571-576.
25. Perkins SJ, Smith KF, Amatayakul S, Ashford D, Rademacher TW, Dwek RA, Lachmann PJ, Harrison RA. 2-DOMAIN STRUCTURE OF THE NATIVE AND REACTIVE CENTER CLEAVED FORMS OF C1BAR INHIBITOR OF HUMAN-COMPLEMENT BY NEUTRON-SCATTERING. Journal of Molecular Biology 1990;214(3):751-763.
26. Caliezi C, Wuillemin WA, Zeerleder S, Redondo M, Eisele B, Hack CE. C1-Esterase inhibitor: an anti-inflammatory agent and its potential use in the treatment of diseases other than hereditary angioedema. Pharmacol Rev 2000;52(1):91-112.
27. Cliff JM, Lee JS, Constantinou N, Cho JE, Clark TG, Ronacher K, King EC, Lukey PT, Duncan K, Van Helden PD and others. Distinct phases of blood gene expression pattern through tuberculosis treatment reflect modulation of the humoral immune response. J Infect Dis 2013;207(1):18-29.
28. Wang Y, Chen J, Chen L, Zheng P, Xu HB, Lu J, Zhong J, Lei Y, Zhou C, Ma Q and others. Urinary peptidomics identifies potential biomarkers for major depressive disorder. Psychiatry Res 2014;217(1-2):25-33.

29. von Zur Mühlen C, Koeck T, Schiffer E, Sackmann C, Zürbig P, Hilgendorf I, Reinöhl J, Rivera J, Zirlik A, Hehrlein C and others. Urine proteome analysis as a discovery tool in patients with deep vein thrombosis and pulmonary embolism. Proteomics Clin Appl 2016;10(5):574-84.
30. Zak DE, Penn-Nicholson A, Scriba TJ, Thompson E, Suliman S, Amon LM, Mahomed H, Erasmus M, Whatney W, Hussey GD and others. A blood RNA signature for tuberculosis disease risk: a prospective cohort study. Lancet 2016;387(10035):2312-22.
31. Jain R, Dey B, Tyagi AK. Development of the first oligonucleotide microarray for global gene expression profiling in guinea pigs: defining the transcription signature of infectious diseases. BMC Genomics 2012;13:520.
32. Beisiegel M, Mollenkopf HJ, Hahnke K, Koch M, Dietrich I, Reece ST, Kaufmann SH. Combination of host susceptibility and Mycobacterium tuberculosis virulence define gene expression profile in the host. Eur J Immunol 2009;39(12):3369-84.
33. Mehra S, Alvarez X, Didier PJ, Doyle LA, Blanchard JL, Lackner AA, Kaushal D. Granuloma correlates of protection against tuberculosis and mechanisms of immune modulation by Mycobacterium tuberculosis. J Infect Dis 2013;207(7):1115-27.
34. Metzger J, Kirsch T, Schiffer E, Ulger P, Mentes E, Brand K, Weissinger EM, Haubitz M, Mischak H, Herget-Rosenthal S. Urinary excretion of twenty peptides forms an early and accurate diagnostic pattern of acute kidney injury. Kidney Int 2010;78(12):1252-62.
35. Zhu W, Liu M, Wang GC, Peng B, Yan Y, Che JP, Ma QW, Yao XD, Zheng JH. Fibrinogen alpha chain precursor and apolipoprotein A-I in urine as biomarkers for noninvasive diagnosis of calcium oxalate nephrolithiasis: a proteomics study. Biomed Res Int 2014;2014:415651.
36. Zauner G, Hoffmann M, Rapp E, Koeleman CA, Dragan I, Deelder AM, Wuhrer M, Hensbergen PJ. Glycoproteomic analysis of human fibrinogen reveals novel regions of O-glycosylation. J Proteome Res 2012;11(12):5804-14.
37. Pacchiarotta T, Hensbergen PJ, Wuhrer M, van Nieuwkoop C, Nevedomskaya E, Derks RJ, Schoenmaker B, Koeleman CA, van Dissel J, Deelder AM and others. Fibrinogen alpha chain O-glycopeptides as possible markers of urinary tract infection. J Proteomics 2012;75(3):1067-73.
38. Jacobs R, Tshehla E, Malherbe S, Kriel M, Loxton AG, Stanley K, van der Spuy G, Walzl G, Chegou NN. Host biomarkers detected in saliva show promise as markers for the diagnosis of pulmonary tuberculosis disease and monitoring of the response to tuberculosis treatment. Cytokine 2016;81:50-6.
39. Kager LM, Blok DC, Lede IO, Rahman W, Afroz R, Bresser P, van der Zee JS, Ghose A, Visser CE, de Jong MD and others. Pulmonary tuberculosis induces a systemic hypercoagulable state. J Infect 2015;70(4):324-34.
40. Liu J, Jiang T, Wei L, Yang X, Wang C, Zhang X, Xu D, Chen Z, Yang F, Li JC. The discovery and identification of a candidate proteomic biomarker of active tuberculosis. BMC Infect Dis 2013;13:506.
41. Awodu OA, Ajayi IO, Famodu AA. Haemorheological variables in Nigeria pulmonary tuberculosis patients undergoing therapy. Clin Hemorheol Microcirc 2007;36(4):267-75.
42. Turken O, Kunter E, Sezer M, Solmazgul E, Cerrahoglu K, Bozkanat E, Ozturk A, Ilvan A. Hemostatic changes in active pulmonary tuberculosis. Int J Tuberc Lung Dis 2002;6(10):927-32.

43. Robson SC, White NW, Aronson I, Woollgar R, Goodman H, Jacobs P. Acute-phase response and the hypercoagulable state in pulmonary tuberculosis. Br J Haematol 1996;93(4):943-9.
44. Van den Steen P, Rudd PM, Dwek RA, Opdenakker G. Concepts and principles of O-linked glycosylation. Critical Reviews in Biochemistry and Molecular Biology 1998;33(3):151-208.
45. Sweeley CC, Bentley R, Makita M, Wells WW. GAS-LIQUID CHROMATOGRAPHY OF TRIMETHYLSILYL DERIVATIVES OF SUGARS AND RELATED SUBSTANCES. Journal of the American Chemical Society 1963;85(16):2497-&.
46. Asselta R, Duga S, Tenchini ML. The molecular basis of quantitative fibrinogen disorders. Journal of Thrombosis and Haemostasis 2006;4(10):2115-2129.
47. Storm D, Herz J, Trinder P, Loos M. C1 inhibitor-C1s complexes are internalized and degraded by the low density lipoprotein receptor-related protein. J Biol Chem 1997;272(49):31043-50.
48. Kwaan HC, Barlow GH. NATURE AND BIOLOGICAL-ACTIVITIES OF DEGRADATION PRODUCTS OF FIBRINOGEN AND FIBRIN. Annual Review of Medicine 1973;24:335-344.

CHAPTER 3: STRUCTURAL CHARACTERIZATION OF *M/Z* 203.1390 METABOLITE

3.1 Introduction

A major challenge in advancing differential metabolites towards candidate biomarkers is the characterization of significant, yet structurally unidentified metabolites. Lack of structural information impedes development of more targeted detection techniques and obstructs comparison with other metabolomics studies making validation of these uncharacterized metabolites challenging [1]. Additionally, current groups hoping to proceed with biomarker qualification are limited to compounds in available databases that have been previously identified. We hypothesize that the structural characterization of these significant, yet unknown metabolites will lead to additional or novel host metabolic pathways providing additional compounds to include in a biomarker based prognostic for treatment response in tuberculosis patients.

Previously, an untargeted metabolomics experiment seeking biomarkers indicative of successful anti-TB treatment response detected six metabolites that were significantly different at early time points post treatment [2]. Data from the previous chapter describe the structural characterization of one of these metabolites, however, five remain uncharacterized or have putative, yet unconfirmed identifications. This chapter focuses on the structural characterization of a metabolite that was defined by an *m/z* value of 203.1390. Characterization of this metabolite as *N*-acetylisoputreanine led to the discovery of an additional metabolic pathway that was not previously associated with anti-TB treatment response and the structural identification of another significantly altered metabolite involved in that pathway.

3.2 Materials and Methods

Chemicals

Glycine, *N*-acetylspermine, γ-aminobutyric acid, N^1, N^{12}-diacetylspermine, sodium triacetoxyborohydride were obtained from Sigma Aldrich (St. Louis, MO, USA). LC-MS grade water, methanol and acetonitrile were from Honeywell Burdick & Jackson (Muskegon, MI, USA). Formic Acid from Fischer Scientific (Pittsburgh, PA, USA). Human urine used as a control was obtained from Gemini Bio-Products (West Sacramento, CA, USA).

Clinical Samples

Patient urine for metabolite identification was from a subset of the samples used for metabolite discovery in the previously published study [2]. This subset of samples was obtained from the tuberculosis research unit (TBRU) NAA2m study (DMID 08-0023) conducted in Uganda.

LC-MS and LC-MS/MS Analysis

Chromatography was based on a previously described method using an Agilent 1200 series high-performance liquid chromatography system (Agilent Technologies, Palo Alto, CA, USA) coupled with an Atlantis T3 reverse-phase C_{18} 3.5µm column (2.1 by 150mm; Waters Corp., Milford, MA) [3]. Elution of metabolites was achieved using a 0-90% nonlinear gradient of methanol in 0.1% formic acid at a constant flow rate of 0.25ml/min. Mass spectrometry was performed using an Agilent 6510 quadrupole time of flight (Q-TOF) LC/MS instrument equipped with an Agilent electrospray ionization source that was operated in positive ionization mode. The operating conditions for the mass spectrometer were: gas temperature, 300˚C; drying gas, 8 L/min; nebulizer 45 lb/in^2; capillary voltage, 2,000 V; fragmentation energy for MS and MS/MS, 120 V; fragmentation energy for MS/MS of *m/z* 100.0757 fragment, 200V; skimmer,

60V; and octapole RF setting, 750 V. Specified ions were isolated for MS/MS fragmentation (isolation width of 1.3 Da) by collision induced dissociation at set collision energies (5-40V). Data were collected in profile and centroid mode at a scan rate of 2.0 spectra/sec and scan range of *m/*z 50 – 1,700 using the Agilent MassHunter Data Acquisition software.

Purification of N^1-acetylpolyamine oxidase (APAO)

A plasmid construct (pET15b/hPAO-1) for the recombinant expression of N^1-acetylpolyamine oxidase (hPAO-1), was kindly provided by Robert Casero Jr. (Johns Hopkins University). Recombinant hPAO-1 enzyme was generated as previously described [4]. Briefly, recombinant hPAO-1 protein was produced in *Escherichia coli* BL21(DE3) STAR and purified under denaturing conditions using nickel-nitrilotriacetic acid (Ni-NTA) resin (Qiagen, Valencia, CA, USA). Purified protein was dialyzed in renaturation buffer (250 mM NaCl, 50mM Tris-HCl, 0.1mM EDTA, 1mM DTT, 0.2µM FAD, pH 8.0) and stored at 4˚C until used for synthesizing *N*-acetylisoputreanine.

N-acetylisoputreanine Synthetic Approaches

A modification of a previously described enzyme assay was used for synthesis of *N*-acetylisoputreanine [4]. *N*-acetylspermine at 0.25 mM was combined with purified hPAO-1 enzyme (0.6mg/ml) in 88 mM glycine buffer (pH 8.0) for 30 mins at RT. ɣ-aminobutyric acid at a final concentration of 10 mM was subsequently added. An aliquot (500 µl) of this mixture was added to 4.5 ml 90% ethanol containing 1% (w/v) sodium triacetoxyborohydride and incubated at RT for 4 hours. The reaction was dried in a Savant SpeedVac and resuspended in 500 µl of water at stored at 4˚C until LC-MS analysis. Prior to LC-MS analysis, the sample was diluted 1:10 in water or commercial urine.

Synthesis and Confirmation of Other Polyamine Catabolites

N-(3-Acetamidopropyl) pyrrolidin-2-one (the ɣ-lactam form of *N*-acetylisoputreanine) was synthesized as previously described [5]. Briefly acetylation of N-(3-Aminopropyl) pyrrolidin-2-one (the ɣ-lactam form of isoputreanine) was performed in methanol with acetyl chloride at pH 7. The reaction was dried and resuspended in LC-MS grade water and stored at 4˚C.

Data Analyses

The LC-MS/MS spectra were manually interrogated against available MS/MS spectra in the METLIN metabolite database, the Human Metabolome Database (HMDB), and the National Institutes of Standards and Technology commercial library (NIST)[6-8]. Theoretical fragments were obtained using ACD/MS Fragmenter (Advanced Chemistry Development, Inc., Toronto, On, Canada).

3.3 Results

Development of a hypothesized structure for m/z 203.1390 metabolite

Structural information for the *m/z* 203.1380 metabolite, with a predicted formula of $C_9H_{19}N_2O_3$ and *m/z* 203.1390, was obtained using LC-MS/MS. A representative spectrum for *m/z* 203.1380 from TB patient urine using 20V collision energy is shown in Figure 3.1A. The MS/MS spectrum revealed a dominant fragment ion (*m/z* 100.0758) that was present even with a low collision energy (10V) (fragmentation data not shown). This was indicative of a highly labile bond and led to the hypothesis that the metabolite was composed of two major fragments connected by a C-N bond.

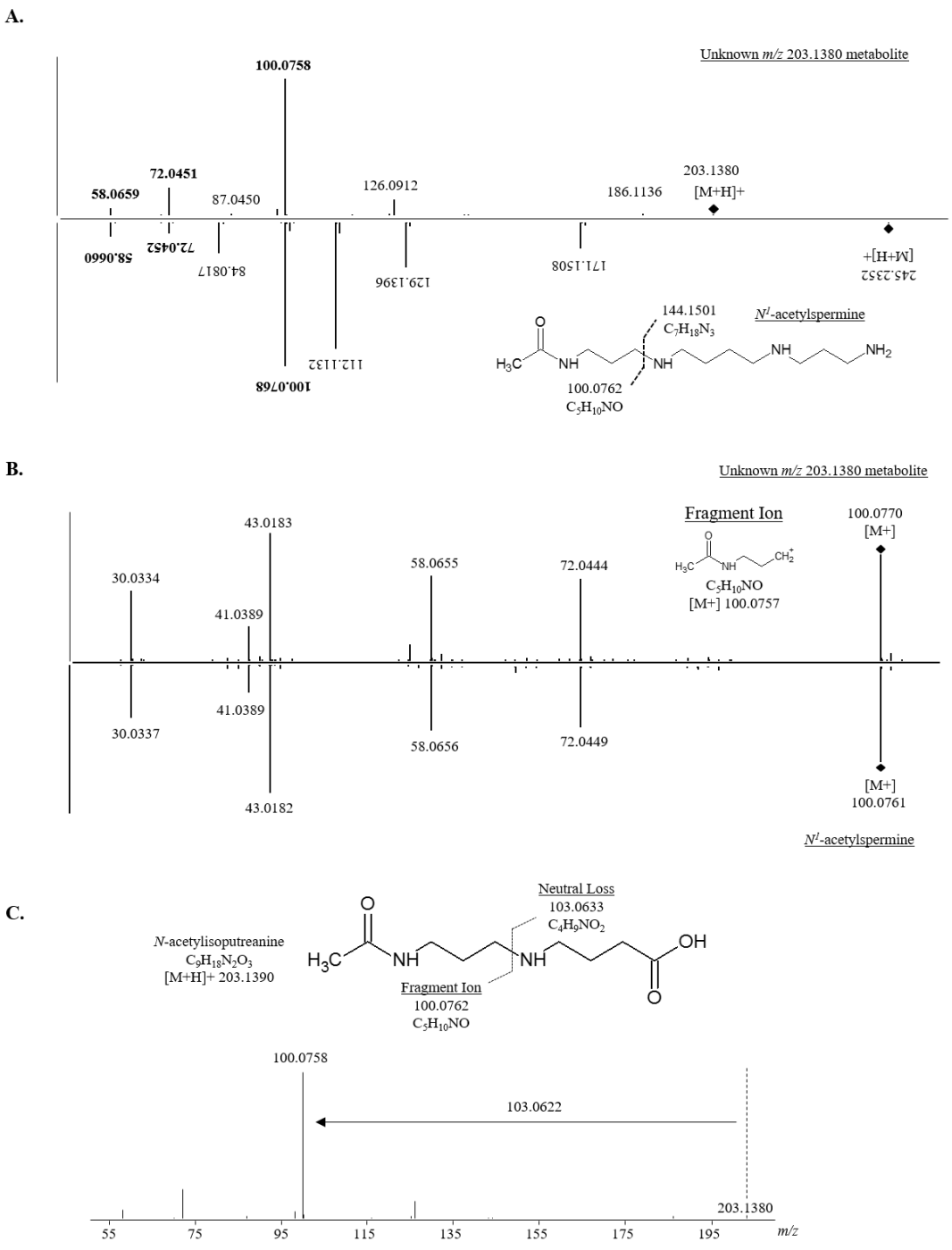

Figure 3.1 Development of Hypothesized Structure
(A) MS/MS comparison of *m/z* 203.1380 metabolite and *N*-acetylspermine. (B) MS/MS comparison of *m/z* 100.0758 fragment ion from *m/z* 203.1380 metabolite (top) and *N*-acetylspermine (bottom). (C) *N*-acetylisoputreanine comprised of *m/z* 100.0758 fragment ion and neutral loss of 103.0622 (γ-aminobutyric acid). Values listed are the experimental values seen in the spectra. All experimental values were within 20 ppm of theoretical values.

Fragment ions from unknown metabolite that are shared with those of defined molecules can be used to help elucidate structural features of the unknown metabolite. Thus, the MS/MS spectrum of the *m/z* 203.1380 feature was compared with available spectra in the National Institute of Standards and Technology (NIST) database [8]. The MS/MS spectra belonging to *N*-acetylspermine had multiple fragment ions in common with the experimental MS/MS spectrum of *m/z* 203.1380 metabolite. This fragment ion overlap (*m/z* 100.0768, *m/z* 72.0452, *m/z* 58.0660) was verified in our laboratory using a standard of *N*-acetylspermine (Figure 3.1A). This indicated a possible structural similarity between *N*-acetylspermine and the *m/z* 203.1390 metabolite.

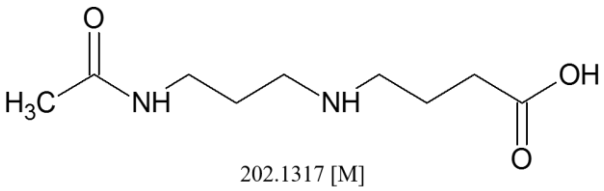

202.1317 [M]
m/z 203.1390
$C_9H_{18}N_2O_3$
N-acetylisoputreanine

Figure 3.3 *N*-acetylisoputreanine, structure of *m/z* 203.1390 metabolite

The structural similarity with *N*-acetylspermine was examined further by targeting the shared fragment ion with a theoretical value of *m/z* 100.0757) for further fragmentation. Increasing the fragmentor voltage of the MS from 120V to 200V induced in-source fragmentation and increased the abundance of the *m/z* 100.0757 fragment ion from both molecules. Fragmentation of the *m/z* 100.0757 daughter ion of both *N*-acetylspermine and the *m/z* 203.1390 feature were virtually identical (Figure 3.1B).

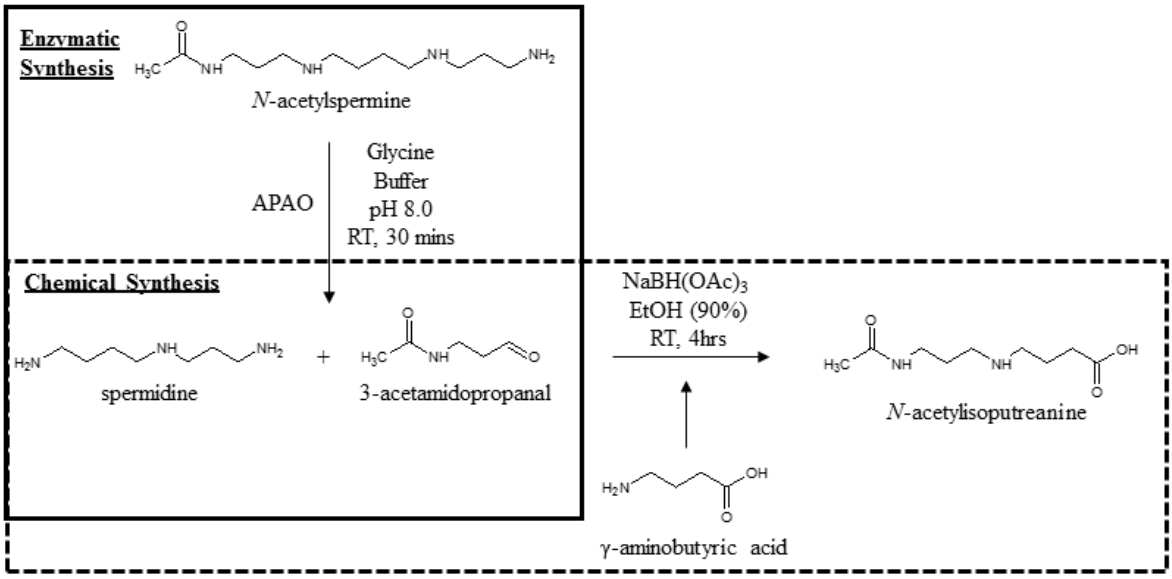

Figure 3.5 Schematic for chemical and enzymatic synthesis of *N*-acetylisoputreanine

ACD/Labs MS Fragmenter and ChemSketch software predict that the *m/z* 100.0757 daughter ion was generated after fragmentation at the C-N bond that separates the acetamidopropyl group (i.e. the *m/z* 100.0757 product) and spermidine in *N*-acetylspermine (Figure 3.1A) [9]. Additional support for the predicted structure of the *m/z* 100.0757 daughter ion was the additional fragment ions *m/z* 58.065 and *m/z* 43.0182, that were predicted to result from fragmentation of the labile C-N bond of the *N*-acetyl group (Figure 3.1B). Thus, it was concluded that both *N*-acetylspermine and the *m/z* 203.1390 metabolite possessed an acetamidopropyl group.

The MS/MS spectra of the *m/z* 203.1390 metabolite was re-examined, without success, to determine whether fragment ions could define the other half of the molecule. Thus, it was proposed that the other portion of the molecule was defined by a neutral loss of 103.0633 (Figure 3.1C). Querying the ChemSpider database resulted in 150 matches with the highest ranked match belonging to γ-aminobutyric acid (GABA) [10]. GABA is an endogenous metabolite in humans and

a component of different metabolic pathways including polyamine metabolism, so its structure was proposed as the other half of the *m/z* 203.1390 metabolite (Figure 3.1C). Additional support for GABA as part of the structure is the easily removable –OH group from its terminal carboxylic acid, which could result in the observed *m/z* 185.1285 fragment from loss of water seen in the MS/MS spectra at lower collision energies (data not shown). The hypothesized structure for the *m/z* 203.1390 metabolite matched with a previously predicted, yet never detected polyamine catabolite, *N*-acetylisoputreanine (Figure 3.2) [11].

Synthesis and Structural Confirmation of N-acetylisoputreanine

A commercial standard of *N*-acetylisoputreanine was not available so structural confirmation was achieved using a combined enzymatic and chemical synthetic approach (Figure 3.3). The final reaction mixture was analyzed by LC-MS/MS and the EIC revealed a peak with the same retention time and MS/MS fragmentation as the endogenous *m/z* 203.1390 metabolite in urine (Figure 3.4). Furthermore, this endogenous peak was increased when the reaction mixture was added to urine (Fig. 3.4A), thus confirming the proposed structure as *N*-acetylisoputreanine.

Assessment of interconversion

N-acetylisoputreanine had not been identified; however, another form of this molecule, *N*-acetylisoputreanine-ɣ-lactam, has been detected in urine[12-14]. In those studies, however, the sample processing used for GC-MS analysis could have resulted in dehydration of *N*-acetylisoputreanine to create the *N*-acetylisoputreanine-γ-lactam [15]. To determine whether *N*-acetylisoputreanine-γ-lactam is an endogenous component of human urine, we extracted the LC-

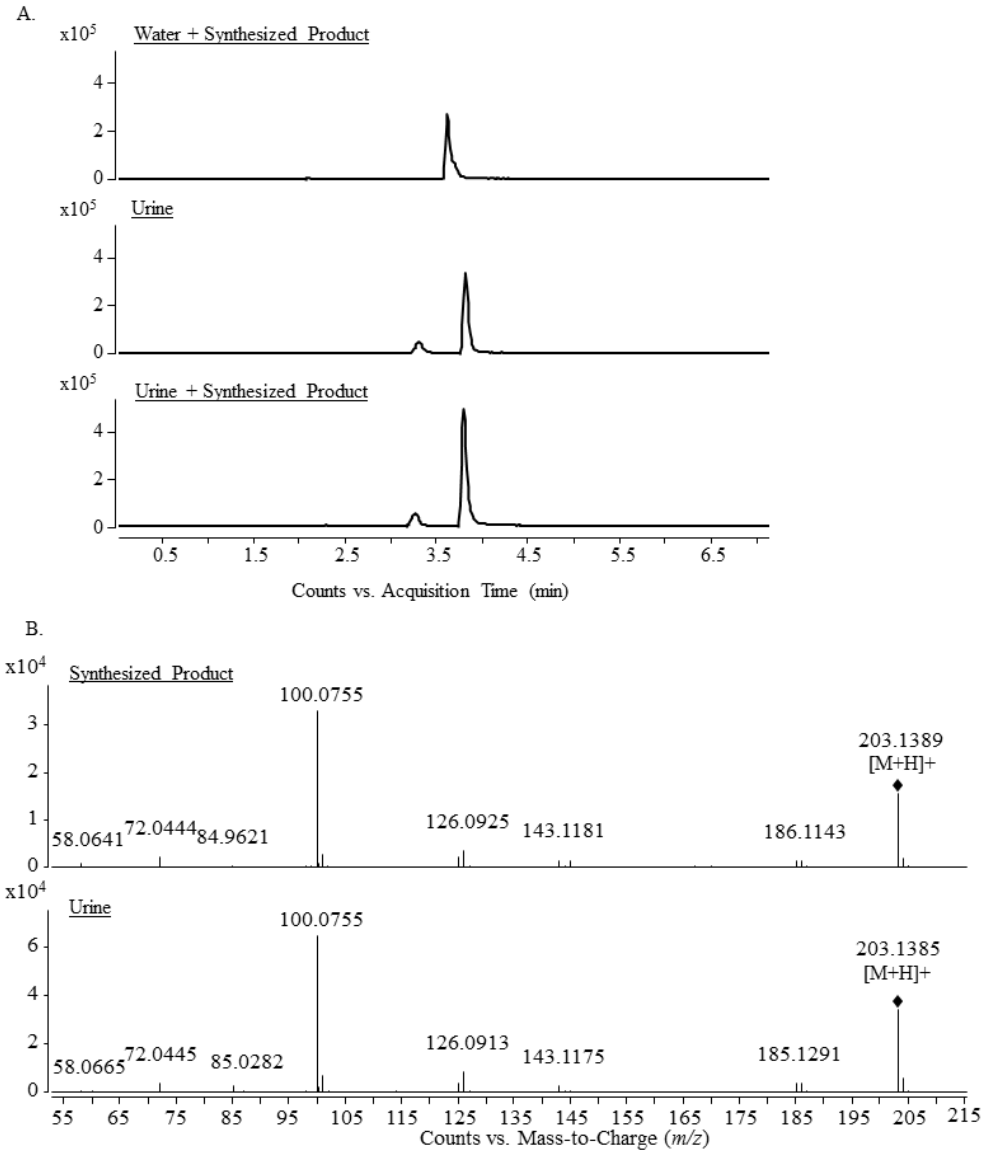

Figure 3.7 Confirmation of N-acetylisoputreanine
(A)The extracted ion chromatogram (EIC) peak for *m/z* 203.1390 in water (top) and urine (bottom) spiked with reaction mixture containing N-acetylisoputreanine matches in retention time with the EIC for *m/z* 203.1390 in urine (middle). (B) MS/MS fragmentation of *m/z* 203.1389 metabolite in urine (bottom) and reaction mixture containing N-acetylisoputreanine in water (top) have similar fragmentation patterns. The increased EIC peak, matching retention time and fragmentation patterns provide confidence that the unknown *m/z* 203.1390 metabolite is N-acetylisoputreanine.

MS data of TB patient urine to search for an *m/z* 185.1285 product. As shown in Figure 3.4A the extracted ion chromatogram (EIC) revealed a peak for this mass in the urine. The synthesized product had a matching retention time and MS/MS spectrum as well as an increase in the endogenous peak when added to urine (Figure 3.6A&B). This confirmed that *N*-acetylisoputreanine-γ-lactam is an endogenous component of human urine. Hydrolysis of the γ-lactam ring is all that is needed to convert *N*-acetylisoputreanine-γ-lactam to *N*-acetylisoputreanine. LC-MS analysis of *N*-acetylisoputreanine-γ-lactam in water and in urine did not change the endogenous *N*-acetylisoputreanine peak or create one in water (Figure 3.6A). This

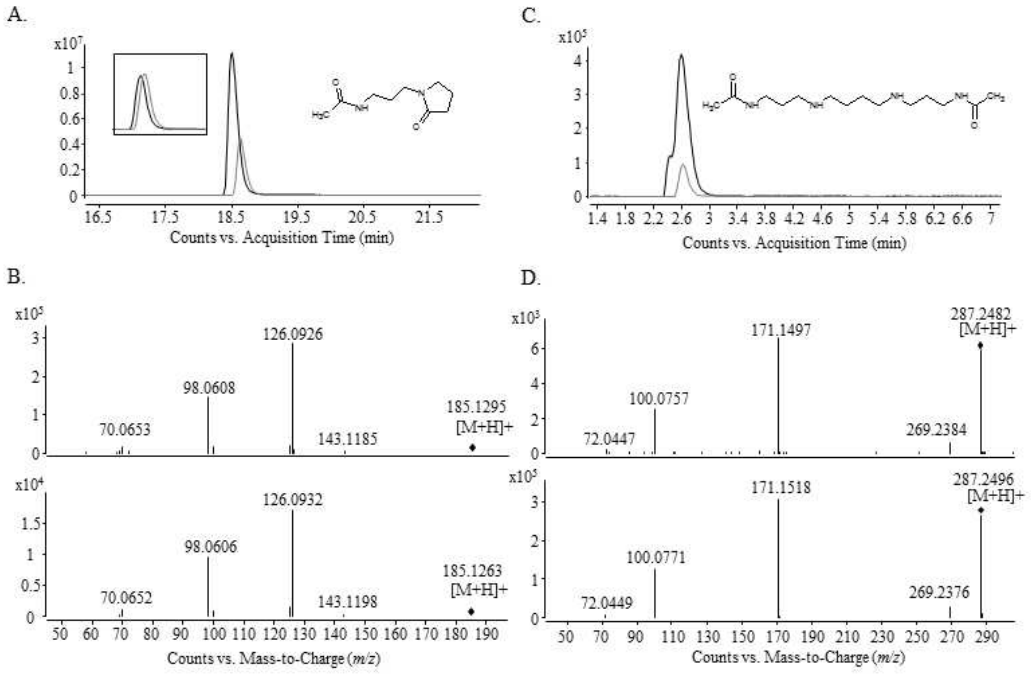

Figure 3.9 Confirmation of Other Polyamine Catabolites
(A) The EIC peak for *m/z* 185.1285 (*N*-acetylisoputreanine-γ-lactam) in urine (gray line) increases after addition of synthesized *N*-acetylisoputreanine-γ-lactam (black line), inset is EIC peak for *m/z* 203.1390 (*N*-acetylisoputreanine) (B) MS/MS fragmentation patterns for *m/z* 185.1285 in urine (top) and synthetic *N*-acetylisoputreanine-γ-lactam in water (bottom) (C) The EIC peak for *m/z* 287.2443 (N^1, N^{12}-diacetylspermine) in urine (gray line) is increased after addition of N^1, N^{12}-diacetylspermine standard (black line)(D) MS/MS fragmentation patterns for *m/z* 287.2443 in urine (top) and commercial N^1, N^{12}-diacetylspermine standard in water (bottom).

provides evidence that *N*-acetylisoputreanine and *N*-acetylisoputreanine-γ-lactam were both normal components of human urinary metabolome.

Structural Confirmation of N^1, N^{12}-diacetylspermine

Another metabolite (*m/z* 287.2443) that differed significantly between the D0 and during treatment time points for tuberculosis patients undergoing therapy was putatively identified as N^1, N^{12}-diacetylspermine [2]. MS/MS fragmentation of this metabolite also resulted in a dominant *m/z* 100.0757 fragment ion similar to *N*-acetylspermine and *N*-acetylisoputreanine which can be explained by the two acetamidopropyl moieties in N^1, N^{12}-diacetylspermine (Figure 3.4C). Further efforts into the structural confirmation of this metabolite was desirable because N^1, N^{12}-diacetylspermine is also a component of polyamine catabolism. Matching retention times and MS/MS spectra between the commercial standard and the *m/z* 287.2443 metabolite confirmed its identity as N^1, N^{12}-diacetylspermine (Figure 3.4C&D). Additional confirmation is the increase in the endogenous peak when the commercial standard is spiked into the urine (Figure 3.4C).

3.4 Discussion

As stated in Chapter 2, a major hindrance in development of clinically useful biomarkers is the large proportion of metabolites with unconfirmed identities. In this chapter, the structural characterization of one of these significantly altered, yet unidentified metabolites as *N*-acetylisoputreanine led to the discovery of an additional metabolic pathway, polyamine metabolism, and additional metabolites, *N*-acetylisoputreanine-γ-lactam and N^1, N^{12}-diacetylspermine. Not only did this research identify a metabolite not previously known to be a component of the human urinary metabolome, but this is the first time that alterations in polyamine metabolism have been associated with anti-TB treatment.

Polyamines are polycationic molecules found in all living organisms that are important for cell proliferation and differentiation. At neutral pH, these molecules are positively charged enabling regulation of biological processes through reversible ionic interactions with negatively charged molecules such as nucleic acids, proteins, and phospholipids[16-21]. This widespread involvement in important cellular processes requires stringent regulation of polyamine levels which is achieved by the polyamine interconversion cycle and transport. The polyamine interconversion cycle consists of synthesis through aminopropylation of putrescine and spermidine and catabolism through acetylation and oxidative degradation of putrescine, spermine, and spermidine [11]. The two metabolites discussed in this chapter are terminal polyamine catabolites resulting from the catabolic branch of the interconversion pathway (Figure 3.6).

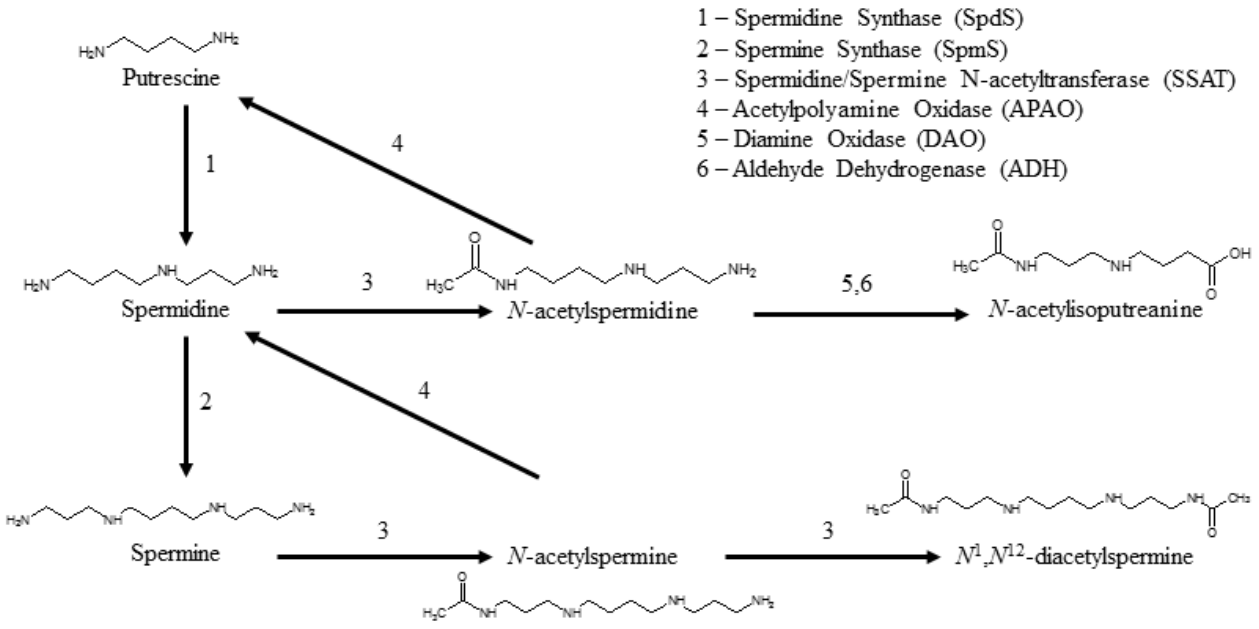

Figure 3.6 Polyamine interconversion pathway

N-acetylisoputreanine and N^1, N^{12}-diacetylspermine were significantly decreased during anti-TB treatment [2]. This decrease could indicate increased polyamine metabolism due to *Mtb* infection that normalizes as the patient returns to a healthy state due to antibiotic treatment. Alternatively, the decreased could result from non-specific action of the antibiotics on host gut microbiota. The gut microbiota are a major source of polyamines in the intestinal lumen and could influence polyamine levels in urine[22-25]. Specifically, the microbial metabolism in the gut, such as catabolism of dietary choline, has been shown to influence the metabolic profile of the host by altering levels of metabolites like dimethylamine in the urine and serum of the host[22,26,27]. Additionally, the presence of colonic bacterial biofilms correlated with an increase in the already elevated levels of N^1, N^{12}-diacetylspermine in colon cancer patients [28].. Thus, during anti-TB treatment, killing of gut microbiota would decrease intestinal polyamine levels potentially leading to decreased levels of *N*-acetylisoputreanine and N^1, N^{12}-diacetylspermine in the urine.

The alternative scenario in which changes in *N*-acetylisoputreanine and N^1, N^{12}-diacetylspermine levels are reflective of *Mtb* infection status is also plausible. In this scenario, the levels of these metabolites would increase at the site of infection and their decrease would be due to specific mycobacterial killing and the resolution of the infection. Similarly, alterations in host polyamine catabolism have been observed in other infections[29-36]. During leishmaniosis, polyamine biosynthesis at the infection site is altered by the parasite as well as the vector to promote parasite growth and pathogenesis [36]. Epstein-Barr virus alters polyamine homeostasis to favor increased polyamine levels, by concurrently inducing polyamine synthesis and reducing polyamine catabolism [30]. Infection with *Chlamydia trachomatis* increases polyamine synthesis due to induction of ornithine decarboxylase which subsequently interferes with NO production and promotes bacterial growth [33]. Alternatively, *Pneumocystis* organisms alter polyamine

homeostasis in favor of polyamine catabolism to allow for pathogen evasion of host immune response[34]. There are many ways that pathogens can influence host polyamine metabolism for their benefit, however, it is unclear whether changes in the levels *N*-acetylisoputreanine and N^1, N^{12}-diacetylspermine are due to specific manipulation by *Mtb* or a general host response to infection.

Limited research is available that relates polyamine metabolism to *Mtb* infection. In the 1950s, it was reported that exogenous spermine inhibited the growth of *Mtb in vitro* [37]. Previous examinations of spermine levels human tissue revealed that diseased tissue from tuberculosis patients contained increased spermine levels, higher than those used to inhibit *in vitro* growth [37,38]. These findings confirm that polyamine metabolism is increased during *Mtb* infection and this increase might be a potential host mechanism control *Mtb* growth, however, the effect of spermine on *Mtb* growth *in vivo* has not been determined. Interestingly, increased polyamine levels during *Mtb* infection could also contribute in the development of a non-replicating phenotype. Spermine and spermidine reduced fluoroquinolone uptake in *M. bovis* BCG *in vitro* presumably by blocking mycobacterial porins [39]. In addition to inhibiting porin-mediated uptake of antibiotics, increased polyamine levels could block porin-mediated uptake of essential nutrients required for bacterial growth. The structural identification described in this chapter adds to the previous literature in highlighting a potential importance for host polyamine metabolism during tuberculosis disease and anti-TB treatment.

The pathway proposed for the formation of *N*-acetylisoputreanine and *N*-acetylisoputreanine-γ-lactam involves oxidative deamination of *N*-acetylspermidine by diamine oxidase (DAO), a copper dependent amine oxidase (CuAO) [11]. Urinary *N*-acetylisoputreanine-γ-lactam levels are decreased in rats treated with the CuAO inhibitor, aminoguanidine,

corroborating involvement of DAO in the formation of *N*-acetylisoputreanine [13]. DAO is mainly expressed in the placenta, small intestines and kidney, though low levels are detectable in the lungs[11,40,41]. It is possible that increased polyamine catabolism in the lungs during *Mtb* infection results in increased export of N^1, N^{12}-diacetylspermine and N-acetylspermidine into circulation. These products then end up in the kidney where *N*-acetylspermidine is oxidatively deaminated by DAO and both *N*-acetylisoputreanine and N^1, N^{12}-diacetylspermine are excreted in the urine. Another possibility is that *N*-acetylisoputreanine is produced via non-enzymatic oxidative deamination of *N*-acetylspermidine independent of DAO. Pyridoxal phosphate (PLP), an active form of vitamin B_6 and cofactor in a variety of enzymes, has been shown to catalyze the oxidative deamination of five amino acids providing evidence that a non-enzymatic process could be involved[42]. However, further investigation of the biochemical pathways involved in the formation of these enzymes is needed. Analysis of these two polyamine catabolites and other polyamines using active TB patient urine and *Mtb* infected tissue are being conducted. These studies will help to elucidate the roles of polyamine catabolism during tuberculosis and anti-TB treatment.

REFERENCES

1. Koulman A, Lane GA, Harrison SJ, Volmer DA. From differentiating metabolites to biomarkers. Anal Bioanal Chem 2009;394(3):663-70.
2. Mahapatra S, Hess AM, Johnson JL, Eisenach KD, DeGroote MA, Gitta P, Joloba ML, Kaplan G, Walzl G, Boom WH and others. A metabolic biosignature of early response to anti-tuberculosis treatment. BMC Infect Dis 2014;14:53.
3. Mahapatra S, Hess AM, Johnson JL, Eisenach KD, DeGroote MA, Gitta P, Joloba ML, Kaplan G, Walzl G, Boom WH and others. A metabolic biosignature of early response to anti-tuberculosis treatment. BMC Infectious Diseases 2014 14(1):53.
4. Wang Y, Hacker A, Stewart TM, Frydman B, Valasinas A, Fraser AV, Worster PM, Robert A. Casero J. Properties of recombinant human N^1-acetylpolyamine oxidase (hPAO): potential role in determining drug sensitivity. Cancer Chemotherapy and Pharmacology 2005;56:83-90.
5. Van den berg GA KA, Elzinga H, and Muskiet FAJ. Determination of N-(3-acetamidopropyl)pyrrolidin-2-one, a Metabolite of Spermidine, in Urine by Isotope Dilution Mass Fragmentography. Journal of Chromatography 1986;383:251-258.
6. Wishart DS, Jewison T, Guo AC, Wilson M, Knox C, Liu Y, Djoumbou Y, Mandal R, Aziat F, Dong E and others. HMDB 3.0 - The Human Metabolome Database in 2013. Nucleic Acids Research 2013;41 (Database Issue):D801-D807.
7. Smith CA, O'Maille G, Want EJ, Qin C, Trauger SA, Brandon TR, Custodio DE, Abagyan R, Siuzdak G. METLIN: A Metabolite Mass Spectral Database. Therapeutic Drug Monitoring 2005;27(6):747-751.
8. Simon-Manso Y, Lowenthal MS, Kilpatrick LE, Sampson ML, Telu KH, Rudnick PA, Mallard WG, II DWB, II TBS, Tchekhovskoi DV and others. Metabolite Profiling of a NIST Standard Reference Material for Human Plasma (SRM 1950): GC-MS, LC-MS, NMR, and Clinical Laboratory Analyses, Libraries, and Web-Based Resources. Analytical Chemistry 2013;85(24):11725-11731.
9. Fragmenter ALM, ChemSketch AL. 2015 www.acdlabs.com. Advanced Chemistry Development, Inc.
10. Pence HE, Williams A. ChemSpider: An Online Chemical Information Resource. Journal of Chemical Education 2010;87(11):1123-1124.
11. Seiler N. Catabolism of polyamines. Amino Acids 2004;26(3):217-33.
12. van den Berg GA, Kingma AW, Elzinga H, Muskiet FA. Determination of N-(3-acetamidopropyl)pyrrolidin-2-one, a metabolite of spermidine, in urine by isotope dilution mass fragmentography. J Chromatogr 1986;383(2):251-8.
13. Hessels J, Kingma AW, Sturkenboom MC, Elzinga H, van den Berg GA, Muskiet FA. Gas chromatographic determination of N-acetylisoputreanine-gamma-lactam, a unique catabolite of N1-acetylspermidine. J Chromatogr 1991;563(1):1-9.
14. Seiler N, Knödgen B, Haegele K. N-(3-aminopropyl)pyrrolidin-2-one, a product of spermidine catabolism in vivo. Biochem J 1982;208(1):189-97.
15. Muskiet FAJ, Stratingh CM, Fremouwottevangers DC, Halie MR. MASS-SPECTROMETRIC IDENTIFICATION OF ISOPUTREANINE, A METABOLITE OF

SPERMIDINE AND OR SPERMINE, IN HUMAN-URINE. Journal of Chromatography 1982;230(1):142-147.
16. Wallace HM, Fraser AV, Hughes A. A perspective of polyamine metabolism. Biochem J 2003;376(Pt 1):1-14.
17. Kurata HT, Marton LJ, Nichols CG. The polyamine binding site in inward rectifier K+ channels. J Gen Physiol 2006;127(5):467-80.
18. Ha HC, Sirisoma NS, Kuppusamy P, Zweier JL, Woster PM, Casero RA. The natural polyamine spermine functions directly as a free radical scavenger. Proc Natl Acad Sci U S A 1998;95(19):11140-5.
19. Celano P, Baylin SB, Casero RA. Polyamines differentially modulate the transcription of growth-associated genes in human colon carcinoma cells. J Biol Chem 1989;264(15):8922-7.
20. Zhang M, Caragine T, Wang H, Cohen PS, Botchkina G, Soda K, Bianchi M, Ulrich P, Cerami A, Sherry B and others. Spermine inhibits proinflammatory cytokine synthesis in human mononuclear cells: a counterregulatory mechanism that restrains the immune response. J Exp Med 1997;185(10):1759-68.
21. Schuber F. Influence of polyamines on membrane functions. Biochem J 1989;260(1):1-10.
22. Matsumoto M, Kibe R, Ooga T, Aiba Y, Kurihara S, Sawaki E, Koga Y, Benno Y. Impact of Intestinal Microbiota on Intestinal Luminal Metabolome. Scientific Reports 2012;2:10.
23. Matsumoto M, Kurihara S, Kibe R, Ashida H, Benno Y. Longevity in Mice Is Promoted by Probiotic-Induced Suppression of Colonic Senescence Dependent on Upregulation of Gut Bacterial Polyamine Production. Plos One 2011;6(8):12.
24. Noack J, Kleessen B, Proll J, Dongowski G, Blaut M. Dietary guar gum and pectin stimulate intestinal microbial polyamine synthesis in rats. Journal of Nutrition 1998;128(8):1385-1391.
25. Kibe R, Kurihara S, Sakai Y, Suzuki H, Ooga T, Sawaki E, Muramatsu K, Nakamura A, Yamashita A, Kitada Y and others. Upregulation of colonic luminal polyamines produced by intestinal microbiota delays senescence in mice. Scientific Reports 2014;4:11.
26. Li M, Wang BH, Zhang MH, Rantalainen M, Wang SY, Zhou HK, Zhang Y, Shen J, Pang XY, Zhang ML and others. Symbiotic gut microbes modulate human metabolic phenotypes. Proceedings of the National Academy of Sciences of the United States of America 2008;105(6):2117-2122.
27. Nicholson JK, Holmes E, Wilson ID. Gut microorganisms, mammalian metabolism and personalized health care. Nat Rev Microbiol 2005;3(5):431-8.
28. Johnson CH, Dejea CM, Edler D, Hoang LT, Santidrian AF, Felding BH, Ivanisevic J, Cho K, Wick EC, Hechenbleikner EM and others. Metabolism links bacterial biofilms and colon carcinogenesis. Cell Metab 2015;21(6):891-7.
29. Mastrantonio R, Cervelli M, Pietropaoli S, Mariottini P, Colasanti M, Persichini T. HIV-Tat Induces the Nrf2/ARE Pathway through NMDA Receptor-Elicited Spermine Oxidase Activation in Human Neuroblastoma Cells. PLoS One 2016;11(2):e0149802.
30. Shi M, Gan YJ, Davis TO, Scott RS. Downregulation of the polyamine regulator spermidine/spermine N(1)-acetyltransferase by Epstein-Barr virus in a Burkitt's lymphoma cell line. Virus Res 2013;177(1):11-21.

31. Chaturvedi R, de Sablet T, Asim M, Piazuelo MB, Barry DP, Verriere TG, Sierra JC, Hardbower DM, Delgado AG, Schneider BG and others. Increased Helicobacter pylori-associated gastric cancer risk in the Andean region of Colombia is mediated by spermine oxidase. Oncogene 2015;34(26):3429-40.
32. Chaturvedi R, Asim M, Hoge S, Lewis ND, Singh K, Barry DP, de Sablet T, Piazuelo MB, Sarvaria AR, Cheng Y and others. Polyamines Impair Immunity to Helicobacter pylori by Inhibiting L-Arginine Uptake Required for Nitric Oxide Production. Gastroenterology 2010;139(5):1686-98, 1698.e1-6.
33. Abu-Lubad M, Meyer TF, Al-Zeer MA. Chlamydia trachomatis inhibits inducible NO synthase in human mesenchymal stem cells by stimulating polyamine synthesis. J Immunol 2014;193(6):2941-51.
34. Liao CP, Lasbury ME, Wang SH, Zhang C, Durant PJ, Murakami Y, Matsufuji S, Lee CH. Pneumocystis mediates overexpression of antizyme inhibitor resulting in increased polyamine levels and apoptosis in alveolar macrophages. J Biol Chem 2009;284(12):8174-84.
35. Stempin C, Giordanengo L, Gea S, Cerbán F. Alternative activation and increase of Trypanosoma cruzi survival in murine macrophages stimulated by cruzipain, a parasite antigen. J Leukoc Biol 2002;72(4):727-34.
36. Rogers M, Kropf P, Choi BS, Dillon R, Podinovskaia M, Bates P, Müller I. Proteophosophoglycans regurgitated by Leishmania-infected sand flies target the L-arginine metabolism of host macrophages to promote parasite survival. PLoS Pathog 2009;5(8):e1000555.
37. HIRSCH JG, DUBOS RJ. The effect of spermine on tubercle bacilli. J Exp Med 1952;95(2):191-208.
38. Harrison GA. Spermine in human tissues. Biochem J 1931;25(6):1885-92.
39. Sarathy JP, Lee E, Dartois V. Polyamines inhibit porin-mediated fluoroquinolone uptake in mycobacteria. PLoS One 2013;8(6):e65806.
40. Finney J, Moon HJ, Ronnebaum T, Lantz M, Mure M. Human copper-dependent amine oxidases. Arch Biochem Biophys 2014;546:19-32.
41. Elmore BO, Bollinger JA, Dooley DM. Human kidney diamine oxidase: heterologous expression, purification, and characterization. Journal of Biological Inorganic Chemistry 2002;7(6):565-579.
42. Choi KY. Non-enzymatic PLP-dependent oxidative deamination of amino acids induces higher alcohol synthesis. Biotechnology and Bioprocess Engineering 2015;20(6):988-994.

CHAPTER 4: METABOLITE ASSOCIATIONS WITH ACTIVE TB DISEASE

4.1 Introduction

While the detection and structural identification of differential metabolites is important for discovering biomarkers, follow up mechanistic studies are essential to understand the functions of these metabolites and their patho-physiological roles during disease [1]. Using the blood of 7,824 adults for genome wide association studies along with metabolic profiling, Shin *et al.* created a comprehensive network of associations between genetic variations and metabolic pathway alterations[2]. This allows for elucidation of genetic influences on metabolites in the human blood allowing for development of better understanding of diseases and drug development. The use of stable isotope labeled tracers can help to elucidate the specific enzymatic alterations that result in altered metabolite abundances. Sellers *et al.* demonstrated enhanced activity of pyruvate carboxylase over that of glutaminase-1 during non-small-cell lung cancer using stable isotope labeled tracers[3]. Exchanging the diets between African Americans and rural Africans altered gut microbial metabolism as well as inflammation and proliferation biomarkers, confirming the influence of diet on gut microbiota and colon cancer risk[4]. Increased levels of N^1, N^{12}-diacetylspermine associated with colon cancer patients were further investigated using stable isotopes and antibiotics to confirmed that N^1, N^{12}-diacetylspermine is an metabolic end product and its altered levels are associated with the presence of gut biofilms [5]. These mechanistic studies provided an understanding of the biological significance behind metabolic profiles associated with different phenotypes. This insight enables selection of the metabolites that are acceptable biomarkers for a particular phenotype and metabolic pathways that would be good targets for therapeutic intervention. .

The previous chapters described the structural characterization of two novel urinary metabolites that decreased during anti-TB treatment. The mechanisms behind their decreased abundance is unknown. The decrease of these metabolites during anti-TB treatment was hypothesized to be due to these metabolites returning to their normal levels, however, it is also possible that these metabolites decreased due to non-specific antibiotic interactions irrespective of patient disease status [6]. To address this hypothesis, the three polyamine metabolites (*N*-acetylisoputreanine, *N*-acetylisoputreanine-γ-lactam, and N^1, N^{12}-diacetylspermine) and the glycosylated serine-leucine dipeptide were assessed in the urine from index tuberculosis patients and tuberculin skin test positive and negative (TST+ and TST-) household contacts as well as in infected and uninfected Balb/c mouse lung tissue.

4.2 Materials and Methods

Chemicals

N^1, N^{12}-diacetylspermine, diaminohexane and heptofluorobutyric acid (HFBA) were obtained from Sigma Aldrich (St. Louis, MO, USA). *N*-acetylisoputreanine was synthesized as previously described in Chapter 3. LC-MS grade water, methanol and acetonitrile were from Honeywell (Morristown, NJ, USA). Formic Acid (FA) was obtained from Fischer Scientific (Pittsburgh, PA, USA).

Clinical Samples and Sample Preparation

Patient urine for metabolite quantification was obtained from the Tuberculosis Research Unit (TBRU) Kawempe Community Health Study (KCHS) conducted in Uganda (http://www.case.edu/affil/tbru/research_dmid01005.html). The KCHS urine samples represented 10 index cases of tuberculosis and, 14 household contacts (HC) that were TST- and 12 HC that were TST+. All KCHS subjects were from 30 to 60 years of age and represented both

sexes, and were without HIV co-morbidity. Patient urine samples from the KCHS were diluted 1:3 in LC-MS grade water as previously described [7]. Pooled urine was prepared as a quality control (QC) sample.

Lung tissue samples, kindly provided by Mercedes Gonzalez-Juarrero, were harvested from Balb/c mice infected with *Mtb* Erdman via low-dose aerosol. Samples were prepared based on previously described protocols[8,9]. The internal standard (IS) diaminohexane was added to microcentrifuge tube at 24.5ng/ml followed by lung tissue (approx. 50mg) and 500µl 80% methanol. Tissue was homogenized using a bullet blender (Next Advance, NY) followed by sonication. Samples were incubated at -20˚C for at least 1 hour and centrifuged at 13,000 rpm for 15 minutes at 4˚C using a table top centrifuge to pellet precipitated proteins. The supernatant was filtered with Ultrafree-MC 0.22µm centrifugal filter (EMD Millipore). The pooled QC sample was prepared by combining 50µl of filtered supernatant from each tissue sample in a microcentrifuge tube. The filtered supernatant from each sample along with the pooled QC sample were evaporated using a savant and the dried metabolite residue was stored at -80˚C. Prior to LC-MS analysis, the dried tissue sample residues were resuspended in 100µl of LC-MS grade water and the dried pooled QC sample residues was resuspended in 1550µl of LC-MS grade water, sonicated for 10 minutes and centrifuged at 14,000xg for 10 minutes at 4˚C. 40µl were transferred to autosampler vials for LC-MS analysis. The precipitated proteins were solubilized in 5% SDS and further diluted with PBS for protein concentration determination using the bicinchoninic acid (BCA) protein assay kit (Pierce, Rockford, IL) as per manufacturer's instructions.

LC-MS Analysis

Two chromatographic separations were used, the first was based on the previously published method, hereby called Method 1 [6]. The second is an adaptation of another method developed for the targeted analysis of polyamine metabolites, hereby called Method 2[10,11]. Both methods utilized an Agilent 1200 series high-performance liquid chromatography system (Agilent Technologies, Palo Alto, CA, USA) coupled with either an Atlantis T3 reverse-phase C_{18} 3.5µm column (2.1 by 150mm; Waters Corp., Milford, MA) for Method 1 or a Poroshell 120 EC-C8 reverse-phase 2.7µm column (2.1 by 100mm; Agilent Technologies, Palo Alto, CA) for Method 2. For Method 1, elution of analytes was achieved using a 0-90% nonlinear gradient of water and methanol supplemented with 0.1% formic acid at a constant flow rate of 0.25ml/min. For Method 2, analytes were eluted with a 5-100% nonlinear gradient of water and acetonitrile supplemented with 0.1% HFBA at a constant flow rate of 0.3ml/min. MS was performed using an Agilent 6224 time of flight (TOF) LC/MS instrument equipped with an Agilent electrospray ionization source that was operated in positive ionization mode. The MS operating conditions for both methods were set as follows: gas temperature, 300˚C; drying gas at 11 liters/minute; nebulizer 40 lb/in^2; capillary voltage, 2,000 V for Method 1 and 4,000 V for Method 2; fragmentor voltage, 120 V; skimmer, 65V; and octapole RF setting, 750 V. Data were collected in profile and centroid mode at a scan rate of 1.0 spectra/sec and scan range of *m/*z 100 – 1,700 using the Agilent MassHunter Data Acquisition software.

Data Analyses

Urine Samples

Molecular features present in LC-MS data were extracted with the Molecular Feature Extractor (MFE) algorithm of the Agilent MassHunter Qualitative Analysis software [12,13]. The

Agilent Mass Profiler Pro (MPP) software was used for retention time alignment, normalization and filtering of extracted molecular features. The parameters used were a 0.25 minute retention time window with 15ppm mass tolerance, each molecular feature was baselined to the median across all samples, and filtered based on their presence in 30% of samples in at least one group. The abundances of these filtered molecular features were determined using the Agilent MassHunter Quantitative Analysis software and exported as a Microsoft Excel spreadsheet for further statistical analyses.

The normalization technique used to adjust molecular feature abundances between samples to a common scale was the median fold change normalization [14]. The median profile of the pooled QCs was used as the target profile. The boxplots of the log2 transformed normalized and unnormalized metabolite abundances were created in R [15].

One way ANOVA and multiple comparisons were used to test if there was any statistical significant differences between the groups. Statistical analyses of the log2 transformed normalized abundances for *N*-acetylisoputreanine and N^1, N^{12}-diacetylspermine were performed using GraphPad Prism version 6.04 for Windows (GraphPad Software, La Jolla California USA).

Tissue Samples

The abundances for targeted metabolites were determined using the Agilent MassHunter Quantitative Analysis software and exported as a Microsoft Excel spreadsheet for further analysis. The abundances for each metabolite were normalized to the total protein content. One way ANOVA and multiple comparisons were used to test if there was any statistical significant differences between the groups. Statistical analyses of normalized abundances for *N*-

acetylisoputreanine and N^1, N^{12}-diacetylspermine were performed using GraphPad Prism version 6.04 for Windows (GraphPad Software, La Jolla California USA).

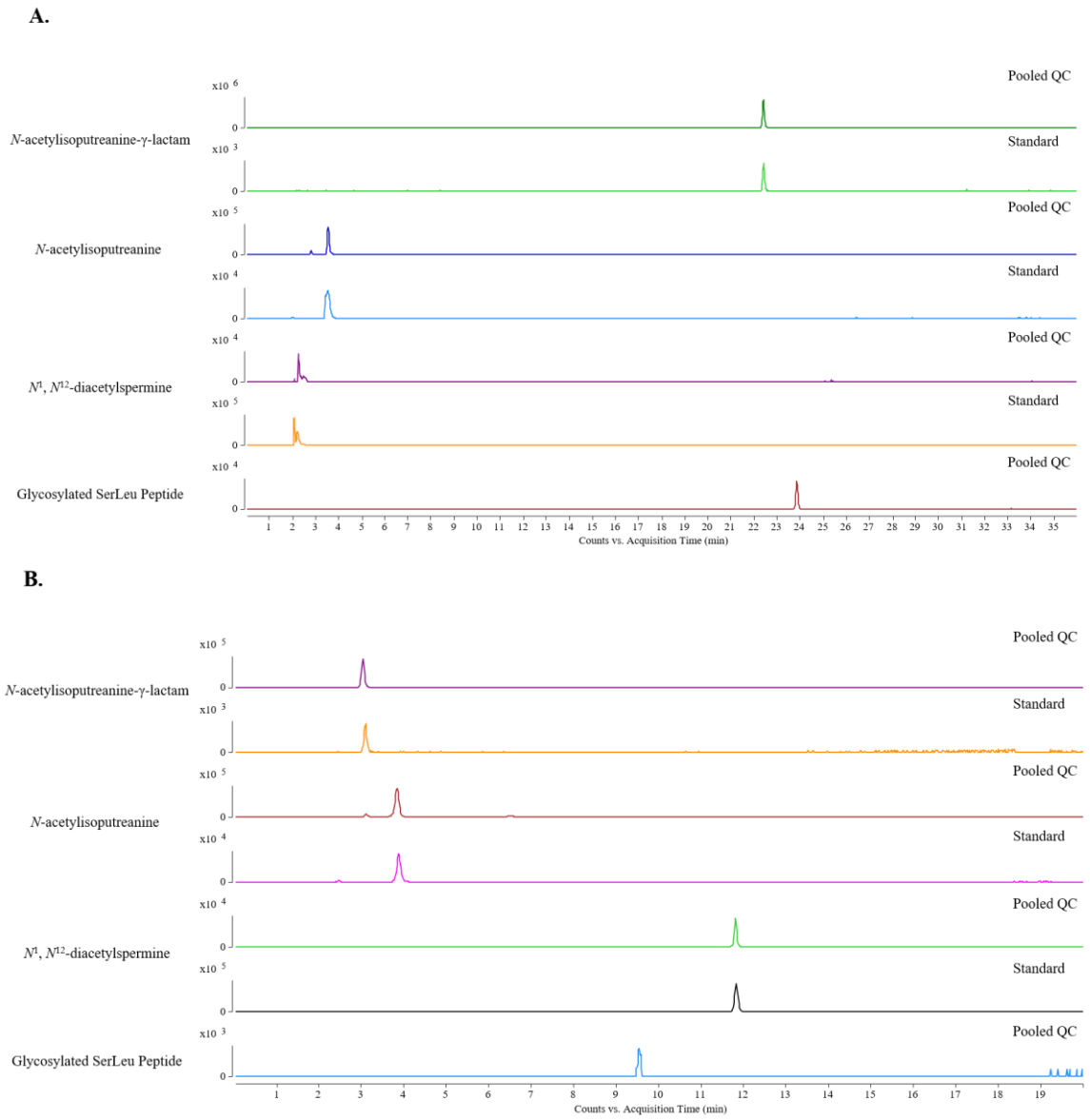

Figure 4.1
Chromatograms demonstrating shift in the retention time of metabolites using either Method 1 chromatography (A) or Method 2 chromatography (B). All chromatograms were generated using either the pooled QC urine sample or a standard of N^1, N^{12}-diacetylspermine, *N*-acetylisoputreanine and *N*-acetylisoputreanine-ɣ-lactam.

4.3 Results

Chromatography

A chromatographic method previously developed for the targeted detection of polyamine metabolites was assessed for analysis of *N*-acetylisoputreanine and N^1, N^{12}-diacetylspermine[10,11]. This method used HFBA instead of FA as the ion pairing agent. HFBA increases the retention time of the positively charged polar polyamine metabolites by neutralizing their positive charge (decreasing the hydrophilicity) and increasing their affinity for the reversed-phase sorbent [16]. Addition of HFBA did increased the retention time of N^1, N^{12}-diacetylspermine from 2.7 to 11.9 minutes, however, it did not change the retention time of *N*-acetylisoputreanine (Figure 4.1). Thus, this chromatographic method (Method 2) along with the previously published chromatographic method (Method 1) were both used for the data collection [6].

Urine Samples

Typically, the creatinine concentration in each sample is used for normalization, however, creatinine can vary due to other factors aside from dilution [17]. In 1908, Shaffer stated that the amount of creatinine excreted in the urine depends primarily on an individual's body weight and that the amount excreted is not only uniform from day to day, but also throughout a 24 hour period independent of the volume excreted [18]. Based on these observations, it was concluded that creatinine is being constantly formed by a bodily process taking place largely in the muscles and that this process has little variation [18]. The consistency of creatinine regardless of volume led researchers to use this as a marker for completeness of urine excretion which could be used to minimize the effect of incomplete excretion or dilution on other excreted urinary metabolites [19]. However, numerous studies have shown that while creatinine excretion may be constant in some individuals, it is not constant in most and is not an adequate estimator

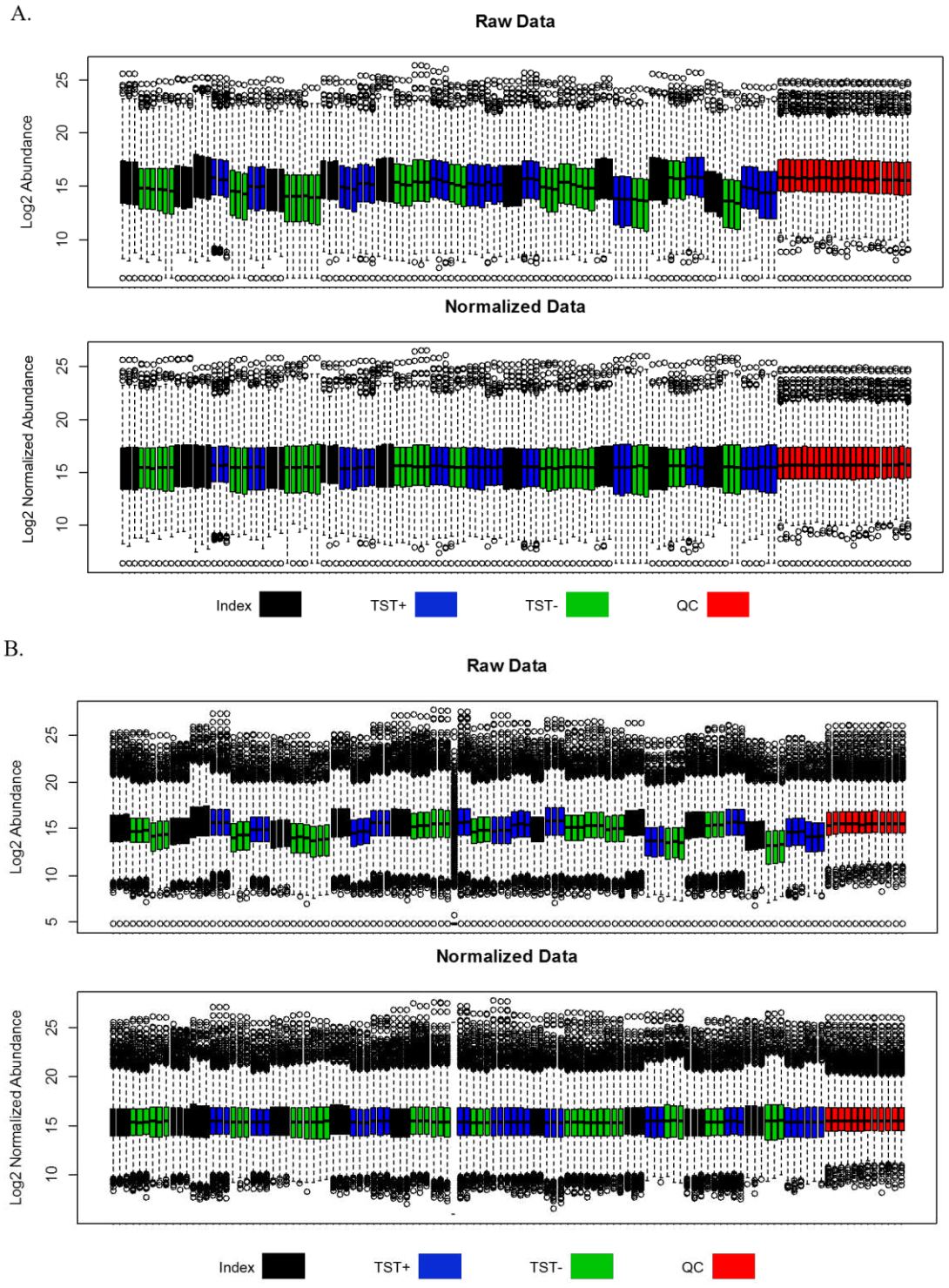

Figure 4.3
Box plots of the log2 abundances for the unnormalized data (Raw Data) and the data normalized with median fold change (Normalized Data) for Method 2 (A) and Method 1 (B).

abundance of all metabolites detected in a pooled QC sample to correct for the different urine concentrations in patient samples, was thought to be less biased and was used to correct for dilution variation amongst patient samples [14]. Figure 4.2 demonstrates the reduction in variability of samples after median fold change normalization. A log2 transformation of the normalized abundances for the metabolites of interest was used to bring them closer to a normal distribution for statistical analysis [14].

Method 1 was used for the analysis of *N*-acetylisoputreanine because inconsistent peak shapes were obtained in some patient urine samples using the Method 2 (data not shown). There was no significant difference between the abundances of *N*-acetylisoputreanine between all three groups (Figure 4.3). Method 2 was used for the analysis of N^1, N^{12}-diacetylspermine due to the increased retention time. The abundances of N^1, N^{12}-diacetylspermine in the index group were significantly higher than the TST- group (Figure 4.3). Since the retention time of *N*-acetylisoputreanine-γ-lactam was already increased using Method 1, the data obtained using this method were used for statistical analysis. The abundance of *N*-acetylisoputreanine-γ-lactam was significantly lower in the index group compared with the both TST- and TST+ household contacts (Figure 4.3). The data obtained from Method 1 was used for the statistical analysis of the glycosylated serine-leucine dipeptide. This peptide was significantly higher in index patients compared with both TST- and TST+ household contacts (Figure 4.3). Though there were some significant differences between index patients and household contacts, none of the metabolites of interest were significantly different between the two household contact groups (Figure 4.3).

Tissue Samples

Initially, the molecular features present in the LC-MS data were extracted and processed as described for the urine. However, the metabolites of interest were not present in the list of

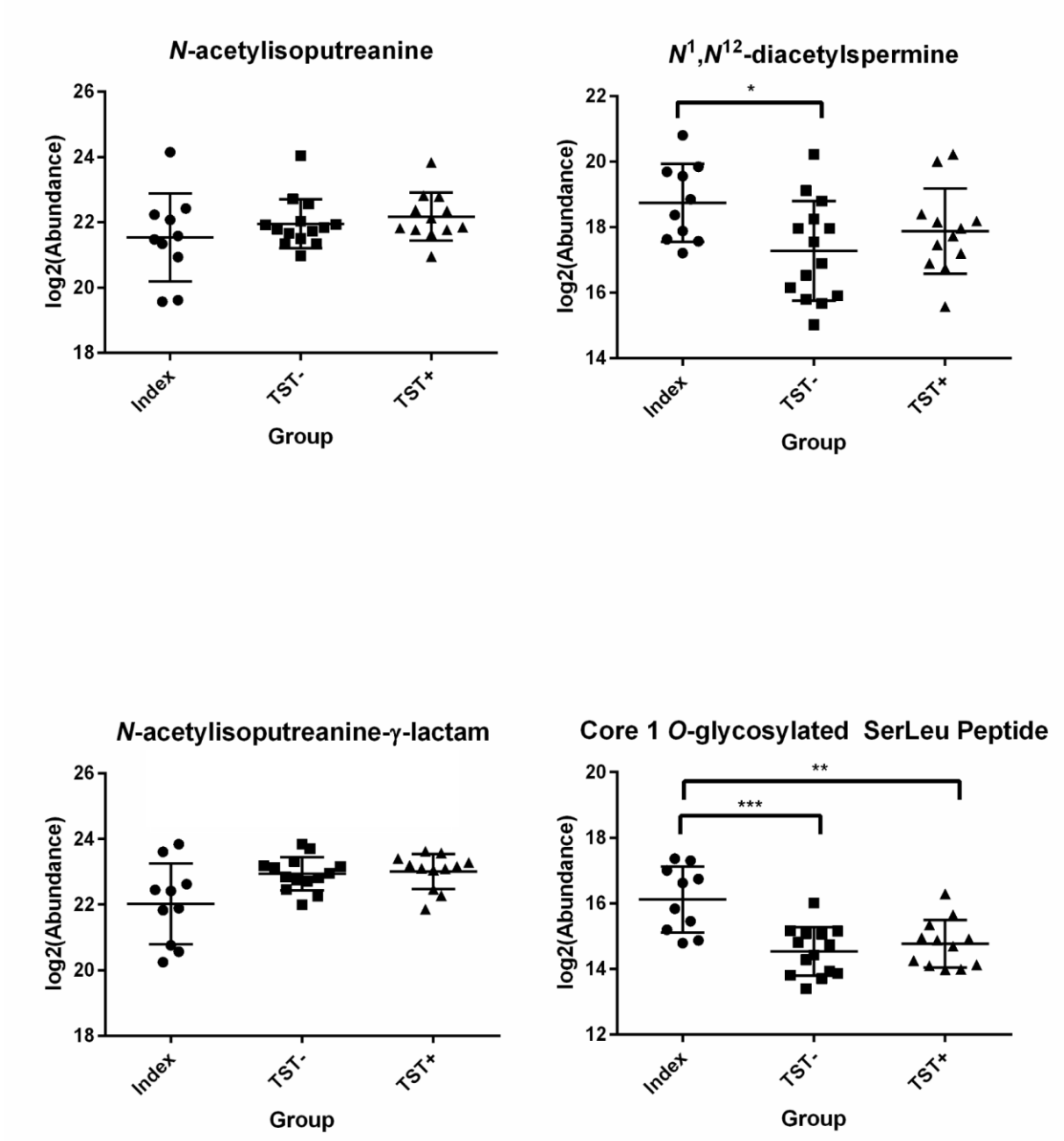

Figure 4.5
Column scatter graphs for quantified metabolites in urine. Each point represents the log2 abundance for a single patient. Data are shown as the mean ± SD and are representative of one experiment. *p<0.05, **p<0.01, ***p<0.001

filtered molecular features. The MassHunter Quantitative software was used for detection and integration of target peaks and to obtain their abundances. Only *N*-acetylisoputreanine was detected in the samples using both chromatographic methods. Since Method 2 was not used for analysis of *N*-acetylisoputreanine in urine samples, the data from Method 1 was used for quantitation and statistical analysis of *N*-acetylisoputreanine in tissue samples. Using this method, the internal standard eluted early and had inconsistent peak shape, thus the abundances of *N*-acetylisoputreanine were only normalized to the total protein content of each sample. Figure 4.4 demonstrates *N*-acetylisoputreanine levels in the lung tissue of naïve mice compared to those 2 weeks and 4 weeks post infection with *Mtb* Erdman. There were not any significant differences between the groups.

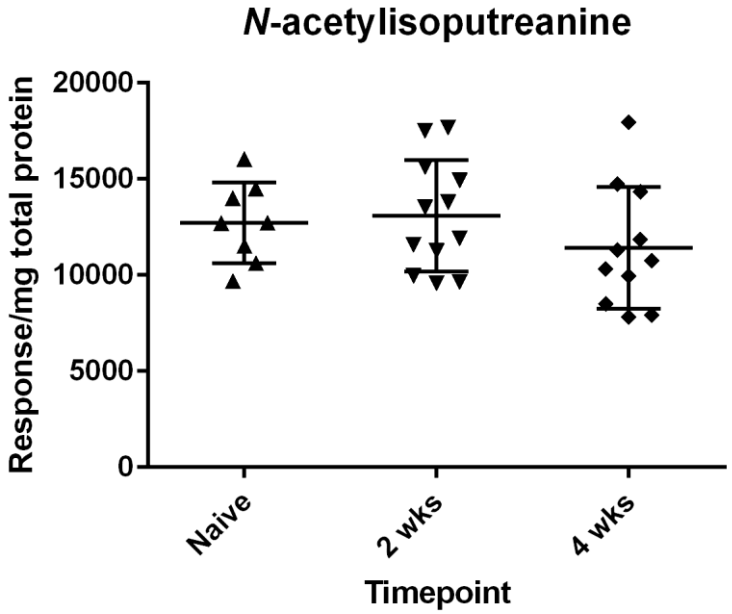

Figure 4.7
Column scatter graph for *N*-acetylisoputreanine in Balb/c mouse tissue. Each point represents response normalized to total protein content for a single sample. Data are shown as the mean ± SD and are representative of one experiment.

4.4 Discussion

The discovery of altered metabolites in untargeted metabolomics experiments warrants further mechanistic studies to determine the mechanisms behind their formation and whether they are actually suitable biomarkers for specified biological processes [1]. This chapter described preliminary mechanistic studies of four metabolites that are altered during anti-TB therapy. Relative LC-MS quantitation of *N*-acetylisoputreanine, *N*-acetylisoputreanine-γ-lactam, N^1, N^{12}-diacetylspermine, and the *O*-glycosylated SerLeu peptide in *Mtb* infected humans and mice helped to elucidate whether these metabolites were altered during active TB disease and should be pursued as adequate markers of resolution of infection during anti-TB treatment.

The structural characterization of *N*-acetylisoputreanine and N^1, N^{12}-diacetylspermine in Chapter 3 indicated that polyamine catabolism was altered during anti-TB treatment. These metabolites were quantified in the urine of tuberculosis patients and household contacts to assess changes in polyamine catabolism during active disease. Significantly increased levels of N^1, N^{12}-diacetylspermine were observed in tuberculosis patients relative to TST- household contacts, suggesting that polyamine catabolism is altered (Fig 4.3). In contrast, the levels of *N*-acetylisoputreanine and *N*-acetylisoputreanine-γ-lactam, other polyamine catabolites, were not significantly different between active tuberculosis patients and household contacts nor infected and uninfected mice (Fig 4.3 and 4.4). This incongruity highlights the complexity of metabolic pathways and the importance in determining the functional roles of individual metabolites.

Though these three metabolites are all terminal polyamine catabolites, different enzymes are involved in their formation [23]. Formation of all three metabolites is initiated with acetylation by spermidine/spermine *N*-acetyltransferase (SSAT) [23]. Further acetylation of *N*-acetylspermine by SSAT yields N^1, N^{12}-diacetylspermine [23]. While two additional enzymes are needed for the

formation of *N*-acetylisoputreanine and *N*-acetylisoputreanine-γ-lactam from *N*-acetylspermidine, diamine oxidase (DAO) and aldehyde dehydrogenase (ADH) [23]. One possible explanation for their different trends is that SSAT activity is upregulated in TB patients resulting in increased levels of N^1, N^{12}-diacetylspermine, while DAO and ADH activity remains unchanged. Reactive oxygen species and TNF-α, both present during *Mtb* infection, have been shown to increase expression of SSAT in cancer cell lines[24,25]. The human genome contains 19 putatively functional ADH genes and the specific ADH involved in formation of *N*-acetylisoputreanine and *N*-acetylisoputreanine-γ-lactam has not been defined [26]. It is possible that two separate, differentially regulated ADH enzymes are involved in the formation of *N*-acetylisoputreanine and *N*-acetylisoputreanine-γ-lactam which could explain why *N*-acetylisoputreanine-γ-lactam was not previously detected as significantly decreasing during anti-TB treatment [6]. Additionally, administration of INH to TB patients can cause histamine toxicity due to its inhibition of DAO and monoamine oxidase which prevents metabolism of histamine[27-29]. Thus, DAO activity might be unchanged during active TB, but during treatment with INH, there might be inhibition of *N*-acetylisoputreanine formation resulting in decreased levels. Further assessment of metabolic enzymes including SSAT and DAO and other acetylated polyamine metabolites during tuberculosis are needed to decipher the mechanisms behind alterations in polyamine catabolism during TB and anti-TB treatment.

The assessment of the *O*-glycosylated SerLeu peptide revealed a significant increase in active TB patients relative to both TST+ and TST- household contacts. Thus, the decrease in this metabolite during treatment could be due to the resolution of infection. However, this hypothesis is difficult to test as the origin of this metabolite has not been confirmed. Despite not knowing the pathways involved, this chapter confirmed the *O*-glycosylated SerLeu peptide as a biomarker

of active TB disease in addition to successful treatment outcome. Further validation of this metabolite using a larger set of patient samples representing different stages of disease and treatment outcomes is needed.

This was a preliminary experiment to assess the levels of metabolites in *Mtb* infected tissues and the detection of only *N*-acetylisoputreanine and none of the other targeted metabolites was unexpected. This could be due to the extraction protocol and analysis methods. The metabolites of interest are polar, thus an 80% methanol extraction protocol was used based on previously published methods[8,9]. Though homogenization via bead beating and methanol extraction have been shown to efficiently extract polar metabolites from tissue, other extraction methods need to be evaluated to determine which provides the best yield of the metabolites targeted in this chapter. Previously, N^1, N^{12}-diacetylspermine was detected and quantified in the tissues of human colon cancer patients demonstrating that it can be extracted and detected from human tissue [5]. Thus, the limited detection of N^1, N^{12}-diacetylspermine in this chapter might be due using whole lungs as opposed to separating out affected and unaffected tissues. The levels of N^1, N^{12}-diacetylspermine in healthy human urine are extremely low, approximately 0.5% of total excreted polyamines [30]. Thus, the levels in healthy tissue might be even less and by combining affected and unaffected tissue, any increase in N^1, N^{12}-diacetylspermine may have been diluted out. A more targeted method such as ELISA or MRM may improve the detection of low abundance metabolites. Additionally, another model could aid in assessing unaffected vs. affected tissue such as non-human primates which have more defined granulomas similar to those seen in humans [31].

Another possible explanation is that these metabolites are not produced at the site of infection. Degradation of both C1INH and fibrinogen, potential sources of the glycopeptide,

generally occurs in the liver, kidneys or urine. C1INH, at the site of infection, binds to its target proteases and this complex is removed from circulation through receptor-mediated endocytosis, resulting in degradation and excretion in the urine [32]. Fibrinogen can be degraded during fibrinolysis which can occur at the site of infection or in other organs, even in the urine[33,34].

Another limitation of this study was not including a healthy control group. The household contacts were samples representative of patients without active TB, however, at the time of diagnosis, they may have been infected but not reactive as it can take three to eight weeks to convert to tuberculin reactivity [35]. Another study in Uganda reported that 6% of household contacts developed active disease and that the majority of these cases were in children under 5 years of age [36]. N^1, N^{12}-diacetylspermine levels in healthy individuals are typically very low [30]. This chapter reported similar levels of N^1, N^{12}-diacetylspermine detected in both active TB patients and household contacts, which could indicate that the household contacts are not healthy or that the levels in active TB patients are not substantially increased. During biomarker validation, household contacts are essential for confirming those robust, differential metabolites, however, during mechanistic studies, a confirmed healthy control group would be beneficial. Inclusion of a healthy control group and a more quantitative method, such as a MRM, is needed to determine how these metabolites are altered during active TB.

These preliminary mechanistic experiments demonstrated a potential association between the core 1 *O*-glycosylated peptide and N^1, N^{12}-diacetylspermine with TB disease pathology and bacterial burden indicating that they will be robust biomarkers for monitoring anti-TB treatment and should be pursued further during validation studies. On the other hand, *N*-acetylisoputreanine was not significantly associated with *Mtb* infection and might be a marker of

off-target drug interactions during anti-TB treatment and will most likely not be a robust biomarker for monitoring anti-TB treatment.

REFERENCES

1. Johnson CH, Ivanisevic J, Siuzdak G. Metabolomics: beyond biomarkers and towards mechanisms. Nat Rev Mol Cell Biol 2016;17(7):451-9.
2. Shin SY, Fauman EB, Petersen AK, Krumsiek J, Santos R, Huang J, Arnold M, Erte I, Forgetta V, Yang TP and others. An atlas of genetic influences on human blood metabolites. Nat Genet 2014;46(6):543-50.
3. Sellers K, Fox MP, Bousamra M, Slone SP, Higashi RM, Miller DM, Wang Y, Yan J, Yuneva MO, Deshpande R and others. Pyruvate carboxylase is critical for non-small-cell lung cancer proliferation. J Clin Invest 2015;125(2):687-98.
4. O'Keefe SJ, Li JV, Lahti L, Ou J, Carbonero F, Mohammed K, Posma JM, Kinross J, Wahl E, Ruder E and others. Fat, fibre and cancer risk in African Americans and rural Africans. Nat Commun 2015;6:6342.
5. Johnson CH, Dejea CM, Edler D, Hoang LT, Santidrian AF, Felding BH, Ivanisevic J, Cho K, Wick EC, Hechenbleikner EM and others. Metabolism links bacterial biofilms and colon carcinogenesis. Cell Metab 2015;21(6):891-7.
6. Mahapatra S, Hess AM, Johnson JL, Eisenach KD, DeGroote MA, Gitta P, Joloba ML, Kaplan G, Walzl G, Boom WH and others. A metabolic biosignature of early response to anti-tuberculosis treatment. BMC Infect Dis 2014;14:53.
7. Want EJ, Wilson ID, Gika H, Theodoridis G, Plumb RS, Shockcor J, Holmes E, Nicholson JK. Global metabolic profiling procedures for urine using UPLC-MS. Nature Protocols 2010;5(6):1005-1008.
8. Metabolomic Extraction Protocols Johnson C. YouTube2015.
9. Want EJ, Masson P, Michopoulos F, Wilson ID, Theodoridis G, Plumb RS, Shockcor J, Loftus N, Holmes E, Nicholson JK. Global metabolic profiling of animal and human tissues via UPLC-MS. Nature Protocols 2013;8(1):17-32.
10. Häkkinen MR. Polyamine analysis by LC-MS. Methods Mol Biol 2011;720:505-18.
11. Häkkinen MR, Roine A, Auriola S, Tuokko A, Veskimäe E, Keinänen TA, Lehtimäki T, Oksala N, Vepsäläinen J. Analysis of free, mono- and diacetylated polyamines from human urine by LC-MS/MS. J Chromatogr B Analyt Technol Biomed Life Sci 2013;941:81-9.
12. Mahapatra S, Hess AM, Johnson JL, Eisenach KD, DeGroote MA, Gitta P, Joloba ML, Kaplan G, Walzl G, Boom WH and others. A metabolic biosignature of early response to anti-tuberculosis treatment. BMC Infectious Diseases 2014 14(1):53.
13. Molins CR, Ashton LV, Wormser GP, Hess AM, Delorey MJ, Mahapatra S, Schriefer ME, Belisle JT. Development of a Metabolic Biosignature for Detection of Early Lyme Disease. Clinical Infectious Diseases 2015;60(12):1767-1775.
14. Veselkov KA, Vingara LK, Masson P, Robinette SL, Want E, Li JV, Barton RH, Boursier-Neyret C, Walther B, Ebbels TM and others. Optimized preprocessing of ultra-performance liquid chromatography/mass spectrometry urinary metabolic profiles for improved information recovery. Anal Chem 2011;83(15):5864-72.
15. Team RC. R: A language and environment for statistical computing. . Vienna, Austria: R Foundation for Statistical Computing; 2013.

16. Shibue M, Mant CT, Hodges RS. Effect of anionic ion-pairing reagent hydrophobicity on selectivity of peptide separations by reversed-phase liquid chromatography. J Chromatogr A 2005;1080(1):68-75.
17. Ram MM, Reddy V. Variability in urinary creatinine. Lancet 1970;2(7674):674.
18. Shaffer P. The excretion of kreatinin and kreatin in health and disease. American Journal of Physiology 1908;23(1):1-22.
19. Vestergaard P, Leverett R. CONSTANCY OF URINARY CREATININE EXCRETION. Journal of Laboratory and Clinical Medicine 1958;51(2):211-218.
20. Alessio L, Berlin A, Dellorto A, Toffoletto F, Ghezzi I. RELIABILITY OF URINARY CREATININE AS A PARAMETER USED TO ADJUST VALUES OF URINARY BIOLOGICAL INDICATORS. International Archives of Occupational and Environmental Health 1985;55(2):99-106.
21. Curtis G, Fogel M. CREATININE EXCRETION - DIURNAL VARIATION AND VARIABILITY OF WHOLE AND PART-DAY MEASURES - A METHODOLOGIC ISSUE IN PSYCHOENDOCRINE RESEARCH. Psychosomatic Medicine 1970;32(4):337-&.
22. James GD, Sealey JE, Alderman M, Ljungman S, Mueller FB, Pecker MS, Laragh JH. A LONGITUDINAL-STUDY OF URINARY CREATININE AND CREATININE CLEARANCE IN NORMAL SUBJECTS - RACE, SEX, AND AGE-DIFFERENCES. American Journal of Hypertension 1988;1(2):124-131.
23. Seiler N. Catabolism of polyamines. Amino Acids 2004;26(3):217-33.
24. Babbar N, Hacker A, Huang Y, Casero RA. Tumor necrosis factor alpha induces spermidine/spermine N1-acetyltransferase through nuclear factor kappaB in non-small cell lung cancer cells. J Biol Chem 2006;281(34):24182-92.
25. Chopra S, Wallace HM. Induction of spermidine/spermine N1-acetyltransferase in human cancer cells in response to increased production of reactive oxygen species. Biochem Pharmacol 1998;55(7):1119-23.
26. Vasiliou V, Nebert DW. Analysis and update of the human aldehyde dehydrogenase (ALDH) gene family. Hum Genomics 2005;2(2):138-43.
27. Baciewicz AM, Self TH. Isoniazid interactions. South Med J 1985;78(6):714-8.
28. Kaneko T, Ishigatsubo Y. Isoniazid and food interactions: --fish, cheese, and wine. Intern Med 2005;44(11):1120-1.
29. Morinaga S, Kawasaki A, Hirata H, Suzuki S, Mizushima Y. Histamine poisoning after ingestion of spoiled raw tuna in a patient taking isoniazid. Intern Med 1997;36(3):198-200.
30. Hiramatsu K, Sugimoto M, Kamei S, Hoshino M, Kinoshita K, Iwasaki K, Kawakita M. Determination of amounts of polyamines excreted in urine: demonstration of N1,N8-diacetylspermidine and N1,N12-diacetylspermine as components commonly occurring in normal human urine. J Biochem 1995;117(1):107-12.
31. Flynn JL, Capuano SV, Croix D, Pawar S, Myers A, Zinovik A, Klein E. Non-human primates: a model for tuberculosis research. Tuberculosis 2003;83(1-3):116-118.
32. Storm D, Herz J, Trinder P, Loos M. C1 inhibitor-C1s complexes are internalized and degraded by the low density lipoprotein receptor-related protein. J Biol Chem 1997;272(49):31043-50.

33. Kwaan HC, Barlow GH. NATURE AND BIOLOGICAL-ACTIVITIES OF DEGRADATION PRODUCTS OF FIBRINOGEN AND FIBRIN. Annual Review of Medicine 1973;24:335-344.
34. Pacchiarotta T, Hensbergen PJ, Wuhrer M, van Nieuwkoop C, Nevedomskaya E, Derks RJ, Schoenmaker B, Koeleman CA, van Dissel J, Deelder AM and others. Fibrinogen alpha chain O-glycopeptides as possible markers of urinary tract infection. J Proteomics 2012;75(3):1067-73.
35. Smith I. Mycobacterium tuberculosis pathogenesis and molecular determinants of virulence. Clin Microbiol Rev 2003;16(3):463-96.
36. Guwatudde D, Nakakeeto M, Jones-Lopez EC, Maganda A, Chiunda A, Mugerwa RD, Ellner JJ, Bukenya G, Whalen CC. Tuberculosis in household contacts of infectious cases in Kampala, Uganda. Am J Epidemiol 2003;158(9):887-98.

CHAPTER 5: MRM ASSAY DEVELOPMENT

5.1 Introduction

Untargeted LC-MS metabolomics experiments have been successful in detecting altered host metabolites that could aid in TB diagnosis and treatment response monitoring[1-5]. However, confirmation of these alterations and their utility as biomarkers using targeted techniques and independent patient populations has not been completed. This lack of confirmation is a major impediment in the development of clinically useful biosignatures for diagnosis and treatment outcome prediction.

This lack of biomarker qualification is apparent in other metabolic biomarker studies as well, with very few research groups validating metabolites identified in the discovery phase [6]. Berger *et al.* detected a differentiating metabolite, in an untargeted metabolomics experiment, of children with acute kidney injury[7]. This metabolite was identified as homovanillic acid sulfate and further validated using an independent set of patient samples and selected reaction monitoring (SRM)[7]. A separate study to identify and assess biomarkers for epithelium ovarian cancer, identified six differentiating metabolites, however, only one remained significant after validation using single ion monitoring (SIM) in a larger patient set[8]. Validation using a SRM method for 52 differentiating metabolites esophageal squamous cell carcinoma with the same set of samples used for discovery, reduced the number of differentiating metabolites to 32 [9]. Validation of differentiating metabolites detected in untargeted experiments reveals which candidates are true biomarkers for the pathologies of interest and brings these metabolites closer to clinical applications.

A common targeted MS based technique for validation of differentiating metabolites is utilizing MS/MS data for exact or relative quantification. This includes SRM or more commonly multiple reaction monitoring (MRM) [10]. Reaction monitoring increases the sensitivity for the particular molecules of interest by targeting specific parent to fragment ion transitions simultaneously which improves the signal to noise ratio [10]. MRM methods have been developed for different classes of compounds to assess vitamin deficiency, inborn errors in metabolism, and xenobiotics[11-16]. The increased specificity and sensitivity make MRM ideal for the validation of differentiating metabolites identified in untargeted metabolomics experiments.

Previously, thirteen urinary metabolites were highlighted as potential biomarkers for anti-TB treatment response due to their decreased abundance following two weeks of treatment (Mahapatra, S., CSU, unpublished data). Validation of these analytes as biomarkers requires quantification of these analytes in a larger and more diverse patient cohort. However, a quantitative method containing all thirteen of these metabolites has not been previously developed. This chapter describes the development of a quantitative MRM assay for quick, selective, and sensitive quantification of all thirteen urinary metabolites in a single run. Development of this method will enable confirmation of the hypothesis that the biomarker discovery methods were robust and that these metabolites are good prognostic biomarkers for successful treatment response outcomes in TB patients.

5.2 Materials and Methods

Chemicals

Analyte standards, analyte structural analogs and creatinine were obtained from Sigma-Aldrich (St. Louis, MO, USA). Stable isotope-labelled analytes were obtained from CDN Isotopes (Pointe-Claire, Quebec, Canada). All solutions were prepared using LC-MS grade water

and LC-MS grade methanol (Honeywell Burdick & Jackson, Muskegon, MI). Formic Acid (FA), sodium phosphate monobasic, sodium phosphate dibasic, and sodium hydroxide were obtained from Fischer Scientific (Pittsburg, PA, USA). Sodium chloride was obtained from J.T. Baker. Urea was obtained from GE Healthcare Bio-sciences AB (Uppsala, Sweden). Human Urine used as a control was obtained from Gemini Bio-Products (West Sacramento, CA, USA).

Patient Samples

Patient urine samples were obtained from the tuberculosis research unit (TBRU) NAA2m study (DMID 08-0023) conducted in Uganda [1]. These samples consisted of urine from ten patients taken at four different time points; TB diagnosis (D0), week 2 (W2), week 8 (W8) and month 6 (M6).

Sterile-filtered (0.2μm) commercial control human urine from normal healthy male donors was obtained from Gemini BioProducts (West Sacramento, CA).

Analytical Standards

A 10mM stock solution of each analyte and internal standard was prepared individually in 0.1% FA. Synthetic urine was prepared as previously described without sodium azide or yellow food coloring [17]. The calibration stock solution contained a mixture of all analytes in synthetic urine at a concentration of 100μM, except for N-acetyl cysteine (10 μM). Using the calibration stock solution, subsequent dilutions were made to get the different calibration standards (0.1-100μM). The quality control (QC) stock solution for method validation was prepared in synthetic urine containing 40μM of trigonelline, 15μM of N-acetyl cysteine, and 150μM of all other analytes. This stock solution was diluted further in synthetic urine to obtain the QC standards. The internal standard (IS) stock solution contained 200μM of d_3-hydroxyproline, 25μM of d_5-phenylalanine, 25μM of d_4-tyrosine, and 25μM of dimethylaspartic

acid in 0.1% FA. Prior to LC-MS/MS analysis, 10µl of IS stock solution was added to 100µl of each calibration standard and QC standard in autosampler vials with 200µl insert using a Hamilton syringe and stored at -20˚C (maximum of three days).

Creatinine Concentration Determination

Patient sample urine was diluted 1:10,000 in 0.1% formic acid in water. After dilution, samples were vortexed and stored at either 4˚C (less than 24 hours) or -20˚C (more than 24 hours) prior to LC-MS/MS analysis. Creatinine concentration for each sample was determined by Greg Dooley (CSU) using an Agilent 6460 series Triple Quadrupole Mass Spectrometer. Briefly, the instrument parameters were as follows: gas temp (250˚C), gas flow (10L/min), nebulizer (25 psi), sheath gas heater (375˚C), sheath gas flow (10L), capillary voltage (4000 V). The instrument was operated in dynamic multiple reaction monitoring (DMRM) mode and the two transitions monitored were 114.1>86 and 114.1 > 44.1.

Sample preparation for LC-MS/MS analysis

Patient samples were stored at -80˚C and thawed on ice. Samples were vortex mixed and 125, 75 or 30µl were transferred to microcentrifuge tubes containing either 0, 75 or 120µl of synthetic urine resulting in three dilutions; undiluted, 1:2 and 1:5. After dilution, urine samples were vortexed and centrifuged at 14,000 rpm using a Microfuge 2R centrifuge (Beckman Coulter) for 15 minutes to remove any particulates. IS stock solution (10µl) was added to an aliquot (100µl) of clarified urine in autosampler vials containing 200µl insert using a Hamilton syringe. Urine samples were stored at -20˚C until LC-MS/MS analysis (maximum of three days).

Liquid chromatography conditions

Liquid chromatography was performed using an Agilent 1200 series LC system equipped with a Waters XSelect XP HSS T3 column (1.5x75mm, 2.5µm) at 30˚C. The gradient system

consisted of mobile phases buffer A: 0.1% FA and buffer B: 0.1% FA in methanol with a constant flow rate of 250µl/min. The gradient program used was: 100% buffer A for 0-3 min, a 2 min linear gradient to 10% buffer B, 2.5 min linear gradient to 90% buffer B, hold for 2 min at 90% buffer B, and a 1.5 min linear gradient to 100% buffer A. Equilibration time between each run was 5 min at 100% buffer A. The sample injection volume was 2.5µl.

MS/MS conditions

Method optimization and MS experiments were performed using an Agilent 6460 series Triple Quadrupole Mass Spectrometer. The mass spectrometer was equipped with an electrospray ionization source operated in positive mode. The ion source parameters consisted of gas temp (300˚C), gas flow (8L/min), nebulizer (35 psi), sheath gas heater (350˚C), sheath gas flow (11L), capillary voltage (3500 V). The instrument was operated in dynamic multiple reaction monitoring mode (DMRM). Direct infusion of a 10µM stock of commercial standards for each analyte was used to optimize the collision energy and fragmentor voltage were by means of the Optimizer Software (Agilent Technologies). MRM transitions were chosen based on abundance of the fragment ions using these optimized parameters. The transitions monitored and the optimized MS/MS parameters are listed in Table 5.1.

Data Processing of Patient Urine Samples

LC-MS/MS data were processed with the Agilent MassHunter Quantitative Analysis software version B.05.02. Each batch of samples were analyzed separately. The calibration standards run prior to each batch were used to generate the calibration curves. The response or peak area for each analyte and internal standard in every sample was obtained using the Agilent MassHunter Quantitative Analysis software to integrate peak for the quantifier transitions. An example of this integration and the calibration curve generated for *N*-acetylaspartic acid is seen

in Figure 5.1A and B. The software's integration was manually inspected and if integration was not consistent, peaks were manually integrated to maintain consistency. For example if there was a split peak as seen in Figure 5.1C and the software integrated both peaks in the one sample and only one peak in all other samples, then the integration would be manually changed to correspond to all the other samples. Additionally, the qualifier ion was used to help with integration and removal of samples for individual analytes. As seen in the left box of Figure 5.1C, the ratio between the quantifier and qualifier transitions is 85.9 for the 5μM alpha amino adipic acid calibration standard. Correspondingly, the ratio between the quantifier and qualifier transitions is 85.4 for patient sample NM7855 providing confidence in the integration and that the left peak does in fact belong to alpha amino adipic acid. However, in patient sample NM7842, the ratio between the quantifier and qualifier transitions is 247.3 which is extremely higher than the expected ratio and justifies removal of this sample from the analysis for this analyte.

Response ratios were generated by dividing the analyte response by the response of the internal standard. The response ratios for the calibration standards were plotted against concentration to generate a calibration curve (Fig 5.1B).The response ratios for the samples were converted into concentrations using the slope and y-intercept derived from the calibration curves for each analyte (Table 5.2). The calculated concentrations were then multiplied by the dilution factor to obtain the final concentrations for each analyte. Individual measurements that were outside the linear range of the calibration curve were removed from the analysis. The values from the 1:5 dilution were used for quantification, however, if these values fell outside the linear range, the next highest dilution within the linear range value was used. Data were normalized according to calculated creatinine concentration for each sample. Patients that had an analyte

value outside quantifiable limits at any time point were not included in statistical analysis for that analyte. One way ANOVA with repeated measures and multiple comparisons were used to test if there was any significant differences between the groups. Statistical analyses of the normalized abundances for each analyte were performed using GraphPad Prism version 6.04 for Windows (GraphPad Software, La Jolla California USA).

5.3 Results

Optimizing Method Parameters

MRM transitions

The fragment ion with the highest abundance using the optimized MS condition was chosen as the quantifier transition and was used for analyte concentration calculations. The second most abundant ion that differed by more than 2 amu was selected as the qualifier transition and was used to validate that the peak belonged to the targeted analyte. Both quantifier and qualifier transitions needed to be present in order to confirm and quantify target analytes. Based on the structure of quinolinic acid and alpha amino adipic acid, negative ionization mode was also assessed during optimization of MS parameters, however, these analytes performed better in positive ionization mode, so this mode was used for all analytes. All MRM transitions depicted in Table 5.1 are monitored using positive mode.

Chromatography

Separation of multiple compounds with differing polarities is challenging. Using the previously published chromatographic method, highly polar compounds eluted within 4 min indicating minimal interaction with the column [1]. Several assessments were performed to improve the retention and separation of the targeted polar compounds listed in Table 5.1 using reversed phase chromatography. Specifically, an Agilent ZORBAX SB-Aq column was assessed, however, retention was not improved compared with the Waters Atlantis T3 column

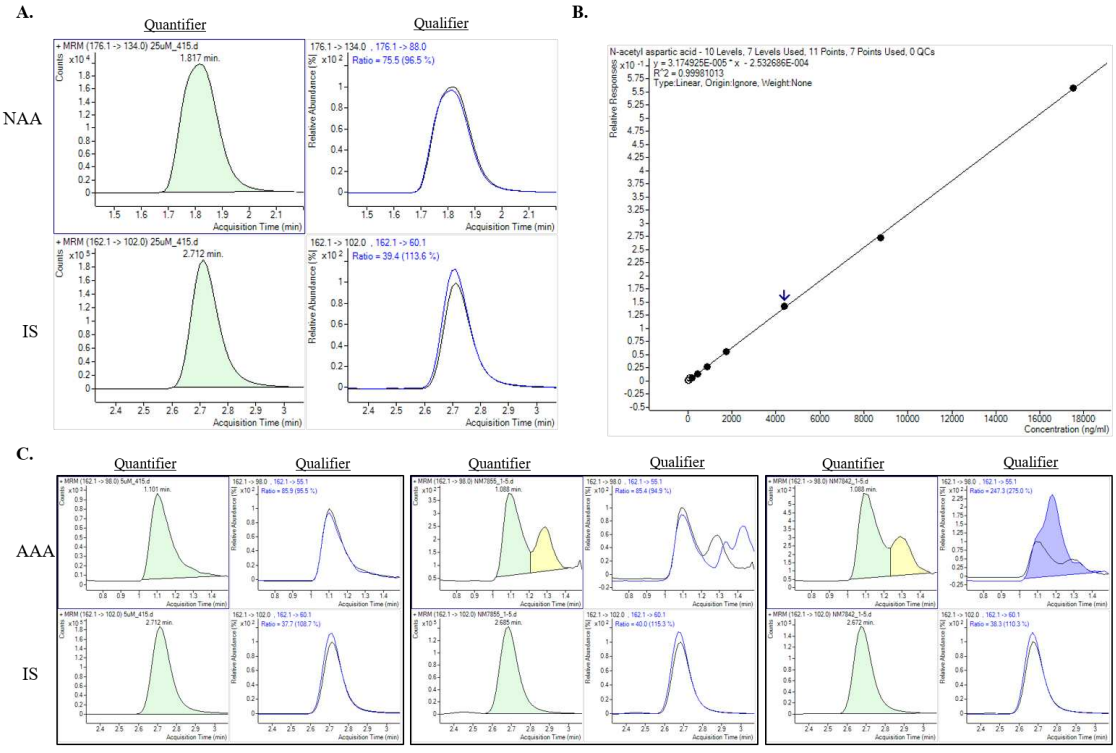

*NAA-*N*-acetylaspartic acid; AAA- alpha amino adipic acid; IS – internal standard

Figure 5.1 Data Analysis Example.
A. The quantifier (top left) and qualifier (top right) transitions for 25µM *N*-acetylaspartic acid calibration standard and the quantifier (bottom left) and qualifier (bottom right) transitions for the internal standard dimethyl aspartic acid. **B.** The calibration curve for *N*-acetylaspartic acid with response ratios plotted on the y-axis and concentrations in ng/mL plotted on the x-axis. **C.** The quantifier (top left of each box) and qualifier (top right of each box) transitions for alpha amino adipic acid in the 5µM calibration standard (left box), NM7855 patient sample (middle box), and NM7842 patient sample (right box). The qualifier and quantifier transitions for the internal standard dimethyl aspartic acid are shown in the bottom left and bottom right of each box.

from the previously published method. Ammonium formate was tested as an alternative ion pairing agent since it might improve peak shape and retention time [18]. While, ammonium formate increased sensitivity of analytes using the ZORBAX SB-Aq column, however, it did not result in an increased retention time. Using the Atlantis T3 column, AF resulted in decreased sensitivity for some compounds and didn't increase the retention time of early eluting polar compounds compared with FA. While, the Atlantis T3 column from the previous method performed best, a shorter column (Waters XSelect HSS T3, 1x75mm, 2.5µm) with similar column chemistry was assessed to shorten run time. This column maintained the chromatographic separation of all compounds with a total run time 15 minutes versus 33 minutes using the longer column and enabled measurement of all analytes in 4 patient samples per hour. Analytes in synthetic urine and commercial urine were assessed before defining the retention time windows for DMRM. A chromatogram for all analytes using this chromatographic method is depicted in Figure 5.2.

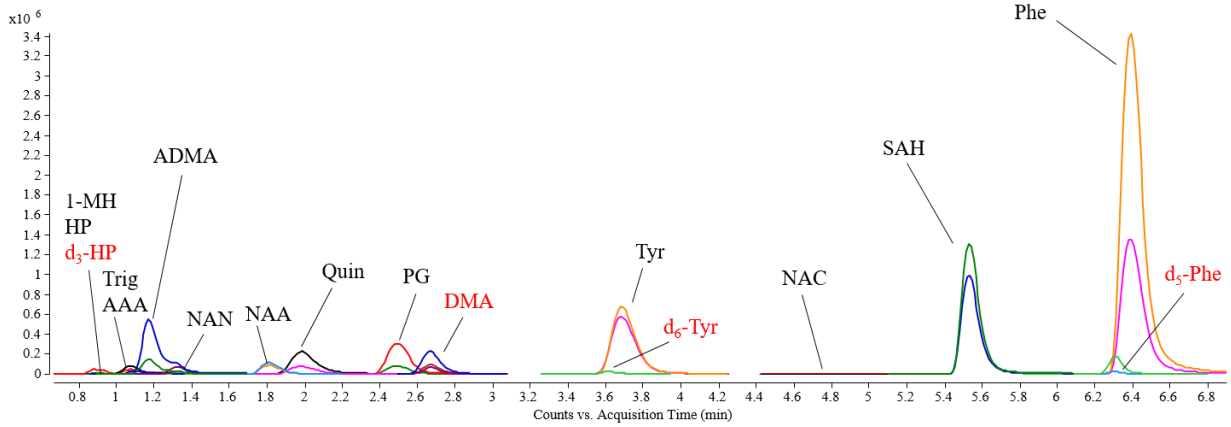

Figure 5.3
Extracted ion chromatograms of the MRM of a 100µM mixture containing all thirteen analytes. Each peak represents the quantifier and qualifier transitions monitored for each analyte. The analytes in red are the internal standards.

1-MH-1-methylhistidine; HP-hydroxyproline; Trig-trigonelline; AAA- alpha amino adipic acid; ADMA-asymmetric dimethyl arginine; NAN-N-acetyl asparagine; NAA-N-acetyl aspartic acid; Quin-quinolinic acid; PG-pyroglutamic acid; DMA-dimethyl aspartic acid; Tyr-tyrosine; NAC-N-acetylcysteine; SAH-S-adenosylhomocysteine; Phe-phenylalanine

Internal Standards

Ideally, stable isotope labeled standards would be obtained for each individual analyte. However, this was not feasible due to cost and availability, so only stable isotope labelled hydroxyproline, tyrosine and phenylalanine were used. Non-endogenous amino acid derivatives, 4-fluoro-D,L-glutamic acid, L-aspartic acid dimethylester, and N, N-dimethylphenylalanine with structural similarity to some of the target analytes were assessed in order to find additional IS. Of these, only L-aspartic acid dimethylester had a retention time near target analytes and did not have interfering signal or was not endogenously present. 4-fluoro-D,L-glutamic acid did not ionize well and the retention time for N, N-dimethylphenylalanine was not near any of the target analytes. The internal standards were assigned to target analytes based on close retention time and similar behavior during method validation (Table 5.1). Due to significant ion suppression, d_3-hydroxyproline was only used as the internal standard for hydroxyproline.

Method Validation

Once the MS/MS conditions, chromatography and internal standards were optimized, method validation was performed.

Method Linearity

Linear range of quantification was assessed using synthetic urine spiked at a final concentration of 100 µM for each analyte, except *N*-acetylcysteine (10µM). These were diluted serially with synthetic urine in triplicate to achieve at least 10 concentration levels ranging from 0.1-100µM.or 0.01-10µM for *N*-acetylcysteine. Lower and upper limits of quantification corresponded to the lowest and highest concentration level falling within linear range (Table 5.2) [19].

Linear calibration curves with a regression coefficient (r^2) greater than 0.99 were obtained for all analytes in synthetic urine covering at least one order of magnitude (Table 5.2). The slope and y-intercept listed in Table 5.2 were obtained from the MassHunter Quantitative Analysis software and used to calculate the concentration of each analyte. Calculated concentrations for analytes at each concentration level in the defined linear range were within 20% of expected value (Table 5.2).

Table 5.1

Monitored MS/MS ion transitions, optimized MS parameters, and retention times of target analytes. [a]Qualifier Transition

Analyte	Internal Standard	Precursor Ion	Product Ion	Fragmentor (V)	Collision Energy (V)	Retention Time (min)
1-Methylhistidine	Aspartic Acid Dimethyl Ester	170.1	124.1[a]	66	12	0.92
			81		48	
Hydroxyproline	d_3-Hydroxyproline	132.1	86.1[a]	51	12	0.96
			68.1		20	
Trigonelline	Aspartic Acid Dimethyl Ester	138.1	92	123	24	1.1
			65.1[a]		36	
Dimethyl Arginine	Aspartic Acid Dimethyl Ester	203.1	88.1	81	12	1.25
			70.1[a]		24	
α-Amino adipic Acid	Aspartic Acid Dimethyl Ester	162.1	98[a]	56	12	1.1
			55.1		28	
N-acetyl Asparagine	Aspartic Acid Dimethyl Ester	175.1	158	61	4	1.35
			88[a]		12	
N-acetyl Aspartic Acid	Aspartic Acid Dimethyl Ester	176.1	134[a]	66	4	1.82
			88		12	
Quinolinic Acid	d_4-Tyrosine	168	106[a]	66	12	2
			78.1		24	
Pyroglutamic Acid	d_4-Tyrosine	130	84[a]	97	12	2.45
			56.1		28	
Tyrosine	d_4-Tyrosine	182.1	136[a]	81	12	3.75
			91		32	
N-acetyl Cysteine	d_4-Tyrosine	164	122[a]	61	4	4.7
			76		20	
S-adenosylhomocysteine	d_5-Phenylalanine	385.1	136[a]	87	16	5.6
			88		48	
Phenylalanine	d_5-Phenylalanine	166.1	120[a]	66	12	6.4
			77		44	

Table 5.2 Calibration Model

Analyte	Linear range (µM)	Slope	Intercept	Regression Coefficient
1-Methylhistidine	0.50 – 5.00	3.96E-05	-1.03E-05	0.9958
Hydroxyproline	2.50 – 100.00	6.38E-04	6.18E-02	0.9975
Trigonelline	0.50 – 50.00	2.06E-05	-4.17E-06	0.9989
Dimethyl Arginine	1.00 – 25.00	1.97E-04	1.07E-02	0.9961
α-Amino adipic Acid	0.50 - 50	1.58E-05	-1.19E-04	0.9995
N-acetyl Asparagine	1.00 – 50.00	8.98E-06	-4.13E-04	0.9989
N-acetyl Aspartic Acid	1.00 – 50.00	5.37E-05	2.09E-03	0.9996
Quinolinic Acid	0.50 – 50.00	3.23E-04	-7.30E-03	0.9991
Pyroglutamic Acid	1.00 – 50.00	1.88E-03	3.90E-02	0.9986
Tyrosine	0.50 – 25.00	2.59E-03	2.04E-02	0.9987
N-acetyl Cysteine	0.03 – 2.50	9.69E-05	3.64E-05	0.9952
S-adenosylhomocysteine	1.00 – 50.00	2.91E-04	-5.48E-02	0.9954
Phenylalanine	0.25 – 10.00	2.78E-03	4.64E-02	0.9932

Precision and Accuracy

Assay precision and reproducibility were evaluated by spiking synthetic urine with 4 concentration levels of each analyte to achieve low and high concentrations. Concentration levels for all analytes except for N-acetylcysteine and trigonelline were 0.6, 3, 6 and 30 µM. Concentration levels for N-acetylcysteine were 0.06, 0.3, 0.6 and 3 µM and concentration levels for trigonelline were 0.16, 0.8, 1.6, and 8 µM. Different values were used for N-acetylcysteine because its endogenous levels are lower than the other analytes. The QC sample concentrations were prepared based on calibration curve data using the previously published method in which the linear range for trigonelline was 0.5-5µM, however, the use of the shorter column resulted in a broader linear range and different QC sample concentrations should be assessed. Three replicates of each concentration level were assessed and the accuracy was determined. All analytes were within 25% of expected values at the three highest concentrations used, except for

1-methylhistidine at 30μM (data not shown). This is expected because 30μM is outside of the linear range for 1-methylhistidine. Further assessment of intra-assay accuracy and precision was performed using five replicate injections of synthetic urine spiked with one concentration level within a single run. Inter-assay accuracy and precision was assessed with five replicate injections of synthetic urine spiked with one concentration level over three separate runs. Accuracy and Precision were calculated as previously described using the equations listed below [19].

Accuracy (% Bias) was calculated using the following equation:

$$\%\ \text{Bias} = \left[\frac{\text{Mean Calculated Concentration}_x\text{-Expected Concentration}_x}{\text{Expected Concentration}_x}\right] \times 100$$

Precision (% coefficient of variation (CV)) was calculated with the following equation:

$$\%\ \text{CV} = \frac{\text{Std. Dev. Calculated Concentration}_x}{\text{Mean Calculated Concentration}_x}$$

Calculated intra-assay and inter-assay % bias and % CV for each analyte is listed in Table 5.3. While the method was extremely precise, the accuracy of the method was not ideal, with only five analytes falling within ±10% of expected values and three compounds (Tyrosine, alpha amino adipic acid and hydroxyproline) falling outside of the ±20% limit (Table 5.3). The intra- and inter- assay precision for most compounds aside was within ±15%. Exceptions were hydroxyproline and 1-methylhistidine with variation greater than 20%. Only 1-methylhistidine and hydroxyproline were removed from the assay due to their inconsistencies. Though other compounds were not accurate, they were consistently higher or lower than the expected value.

Analyte Stability

Analyte stability was assessed using commercial control urine from normal healthy male donors. Urine was left in autosampler at 4˚C for 24 hours to mimic conditions encountered during sample analysis. Five replicate injections of urine was analyzed at three time points during the 24 hour period. Analytes were considered stable until the percent change of average calculated concentration from time zero became greater than ±20%. Table 5.4 lists the percent change relative to time zero for each analyte at each time point.

All analytes that did not have a percent change greater than ±20% were considered stable in the autosampler at 4˚C for 24 hours. The percent changes were higher at the 15 hour time point due to lower abundances detected for the internal standards, which is likely due to an instrument error since the same sample was used for all stability measurements. This highlights the importance of having stable isotope labelled ISs to counteract instrumental variations.

Dilution Integrity and Carryover

Dilution integrity was assessed because samples were previously processed by dilution with water according to creatinine concentration. The effect of analyte ionization following dilution with water was assessed. Samples were prepared using commercial control urine that was undiluted and diluted in either water or synthetic urine. The calculated concentration from the undiluted urine was used to calculate the expected concentration after a 1:10 dilution of the urine. The percent change of the calculated concentration in the diluted urine from the expected value was used to assess dilution integrity (Table 5.4). Analytes must have a percent change of less than ± 20%. Seven metabolites met this criterion in the samples diluted with synthetic urine while only one analyte, tyrosine, met this criterion in the samples diluted with water. For some analytes, the calculated concentration in the undiluted urine was either outside of the linear range

or at a low enough concentration such that dilution of the sample resulted in a calculated concentration outside of the linear range. This could explain the high percent changes following dilution with both water and synthetic urine. Dilution in synthetic urine seemed to be more accurate than dilution with water for most analytes, especially those earlier eluting, polar analytes. However, if adding the same amount of diluent to all urine samples, water might be acceptable.

Carryover was assessed by analysis of blank synthetic urine directly after the analysis of either the highest calibrator or commercial control urine. Analyte responses in blank synthetic urine could not be more than 10% of the signal for the lowest calibrator [19]. Following the highest calibrator or commercial control urine, there was no response for most analytes in blank synthetic urine (Table 5.4). Responses were observed for dimethyl arginine, S-adenosylhomocysteine and phenylalanine, however, the responses for dimethyl arginine and phenylalanine were less than 10% of the lowest calibrator. The response for S-adenosylhomocysteine following the highest calibrator was higher than 10%, indicating that carryover may be an issue for S-adenosylhomocysteine. However, repeated injections of the highest calibrator did not result in an increase in calculated concentrations for S-adenosylhomocysteine of more than ± 20% (data not shown).

Table 5.3 Precision and Accuracy

* Analytes with precision greater than ± 20%, # Analytes with accuracy greater than ± 20%

Analyte	Intra-assay (n=5)				Inter-assay (n=15)			
	Concentration (µM)		Accuracy (% Bias)	Precision (% CV)	Concentration (µM)		Accuracy (% Bias)	Precision (% CV)
	Added	Found			Added	Found		
1-Methylhistidine*	6.00	6.38	6.3	5.1	6.00	5.58	-7.0	29.8
Hydroxyproline*#	6.00	6.82	13.7	33.5	6.00	8.08	34.6	54.4
Trigonelline	1.60	1.53	-4.4	8.3	1.6	1.55	-3.1	14.6
Dimethyl Arginine	6.00	6.78	13.0	5.3	6.00	6.34	5.7	7.4
α-Amino adipic Acid#	6.00	4.63	-22.8	5.3	6.00	4.46	-25.7	17.4
N-acetyl Asparagine	6.00	6.98	16.3	2.6	6.00	6.75	12.5	14.6
N-acetyl Aspartic Acid	6.00	6.02	0.3	1.6	6.00	6.02	0.3	8.0
Quinolinic Acid	6.00	6.56	9.3	2.4	6.00	6.39	6.5	4.9
Pyroglutamic Acid	6.00	6.78	13.0	4.3	6.00	6.74	12.3	7.2
Tyrosine#	6.00	7.48	24.6	1.1	6.00	7.41	23.5	1.5
N-acetyl Cysteine	0.60	0.56	-6.7	2.8	0.60	0.56	-6.7	5.7
S-adenosylhomocysteine	6.00	5.79	-3.5	4.2	6.00	6.14	2.3	8.1
Phenylalanine	6.00	6.83	13.8	1.2	6.00	6.87	14.5	1.1

Table 5.4 Analyte Stability, Dilution Integrity and Carryover

IS was lower than expected causing increased variation, ** undiluted urine above upper limit of quantification, * 1/10 dilution below lower limit of quantification

Analyte	Stability			Dilution Integrity		Carryover	
	% change from T_0			Accuracy		% of lowest calibrator	
	10	15#	24	Synthetic Urine	Water	After Highest Calibrator	After Commercial Control Urine
1-methylhistidine	0.42	16.20	5.27	50.93 **	520.33	ND	ND
hydroxyproline	-1.71	7.59	1.14	-98.67 *	-120.45	ND	ND
Trigonelline	1.45	27.32	16.88	6.44	251.13	ND	ND
Dimethyl arginine	-2.28	18.93	8.60	1.02	54.10	2.99	0.37
alpha amino adipic acid	1.32	23.05	13.26	2.32	525.03	ND	ND
N-acetyl asparagine	-1.33	16.99	7.65	-14.44	198.02	ND	ND
N-acetyl aspartic acid	1.04	21.21	10.39	-2.23	32.27	ND	ND
Quinolinic acid	-0.89	25.87	5.35	-5.52	28.40	ND	ND
Pyroglutamic acid	-5.20	16.29	-3.86	59.75 **	52.14	ND	ND
Tyrosine	-7.63	14.72	-4.35	-2.46	-4.35	ND	ND
N-acetyl cysteine	-7.05	10.27	1.31	107.48 *	123.04	ND	ND
S-adenosylhomocysteine	-9.34	1.16	-11.89	282.81 *	277.91	14.23	0.12
Phenylalanine	-10.59	12.37	-8.96	-131.97 *	-130.16	0.66	0.70

Application of Developed Method

A limited subset of TB patient urine samples were re-analyzed using the developed targeted method to identify any unforeseen issues and assess method performance before analyzing a new set clinical samples . Each sample dilution (undiluted, 1:2, or 1:5) was run on a separate day as an individual batch. Dilutions were chosen based on analyte concentrations observed in commercial control urine during method validation. A set of calibration standards were injected at the beginning of each sample batch in order to establish a calibration curve. The sequence of sample injection was randomized to minimize the effect of instrument variability.

Table 5.5 Average concentrations for each analyte at the different time points during treatment.

Analyte	Concentration (μmol/mmol creatinine) n = 10, mean ± SD			
	Day 0	Week 2	Week 8	Week 24
Trigonelline	489.7 ± 583.4	411.0 ± 197.8	611.7 ± 676.0	388.9 ± 522.5
Dimethyl Arginine	199.5 ± 142.1	170.0 ± 58.84	260.2 ± 128.1	139.9 ± 71.81
α-Amino adipic Acid	20.67 ± 11.69	29.75 ± 17.80	14.22 ± 6.514	19.44 ± 9.175
N-acetyl Asparagine	41.16 ± 34.84	46.22 ± 26.43	58.87 ± 48.35	50.41 ± 20.62
N-acetyl Aspartic Acid	43.12 ± 33.24	46.66 ± 16.16	47.58 ± 23.23	42.62 ± 23.32
Quinolinic Acid	156.9 ± 80.99	160.7 ± 77.75	139.0 ± 49.42	54.40 ± 34.51
Pyroglutamic Acid	112.3 ± 35.23	68.97 ± 14.35	90.13 ± 27.09	80.95 ± 47.47
Tyrosine	62.89 ± 50.03	65.40 ± 44.78	68.18 ± 34.13	81.40 ± 63.37
N-acetyl Cysteine	2.090 ± 1.431	4.478 ± 3.121	2.542 ± 2.435	5.307 ± 3.687
S-adenosylhomocysteine	4.363 ± 5.058	2.952 ± 1.426	2.910 ± 2.042	2.088 ± 1.782
Phenylalanine	33.58 ± 11.26	30.33 ± 13.85	32.83 ± 13.75	34.59 ± 22.93

The creatinine concentration for each urine sample was used to normalize urine dilution variability. Though creatinine excretion may not be an adequate marker of urine dilution, the median fold change normalization method used in Chapter 4 could not be applied due to the targeted method used in this chapter[20-24]. The average, normalized amounts (μmol/mmol creatinine) of each analyte are reported in Table 5.5. Although the purpose of analyzing these samples was to confirm suitability of the developed method for analysis of clinical samples, the analyte trends during anti-TB treatment were investigated to see how they compared to those previously observed (Mahapatra, S., CSU, unpublished data). Figure 5.3 demonstrates the distribution of normalized levels for each analyte at the different time points during anti-TB treatment. Only two analytes were significantly decreased during treatment; pyroglutamic acid was significantly decreased by week 2 of treatment and quinolinic acid was by month 6 of treatment. In an attempt to minimize patient variability, normalized levels at diagnosis (D0, 0

weeks) were equated to one and normalized levels during treatment were expressed as fold change relative to diagnosis. These fold changes were plotted for each individual patient allowing assessment of changes on a per patient basis (Figure 5.4). The analyte levels for a few patients had consistent trends such as patient 4 whose levels were consistently increased at week two and then decreased and patient 6 whose levels consistently decreased by week two and then remained relatively constant. However, the levels for a majority of patients varied depending on the analyte.

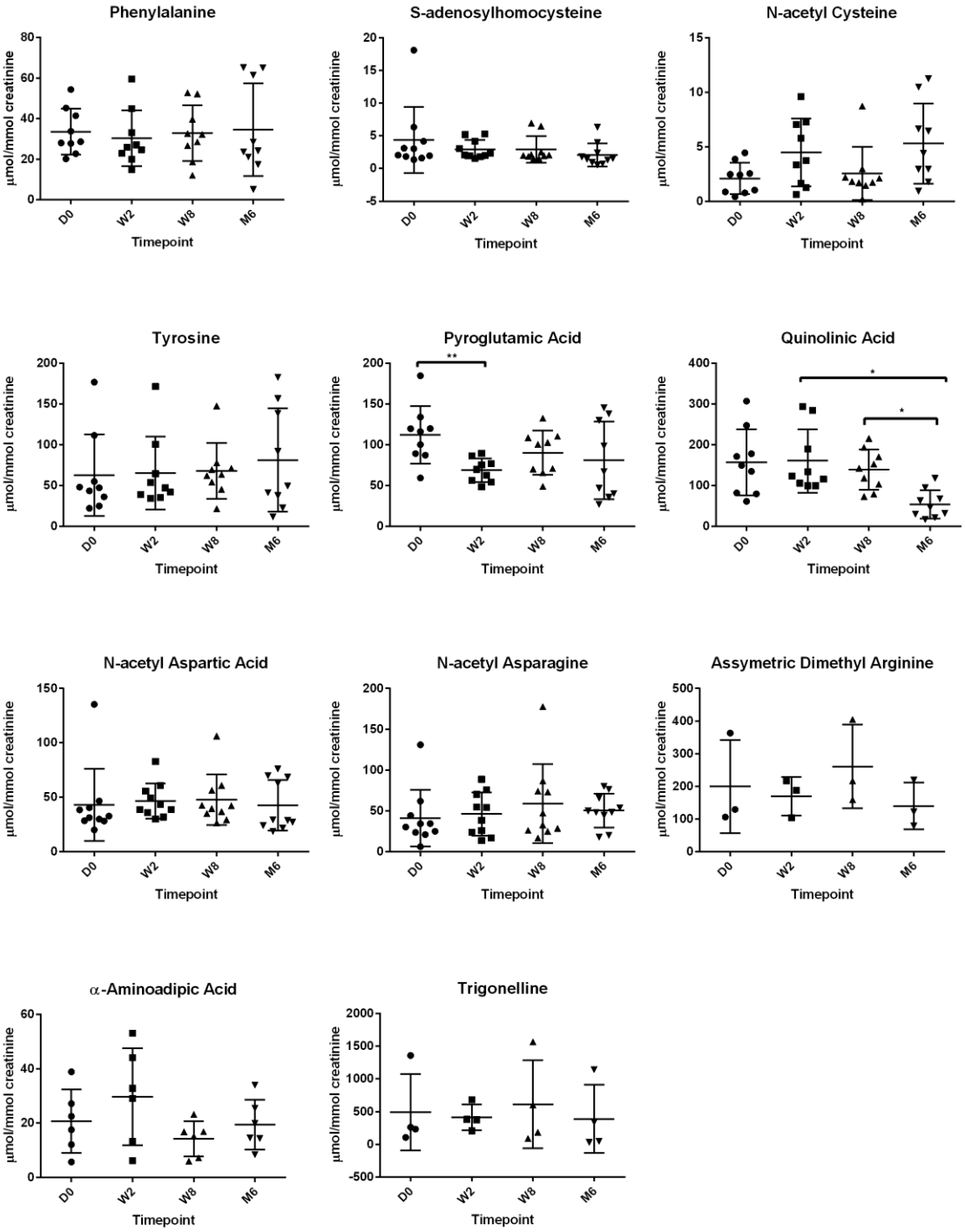

Figure 5.5

Column scatter graphs for quantified analytes. Each point represents the log2 normalized concentration for a single patient. Data are shown as the mean ± SD and are representative of one experiment. *p<0.05, **p<0.01, ***p<0.001

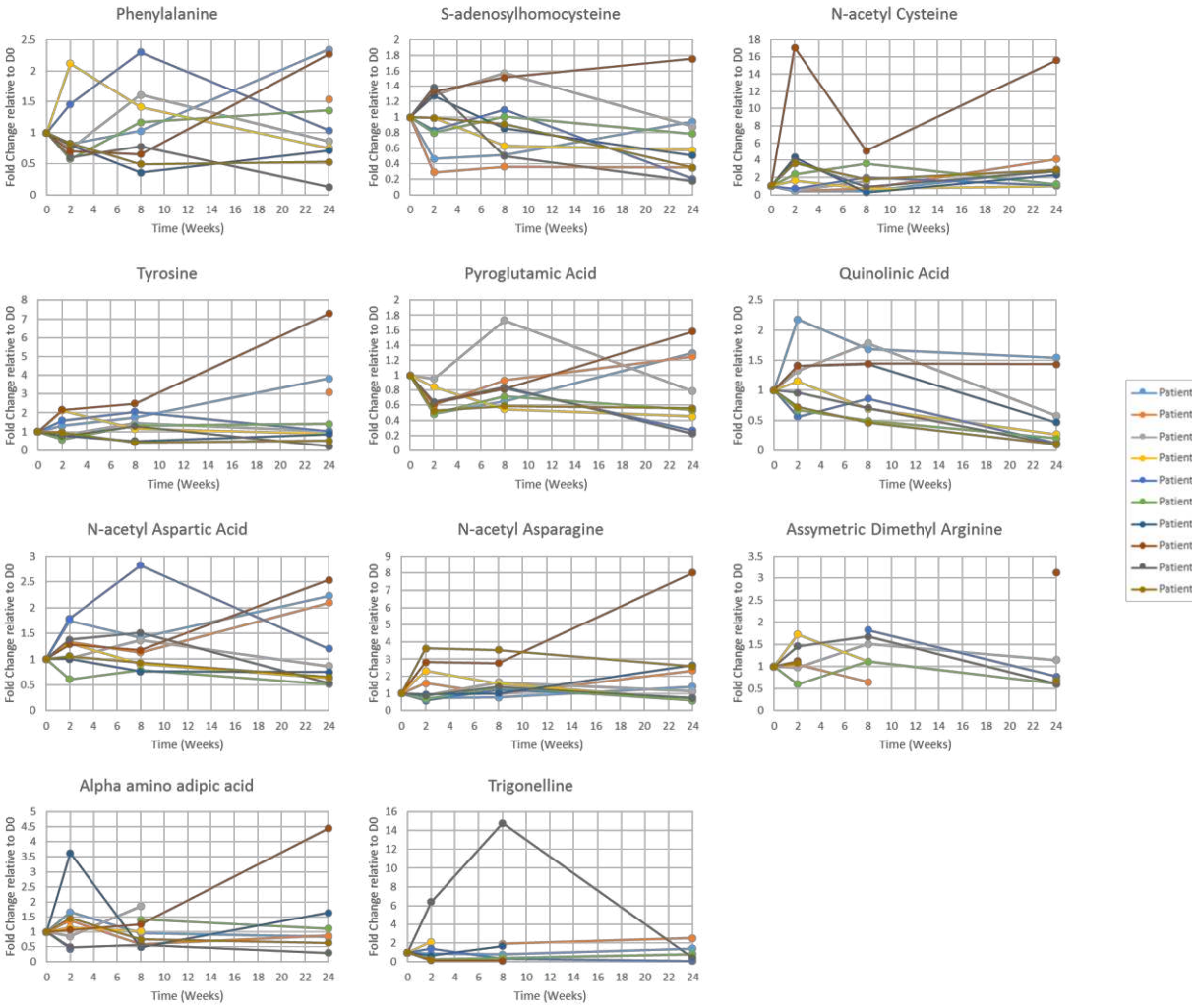

Figure 5 7
Fold changes for quantified analytes in individual patients during treatment relative to diagnosis (D0).

5.4 Discussion

This chapter described the development of a targeted method for thirteen metabolites previously found to decrease during anti-TB treatment (S. Mahapatra, unpublished results, CSU). Though untargeted metabolomics experiments are essential for identifying novel and unexpected metabolic alterations, these new findings must be validated, preferably with targeted methods, before they can be designated as biomarkers for a particular condition. The targeted method development described in this chapter is a critical step in confirming these differentiated metabolites as true biomarkers of anti-TB treatment response.

The targeted method developed is capable of accurate and precise quantification of eleven out of the initial thirteen metabolites. The eleven metabolites were successfully quantified in TB patient urine. The entire method can be completed within 15 minutes and requires minimal sample preparation, allowing for the analysis of many samples in a short period of time. As with all methods, there is associated variation (Table 5.3 - 5.5). However, the variation observed during method validation is similar to that seen by others quantifying urinary metabolites[25-27]. This method variability highlights the importance of adequate ISs and defined criteria for method acceptance. Though this method may not be suitable for decisions based on specific analyte levels due to its limited accuracy, it is suitable for monitoring changes over time, due to its high precision.

Additionally, the high variance seen in patient urine samples, is most likely due to inter-patient variability. Humans are heterogeneous and have different habits that contribute to their urinary metabolite excretion. Not only is this variation from person to person, but a single person can have varying metabolite excretion on multiple days [28]. While matching patients more stringently might lessen the variability and pull out significant changes, the purpose of these

metabolites is to serve as a universal biomarker for the evaluation of a mixed population of patients, and thus alterations in these metabolites should be significant in spite of the inter-patient variability. Another source of variation could be the small number of patient samples analyzed. Increasing the number of patient samples could reduce this variability and allow for significant changes to be observed.

Though it is important to identify metabolites that can serve as universal biomarkers, there is some value in examining these metabolic changes in patients individually. In doing this, the metabolite changes for individual patients during treatment can be observed and these changes can be compared with clinical data to better explain the trends observed individually. This is important because these biomarkers will be evaluated on a per patient basis in the clinics. However, one should exercise caution when analyzing the data in this way as this could lead to flawed explanations of the data and inadequate biomarkers. One way to minimize over-fitting the data, would be to only examine individual trends when a significant difference is observed following a repeated measures ANOVA test. This statistical test highlight significant changes between groups while also taking into account the individual changes. Thus, once the ANOVA has demonstrated the utility of the biomarker in differentiating a population of patients, further evaluation of those individual changes can be examined.

The values of these eleven metabolites in patient urine are above or on the higher end of ranges previously reported in the urine of healthy individuals [29]. Levels different than those observed in healthy individuals are expected in TB patients at diagnosis as these individuals are not healthy. If the patients are cured at the end of treatment, then it can be assumed that their metabolic profiles would be similar to those of healthy individuals. However, there might still be antibiotics in these patients systems at the end of treatment and this could cause metabolic

profiles different than those observed in healthy individuals [30]. Additionally, at the conclusion of anti-TB treatment, lung function of these patients is impaired, which could influence host metabolism and the levels of these analytes[31-36]. These values do not differ drastically from reported values indicating that these differences are likely due to biological reasons and not an error in the developed method.

Despite this high variation, two of the compounds decreased during anti-TB treatment in accordance with previous unpublished observations by S. Mahapatra, Colorado State University. One of the compounds, pyroglutamic acid, was significantly decreased by week 2. In contrast to this result, Che *et al.* reported that pyroglutamic acid increased following anti-TB treatment [37]. The use of a different platform, biofluid, or untargeted method could explain these different results. Alternatively, an understanding of the formation of pyroglutamic acid and the pathways it is involved in might resolve these discrepancies. Pyroglutamic acid can be generated spontaneously from glutamate or glutamine, incomplete reactions involving activated glutamate, degradation of proteins containing an N-terminal pyroglutamic acid residue, or during glutathione degradation[38]. Alterations in glutathione metabolism during *Mtb* infection that have been previously described[2,39-41]. However, not only are there other mechanisms for pyroglutamic acid formation, but *Mtb* could also be contributing to the levels of this metabolite[42]. Further investigation of these mechanisms might provide an explanation for the observed alterations in pyroglutamic acid levels.

The other metabolite, quinolinic acid, was significantly decreased by month six. Quinolinic acid is a product of tryptophan catabolism that can also serve as a precursor for nicotinamide adenosine dinucleotide (NAD) biosynthesis[43,44]. Indoleamine 2,3-dioxygenase-1 is the rate limiting enzyme in tryptophan degradation via the kynurenine pathway[45,46]. Elevated

levels of this enzyme have been detected during *Mtb* infection[45,47-49]. Additionally, numerous studies have reported decreased levels of tryptophan and increased levels of downstream tryptophan degradation products during active TB[2,3,42,50]. During treatment, the killing of bacteria could lead to reduced tryptophan degradation and decreased levels of its degradation products, like quinolinic acid. Further evaluation of other metabolites in the kynurenine pathway during anti-TB treatment is needed to confirm this hypothesis.

A limitation of this study is that two of the thirteen metabolites, 1-methylhistidine and hydroxyproline, were highly variable and could not be quantified using this method. Developing a method to quantify different classes of compounds is not always feasible and a separate method is needed to quantify these two. The short retention times of both of these metabolites contributed to their poor performance due to their minimal interaction with the column as well as potential ion suppression by other early eluting components of the urine such as salt and urea. Other methods have been developed that address these issues and may be used or optimized for analysis of these two analytes. While not increasing the retention time, an 80-fold dilution followed by filtration prior to detection yielded an improved accuracy and precision of $< \pm 11\%$ for 1-methylhistidine [51]. This high dilution probably decreased the amount ion suppression due to interfering urine components allowing for more reproducible measurements. Other methods increased the retention time of 1-methylhistidine and hydroxyproline on reverse-phase columns by changing their polarity through derivatization prior to LC-MS analysis[52-54]. Additionally, methods have been developed using hydrophilic interaction liquid chromatography (HILIC) which typically increases the retention time of polar analytes and may be more suitable for 1-methylhistidine and hydroxyproline[55,56]. Another option to reduce the effects of ion suppression is to use GC-MS. GC-MS is not suitable for the quantification of 1-methylhistidine due to its

thermal instability, however, methods have been developed for the quantification of hydroxyproline and these could be used for its analysis[57,58]. Each of these methods has their own advantages and disadvantages that will have to be evaluated before these two metabolites can be quantified.

Not all of these compounds behaved as described previously, however, this is not unexpected as this was just a test to assess method performance prior to analysis of a larger set of clinical samples. . Due to inherent human variability, a larger sample size than ten patients would be needed to assess significant changes in these analytes during treatment[59]. Prior to applying this method to a larger set of clinical samples, a power analysis can be done using the values obtained from this chapter to determine the appropriate sample size. Additionally, these samples were previously analyzed using an instrument and method designed to detect as many metabolites as possible, while the method developed in this chapter was designed to detect only targeted metabolites. By removing unwanted signals and enabling increased detection of analytes, this MRM method could yield different results than described previously even with the appropriate sample size.. This demonstrates the importance of performing validation with a different method and independent patient subset in order to confirm that changes were not due to original method variability or the particular sample set. Further validation of these compounds as biomarkers of anti-TB treatment respond is currently being pursued using a different patient set representing various treatment outcomes.

REFERENCES

1. Mahapatra S, Hess AM, Johnson JL, Eisenach KD, DeGroote MA, Gitta P, Joloba ML, Kaplan G, Walzl G, Boom WH and others. A metabolic biosignature of early response to anti-tuberculosis treatment. BMC Infect Dis 2014;14:53.
2. Weiner J, Parida SK, Maertzdorf J, Black GF, Repsilber D, Telaar A, Mohney RP, Arndt-Sullivan C, Ganoza CA, Faé KC and others. Biomarkers of inflammation, immunosuppression and stress with active disease are revealed by metabolomic profiling of tuberculosis patients. PLoS One 2012;7(7):e40221.
3. Feng S, Du YQ, Zhang L, Feng RR, Liu SY. Analysis of serum metabolic profile by ultra-performance liquid chromatography-mass spectrometry for biomarkers discovery: application in a pilot study to discriminate patients with tuberculosis. Chin Med J (Engl) 2015;128(2):159-68.
4. Lau SK, Lee KC, Curreem SO, Chow WN, To KK, Hung IF, Ho DT, Sridhar S, Li IW, Ding VS and others. Metabolomic Profiling of Plasma from Patients with Tuberculosis by Use of Untargeted Mass Spectrometry Reveals Novel Biomarkers for Diagnosis. J Clin Microbiol 2015;53(12):3750-9.
5. Frediani JK, Jones DP, Tukvadze N, Uppal K, Sanikidze E, Kipiani M, Tran VT, Hebbar G, Walker DI, Kempker RR and others. Plasma metabolomics in human pulmonary tuberculosis disease: a pilot study. PLoS One 2014;9(10):e108854.
6. Koulman A, Lane GA, Harrison SJ, Volmer DA. From differentiating metabolites to biomarkers. Anal Bioanal Chem 2009;394(3):663-70.
7. Beger RD, Holland RD, Sun J, Schnackenberg LK, Moore PC, Dent CL, Devarajan P, Portilla D. Metabonomics of acute kidney injury in children after cardiac surgery. Pediatr Nephrol 2008;23(6):977-84.
8. Chen J, Zhang X, Cao R, Lu X, Zhao S, Fekete A, Huang Q, Schmitt-Kopplin P, Wang Y, Xu Z and others. Serum 27-nor-5β-cholestane-3,7,12,24,25 pentol glucuronide discovered by metabolomics as potential diagnostic biomarker for epithelium ovarian cancer. J Proteome Res 2011;10(5):2625-32.
9. Xu J, Chen Y, Zhang R, Song Y, Cao J, Bi N, Wang J, He J, Bai J, Dong L and others. Global and targeted metabolomics of esophageal squamous cell carcinoma discovers potential diagnostic and therapeutic biomarkers. Mol Cell Proteomics 2013;12(5):1306-18.
10. Kitteringham NR, Jenkins RE, Lane CS, Elliott VL, Park BK. Multiple reaction monitoring for quantitative biomarker analysis in proteomics and metabolomics. J Chromatogr B Analyt Technol Biomed Life Sci 2009;877(13):1229-39.
11. Hampel D, York ER, Allen LH. Ultra-performance liquid chromatography tandem mass-spectrometry (UPLC-MS/MS) for the rapid, simultaneous analysis of thiamin, riboflavin, flavin adenine dinucleotide, nicotinamide and pyridoxal in human milk. J Chromatogr B Analyt Technol Biomed Life Sci 2012;903:7-13.
12. Kirsch SH, Knapp JP, Herrmann W, Obeid R. Quantification of key folate forms in serum using stable-isotope dilution ultra performance liquid chromatography-tandem mass spectrometry. J Chromatogr B Analyt Technol Biomed Life Sci 2010;878(1):68-75.

13. Stanislaus A, Guo K, Li L. Development of an isotope labeling ultra-high performance liquid chromatography mass spectrometric method for quantification of acylglycines in human urine. Anal Chim Acta 2012;750:161-72.
14. Waterval WA, Scheijen JL, Ortmans-Ploemen MM, Habets-van der Poel CD, Bierau J. Quantitative UPLC-MS/MS analysis of underivatised amino acids in body fluids is a reliable tool for the diagnosis and follow-up of patients with inborn errors of metabolism. Clin Chim Acta 2009;407(1-2):36-42.
15. Lutz U, Bittner N, Lutz RW, Lutz WK. Metabolite profiling in human urine by LC-MS/MS: method optimization and application for glucuronides from dextromethorphan metabolism. J Chromatogr B Analyt Technol Biomed Life Sci 2008;871(2):349-56.
16. Wen A, Hang T, Chen S, Wang Z, Ding L, Tian Y, Zhang M, Xu X. Simultaneous determination of amoxicillin and ambroxol in human plasma by LC-MS/MS: validation and application to pharmacokinetic study. J Pharm Biomed Anal 2008;48(3):829-34.
17. Lu G, Toivola B. A Validated Triple Quadrupole LC/MS/MS Method for Quantitative Analysis of Methylenedioxypyrovalerone (MDPV) and Mephedrone, Common Components of "Bath Salts" in Urine. USA: Agilent Technologies, Inc.; 2012.
18. McCalley DV. Effect of buffer on peak shape of peptides in reversed-phase high performance liquid chromatography. J Chromatogr A 2004;1038(1-2):77-84.
19. Toxicology SWGfF. Scientific Working Group for Forensic Toxicology (SWGTOX) standard practices for method validation in forensic toxicology. J Anal Toxicol 2013;37(7):452-74.
20. Ram MM, Reddy V. Variability in urinary creatinine. Lancet 1970;2(7674):674.
21. Alessio L, Berlin A, Dellorto A, Toffoletto F, Ghezzi I. RELIABILITY OF URINARY CREATININE AS A PARAMETER USED TO ADJUST VALUES OF URINARY BIOLOGICAL INDICATORS. International Archives of Occupational and Environmental Health 1985;55(2):99-106.
22. James GD, Sealey JE, Alderman M, Ljungman S, Mueller FB, Pecker MS, Laragh JH. A LONGITUDINAL-STUDY OF URINARY CREATININE AND CREATININE CLEARANCE IN NORMAL SUBJECTS - RACE, SEX, AND AGE-DIFFERENCES. American Journal of Hypertension 1988;1(2):124-131.
23. Curtis G, Fogel M. CREATININE EXCRETION - DIURNAL VARIATION AND VARIABILITY OF WHOLE AND PART-DAY MEASURES - A METHODOLOGIC ISSUE IN PSYCHOENDOCRINE RESEARCH. Psychosomatic Medicine 1970;32(4):337-&.
24. Vestergaard P, Leverett R. CONSTANCY OF URINARY CREATININE EXCRETION. Journal of Laboratory and Clinical Medicine 1958;51(2):211-218.
25. Piraud M, Vianey-Saban C, Petritis K, Elfakir C, Steghens JP, Bouchu D. Ion-pairing reversed-phase liquid chromatography/electrospray ionization mass spectrometric analysis of 76 underivatized amino acids of biological interest: a new tool for the diagnosis of inherited disorders of amino acid metabolism. Rapid Commun Mass Spectrom 2005;19(12):1587-602.
26. Chen SS, Burton C, Kaczmarek A, Shi HL, Ma YF. Simultaneous determination of urinary quinolinate, gentisate, 4-hydroxybenzoate, and alpha-ketoglutarate by high-performance liquid chromatography-tandem mass spectrometry. Analytical Methods 2015;7(16):6572-6578.

27. Orhan H, Vermeulen NP, Tump C, Zappey H, Meerman JH. Simultaneous determination of tyrosine, phenylalanine and deoxyguanosine oxidation products by liquid chromatography-tandem mass spectrometry as non-invasive biomarkers for oxidative damage. J Chromatogr B Analyt Technol Biomed Life Sci 2004;799(2):245-54.
28. Jackson AA, Persaud C, Meakins TS, Bundy R. Urinary excretion of 5-L-oxoproline (pyroglutamic acid) is increased in normal adults consuming vegetarian or low protein diets. J Nutr 1996;126(11):2813-22.
29. Bouatra S, Aziat F, Mandal R, Guo AC, Wilson MR, Knox C, Bjorndahl TC, Krishnamurthy R, Saleem F, Liu P and others. The human urine metabolome. PLoS One 2013;8(9):e73076.
30. Schaaf HS, Parkin DP, Seifart HI, Werely CJ, Hesseling PB, van Helden PD, Maritz JS, Donald PR. Isoniazid pharmacokinetics in children treated for respiratory tuberculosis. Arch Dis Child 2005;90(6):614-8.
31. Byrne AL, Marais BJ, Mitnick CD, Lecca L, Marks GB. Tuberculosis and chronic respiratory disease: a systematic review. Int J Infect Dis 2015;32:138-46.
32. de Vallière S, Barker RD. Residual lung damage after completion of treatment for multidrug-resistant tuberculosis. Int J Tuberc Lung Dis 2004;8(6):767-71.
33. Maguire GP, Anstey NM, Ardian M, Waramori G, Tjitra E, Kenangalem E, Handojo T, Kelly PM. Pulmonary tuberculosis, impaired lung function, disability and quality of life in a high-burden setting. Int J Tuberc Lung Dis 2009;13(12):1500-6.
34. Ngahane BH, Pefura-Yone EW, Mama M, Tengang B, Nganda MM, Wandji A, Olinga U, Nyankiyé E, Afane Ze E, Kuaban C. Evaluation of factors affecting adherence to asthma controller therapy in chest clinics in a sub-Saharan African setting: a cross-sectional study. Afr Health Sci 2016;16(1):194-200.
35. Plit ML, Anderson R, Van Rensburg CE, Page-Shipp L, Blott JA, Fresen JL, Feldman C. Influence of antimicrobial chemotherapy on spirometric parameters and pro-inflammatory indices in severe pulmonary tuberculosis. Eur Respir J 1998;12(2):351-6.
36. Willcox PA, Ferguson AD. Chronic obstructive airways disease following treated pulmonary tuberculosis. Respir Med 1989;83(3):195-8.
37. Che N, Cheng J, Li H, Zhang Z, Zhang X, Ding Z, Dong F, Li C. Decreased serum 5-oxoproline in TB patients is associated with pathological damage of the lung. Clin Chim Acta 2013;423:5-9.
38. Kumar A, Bachhawat AK. Pyroglutamic acid: throwing light on a lightly studied metabolite. Current Science 2012;102(2):288-297.
39. Somashekar BS, Amin AG, Rithner CD, Troudt J, Basaraba R, Izzo A, Crick DC, Chatterjee D. Metabolic profiling of lung granuloma in Mycobacterium tuberculosis infected guinea pigs: ex vivo 1H magic angle spinning NMR studies. J Proteome Res 2011;10(9):4186-95.
40. Shin JH, Yang JY, Jeon BY, Yoon YJ, Cho SN, Kang YH, Ryu DH, Hwang GS. (1)H NMR-based metabolomic profiling in mice infected with Mycobacterium tuberculosis. J Proteome Res 2011;10(5):2238-47.
41. Venketaraman V, Millman A, Salman M, Swaminathan S, Goetz M, Lardizabal A, Hom D, Connell ND. Glutathione levels and immune responses in tuberculosis patients. Microbial Pathogenesis 2008;44(3):255-261.

42. Meissner-Roloff RJ, Koekemoer G, Warren RM, Loots DT. A metabolomics investigation of a hyper- and hypo-virulent phenotype of Beijing lineage M-tuberculosis. Metabolomics 2012;8(6):1194-1203.
43. Guillemin GJ. Quinolinic acid, the inescapable neurotoxin. FEBS J 2012;279(8):1356-65.
44. SARETT HP. Quinolinic acid excretion and metabolism in man. J Biol Chem 1951;193(2):627-34.
45. Blumenthal A, Nagalingam G, Huch JH, Walker L, Guillemin GJ, Smythe GA, Ehrt S, Britton WJ, Saunders BM. M. tuberculosis induces potent activation of IDO-1, but this is not essential for the immunological control of infection. PLoS One 2012;7(5):e37314.
46. Qualls JE, Murray PJ. Immunometabolism within the tuberculosis granuloma: amino acids, hypoxia, and cellular respiration. Semin Immunopathol 2016;38(2):139-52.
47. Almeida AS, Lago PM, Boechat N, Huard RC, Lazzarini LC, Santos AR, Nociari M, Zhu H, Perez-Sweeney BM, Bang H and others. Tuberculosis is associated with a down-modulatory lung immune response that impairs Th1-type immunity. J Immunol 2009;183(1):718-31.
48. Moreau M, Lestage J, Verrier D, Mormede C, Kelley KW, Dantzer R, Castanon N. Bacille Calmette-Guérin inoculation induces chronic activation of peripheral and brain indoleamine 2,3-dioxygenase in mice. J Infect Dis 2005;192(3):537-44.
49. Desvignes L, Ernst JD. Interferon-gamma-responsive nonhematopoietic cells regulate the immune response to Mycobacterium tuberculosis. Immunity 2009;31(6):974-85.
50. Zhou A, Ni J, Xu Z, Wang Y, Lu S, Sha W, Karakousis PC, Yao YF. Application of (1)h NMR spectroscopy-based metabolomics to sera of tuberculosis patients. J Proteome Res 2013;12(10):4642-9.
51. Wang H, Hu P, Jiang J. Measurement of 1- and 3-methylhistidine in human urine by ultra performance liquid chromatography-tandem mass spectrometry. Clin Chim Acta 2012;413(1-2):131-8.
52. Schnackenberg LK, Sun JC, Pence LM, Bhattacharyya S, da Costa GG, Beger RD. Metabolomics evaluation of hydroxyproline as a potential marker of melamine and cyanuric acid nephrotoxicity in male and female Fischer F344 rats. Food and Chemical Toxicology 2012;50(11):3978-3983.
53. Kaspar H, Dettmer K, Chan Q, Daniels S, Nimkar S, Daviglus ML, Stamler J, Elliott P, Oefner PJ. Urinary amino acid analysis: a comparison of iTRAQ-LC-MS/MS, GC-MS, and amino acid analyzer. J Chromatogr B Analyt Technol Biomed Life Sci 2009;877(20-21):1838-46.
54. Fonteh AN, Harrington RJ, Harrington MG. Quantification of free amino acids and dipeptides using isotope dilution liquid chromatography and electrospray ionization tandem mass spectrometry. Amino Acids 2007;32(2):203-12.
55. Idborg H, Zamani L, Edlund PO, Schuppe-Koistinen I, Jacobsson SP. Metabolic fingerprinting of rat urine by LC/MS Part 1. Analysis by hydrophilic interaction liquid chromatography-electrospray ionization mass spectrometry. J Chromatogr B Analyt Technol Biomed Life Sci 2005;828(1-2):9-13.
56. Gika HG, Theodoridis GA, Wilson ID. Hydrophilic interaction and reversed-phase ultra-performance liquid chromatography TOF-MS for metabonomic analysis of Zucker rat urine. J Sep Sci 2008;31(9):1598-608.

57. Kaspar H, Dettmer K, Gronwald W, Oefner PJ. Automated GC-MS analysis of free amino acids in biological fluids. J Chromatogr B Analyt Technol Biomed Life Sci 2008;870(2):222-32.
58. Pasikanti KK, Ho PC, Chan ECY. Development and validation of a gas chromatography/mass spectrometry metabonomic platform for the global profiling of urinary metabolites. Rapid Communications in Mass Spectrometry 2008;22(19):2984-2992.
59. Broadhurst DI, Kell DB. Statistical strategies for avoiding false discoveries in metabolomics and related experiments. Metabolomics 2006;2(4):171-196.

CHAPTER 6: FINAL DISCUSSION AND FUTURE DIRECTIONS

6.1 Final Discussion

Biomarker discovery in the field of tuberculosis is rapidly progressing, however, a transition from biomarker discovery towards biomarker validation is needed to succeed in development of a clinically useful biosignature [1]. Not only can metabolomics data sets be used for biomarker discovery, but they can also provide insights into host-pathogen interactions with further mechanistic studies [2]. The results presented in this dissertation are important for transitioning towards biomarker validation and provided initial insights into host-pathogen interactions.

Aim I was addressed in Chapters 2 and 3 which described the structural characterization of two novel urinary metabolites, a core-1 *O*-glycosylated Ser-Leu peptide and *N*-acetylisoputreanine. In Chapter 2, the use of LC-MS/MS provided structural information about the unknown molecule, including diagnostic carbohydrate ions leading to a hypothesized structure. Enzymatic deglycosylation in combination with commercial standards enabled confirmation of the hypothesized structure. Although, structural characterization of the *m/z* 875.36 metabolite as a core-1 *O*-glycosylated Ser-Leu peptide augments available metabolite databases, it did not yield a direct link to metabolic pathways as anticipated. However, a number of proteins were found that had documented core-1 *O*-glycosylation at sites that matched with the identified glycopeptide. Like the identified glycopeptide, the transcript of one of these proteins, C1INH, decreased during anti-TB treatment. This correlation provided a potential origin of the glycopeptide, linking it to the complement and coagulation pathways. Further investigation of the literature revealed fibrinogen as another possible source protein [3]. As

fibrinogen's glycosylation sites are not documented in the UniProt database, there are probably other proteins with undocumented glycosylation sites that are also potential sources of the identified glycopeptide.

In Chapter 3, LC-MS/MS fragmentation of the unknown molecule generated a key fragment ion (*m/z* 100.0757) that matched with a known compound, *N*-acetylspermine, aiding in development of a hypothesized structure. Chemical and enzymatic synthesis of hypothesized structure lead to its confirmation. The structural identification of this metabolite adds to the number of searchable metabolites and supplied a direct link to a metabolic pathway, polyamine catabolism. Two additional polyamine catabolites, N^1, N^{12}-diacetylspermine and *N*-acetylisoputreanine-γ-lactam, were confirmed as endogenous components of human urine. The abundances of both *N*-acetylisoputreanine and N^1, N^{12}-diacetylspermine decreased during anti-TB treatment, providing evidence that polyamine catabolism could be altered during active TB [4]. However, the gut microbiota are another source of polyamines and non-specific antibiotic killing of the gut microbiota might also lead to the decrease observed. Aim II was addressed in Chapter 4, which dealt with the relative quantification of four metabolites in samples representing active TB disease. LC-MS analyses of active TB patients and household contacts revealed a significant increase in the core-1 *O*-glycosylated peptide and N^1, N^{12}-diacetylspermine in TB patients relative to household contacts. Biomarkers of successful anti-TB treatment response would serve as indicators of disease resolution and bacterial clearance, thus these analyses provided evidence that these two metabolites should be pursued as biomarkers due to their association with *Mtb* infection. . In contrast there was no increase observed for the other two polyamine catabolites, *N*-acetylisoputreanine and *N*-acetylisoputreanine-γ-lactam. This provides evidence for non-specific antibiotic killing of gut microbiota or INH inhibition of DAO playing a role in the altered levels

of these metabolites. Since these activities are not associated with TB disease, these metabolites should not be pursued. Further corroboration that *N*-acetylisoputreanine is an inadequate biomarker for anti-TB treatment response came from the LC-MS analysis of infected and uninfected Balb/c mouse lung tissue which confirmed the stable levels of *N*-acetylisoputreanine during infection. Additionally, the other three metabolites were not detected either due to experimental limitations or production of these metabolites at sites other than the lungs. These analyses also provided evidence for distinct regulation of the different polyamine catabolic enzymes.

Aim III was addressed in Chapter 5, in which an MRM assay for eleven structurally confirmed metabolites was developed. The chromatographic and MS parameters were successfully optimized for all thirteen metabolites. A linear calibration model with a correlation coefficient of greater than 0.99 was achieved for all thirteen metabolites. The inter- and intra-assay accuracy was within ± 20% for most compounds, exceptions were alpha amino adipic acid, tyrosine, and hydroxyproline. The inter- and intra- assay precision was within ± 20% for all compounds except for 1-methylhistidine and hydroxyproline. During method validation, 1-methylhistidine and hydroxyproline did not meet the defined criterion for method precision and were removed from the method. The developed method was applied in the re-analysis of urine samples from TB patients undergoing anti-TB treatment. Though the purpose of re-analyzing these samples was to test the developed method, two analytes, pyroglutamic acid and quinolinic acid, significantly decreased during treatment confirming previous results (S. Mahapatra, unpublished data, CSU). The variation between patients was large, however, its magnitude was similar to that observed in other urine analyses which is to be expected as humans are heterogeneous[5-7]. This variation was amplified by the small sample size and may have obscured

detection of significant changes in other metabolites highlighting the importance of determining the appropriate sample size before analysis of other clinical samples.

6.2 Future Directions

Building upon the research presented in this dissertation is required for continued progression towards a clinically useful biosignature of anti-TB treatment response.

Chapters 2 and 3 demonstrated that structural characterization can aid in development of validated methods and reveal the metabolic pathways involved. Thus, structural characterization of the nine remaining metabolites belonging to the TB-early treatment response biosignature is needed (Table 1.1). Similar to the characterization of *N*-acetylisoputreanine, structural characterization of these other metabolites may reveal additional metabolic pathways and provide additional biomarkers. In contrast, structural characterization may not provide a direct link to metabolic pathways, like the *O*-glycosylated peptide. However, characterization provides important information that can be utilized in development of targeted quantitative assays needed for the validation of these metabolites as biomarkers of anti-TB treatment response.

On a related note, targeted, quantitative assays need to be developed for the three metabolites from Chapters 2 and 3 and the two metabolites, 1-methyl histidine and hydroxyproline, that failed method validation in Chapter 5. Additionally, these metabolites and the eleven metabolites from Chapter 5 need to be validated using a larger, independent sample set with patients representing various treatment outcomes. By using a larger sample set, the effects of patient variability should be reduced which will improve the likelihood of observing significant changes. A variety of treatment outcomes is needed to assess whether these metabolites can also serve as predictors for slow- and fast- responders, relapse, or treatment failure.

Urine was the biological fluid used in this dissertation. Urine is formed in the kidneys as a mechanism to maintain proper osmolality of plasma and to remove metabolic degradation products of foreign and endogenous compounds from the body [8]. It is a preferred biological fluid due to its noninvasive collection methods, ability to obtain large volumes easily, and its metabolic complexity [8]. In contrast to sputum, urine can be collected with minimized risk of infection from most patients regardless of immune status, age, and treatment duration making it an attractive biological specimen for TB patients[9,10].

Despite these advantages, urine concentration variations posed a problem when quantifying urinary metabolic changes in this dissertation. As stated in Chapter 4, urinary creatinine concentration has been commonly used to normalize urinary metabolite excretion based on documentation of its constant excretion [11]. However, several groups have demonstrated that creatinine excretion is not constant and that it is an inadequate marker for urine metabolite excretion[12-15]. In Chapter 4, the median fold change normalization method was utilized to correct for variations in urine dilution. However, since this method requires the abundances of all metabolites detected in a sample to estimate urine concentration, this method could not be used to normalize the metabolite concentration obtained using the MRM method and thus creatinine concentration normalization was used in Chapter 5. Since creatinine concentrations is an inadequate measurement of urine concentration, the use of creatinine concentration for normalization in Chapter 5 might have played an additional role in the large variation observed between patients.

In order to address the challenges posed by urine concentration variations, the osmolality of each urine sample will be used to normalize urine concentration variations during analysis of future samples. Osmolality is the concentration of solutes per kilogram of solution [16]. It is

dependent only on the number of particles in the solution and is not affected by particle size or charge [16]. Osmolality provides a direct measurement of total urine metabolite excretion and thus is the gold standard[16-18]. Additionally, normalization of urine to osmolality reduced the overall variation amongst all samples allowing for detection of metabolites that were truly different between sample groups [17]. Thus, by normalizing to osmolality, the large patient inter-variability observed in Chapter 5 might be reduced as some of this variation could be due to differing urine concentrations amongst patients.

The results from Chapter 4 provided evidence for complex regulation of polyamine catabolism during active TB. Assessment of the expression and activity of host SSAT during *Mtb* infection through protein quantitation and enzyme inhibition will help elucidate the role of host SSAT and whether its increased expression is related to the increased levels of N^1, N^{12}-diacetylspermine in the urine of active TB patients. Measurement of the abundances of other polyamine catabolites, *N*-acetylspermine and *N*-acetylspermidine, during active disease will also aid in understanding the role of host SSAT during *Mtb* infection. Further analyses of tissue samples are required to confirm whether or not these metabolites are produced at the site of infection and if they are increased during active TB. A more focused experiment using tissues and urine of infected and uninfected mice undergoing different treatment regimens is needed to elucidate the role of antibiotics and INH specifically in *N*-acetylisoputreanine levels. Additionally, samples from patients being administered prophylactic INH or RIF could help determine whether non-specific killing of gut microflora or INH inhibition of DAO are responsible for altered *N*-acetylisoputreanine levels.

This link between polyamine catabolism and TB is exciting because studies of this pathway in relation to TB are limited. Interestingly, arginine, an important and highly studied

metabolite in relation to TB, can actually be converted to ornithine, the precursor for the polyamine metabolic pathway by arginase[19,20]. Arginase competes with nitric oxide synthase for available arginine in order to control inflammation and kill intracellular *Mtb* respectively[19,21,22]. Correspondingly, these two enzymes are used to characterize different macrophage populations; arginase is a marker for M2 anti-inflammatory macrophages and nitric oxide synthase is a marker for M1 pro-inflammatory macrophages [23]. Though it is generally accepted that predominantly M1 macrophages exist during *Mtb* infection, macrophage expression of arginase has been detected in the lungs of *Mtb* infected non-human primates and humans and in patient PBMCs[24-26]. The increased expression of arginase during *Mtb* infection would lead to increased production of ornithine which could enter the polyamine metabolic pathway and increase polyamine biosynthesis. Since polyamine metabolism is tightly regulated, polyamine catabolism would be induced to counteract the increased level of polyamines. Thus the polyamine catabolites discussed in this dissertation could be used as markers for M2 macrophages during TB. Further investigations of the role of polyamine metabolism during TB through analysis of the enzymes and metabolites involved in this pathway are needed to elucidate whether this scenario is true.

The core-1 *O*-glycosylated peptide is capable of being a robust predictor of active disease as seen in Chapter 4. Thus, knowledge of its origin and the metabolic pathways involved is even more desirable. Two likely source proteins, C1INH and fibrinogen, both involved in coagulation were described in Chapter 2. Evaluation of urine from patients deficient in either of these proteins may elucidate its origin. Though defining the origin of this peptide would lead to a better understanding of host physiological responses to infection with *Mtb*, without knowing its origin this glycopeptide can still be pursued as a biomarker for anti-TB treatment response.

Assessment of the glycopeptide and other structurally confirmed metabolites in TB patients with different treatment response outcomes as well as in TB patients receiving different treatment regimens is needed to validate them as biomarkers. Chapter 4 demonstrated the likelihood that a causal relationship between core 1 *O*-glycosylated peptide and N^1, N^{12}-diacetylspermine and TB exists due to their increase in active disease and decrease with successful treatment, however, this relationship needs to be confirmed using more targeted methods. Additionally, it has yet to be demonstrated whether such a relationship exist for the other structurally confirmed metabolites. During the assessment of treatment response, it is imperative that all patient at risk for treatment failure or relapse are detected. Thus, these biomarkers need to be assessed as prognostic markers for poor anti-TB treatment outcome. Analysis of samples representative of different treatment response outcomes will enable determination of the sensitivity and specificity when using levels of these biomarkers to classify patients. In this scenario, it is more important to have a high sensitivity, since missing a potential treatment failure or relapse could lead to patient death and continued spread of the pathogen, whereas, classifying a responder as a potential treatment failure still results in a cure though it might lead to a longer treatment duration or more adverse side effects. It is important to keep in mind that the low prevalence of a poor outcome may influence the PPV and that a low PPV doesn't necessarily indicate a deficient prognostic [27].

Following demonstration that these are robust prognostic biomarkers of poor treatment outcome, these markers can be assessed as surrogate markers for treatment efficacy. In order to do this, different treatment regimens and outcomes should be analyzed. This data along with the statistical methods described in Chapter 1 will not only confirm their prognostic capabilities, but will demonstrate that their changes are dependent on anti-TB treatment and can be used to

predict the efficacy of treatment. It also provides more evidence that they are markers of disease resolution and not a marker of one specific therapy. Demonstration that specific biomarkers are for disease resolution would enable these markers to be used in evaluating the efficacy of newly developed compounds and regimens.

The results described in this dissertation demonstrated the complexity of human metabolism. A single metabolite can belong to one or many metabolic pathways and alterations in that metabolite may not be as straightforward as upregulation of biosynthetic or catabolic enzymes. Furthermore, altered levels of metabolites might not arise from changes in metabolic pathways, but may be due to increased degradation of host macromolecules such as nucleic acids, proteins and lipids. Adding to this complexity is the fact that metabolites formed at the site of infection may be further modified at other sites in the body before being excreted in the urine. Analysis of transcript, protein, and metabolite levels involved in the biosynthesis and catabolism of a targeted metabolite in a variety of patient and animal samples is needed to fully comprehend how the metabolite is formed and the mechanisms behind alterations observed. Although understanding the complex metabolism of human beings is challenging, any insights are exciting and provide useful information for developing biomarkers and treatments for human diseases.

REFERENCES

1. Koulman A, Lane GA, Harrison SJ, Volmer DA. From differentiating metabolites to biomarkers. Anal Bioanal Chem 2009;394(3):663-70.
2. Johnson CH, Ivanisevic J, Siuzdak G. Metabolomics: beyond biomarkers and towards mechanisms. Nat Rev Mol Cell Biol 2016;17(7):451-9.
3. Pacchiarotta T, Hensbergen PJ, Wuhrer M, van Nieuwkoop C, Nevedomskaya E, Derks RJ, Schoenmaker B, Koeleman CA, van Dissel J, Deelder AM and others. Fibrinogen alpha chain O-glycopeptides as possible markers of urinary tract infection. J Proteomics 2012;75(3):1067-73.
4. Mahapatra S, Hess AM, Johnson JL, Eisenach KD, DeGroote MA, Gitta P, Joloba ML, Kaplan G, Walzl G, Boom WH and others. A metabolic biosignature of early response to anti-tuberculosis treatment. BMC Infect Dis 2014;14:53.
5. Piraud M, Vianey-Saban C, Petritis K, Elfakir C, Steghens JP, Bouchu D. Ion-pairing reversed-phase liquid chromatography/electrospray ionization mass spectrometric analysis of 76 underivatized amino acids of biological interest: a new tool for the diagnosis of inherited disorders of amino acid metabolism. Rapid Commun Mass Spectrom 2005;19(12):1587-602.
6. Chen SS, Burton C, Kaczmarek A, Shi HL, Ma YF. Simultaneous determination of urinary quinolinate, gentisate, 4-hydroxybenzoate, and alpha-ketoglutarate by high-performance liquid chromatography-tandem mass spectrometry. Analytical Methods 2015;7(16):6572-6578.
7. Orhan H, Vermeulen NP, Tump C, Zappey H, Meerman JH. Simultaneous determination of tyrosine, phenylalanine and deoxyguanosine oxidation products by liquid chromatography-tandem mass spectrometry as non-invasive biomarkers for oxidative damage. J Chromatogr B Analyt Technol Biomed Life Sci 2004;799(2):245-54.
8. Bouatra S, Aziat F, Mandal R, Guo AC, Wilson MR, Knox C, Bjorndahl TC, Krishnamurthy R, Saleem F, Liu P and others. The human urine metabolome. PLoS One 2013;8(9):e73076.
9. Lawn SD. Point-of-care detection of lipoarabinomannan (LAM) in urine for diagnosis of HIV-associated tuberculosis: a state of the art review. BMC Infect Dis 2012;12:103.
10. Minion J, Leung E, Talbot E, Dheda K, Pai M, Menzies D. Diagnosing tuberculosis with urine lipoarabinomannan: systematic review and meta-analysis. European Respiratory Journal 2011;38(6):1398-1405.
11. Shaffer P. The excretion of kreatinin and kreatin in health and disease. American Journal of Physiology 1908;23(1):1-22.
12. Ram MM, Reddy V. Variability in urinary creatinine. Lancet 1970;2(7674):674.
13. Alessio L, Berlin A, Dellorto A, Toffoletto F, Ghezzi I. RELIABILITY OF URINARY CREATININE AS A PARAMETER USED TO ADJUST VALUES OF URINARY BIOLOGICAL INDICATORS. International Archives of Occupational and Environmental Health 1985;55(2):99-106.
14. Curtis G, Fogel M. CREATININE EXCRETION - DIURNAL VARIATION AND VARIABILITY OF WHOLE AND PART-DAY MEASURES - A METHODOLOGIC

ISSUE IN PSYCHOENDOCRINE RESEARCH. Psychosomatic Medicine 1970;32(4):337-&.
15. Vestergaard P, Leverett R. CONSTANCY OF URINARY CREATININE EXCRETION. Journal of Laboratory and Clinical Medicine 1958;51(2):211-218.
16. Chadha V, Garg U, Alon US. Measurement of urinary concentration: a critical appraisal of methodologies. Pediatr Nephrol 2001;16(4):374-82.
17. Warrack BM, Hnatyshyn S, Ott KH, Reily MD, Sanders M, Zhang H, Drexler DM. Normalization strategies for metabonomic analysis of urine samples. J Chromatogr B Analyt Technol Biomed Life Sci 2009;877(5-6):547-52.
18. Wu Y, Li L. Sample normalization methods in quantitative metabolomics. J Chromatogr A 2016;1430:80-95.
19. Qualls JE, Murray PJ. Immunometabolism within the tuberculosis granuloma: amino acids, hypoxia, and cellular respiration. Semin Immunopathol 2016;38(2):139-52.
20. Rapovy SM, Zhao J, Bricker RL, Schmidt SM, Setchell KD, Qualls JE. Differential Requirements for L-Citrulline and L-Arginine during Antimycobacterial Macrophage Activity. J Immunol 2015;195(7):3293-300.
21. El Kasmi KC, Qualls JE, Pesce JT, Smith AM, Thompson RW, Henao-Tamayo M, Basaraba RJ, König T, Schleicher U, Koo MS and others. Toll-like receptor-induced arginase 1 in macrophages thwarts effective immunity against intracellular pathogens. Nat Immunol 2008;9(12):1399-406.
22. Qualls JE, Neale G, Smith AM, Koo MS, DeFreitas AA, Zhang H, Kaplan G, Watowich SS, Murray PJ. Arginine usage in mycobacteria-infected macrophages depends on autocrine-paracrine cytokine signaling. Sci Signal 2010;3(135):ra62.
23. Galván-Peña S, O'Neill LA. Metabolic reprograming in macrophage polarization. Front Immunol 2014;5:420.
24. Pessanha AP, Martins RA, Mattos-Guaraldi AL, Vianna A, Moreira LO. Arginase-1 expression in granulomas of tuberculosis patients. FEMS Immunol Med Microbiol 2012;66(2):265-8.
25. Mattila JT, Ojo OO, Kepka-Lenhart D, Marino S, Kim JH, Eum SY, Via LE, Barry CE, Klein E, Kirschner DE and others. Microenvironments in tuberculous granulomas are delineated by distinct populations of macrophage subsets and expression of nitric oxide synthase and arginase isoforms. J Immunol 2013;191(2):773-84.
26. Zea AH, Culotta KS, Ali J, Mason C, Park HJ, Zabaleta J, Garcia LF, Ochoa AC. Decreased expression of CD3zeta and nuclear transcription factor kappa B in patients with pulmonary tuberculosis: potential mechanisms and reversibility with treatment. J Infect Dis 2006;194(10):1385-93.
27. Pepe MS. The statistical evaluation of medical tests for classification and prediction. USA: Oxford University Press; 2003.

APPENDIX

Phosphorylation of KasA and KasB

A.1 Introduction

The cell envelope of *Mycobacterium tuberculosis* plays an essential role in its pathogenicity [1]. Mycolic acids, a predominant component of this impermeable cell envelope, are essential for the virulence and survival of *M. tuberculosis* in that they form crucial interactions with macrophages during infection and provide an impermeable barrier for drugs and other external molecules[1-5]. There are two fatty acid synthases involved in mycolic acid biosynthesis, fatty acid synthase I (FAS-I) and fatty acid synthase II (FAS II)[4,6]. Of interest to this chapter are the distinct, dissociable enzymes of FAS-II which are responsible for producing the longer chain meromycolates, ranging from 56 – 64 carbons.

FAS-II, typically found in prokaryotes, is composed of separate, dissociable enzymes; β - ketoacyl synthase (KAS), β - ketoacyl reductase (KR), β - hydroxyacyl dehydrase (DH), and enoyl reductase (ER)[6-8]. Additional enzymes, mycolic methyltransferases (MAMTs), modify the meromycolate chain produced by FAS-II[9,10]. The complexity and diversity of meromycolate chains produced by FAS-II indicate a high level of regulation due to post-translational modifications and interactions between the many enzymes involved. Previous studies using recombinant proteins have shown these modifications and interactions occur *in vitro*[11-14]. This led to the hypothesis that post-translational modifications and protein-protein interactions modulate differential associations and functions of FAS-II enzymes allowing for modification of mycolic acid species during infection. This chapter describes the characterization of native KasA and KasB phosphorylation in *Mtb*H37Ra.

A.2 Materials and Methods

Bacterial Strains and Growth Conditions

E. coli strains used for cloning and expression of recombinant KasA and KasB were *E. coli* Top10 (Invitrogen) and *E. coli* BL21 (Novagen).

Mtb H37Ra was grown and maintained on Middlebrook 7H11 agar plates supplemented with OADC or in Sauton medium at 37˚C. When required media were supplemented with 75μg/ml hygromycin.

Cloning Expression and Purification of recombinant KasA and KasB

The following plasmids designed to express KasA and KasB (pET28a-*kasA*, pET28a-*kasB*, pVV16-*kasA*, pVV16-*kasB*) were used. *E. coli* cells transformed with either pET28a-*kasB* or pET28a-*kasA* were used to inoculate LB medium supplemented with 50μg/ml kanamycin. Cultures were grown at 37˚C and induced with 1mM IPTG. Recombinant KasA and KasB were purified with Ni-NTA resin (Qiagen, Valencia, CA). *Mtb*H37Ra cells transformed with either pVV16-*kasA* or pVV16-*kasB* were used to inoculate Sauton medium supplemented with 75μg/ml hygromycin. His-tagged KasA and KasB were purified with Ni-NTA resin (Qiagen, Valencia, CA).

Two Dimensional Gel Electrophoresis

For *in vivo* detection of different KasA and KasB isoforms, cells were harvested and lysed using a French Pressure Cell in lysis buffer containing DNase, RNase, and Halt protease and phosphatase inhibitor cocktail (ThermoFisher Scientific, Waltham, MA, USA) in TBS, pH 7.4. The lysate was cleared by centrifugation at 27,000xg and 100,000xg. The 60% ammonium sulfate fraction was obtained by adding ground ammonium sulfate to cleared lysate containing cytosolic protein, the precipitate was resuspended and buffer exchanged in Tris-Cl pH 7.0. For

both cytosolic proteins and 60% ammonium sulfate enrich fraction, approximately 100 µg of total protein was loaded onto a 7cm Immobiline DryStrip Gel (GE Healthcare, pH 4-7) and the first dimension electrophoresis was performed using a Multiphor II Electrophoresis System (GE Healthcare). The second dimension was performed using either a 4-12% or a 10% IPG Zoom gel (Invitrogen). Approximately 5µg of purified recombinant KasA and KasB proteins from *Mtb* H37Ra was used with the same electrophoresis parameters.

Immunoblotting

For KasA and KasB detection, 2D gels were blotted onto PVDF membrane and probed with rabbit anti-KasA or KasB polyclonal antibodies (1:500000). The secondary antibody was horseradish peroxidase-conjugated anti-rabbit IgG polyclonal antibody at 1:2500 (Promega). Detection was carried out using Pierce ECL Western blotting substrate (Thermo Scientific) according to manufacturer's instructions.

For phospho-amino acid detection, 1D gels were blotted onto PVDF membrane and probed with rabbit anti-phosphothreonine (1:500), rabbit anti-phosphoserine (1:200), and rabbit anti-phosphotyrosine (1:1000) polyclonal antibodies (Life Technologies). The secondary antibody was horseradish peroxidase-conjugated anti-rabbit IgG polyclonal antibody at 1:5000 (Promega). Detection was carried out using Pierce ECL Western blotting substrate (Thermo Scientific) according to manufacturer's instructions.

Phosphopeptide Identification by LC-MS/MS Analyses

Mtb H37Ra cells were harvested and lysed using a French Pressure Cell in lysis buffer (8M Urea, 75 mM NaCl, 50mM Tris, pH 8.2). Halt protease and phosphatase inhibitor cocktail (ThermoFisher Scientific, Waltham, MA, USA) was added according to manufacturer's instructions. 15mg of total protein at a concentration of 10-20mg/ml was reduced with 5mM

DTT and alkylated with 14mM iodoacetamide. In-solution digestion was done with trypsin (Promega, Madison, WI, USA) at an enzyme to substrate ration of 1/200 and incubated overnight at 37˚C. The resulting digest was desalted using Sep-Pak C18 cartridges (Waters, Milford, MA, USA) frozen at -80˚C and lyophilized.

Recombinant KasA and KasB protein bands were excised from 1D gel, destained and digested with 5 µl of 83 ng/µl trypsin (Roche Diagnostics, Indianapolis, IN, USA). The peptide were extracted with 60% ACN and 0.1% TFA in water, dried in Savant SpeedVac.

Offline Phosphopeptide Enrichment

Phosphopeptides were enriched according to the previously published protocol [15]. Briefly peptides were resuspended in 40% ACN and 25mM FA in water (IMAC binding buffer). PHOS-Select Iron Affinity Gel beads (Sigma, St. Louis, MO, USA) were equilibrated in IMAC binding buffer and peptide samples were incubated with beads for 60 minutes. The unphosphorylated peptide flow through was retained for MS analysis and phosphorylated peptides were eluted with 50% ACN and 0.5% acetic acid.

Online Phosphopeptide Enrichment

Peptides were resuspended in 40% ACN and 25mM FA in water. Peptides are loaded onto the Phosphochip (Agilent, Santa Clara, CA, USA) and unphosphorylated peptides are analyzed using a gradient of water and ACN supplemented with 0.6% acetic acid and 0.5% FA. Phosphopeptides are eluted with elution buffer (Agilent, Santa Clara, CA, USA) and analyzed with a gradient of water and ACN supplemented with 0.6% acetic acid and 0.5% FA.

LC-MS Analyses

The samples were analyzed using and Agilent 6550 QTOF or a Thermo Scientific Orbitrap Velos MS coupled with nanoHPLC. Spectrum Mill was set up to search the Mycobacterium database assuming digestion with enzyme trypsin. Spectrum Mill was searched with a fragment ion tolerance of 50 PPM and a parent ion tolerance of 20 PPM. Oxidation of methionine and deamidated asparagine were specified as variable modifications. Mascot was set up to search the MtbRv_Rev_R20_041212 database assuming the digestion enzyme trypsin. Mascot was searched with a fragment ion mass tolerance of 0.80 Da and a parent ion tolerance of 20 PPM. Oxidation of methionine and phosphorylation of serine, threonine and tyrosine were specified in Mascot as variable modifications. Scaffold (version Scaffold_4.1.1, Proteome Software Inc., Portland, OR) was used to validate MS/MS based peptide and protein identifications. Peptide identifications were accepted if they could be established at greater than 95.0% probability by the Scaffold Local FDR algorithm. Protein identifications were accepted if they could be established at greater than 99.9% probability and contained at least 2 identified peptides. Protein probabilities were assigned by the Protein Prophet algorithm (Nesvizhskii, Al et al Anal. Chem. 2003; 75(17):4646-58). Proteins that contained similar peptides and could not be differentiated based on MS/MS analysis alone were grouped to satisfy the principles of parsimony.

A.3 Results

Two dimensional gel electrophoresis of KasA and KasB from *M. bovis* BCG lysates expressing native and recombinant proteins yielded multiple spots [13]. This spot profile was confirmed using lysates from *Mtb* H37Ra (Figure A.1A). KasA and KasB proteins were present in the 60% fraction after ammonium sulfate precipitation (data not shown). Analysis of this fraction using MES running buffer allowed for a cleaner separation and better visualization of native KasA and KasB spots in the *Mtb* H37Ra lysate (Figure A.1B). While this spot profile is different than that previously shown for *M. bovis* BCG native proteins, it is similar to what is depicted for recombinant *Mtb* KasA and KasB expressed in *M. bovis* BCG [13]. Due to this

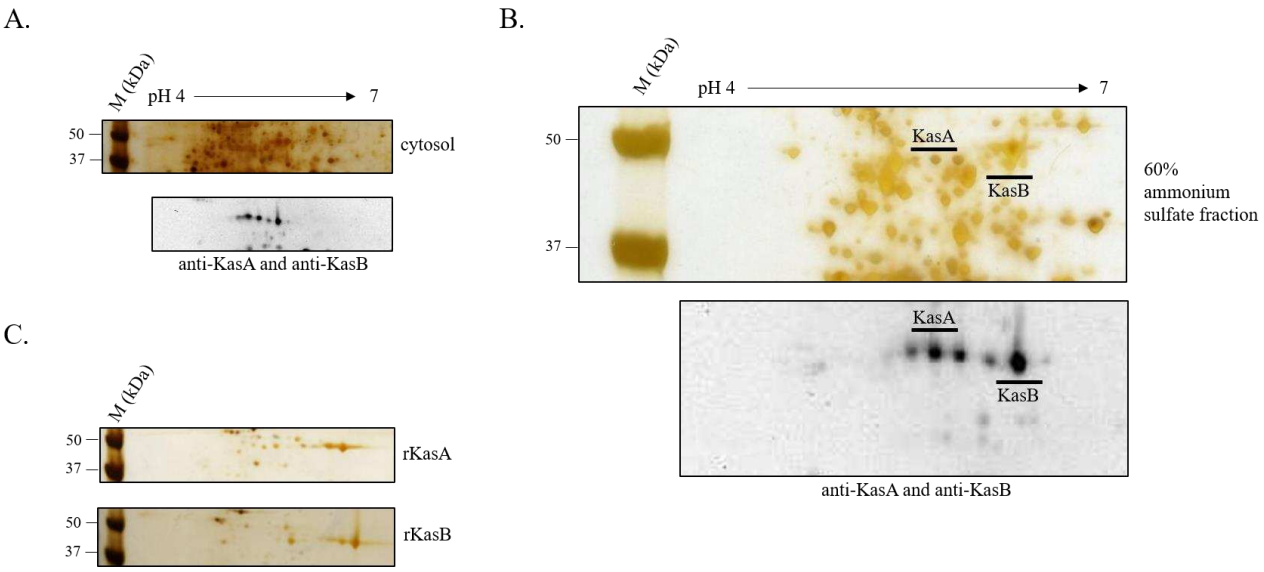

Figure A.1
Confirmation of KasA and KasB spot profile. *Mtb*H37Ra cytosolic proteins (A) 60% ammonium sulfate fraction of *Mtb*H37Ra cytosolic proteins (B) rKasA and rKasB expressed in *Mtb*H37Ra

difference, the spots corresponding predicted to belong to KasA and KasB based on reactivity with KasA and KasB antibodies were cut out and analyzed by MS following trypsin digestion. The MS results confirmed that these spots belonged to KasA and KasB (data not shown).

In order to obtain more protein for determination of phosphorylation sites, KasA and KasB were overexpressed in *Mtb* H37Ra. The spot profile of the purified, recombinant proteins expressed in *Mtb* H37Ra resembled that of the native *Mtb* H37Ra proteins, confirming that overexpression didn't affect the phosphorylation state of these proteins (Figure A.1C). Previously, it was shown that *Mtb* KasA and KasB expressed in *E. coli* didn't react with phosphoserine and phosphothreonine antibodies and that expression in *M. bovis* BCG was required for reactivity [13]. Phosphoantibody reactivity of recombinant *Mtb* KasA and KasB expressed in *Mtb* H37Ra was assessed using one dimensional gel electrophoresis (Figure A.2). Minor reactivity against all three antibodies tested (phosphoserine, phosphothreonine and phosphotyrosine) was observed for KasA and KasB expressed in both *Mtb* H37Ra as well as in *E. coli* (Figure A.2). The reactivity against the phosphoserine antibody was not as strong as that observed for the positive control ovalbumin which is known to be phosphorylated on two serine residues [16]. Similar reactivity against the phosphothreonine antibody was observed for ovalbumin, which is not described as having any phosphorylated threonine sites [16]. More reactivity was observed for the positive control BSA conjugated with phosphotyrosine amino acid than with the recombinant KasA and KasB proteins and minor reactivity of all proteins with the secondary antibody alone was observed (Figure A.2). KasA and KasB were previously shown to be phosphorylated on threonine residues, however, the reactivity observed against the phosphothreonine antibody is similar to that of ovalbumin, making it seem like the reactivity observed is non-specific [13]. Based on the above results, no conclusive determinations can be made about phosphorylation of KasA and KasB.

In attempt to increase the amount of KasA and KasB phosphopeptides available for detection, an off-line phosphopeptide enrichment was performed on an in-solution digest of native proteins from *Mtb*H37Ra whole cell lysate. This phosphopeptide enrichment was analyzed by LC-MS on a LTQ Orbitrap and no phosphopeptides for KasA and KasB were identified, however, other phosphopeptides were detected (Table A.1 and Table A.2). On-line phosphopeptide enrichment of native proteins from *Mtb*H37Ra whole cell lysate using an Agilent phosphochip and QTOF was performed. Though other phosphopeptides were detected, no phosphopeptides were identified for KasA and KasB (Table A.3). In order to increase the amount of KasA and KasB protein and chances of identifying phosphopeptides, LC-MS analysis of purified, recombinant KasA and KasB expressed in *Mtb*H37Ra was performed. In gel digestion of the purified, recombinant KasA and KasB protein bands from a 1D gel and subsequent analysis with LC-MS on LTQ Orbitrap yielded some phosphopeptides. These sequences indicated putative phosphorylation sites for KasA (T165) and KasB (S188, S192 and

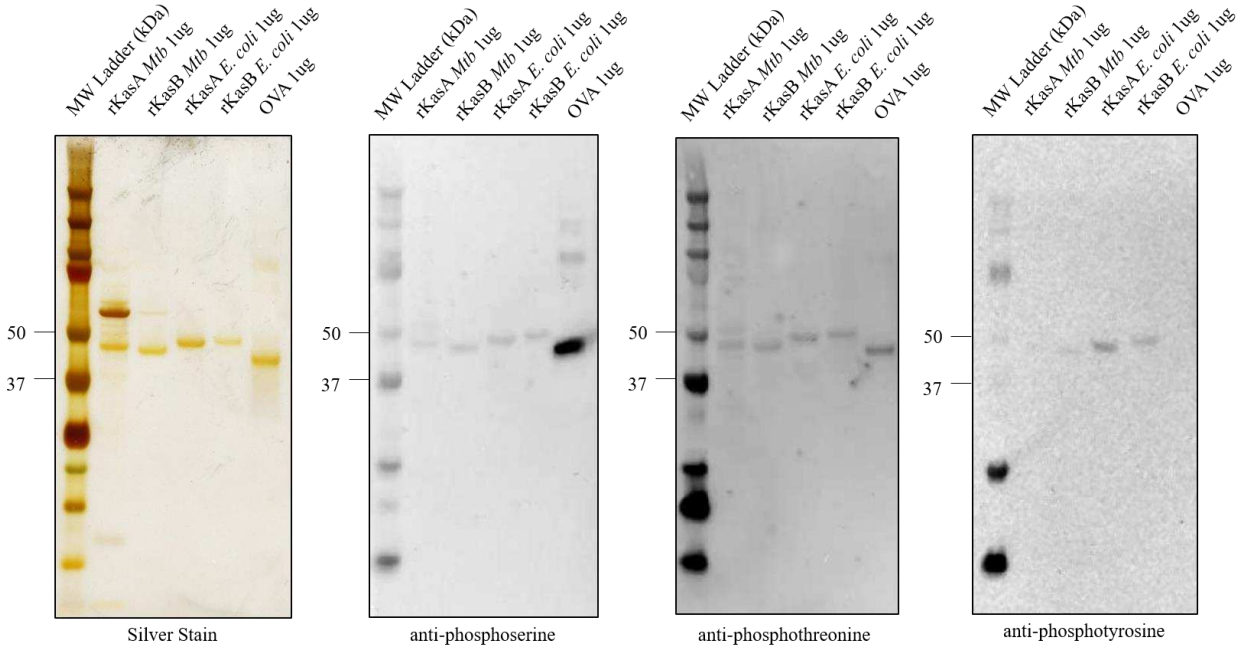

Figure A.3 Reactivity of KasA and KasB with phosphoantibodies

KasB (K)AVSPLTVQKyMPNGAAAAVGLER(H)

MS^2

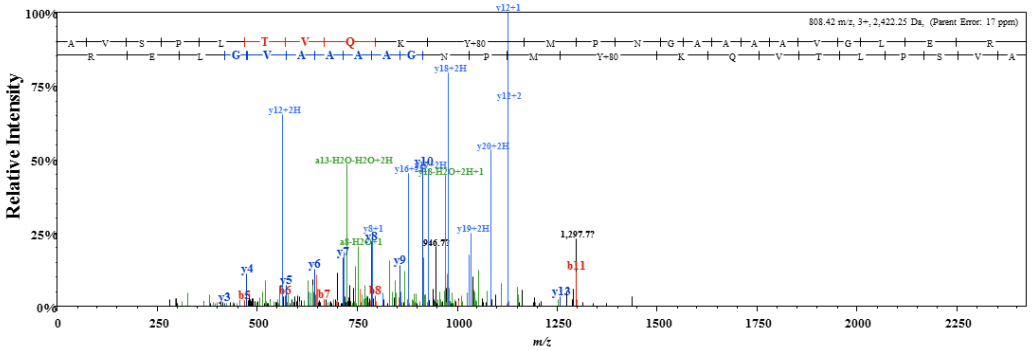

(K)AGVMTPVsACASGAEAIAR(A)

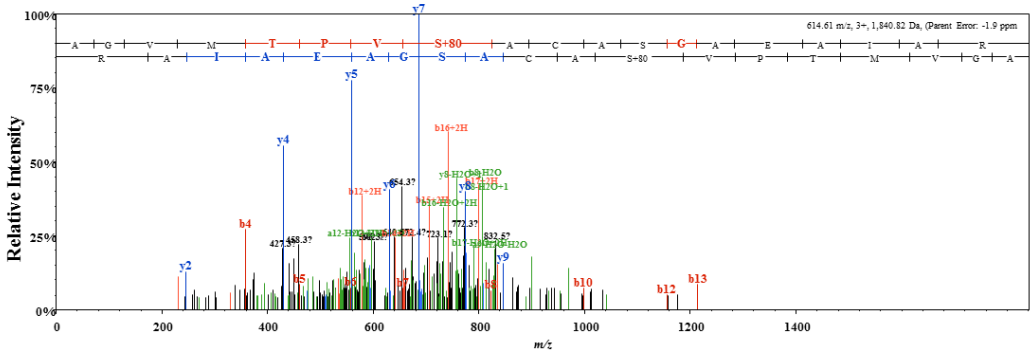

(K)AGVmTPVSACAsGAEAIAR(A)

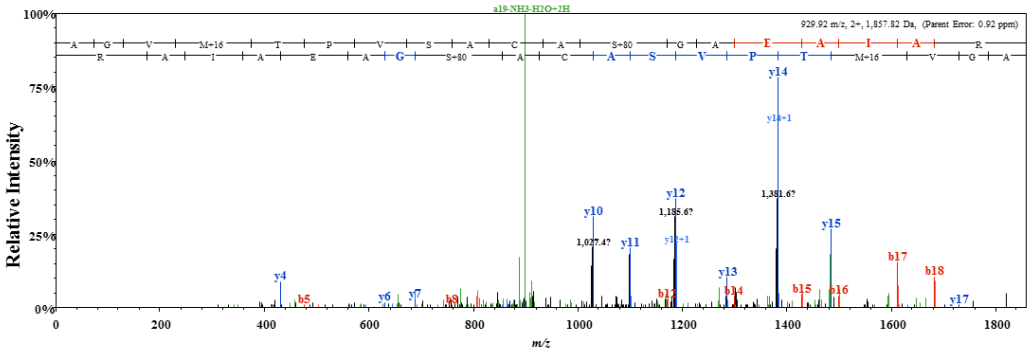

KasA (R)AGVmtPVSACSSGSEAIAHAWR(Q)

MS^2

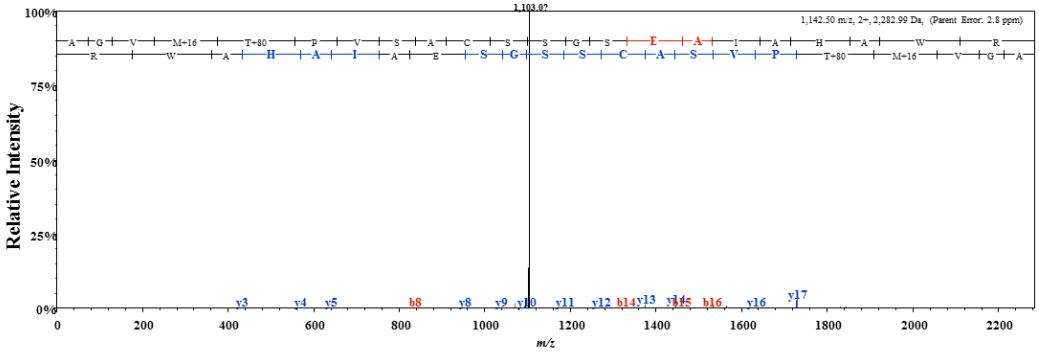

Figure A.5 KasA and KasB phosphopeptides

Y164) (Figure A.3). However, very few spectra for each phosphopeptide were identified and there was a lot of background in the spectra (Figure A.3). On-line phosphopeptide enrichment of in-gel digested purified, recombinant KasA and KasB using Agilent phosphochip and QTOF, had good sequence coverage of both proteins, but yielded no phosphopeptides for KasA and KasB (Figure A.4). Peptides for both proteins were detected in both the phosphoprotein eluate and nonphosphoprotein eluate.

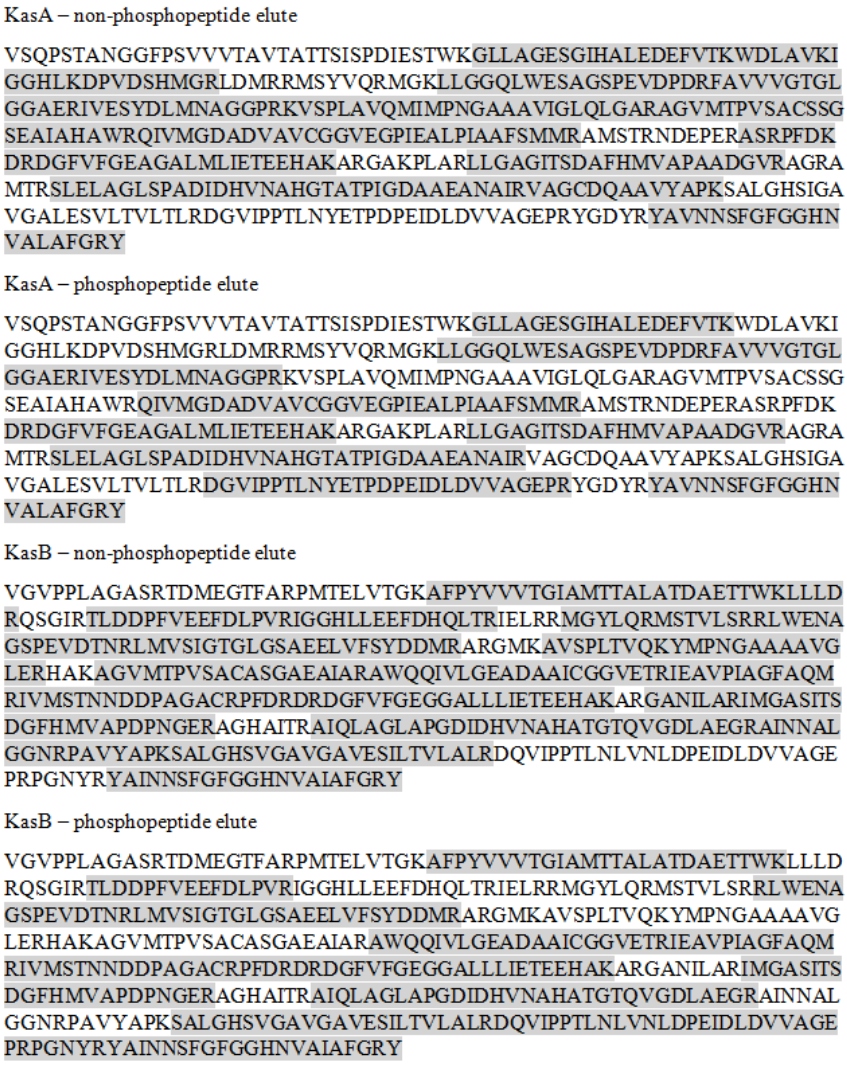

Figure A.7
Sequence coverage of KasA and KasB from phosphochip and Q-TOF analysis. Peptides detected are highlighted in gray.

A.4 Discussion

Previous research suggested that KasA and KasB were phosphorylated on threonine residues[13,17]. Confirmation of the spot profile of KasA and KasB observed in this previous study was achieved [13]. However, multiple analyses failed to confirm the phosphorylated residues and sites of phosphorylation for both of these proteins. Though there was minor reactivity with phospho-antibodies, this reactivity was concluded to be nonspecific. This is in contrast with the previous studies which demonstrated reactivity with a phosphothreonine antibody[13,17]. However, a positive or negative control is not shown, making it hard to compare their signal with the signal seen in Fig A.2. One explanation for these differing results could be the two different strains used, *M. bovis* BCG vs. *Mtb* H37Ra. Interestingly, though KasA has a lower molecular weight than KasB, KasA ran higher than KasB (Fig A.1 and A.2). However, in the previous study using *M bovis* BCG, KasA runs lower than KasB [13].

Although, KasA and KasB were shown to be phosphorylated on two threonine residues (T334 and T 336), attempts to detect KasA and KasB phosphopeptides were unsuccessful[17]. However, the MS data and conditions used are not reported, making it difficult to compare with the results presented in this chapter. Although care was taken to preserve phosphorylation, this modification is extremely labile and it's possible that phosphates were removed prior to or during LC-MS analysis. However, in our analyses of the whole cell lysate, phosphopeptides were detected, indicating that some phosphorylation was preserved. If KasA and KasB were truly phosphorylated, one would expect to detect at least some phosphopeptides from the whole cell lysate. LC-MS analysis using recombinant purified KasA and KasB did yield some phosphopeptides, however, there were not many and the spectra was noisy, making it hard to interpret the fragmentation. Additionally, the peptide sequences that fragmentation could be

determined for, didn't contain the part of the sequence with the phosphorylation site. Though putative phosphorylation sites were assigned, there is little confidence behind them.

The previous groups further confirmed phosphorylation of KasA and KasB by demonstrating disappearance of other proteins spots upon phosphatase treatment [13]. This experiment would need to be repeated to confirm their results or demonstrate that KasA and KasB are not phosphorylated. At this point, it seems like the data are indicating that the spot profile observed after two dimensional gel electrophoresis is due to some other modification aside from phosphorylation. Further analysis is needed to confirm this and to determine the reason for the multiple KasA and KasB spots.

Table A.1

List of all proteins detected in WCL phosphopeptide enrichment fraction. Off-line phosphopeptide enrichment.

Protein Accession Number/Protein name
Rv0002.1 | Rv0002 | Mycobacterium tuberculosis H37Rv DNA polymerase III beta chain dnaN (403 aa)
Rv0005.1 | Rv0005 | Mycobacterium tuberculosis H37Rv DNA gyrase subunit B gyrB (715 aa)
Rv0006.1 | Rv0006 | Mycobacterium tuberculosis H37Rv DNA gyrase subunit A gyrA (839 aa)
Rv0007.1 | Rv0007 | Mycobacterium tuberculosis H37Rv conserved membrane protein (305 aa)
Rv0009.1 | Rv0009 | Mycobacterium tuberculosis H37Rv iron-regulated peptidyl-prolyl-cis-trans-isomerase A ppiA (183 aa)
Rv0014c.1 | Rv0014c | Mycobacterium tuberculosis H37Rv transmembrane serine/threonine-protein kinase B pknB (627 aa)
Rv0015c.1 | Rv0015c | Mycobacterium tuberculosis H37Rv transmembrane serine/threonine-protein kinase A pknA (432 aa)
Rv0020c.1 | Rv0020c | Mycobacterium tuberculosis H37Rv conserved hypothetical protein (528 aa)
Rv0036c.1 | Rv0036c | Mycobacterium tuberculosis H37Rv conserved hypothetical protein (258 aa)
Rv0053.1 | Rv0053 | Mycobacterium tuberculosis H37Rv 30S ribosomal protein S6 rpsF (97 aa)
Rv0054.1 | Rv0054 | Mycobacterium tuberculosis H37Rv single-strand binding protein ssb (165 aa)
Rv0055.1 | Rv0055 | Mycobacterium tuberculosis H37Rv 30S ribosomal protein rpsR1 (85 aa)
Rv0056.1 | Rv0056 | Mycobacterium tuberculosis H37Rv 50S ribosomal protein L9 rplI (153 aa)
Rv0066c.1 | Rv0066c | Mycobacterium tuberculosis H37Rv isocitrate dehydrogenase icd2 (746 aa)
Rv0088.1 | Rv0088 | Mycobacterium tuberculosis H37Rv hypothetical protein (225 aa)
Rv0129c.1 | Rv0129c | Mycobacterium tuberculosis H37Rv secreted fibronectin-binding protein C antigen 85-C fbpC (341 aa)
Rv0147.1 | Rv0147 | Mycobacterium tuberculosis H37Rv aldehyde dehydrogenase NAD-dependent (507 aa)
Rv0148.1 | Rv0148 | Mycobacterium tuberculosis H37Rv short-chain type dehydrogenase/reductase (287 aa)
Rv0154c.1 | Rv0154c | Mycobacterium tuberculosis H37Rv acyl-CoA dehydrogenase fadE2 (404 aa)
Rv0155.1 | Rv0155 | Mycobacterium tuberculosis H37Rv NAD(P) transhydrogenase alpha subunit pntAa (367 aa)
Rv0157.1 | Rv0157 | Mycobacterium tuberculosis H37Rv NAD(P) transhydrogenase beta subunit pntB (476 aa)
Rv0175.1 | Rv0175 | Mycobacterium tuberculosis H37Rv MCE-associated membrane protein (214 aa)
Rv0178.1 | Rv0178 | Mycobacterium tuberculosis H37Rv MCE-associated membrane protein (245 aa)
Rv0183.1 | Rv0183 | Mycobacterium tuberculosis H37Rv lysophospholipase (280 aa)
Rv0206c.1 | Rv0206c | Mycobacterium tuberculosis H37Rv transmembrane transport protein mmpL3 (945 aa)
Rv0207c.1 | Rv0207c | Mycobacterium tuberculosis H37Rv conserved hypothetical protein (243 aa)
Rv0211.1 | Rv0211 | Mycobacterium tuberculosis H37Rv iron-regulated phosphoenolpyruvate carboxykinase pckA (607 aa)

Rv0227c.1 | Rv0227c | Mycobacterium tuberculosis H37Rv conserved membrane protein (422 aa)
Rv0234c.1 | Rv0234c | Mycobacterium tuberculosis H37Rv succinate-semialdehyde dehydrogenase dependent gabD1 (512 aa)
Rv0241c.1 | Rv0241c | Mycobacterium tuberculosis H37Rv conserved hypothetical protein (281 aa)
Rv0242c.1 | Rv0242c | Mycobacterium tuberculosis H37Rv 3-oxoacyl-[acyl-carrier protein] reductase fabG4 (455 aa)
Rv0243.1 | Rv0243 | Mycobacterium tuberculosis H37Rv acetyl-CoA acyltransferase fadA2 (441 aa)
Rv0247c.1 | Rv0247c | Mycobacterium tuberculosis H37Rv succinate dehydrogenase iron-sulfur subunit (249 aa)
Rv0248c.1 | Rv0248c | Mycobacterium tuberculosis H37Rv succinate dehydrogenase iron-sulfur subunit (647 aa)
Rv0250c.1 | Rv0250c | Mycobacterium tuberculosis H37Rv conserved hypothetical protein (98 aa)
Rv0251c.1 | Rv0251c | Mycobacterium tuberculosis H37Rv heat shock protein hsp (160 aa)
Rv0270.1 | Rv0270 | Mycobacterium tuberculosis H37Rv fatty-acid-CoA ligase fadD2 (561 aa)
Rv0292.1 | Rv0292 | Mycobacterium tuberculosis H37Rv conserved membrane protein (332 aa)
Rv0341.1 | Rv0341 | Mycobacterium tuberculosis H37Rv isoniazid inductible gene protein iniB (480 aa)
Rv0342.1 | Rv0342 | Mycobacterium tuberculosis H37Rv isoniazid inductible gene protein iniA (641 aa)
Rv0350.1 | Rv0350 | Mycobacterium tuberculosis H37Rv chaperone protein dnaK (626 aa)
Rv0351.1 | Rv0351 | Mycobacterium tuberculosis H37Rv chaperone grpE (236 aa)
Rv0363c.1 | Rv0363c | Mycobacterium tuberculosis H37Rv fructose-bisphosphate aldolase fba (345 aa)
Rv0379.1 | Rv0379 | Mycobacterium tuberculosis H37Rv protein transport protein secE2 (72 aa)
Rv0383c.1 | Rv0383c | Mycobacterium tuberculosis H37Rv conserved secreted protein (285 aa)
Rv0384c.1 | Rv0384c | Mycobacterium tuberculosis H37Rv endopeptidase ATP binding protein chain B clpB (849 aa)
Rv0407.1 | Rv0407 | Mycobacterium tuberculosis H37Rv F420-dependent glucose-6-phosphate dehydrogenase fgd1 (337 aa)
Rv0421c.1 | Rv0421c | Mycobacterium tuberculosis H37Rv conserved hypothetical protein (210 aa)
Rv0439c.1 | Rv0439c | Mycobacterium tuberculosis H37Rv dehydrogenase/reductase (312 aa)
Rv0440.1 | Rv0440 | Mycobacterium tuberculosis H37Rv 60 kda chaperonin 2 groEL2 (541 aa)
Rv0458.1 | Rv0458 | Mycobacterium tuberculosis H37Rv aldehyde dehydrogenase (508 aa)
Rv0475.1 | Rv0475 | Mycobacterium tuberculosis H37Rv iron-regulated heparin binding hemagglutinin hbhA (200 aa)
Rv0489.1 | Rv0489 | Mycobacterium tuberculosis H37Rv phosphoglycerate mutase 1 gpm1 (250 aa)
Rv0530.1 | Rv0530 | Mycobacterium tuberculosis H37Rv conserved hypothetical protein (406 aa)
Rv0552.1 | Rv0552 | Mycobacterium tuberculosis H37Rv conserved hypothetical protein (535 aa)
Rv0566c.1 | Rv0566c | Mycobacterium tuberculosis H37Rv conserved hypothetical protein (164 aa)
Rv0580c.1 | Rv0580c | Mycobacterium tuberculosis H37Rv conserved hypothetical protein (164 aa)
Rv0613c.1 | Rv0613c | Mycobacterium tuberculosis H37Rv hypothetical protein (856 aa)
Rv0632c.1 | Rv0632c | Mycobacterium tuberculosis H37Rv enoyl-CoA hydratase echA3 (232 aa)
Rv0634B.1 | Rv0634B | Mycobacterium tuberculosis H37Rv 50S ribosomal protein L33 rpmG2 (56 aa)
Rv0636.1 | Rv0636 | Mycobacterium tuberculosis H37Rv conserved hypothetical protein (143 aa)
Rv0638.1 | Rv0638 | Mycobacterium tuberculosis H37Rv preprotein translocase secE1 (162 aa)
Rv0640.1 | Rv0640 | Mycobacterium tuberculosis H37Rv 50S ribosomal protein L11 rplK (143 aa)
Rv0641.1 | Rv0641 | Mycobacterium tuberculosis H37Rv 50S ribosomal protein L1 rplA (236 aa)
Rv0651.1 | Rv0651 | Mycobacterium tuberculosis H37Rv 50S ribosomal protein L10 rplJ (179 aa)
Rv0652.1 | Rv0652 | Mycobacterium tuberculosis H37Rv 50S ribosomal protein L7/L12 rplL (131 aa)
Rv0667.1 | Rv0667 | Mycobacterium tuberculosis H37Rv DNA-directed RNA polymerase beta chain rpoB (1173 aa)
Rv0668.1 | Rv0668 | Mycobacterium tuberculosis H37Rv DNA-directed RNA polymerase beta chain rpoC (1317 aa)
Rv0683.1 | Rv0683 | Mycobacterium tuberculosis H37Rv 30S ribosomal protein S7 rpsG (157 aa)
Rv0685.1 | Rv0685 | Mycobacterium tuberculosis H37Rv iron-regulated elongation factor tu tuf (397 aa)
Rv0686.1 | Rv0686 | Mycobacterium tuberculosis H37Rv membrane protein (266 aa)
Rv0700.1 | Rv0700 | Mycobacterium tuberculosis H37Rv 30S ribosomal protein S10 rpsJ (102 aa)
Rv0701.1 | Rv0701 | Mycobacterium tuberculosis H37Rv 50S ribosomal protein L3 rplC (218 aa)
Rv0704.1 | Rv0704 | Mycobacterium tuberculosis H37Rv 50S ribosomal protein L2 rplB (281 aa)
Rv0705.1 | Rv0705 | Mycobacterium tuberculosis H37Rv 30S ribosomal protein S19 rpsS (94 aa)
Rv0706.1 | Rv0706 | Mycobacterium tuberculosis H37Rv 50S ribosomal protein L22 rplV (198 aa)
Rv0707.1 | Rv0707 | Mycobacterium tuberculosis H37Rv 30S ribosomal protein S3 rpsC (275 aa)
Rv0710.1 | Rv0710 | Mycobacterium tuberculosis H37Rv 30S ribosomal protein S17 rpsQ (137 aa)
Rv0714.1 | Rv0714 | Mycobacterium tuberculosis H37Rv 50S ribosomal protein L14 rplN (123 aa)
Rv0715.1 | Rv0715 | Mycobacterium tuberculosis H37Rv 50S ribosomal protein L24 rplX (106 aa)
Rv0716.1 | Rv0716 | Mycobacterium tuberculosis H37Rv 50S ribosomal protein L5 rplE (188 aa)
Rv0718.1 | Rv0718 | Mycobacterium tuberculosis H37Rv 30S ribosomal protein S8 rpsH (133 aa)
Rv0719.1 | Rv0719 | Mycobacterium tuberculosis H37Rv 50S ribosomal protein L6 rplF (180 aa)
Rv0720.1 | Rv0720 | Mycobacterium tuberculosis H37Rv 50S ribosomal protein L18 rplR (123 aa)
Rv0721.1 | Rv0721 | Mycobacterium tuberculosis H37Rv 30S ribosomal protein S5 rpsE (221 aa)
Rv0724.1 | Rv0724 | Mycobacterium tuberculosis H37Rv protease IV sppA (624 aa)
Rv0730.1 | Rv0730 | Mycobacterium tuberculosis H37Rv conserved hypothetical protein (243 aa)
Rv0733.1 | Rv0733 | Mycobacterium tuberculosis H37Rv adenylate kinase adk (182 aa)
Rv0757.1 | Rv0757 | Mycobacterium tuberculosis H37Rv two component system transcriptional regulator phoP (248 aa)
Rv0761c.1 | Rv0761c | Mycobacterium tuberculosis H37Rv zinc-type alcohol dehydrogenase NAD dependent adhB (376 aa)
Rv0798c.1 | Rv0798c | Mycobacterium tuberculosis H37Rv 29 kda antigen cfp29 (266 aa)
Rv0810c.1 | Rv0810c | Mycobacterium tuberculosis H37Rv conserved hypothetical protein (61 aa)
Rv0814c.1 | Rv0814c | Mycobacterium tuberculosis H37Rv hypothetical protein sseC2 (101 aa)

Rv0815c.1 | Rv0815c | Mycobacterium tuberculosis H37Rv thiosulfate sulfurtransferase cysA2 (278 aa)
Rv0818.1 | Rv0818 | Mycobacterium tuberculosis H37Rv transcriptional regulator (256 aa)
Rv0824c.1 | Rv0824c | Mycobacterium tuberculosis H37Rv acyl-[acyl-carrier protein] desaturase desA1 (339 aa)
Rv0831c.1 | Rv0831c | Mycobacterium tuberculosis H37Rv conserved hypothetical protein (272 aa)
Rv0860.1 | Rv0860 | Mycobacterium tuberculosis H37Rv fatty-acid oxidation protein fadB (721 aa)
Rv0873.1 | Rv0873 | Mycobacterium tuberculosis H37Rv acyl-CoA dehydrogenase fadE10 (651 aa)
Rv0884c.1 | Rv0884c | Mycobacterium tuberculosis H37Rv phosphoserine aminotransferase serC (377 aa)
Rv0896.1 | Rv0896 | Mycobacterium tuberculosis H37Rv citrate synthase I gltA2 (432 aa)
Rv0898c.1 | Rv0898c | Mycobacterium tuberculosis H37Rv conserved hypothetical protein (88 aa)
Rv0905.1 | Rv0905 | Mycobacterium tuberculosis H37Rv enoyl-CoA hydratase echA6 (244 aa)
Rv0931c.1 | Rv0931c | Mycobacterium tuberculosis H37Rv transmembrane serine/threonine-protein kinase D pknD (665 aa)
Rv0934.1 | Rv0934 | Mycobacterium tuberculosis H37Rv periplasmic phosphate-binding lipoprotein pstS1 (375 aa)
Rv0951.1 | Rv0951 | Mycobacterium tuberculosis H37Rv succinyl-CoA synthetase beta chain sucC (388 aa)
Rv0952.1 | Rv0952 | Mycobacterium tuberculosis H37Rv succinyl-CoA synthetase alpha chain sucD (304 aa)
Rv0993.1 | Rv0993 | Mycobacterium tuberculosis H37Rv UTP-glucose-1-phosphate uridylyltransferase galU (307 aa)
Rv1017c.1 | Rv1017c | Mycobacterium tuberculosis H37Rv ribose-phosphate pyrophosphokinase prsA (327 aa)
Rv1018c.1 | Rv1018c | Mycobacterium tuberculosis H37Rv UDP-N-acetylglucosamine pyrophosphorylase glmU (496 aa)
Rv1023.1 | Rv1023 | Mycobacterium tuberculosis H37Rv enolase eno (430 aa)
Rv1038c.1 | Rv1038c | Mycobacterium tuberculosis H37Rv Esat-6 like protein esxJ (99 aa)
Rv1056.1 | Rv1056 | Mycobacterium tuberculosis H37Rv conserved hypothetical protein (255 aa)
Rv1074c.1 | Rv1074c | Mycobacterium tuberculosis H37Rv beta-ketoacyl CoA thiolase fadA3 (406 aa)
Rv1080c.1 | Rv1080c | Mycobacterium tuberculosis H37Rv transcription elongation factor greA (165 aa)
Rv1093.1 | Rv1093 | Mycobacterium tuberculosis H37Rv serine hydroxymethyltransferase 1 glyA1 (427 aa)
Rv1094.1 | Rv1094 | Mycobacterium tuberculosis H37Rv acyl-[acyl-carrier protein] desaturase desA2 (276 aa)
Rv1098c.1 | Rv1098c | Mycobacterium tuberculosis H37Rv fumarase fum (475 aa)
Rv1133c.1 | Rv1133c | Mycobacterium tuberculosis H37Rv 5-methyltetrahydropteroyltriglutamate-homocysteine methyltransferase metE (760 aa)
Rv1177.1 | Rv1177 | Mycobacterium tuberculosis H37Rv ferredoxin fdxC (109 aa)
Rv1196.1 | Rv1196 | Mycobacterium tuberculosis H37Rv PPE family protein (392 aa)
Rv1198.1 | Rv1198 | Mycobacterium tuberculosis H37Rv esat-6 like protein esxL (95 aa)
Rv1201c.1 | Rv1201c | Mycobacterium tuberculosis H37Rv transferase (318 aa)
Rv1223.1 | Rv1223 | Mycobacterium tuberculosis H37Rv serine protease htrA (529 aa)
Rv1240.1 | Rv1240 | Mycobacterium tuberculosis H37Rv malate dehydrogenase mdh (330 aa)
Rv1245c.1 | Rv1245c | Mycobacterium tuberculosis H37Rv short-chain type dehydrogenase/reductase (277 aa)
Rv1248c.1 | Rv1248c | Mycobacterium tuberculosis H37Rv 2-oxoglutarate dehydrogenase sucA (1215 aa)
Rv1284.1 | Rv1284 | Mycobacterium tuberculosis H37Rv conserved hypothetical protein (164 aa)
Rv1297.1 | Rv1297 | Mycobacterium tuberculosis H37Rv transcription termination factor rho (603 aa)
Rv1307.1 | Rv1307 | Mycobacterium tuberculosis H37Rv ATP synthase delta chain atpH (447 aa)
Rv1308.1 | Rv1308 | Mycobacterium tuberculosis H37Rv ATP synthase alpha chain atpA (550 aa)
Rv1309.1 | Rv1309 | Mycobacterium tuberculosis H37Rv ATP synthase gamma chain atpG (306 aa)
Rv1310.1 | Rv1310 | Mycobacterium tuberculosis H37Rv ATP synthase beta chain atpD (487 aa)
Rv1323.1 | Rv1323 | Mycobacterium tuberculosis H37Rv acetyl-CoA acetyltransferase fadA4 (390 aa)
Rv1328.1 | Rv1328 | Mycobacterium tuberculosis H37Rv glycogen phosphorylase glgP (864 aa)
Rv1388.1 | Rv1388 | Mycobacterium tuberculosis H37Rv integration host factor mihF (191 aa)
Rv1392.1 | Rv1392 | Mycobacterium tuberculosis H37Rv S-adenosylmethionine synthetase metK (404 aa)
Rv1393c.1 | Rv1393c | Mycobacterium tuberculosis H37Rv monooxygenase (493 aa)
Rv1423.1 | Rv1423 | Mycobacterium tuberculosis H37Rv transcriptional regulator whiA (326 aa)
Rv1436.1 | Rv1436 | Mycobacterium tuberculosis H37Rv glyceraldehyde 3-phosphate dehydrogenase gap (340 aa)
Rv1448c.1 | Rv1448c | Mycobacterium tuberculosis H37Rv transaldolase tal (374 aa)
Rv1449c.1 | Rv1449c | Mycobacterium tuberculosis H37Rv transketolase tkt (701 aa)
Rv1475c.1 | Rv1475c | Mycobacterium tuberculosis H37Rv iron-regulated aconitate hydratase acn (944 aa)
Rv1479.1 | Rv1479 | Mycobacterium tuberculosis H37Rv transcriptional regulator moxR1 (378 aa)
Rv1480.1 | Rv1480 | Mycobacterium tuberculosis H37Rv conserved hypothetical protein (318 aa)
Rv1488.1 | Rv1488 | Mycobacterium tuberculosis H37Rv conserved hypothetical protein (382 aa)
Rv1521.1 | Rv1521 | Mycobacterium tuberculosis H37Rv fatty-acid-CoA ligase fadD25 (584 aa)
Rv1543.1 | Rv1543 | Mycobacterium tuberculosis H37Rv fatty-acyl-CoA reductase (342 aa)
Rv1544.1 | Rv1544 | Mycobacterium tuberculosis H37Rv ketoacyl reductase (268 aa)
Rv1558.1 | Rv1558 | Mycobacterium tuberculosis H37Rv conserved hypothetical protein (149 aa)
Rv1617.1 | Rv1617 | Mycobacterium tuberculosis H37Rv pyruvate kinase pykA (473 aa)
Rv1626.1 | Rv1626 | Mycobacterium tuberculosis H37Rv two component system transcriptional regulator (206 aa)
Rv1627c.1 | Rv1627c | Mycobacterium tuberculosis H37Rv nonspecific lipid-transfer protein (403 aa)
Rv1630.1 | Rv1630 | Mycobacterium tuberculosis H37Rv 30S ribosomal protein S1 rpsA (482 aa)
Rv1636.1 | Rv1636 | Mycobacterium tuberculosis H37Rv iron-regulated conserved hypothetical protein (147 aa)
Rv1641.1 | Rv1641 | Mycobacterium tuberculosis H37Rv initiation factor IF-3 infC (202 aa)
Rv1707.1 | Rv1707 | Mycobacterium tuberculosis H37Rv conserved membrane protein (487 aa)
Rv1719.1 | Rv1719 | Mycobacterium tuberculosis H37Rv transcriptional regulator (260 aa)

Rv1746.1 | Rv1746 | Mycobacterium tuberculosis H37Rv anchored-membrane serine/threonine-protein kinase pknF (477 aa)
Rv1747.1 | Rv1747 | Mycobacterium tuberculosis H37Rv conserved transmembrane ATP-binding protein ABC transporter (866 aa)
Rv1771.1 | Rv1771 | Mycobacterium tuberculosis H37Rv oxidoreductase (429 aa)
Rv1782.1 | Rv1782 | Mycobacterium tuberculosis H37Rv conserved membrane protein (507 aa)
Rv1784.1 | Rv1784 | Mycobacterium tuberculosis H37Rv conserved hypothetical protein (933 aa)
Rv1794.1 | Rv1794 | Mycobacterium tuberculosis H37Rv conserved hypothetical protein (301 aa)
Rv1821.1 | Rv1821 | Mycobacterium tuberculosis H37Rv preprotein translocase ATPase secA2 (809 aa)
Rv1827.1 | Rv1827 | Mycobacterium tuberculosis H37Rv hypothetical protein cfp17 (163 aa)
Rv1836c.1 | Rv1836c | Mycobacterium tuberculosis H37Rv conserved hypothetical protein (678 aa)
Rv1837c.1 | Rv1837c | Mycobacterium tuberculosis H37Rv malate synthase G glcB (742 aa)
Rv1843c.1 | Rv1843c | Mycobacterium tuberculosis H37Rv inosine-5-monophosphate dehydrogenase guaB1 (480 aa)
Rv1855c.1 | Rv1855c | Mycobacterium tuberculosis H37Rv oxidoreductase (308 aa)
Rv1869c.1 | Rv1869c | Mycobacterium tuberculosis H37Rv reductase (412 aa)
Rv1871c.1 | Rv1871c | Mycobacterium tuberculosis H37Rv conserved hypothetical protein (130 aa)
Rv1872c.1 | Rv1872c | Mycobacterium tuberculosis H37Rv L-lactate dehydrogenase lldD2 (415 aa)
Rv1875.1 | Rv1875 | Mycobacterium tuberculosis H37Rv conserved hypothetical protein (148 aa)
Rv1880c.1 | Rv1880c | Mycobacterium tuberculosis H37Rv cytochrome P450 140 cyp140 (439 aa)
Rv1886c.1 | Rv1886c | Mycobacterium tuberculosis H37Rv secreted fibronectin-binding protein antigen 85-B fbpB (326 aa)
Rv1908c.1 | Rv1908c | Mycobacterium tuberculosis H37Rv catalase-peroxidase-peroxynitritase T katG (741 aa)
Rv1919c.1 | Rv1919c | Mycobacterium tuberculosis H37Rv conserved hypothetical protein (155 aa)
Rv1925.1 | Rv1925 | Mycobacterium tuberculosis H37Rv acyl-CoA ligase fadD31 (621 aa)
Rv1978.1 | Rv1978 | Mycobacterium tuberculosis H37Rv conserved hypothetical protein (283 aa)
Rv2030c.1 | Rv2030c | Mycobacterium tuberculosis H37Rv conserved hypothetical protein (682 aa)
Rv2031c.1 | Rv2031c | Mycobacterium tuberculosis H37Rv heat shock protein hspX (145 aa)
Rv2050.1 | Rv2050 | Mycobacterium tuberculosis H37Rv conserved hypothetical protein (112 aa)
Rv2091c.1 | Rv2091c | Mycobacterium tuberculosis H37Rv membrane protein (245 aa)
Rv2094c.1 | Rv2094c | Mycobacterium tuberculosis H37Rv SEC-independent protein translocase membrane-bound protein tatA (84 aa)
Rv2111c.1 | Rv2111c | Mycobacterium tuberculosis H37Rv conserved hypothetical protein (65 aa)
Rv2112c.1 | Rv2112c | Mycobacterium tuberculosis H37Rv conserved hypothetical protein (555 aa)
Rv2115c.1 | Rv2115c | Mycobacterium tuberculosis H37Rv ATPase (610 aa)
Rv2127.1 | Rv2127 | Mycobacterium tuberculosis H37Rv L-asparagine permease ansP1 (490 aa)
Rv2140c.1 | Rv2140c | Mycobacterium tuberculosis H37Rv conserved hypothetical protein (177 aa)
Rv2145c.1 | Rv2145c | Mycobacterium tuberculosis H37Rv hypothetical protein wag31 (261 aa)
Rv2147c.1 | Rv2147c | Mycobacterium tuberculosis H37Rv conserved hypothetical protein (242 aa)
Rv2151c.1 | Rv2151c | Mycobacterium tuberculosis H37Rv cell division protein ftsQ (315 aa)
Rv2159c.1 | Rv2159c | Mycobacterium tuberculosis H37Rv conserved hypothetical protein (345 aa)
Rv2185c.1 | Rv2185c | Mycobacterium tuberculosis H37Rv conserved hypothetical protein (145 aa)
Rv2187.1 | Rv2187 | Mycobacterium tuberculosis H37Rv long-chain fatty-acid-CoA ligase fadD15 (601 aa)
Rv2195.1 | Rv2195 | Mycobacterium tuberculosis H37Rv Rieske iron-sulfur protein qcrA (430 aa)
Rv2196.1 | Rv2196 | Mycobacterium tuberculosis H37Rv ubiquinol-cytochrome C reductase qcrB cytochrome B subunit (550 aa)
Rv2197c.1 | Rv2197c | Mycobacterium tuberculosis H37Rv conserved membrane protein (215 aa)
Rv2198c.1 | Rv2198c | Mycobacterium tuberculosis H37Rv membrane protein mmpS3 (300 aa)
Rv2202c.1 | Rv2202c | Mycobacterium tuberculosis H37Rv carbohydrate kinase cbhK (325 aa)
Rv2204c.1 | Rv2204c | Mycobacterium tuberculosis H37Rv conserved hypothetical protein (119 aa)
Rv2211c.1 | Rv2211c | Mycobacterium tuberculosis H37Rv aminomethyltransferase gcvT (380 aa)
Rv2213.1 | Rv2213 | Mycobacterium tuberculosis H37Rv aminopeptidase pepB (516 aa)
Rv2215.1 | Rv2215 | Mycobacterium tuberculosis H37Rv pyruvate dehydrogenase E2 component sucB (554 aa)
Rv2220.1 | Rv2220 | Mycobacterium tuberculosis H37Rv glutamine synthetase glnA1 (479 aa)
Rv2241.1 | Rv2241 | Mycobacterium tuberculosis H37Rv pyruvate dehydrogenase E1 component aceE (902 aa)
Rv2244.1 | Rv2244 | Mycobacterium tuberculosis H37Rv meromycolate extension acyl carrier protein acpM (116 aa)
Rv2245.1 | Rv2245 | Mycobacterium tuberculosis H37Rv 3-oxoacyl-[acyl-carrier protein] synthase 1 kasA (417 aa)
Rv2246.1 | Rv2246 | Mycobacterium tuberculosis H37Rv 3-oxoacyl-[acyl-carrier protein] synthase 2 kasB (439 aa)
Rv2247.1 | Rv2247 | Mycobacterium tuberculosis H37Rv acetyl/propionyl-CoA carboxylase beta subunit accD6 (474 aa)
Rv2259.1 | Rv2259 | Mycobacterium tuberculosis H37Rv zinc-type alcohol dehydrogenase adhE2 (362 aa)
Rv2280.1 | Rv2280 | Mycobacterium tuberculosis H37Rv dehydrogenase (460 aa)
Rv2296.1 | Rv2296 | Mycobacterium tuberculosis H37Rv haloalkane dehalogenase (301 aa)
Rv2298.1 | Rv2298 | Mycobacterium tuberculosis H37Rv conserved hypothetical protein (324 aa)
Rv2299c.1 | Rv2299c | Mycobacterium tuberculosis H37Rv chaperone protein htpG (648 aa)
Rv2338c.1 | Rv2338c | Mycobacterium tuberculosis H37Rv molybdopterin biosynthesis protein moeW (319 aa)
Rv2345.1 | Rv2345 | Mycobacterium tuberculosis H37Rv conserved membrane protein (661 aa)
Rv2400c.1 | Rv2400c | Mycobacterium tuberculosis H37Rv sulfate-binding lipoprotein subI (357 aa)
Rv2444c.1 | Rv2444c | Mycobacterium tuberculosis H37Rv ribonuclease E rne (954 aa)
Rv2455c.1 | Rv2455c | Mycobacterium tuberculosis H37Rv oxidoreductase alpha subunit (654 aa)
Rv2460c.1 | Rv2460c | Mycobacterium tuberculosis H37Rv ATP-dependent clp protease proteolytic subunit 2 clpP2 (215 aa)
Rv2461c.1 | Rv2461c | Mycobacterium tuberculosis H37Rv ATP-dependent clp protease proteolytic subunit 1 clpP1 (201 aa)
Rv2462c.1 | Rv2462c | Mycobacterium tuberculosis H37Rv trigger factor protein tig (467 aa)

Rv2467.1 | Rv2467 | Mycobacterium tuberculosis H37Rv aminopeptidase N pepN (862 aa)
Rv2476c.1 | Rv2476c | Mycobacterium tuberculosis H37Rv NAD-dependent glutamate dehydrogenase gdh (1625 aa)
Rv2477c.1 | Rv2477c | Mycobacterium tuberculosis H37Rv macrolide-transport ATP-binding protein ABC transporter (559 aa)
Rv2496c.1 | Rv2496c | Mycobacterium tuberculosis H37Rv pyruvate dehydrogenase E1 component beta subunit pdhB (349 aa)
Rv2520c.1 | Rv2520c | Mycobacterium tuberculosis H37Rv conserved membrane protein (76 aa)
Rv2524c.1 | Rv2524c | Mycobacterium tuberculosis H37Rv fatty-acid synthase fas (3070 aa)
Rv2536.1 | Rv2536 | Mycobacterium tuberculosis H37Rv conserved membrane protein (231 aa)
Rv2555c.1 | Rv2555c | Mycobacterium tuberculosis H37Rv alanyl-tRNA synthetase alaS (905 aa)
Rv2563.1 | Rv2563 | Mycobacterium tuberculosis H37Rv glutamine-transport transmembrane protein ABC transporter (350 aa)
Rv2565.1 | Rv2565 | Mycobacterium tuberculosis H37Rv conserved hypothetical protein (584 aa)
Rv2583c.1 | Rv2583c | Mycobacterium tuberculosis H37Rv GTP pyrophosphokinase relA (791 aa)
Rv2586c.1 | Rv2586c | Mycobacterium tuberculosis H37Rv protein-export membrane protein secF (443 aa)
Rv2606c.1 | Rv2606c | Mycobacterium tuberculosis H37Rv pyridoxine biosynthesis protein (300 aa)
Rv2614c.1 | Rv2614c | Mycobacterium tuberculosis H37Rv threonyl-tRNA synthetase thrS (693 aa)
Rv2623.1 | Rv2623 | Mycobacterium tuberculosis H37Rv conserved hypothetical protein (298 aa)
Rv2625c.1 | Rv2625c | Mycobacterium tuberculosis H37Rv conserved alanine and leucine rich membrane protein (394 aa)
Rv2626c.1 | Rv2626c | Mycobacterium tuberculosis H37Rv conserved hypothetical protein (144 aa)
Rv2629.1 | Rv2629 | Mycobacterium tuberculosis H37Rv conserved hypothetical protein (375 aa)
Rv2696c.1 | Rv2696c | Mycobacterium tuberculosis H37Rv conserved alanine, glycine and valine rich protein (260 aa)
Rv2703.1 | Rv2703 | Mycobacterium tuberculosis H37Rv RNA polymerase sigma factor sigA (529 aa)
Rv2711.1 | Rv2711 | Mycobacterium tuberculosis H37Rv iron-dependent repressor and activator ideR (231 aa)
Rv2731.1 | Rv2731 | Mycobacterium tuberculosis H37Rv conserved alanine and arginine rich protein (451 aa)
Rv2744c.1 | Rv2744c | Mycobacterium tuberculosis H37Rv conserved alanine rich protein (271 aa)
Rv2773c.1 | Rv2773c | Mycobacterium tuberculosis H37Rv dihydrodipicolinate reductase dapB (246 aa)
Rv2780.1 | Rv2780 | Mycobacterium tuberculosis H37Rv 40 kda secreted L-alanine dehydrogenase ald (372 aa)
Rv2783c.1 | Rv2783c | Mycobacterium tuberculosis H37Rv bifunctional polyribonucleotide nucleotidyltransferase gpsI (753 aa)
Rv2831.1 | Rv2831 | Mycobacterium tuberculosis H37Rv enoyl-CoA hydratase echA16 (250 aa)
Rv2839c.1 | Rv2839c | Mycobacterium tuberculosis H37Rv translation initiation factor IF-2 infB (901 aa)
Rv2841c.1 | Rv2841c | Mycobacterium tuberculosis H37Rv N utilization substance protein A nusA (348 aa)
Rv2868c.1 | Rv2868c | Mycobacterium tuberculosis H37Rv 4-hydroxy-3-methylbut-2-en-1-yl diphosphate synthase gcpE (388 aa)
Rv2882c.1 | Rv2882c | Mycobacterium tuberculosis H37Rv ribosome recycling factor frr (186 aa)
Rv2887.1 | Rv2887 | Mycobacterium tuberculosis H37Rv transcriptional regulator (140 aa)
Rv2889c.1 | Rv2889c | Mycobacterium tuberculosis H37Rv elongation factor tsf (272 aa)
Rv2890c.1 | Rv2890c | Mycobacterium tuberculosis H37Rv 30S ribosomal protein S2 rpsB (288 aa)
Rv2909c.1 | Rv2909c | Mycobacterium tuberculosis H37Rv 30S ribosomal protein S16 rpsP (163 aa)
Rv2916c.1 | Rv2916c | Mycobacterium tuberculosis H37Rv signal recognition particle protein ffh (526 aa)
Rv2933.1 | Rv2933 | Mycobacterium tuberculosis H37Rv phenolpthiocerol synthesis type-I polyketide synthase ppsC (2189 aa)
Rv2935.1 | Rv2935 | Mycobacterium tuberculosis H37Rv phenolpthiocerol synthesis type-I polyketide synthase ppsE (1489 aa)
Rv2940c.1 | Rv2940c | Mycobacterium tuberculosis H37Rv multifunctional mycocerosic acid synthase membrane-associated mas (2112 aa)
Rv2941.1 | Rv2941 | Mycobacterium tuberculosis H37Rv fatty-acid-CoA ligase fadD28 (581 aa)
Rv2969c.1 | Rv2969c | Mycobacterium tuberculosis H37Rv conserved membrane protein (256 aa)
Rv2970c.1 | Rv2970c | Mycobacterium tuberculosis H37Rv lipase/esterase lipN (377 aa)
Rv2971.1 | Rv2971 | Mycobacterium tuberculosis H37Rv oxidoreductase (283 aa)
Rv2984.1 | Rv2984 | Mycobacterium tuberculosis H37Rv polyphosphate kinase ppk (743 aa)
Rv2986c.1 | Rv2986c | Mycobacterium tuberculosis H37Rv histone-like DNA-binding protein hupB (215 aa)
Rv2987c.1 | Rv2987c | Mycobacterium tuberculosis H37Rv 3-isopropylmalate dehydratase small subunit leuD (199 aa)
Rv2992c.1 | Rv2992c | Mycobacterium tuberculosis H37Rv glutamyl-tRNA synthetase gltS (491 aa)
Rv2996c.1 | Rv2996c | Mycobacterium tuberculosis H37Rv D-3-phosphoglycerate dehydrogenase serA1 (529 aa)
Rv3001c.1 | Rv3001c | Mycobacterium tuberculosis H37Rv ketol-acid reductoisomerase ilvC (334 aa)
Rv3009c.1 | Rv3009c | Mycobacterium tuberculosis H37Rv glutamyl-tRNA(gln) amidotransferase subunit B gatB (510 aa)
Rv3028c.1 | Rv3028c | Mycobacterium tuberculosis H37Rv electron transfer flavoprotein alpha subunit fixB (319 aa)
Rv3029c.1 | Rv3029c | Mycobacterium tuberculosis H37Rv electron transfer flavoprotein beta subunit fixA (267 aa)
Rv3043c.1 | Rv3043c | Mycobacterium tuberculosis H37Rv cytochrome C oxidase polypeptide I ctaD (574 aa)
Rv3045.1 | Rv3045 | Mycobacterium tuberculosis H37Rv NADP-dependent alcohol dehydrogenase adhC (347 aa)
Rv3051c.1 | Rv3051c | Mycobacterium tuberculosis H37Rv ribonucleoside-diphosphate reductase alpha chain nrdE (694 aa)
Rv3127.1 | Rv3127 | Mycobacterium tuberculosis H37Rv conserved hypothetical protein (345 aa)
Rv3139.1 | Rv3139 | Mycobacterium tuberculosis H37Rv acyl-CoA dehydrogenase fadE24 (469 aa)
Rv3161c.1 | Rv3161c | Mycobacterium tuberculosis H37Rv dioxygenase (383 aa)
Rv3193c.1 | Rv3193c | Mycobacterium tuberculosis H37Rv conserved membrane protein (993 aa)
Rv3200c.1 | Rv3200c | Mycobacterium tuberculosis H37Rv transmembrane cation transporter (356 aa)
Rv3206c.1 | Rv3206c | Mycobacterium tuberculosis H37Rv molybdenum cofactor biosynthesis protein moeB1 (393 aa)
Rv3223c.1 | Rv3223c | Mycobacterium tuberculosis H37Rv alternative RNA polymerase sigma factor sigH (217 aa)
Rv3224.1 | Rv3224 | Mycobacterium tuberculosis H37Rv iron-regulated short-chain dehydrogenase/reductase (283 aa)
Rv3240c.1 | Rv3240c | Mycobacterium tuberculosis H37Rv preprotein translocase secA1 (950 aa)
Rv3246c.1 | Rv3246c | Mycobacterium tuberculosis H37Rv two component system transcriptional regulator mtrA (229 aa)
Rv3248c.1 | Rv3248c | Mycobacterium tuberculosis H37Rv adenosylhomocysteinase sahH (496 aa)

Rv3269.1 | Rv3269 | Mycobacterium tuberculosis H37Rv conserved hypothetical protein (94 aa)
Rv3273.1 | Rv3273 | Mycobacterium tuberculosis H37Rv transmembrane carbonic anhydrase (765 aa)
Rv3274c.1 | Rv3274c | Mycobacterium tuberculosis H37Rv acyl-CoA dehydrogenase fadE25 (390 aa)
Rv3280.1 | Rv3280 | Mycobacterium tuberculosis H37Rv propionyl-CoA carboxylase beta chain 5 accD5 (549 aa)
Rv3283.1 | Rv3283 | Mycobacterium tuberculosis H37Rv thiosulfate sulfurtransferase sseA (298 aa)
Rv3285.1 | Rv3285 | Mycobacterium tuberculosis H37Rv bifunctional acetyl-/propionyl-coenzyme A carboxylase alpha chain accA3 (601 aa)
Rv3292.1 | Rv3292 | Mycobacterium tuberculosis H37Rv conserved hypothetical protein (416 aa)
Rv3311.1 | Rv3311 | Mycobacterium tuberculosis H37Rv conserved hypothetical protein (421 aa)
Rv3356c.1 | Rv3356c | Mycobacterium tuberculosis H37Rv bifunctional methylenetetrahydrofolate dehydrogenase folD (282 aa)
Rv3389c.1 | Rv3389c | Mycobacterium tuberculosis H37Rv dehydrogenase (291 aa)
Rv3411c.1 | Rv3411c | Mycobacterium tuberculosis H37Rv inosine-5-monophosphate dehydrogenase guaB2 (530 aa)
Rv3417c.1 | Rv3417c | Mycobacterium tuberculosis H37Rv 60 kda chaperonin 1 groEL1 (540 aa)
Rv3418c.1 | Rv3418c | Mycobacterium tuberculosis H37Rv 10 kda chaperonin groES (101 aa)
Rv3436c.1 | Rv3436c | Mycobacterium tuberculosis H37Rv glucosamine-fructose-6-phosphate aminotransferase glmS (625 aa)
Rv3441c.1 | Rv3441c | Mycobacterium tuberculosis H37Rv phospho-sugar mutase mrsA (449 aa)
Rv3443c.1 | Rv3443c | Mycobacterium tuberculosis H37Rv 50S ribosomal protein L13 rplM (148 aa)
Rv3457c.1 | Rv3457c | Mycobacterium tuberculosis H37Rv DNA-directed RNA polymerase alpha chain rpoA (348 aa)
Rv3458c.1 | Rv3458c | Mycobacterium tuberculosis H37Rv 30S ribosomal protein S4 rpsD (202 aa)
Rv3460c.1 | Rv3460c | Mycobacterium tuberculosis H37Rv 30S ribosomal protein S13 rpsM (125 aa)
Rv3462c.1 | Rv3462c | Mycobacterium tuberculosis H37Rv translation initiation factor IF-1 infA (74 aa)
Rv3463.1 | Rv3463 | Mycobacterium tuberculosis H37Rv conserved hypothetical protein (286 aa)
Rv3464.1 | Rv3464 | Mycobacterium tuberculosis H37Rv dTDP-glucose 4,6-dehydratase rmlB (332 aa)
Rv3509c.1 | Rv3509c | Mycobacterium tuberculosis H37Rv acetohydroxyacid synthase ilvX (516 aa)
Rv3528c.1 | Rv3528c | Mycobacterium tuberculosis H37Rv hypothetical protein (238 aa)
Rv3547.1 | Rv3547 | Mycobacterium tuberculosis H37Rv conserved hypothetical protein (152 aa)
Rv3584.1 | Rv3584 | Mycobacterium tuberculosis H37Rv lipoprotein lpqE (183 aa)
Rv3588c.1 | Rv3588c | Mycobacterium tuberculosis H37Rv carbonic anhydrase (208 aa)
Rv3592.1 | Rv3592 | Mycobacterium tuberculosis H37Rv conserved hypothetical protein (106 aa)
Rv3596c.1 | Rv3596c | Mycobacterium tuberculosis H37Rv ATP-dependent protease ATP-binding subunit clpC1 (849 aa)
Rv3597c.1 | Rv3597c | Mycobacterium tuberculosis H37Rv iron-regulated lsr2 protein precursor (113 aa)
Rv3604c.1 | Rv3604c | Mycobacterium tuberculosis H37Rv conserved alanine, arginine and proline rich membrane protein (398 aa)
Rv3610c.1 | Rv3610c | Mycobacterium tuberculosis H37Rv membrane-bound ell division protein ftsH (761 aa)
Rv3676.1 | Rv3676 | Mycobacterium tuberculosis H37Rv transcriptional regulator, crp/fnr-family (225 aa)
Rv3688c.1 | Rv3688c | Mycobacterium tuberculosis H37Rv conserved hypothetical protein (155 aa)
Rv3699.1 | Rv3699 | Mycobacterium tuberculosis H37Rv conserved hypothetical protein (234 aa)
Rv3716c.1 | Rv3716c | Mycobacterium tuberculosis H37Rv conserved hypothetical protein (134 aa)
Rv3719.1 | Rv3719 | Mycobacterium tuberculosis H37Rv conserved hypothetical protein (471 aa)
Rv3720.1 | Rv3720 | Mycobacterium tuberculosis H37Rv fatty-acid synthase (421 aa)
Rv3722c.1 | Rv3722c | Mycobacterium tuberculosis H37Rv conserved hypothetical protein (436 aa)
Rv3734c.1 | Rv3734c | Mycobacterium tuberculosis H37Rv conserved hypothetical protein (455 aa)
Rv3763.1 | Rv3763 | Mycobacterium tuberculosis H37Rv 19 kda lipoprotein antigen precursor lpqH (160 aa)
Rv3800c.1 | Rv3800c | Mycobacterium tuberculosis H37Rv polyketide synthase pks13 (1734 aa)
Rv3801c.1 | Rv3801c | Mycobacterium tuberculosis H37Rv fatty-acid-CoA ligase fadD32 (638 aa)
Rv3804c.1 | Rv3804c | Mycobacterium tuberculosis H37Rv secreted fibronectin-binding protein antigen fbpA (339 aa)
Rv3814c.1 | Rv3814c | Mycobacterium tuberculosis H37Rv acyltransferase (262 aa)
Rv3817.1 | Rv3817 | Mycobacterium tuberculosis H37Rv phosphotransferase (252 aa)
Rv3841.1 | Rv3841 | Mycobacterium tuberculosis H37Rv bacterioferritin bfrB (182 aa)
Rv3846.1 | Rv3846 | Mycobacterium tuberculosis H37Rv superoxide dismutase sodA (208 aa)
Rv3849.1 | Rv3849 | Mycobacterium tuberculosis H37Rv conserved hypothetical protein (133 aa)
Rv3852.1 | Rv3852 | Mycobacterium tuberculosis H37Rv histone-like protein hns (135 aa)
Rv3860.1 | Rv3860 | Mycobacterium tuberculosis H37Rv conserved hypothetical protein (391 aa)
Rv3865.1 | Rv3865 | Mycobacterium tuberculosis H37Rv conserved hypothetical protein (104 aa)
Rv3868.1 | Rv3868 | Mycobacterium tuberculosis H37Rv conserved hypothetical protein (574 aa)
Rv3871.1 | Rv3871 | Mycobacterium tuberculosis H37Rv conserved hypothetical protein (592 aa)
Rv3874.1 | Rv3874 | Mycobacterium tuberculosis H37Rv 10 kda culture filtrate antigen esxB (101 aa)
Rv3875.1 | Rv3875 | Mycobacterium tuberculosis H37Rv 6 kda early secretory antigenic target esxA (96 aa)
Rv3876.1 | Rv3876 | Mycobacterium tuberculosis H37Rv conserved alanine and proline rich protein (667 aa)
Rv3880c.1 | Rv3880c | Mycobacterium tuberculosis H37Rv conserved hypothetical protein (116 aa)
Rv3894c.1 | Rv3894c | Mycobacterium tuberculosis H37Rv conserved membrane protein (1397 aa)
Rv3910.1 | Rv3910 | Mycobacterium tuberculosis H37Rv conserved membrane protein (1185 aa)
Rv3913.1 | Rv3913 | Mycobacterium tuberculosis H37Rv thioredoxin reductase trxB2 (336 aa)
Rv3914.1 | Rv3914 | Mycobacterium tuberculosis H37Rv thioredoxin trxC (117 aa)
Rv3920c.1 | Rv3920c | Mycobacterium tuberculosis H37Rv hypothetical protein (188 aa)

Table A.2

List of proteins containing phosphopeptides in WCL phosphopeptide enriched fraction. Off-line phosphopeptide enrichment.

Protein Accession Number/Protein Name
Rv0007.1 | Rv0007 | Mycobacterium tuberculosis H37Rv conserved membrane protein (305 aa)
Rv0014c.1 | Rv0014c | Mycobacterium tuberculosis H37Rv transmembrane serine/threonine-protein kinase B pknB (627 aa)
Rv0015c.1 | Rv0015c | Mycobacterium tuberculosis H37Rv transmembrane serine/threonine-protein kinase A pknA (432 aa)
Rv0020c.1 | Rv0020c | Mycobacterium tuberculosis H37Rv conserved hypothetical protein (528 aa)
Rv0056.1 | Rv0056 | Mycobacterium tuberculosis H37Rv 50S ribosomal protein L9 rplI (153 aa)
Rv0175.1 | Rv0175 | Mycobacterium tuberculosis H37Rv MCE-associated membrane protein (214 aa)
Rv0178.1 | Rv0178 | Mycobacterium tuberculosis H37Rv MCE-associated membrane protein (245 aa)
Rv0206c.1 | Rv0206c | Mycobacterium tuberculosis H37Rv transmembrane transport protein mmpL3 (945 aa)
Rv0227c.1 | Rv0227c | Mycobacterium tuberculosis H37Rv conserved membrane protein (422 aa)
Rv0242c.1 | Rv0242c | Mycobacterium tuberculosis H37Rv 3-oxoacyl-[acyl-carrier protein] reductase fabG4 (455 aa)
Rv0341.1 | Rv0341 | Mycobacterium tuberculosis H37Rv isoniazid inductible gene protein iniB (480 aa)
Rv0350.1 | Rv0350 | Mycobacterium tuberculosis H37Rv chaperone protein dnaK (626 aa)
Rv0351.1 | Rv0351 | Mycobacterium tuberculosis H37Rv chaperone grpE (236 aa)
Rv0363c.1 | Rv0363c | Mycobacterium tuberculosis H37Rv fructose-bisphosphate aldolase fba (345 aa)
Rv0383c.1 | Rv0383c | Mycobacterium tuberculosis H37Rv conserved secreted protein (285 aa)
Rv0384c.1 | Rv0384c | Mycobacterium tuberculosis H37Rv endopeptidase ATP binding protein chain B clpB (849 aa)
Rv0421c.1 | Rv0421c | Mycobacterium tuberculosis H37Rv conserved hypothetical protein (210 aa)
Rv0440.1 | Rv0440 | Mycobacterium tuberculosis H37Rv 60 kda chaperonin 2 groEL2 (541 aa)
Rv0458.1 | Rv0458 | Mycobacterium tuberculosis H37Rv aldehyde dehydrogenase (508 aa)
Rv0530.1 | Rv0530 | Mycobacterium tuberculosis H37Rv conserved hypothetical protein (406 aa)
Rv0580c.1 | Rv0580c | Mycobacterium tuberculosis H37Rv conserved hypothetical protein (164 aa)
Rv0634B.1 | Rv0634B | Mycobacterium tuberculosis H37Rv 50S ribosomal protein L33 rpmG2 (56 aa)
Rv0638.1 | Rv0638 | Mycobacterium tuberculosis H37Rv preprotein translocase secE1 (162 aa)
Rv0686.1 | Rv0686 | Mycobacterium tuberculosis H37Rv membrane protein (266 aa)
Rv0710.1 | Rv0710 | Mycobacterium tuberculosis H37Rv 30S ribosomal protein S17 rpsQ (137 aa)
Rv0733.1 | Rv0733 | Mycobacterium tuberculosis H37Rv adenylate kinase adk (182 aa)
Rv0757.1 | Rv0757 | Mycobacterium tuberculosis H37Rv two component system transcriptional regulator phoP (248 aa)
Rv0896.1 | Rv0896 | Mycobacterium tuberculosis H37Rv citrate synthase I gltA2 (432 aa)
Rv0931c.1 | Rv0931c | Mycobacterium tuberculosis H37Rv transmembrane serine/threonine-protein kinase D pknD (665 aa)
Rv0993.1 | Rv0993 | Mycobacterium tuberculosis H37Rv UTP-glucose-1-phosphate uridylyltransferase galU (307 aa)
Rv1038c.1 | Rv1038c | Mycobacterium tuberculosis H37Rv Esat-6 like protein esxJ (99 aa)
Rv1080c.1 | Rv1080c | Mycobacterium tuberculosis H37Rv transcription elongation factor greA (165 aa)
Rv1133c.1 | Rv1133c | Mycobacterium tuberculosis H37Rv 5-methyltetrahydropteroyltriglutamate-homocysteine methyltransferase metE (760 aa)
Rv1196.1 | Rv1196 | Mycobacterium tuberculosis H37Rv PPE family protein (392 aa)
Rv1307.1 | Rv1307 | Mycobacterium tuberculosis H37Rv ATP synthase delta chain atpH (447 aa)
Rv1423.1 | Rv1423 | Mycobacterium tuberculosis H37Rv transcriptional regulator whiA (326 aa)
Rv1479.1 | Rv1479 | Mycobacterium tuberculosis H37Rv transcriptional regulator moxR1 (378 aa)
Rv1488.1 | Rv1488 | Mycobacterium tuberculosis H37Rv conserved hypothetical protein (382 aa)
Rv1636.1 | Rv1636 | Mycobacterium tuberculosis H37Rv iron-regulated conserved hypothetical protein (147 aa)
Rv1707.1 | Rv1707 | Mycobacterium tuberculosis H37Rv conserved membrane protein (487 aa)
Rv1719.1 | Rv1719 | Mycobacterium tuberculosis H37Rv transcriptional regulator (260 aa)
Rv1746.1 | Rv1746 | Mycobacterium tuberculosis H37Rv anchored-membrane serine/threonine-protein kinase pknF (477 aa)
Rv1747.1 | Rv1747 | Mycobacterium tuberculosis H37Rv conserved transmembrane ATP-binding protein ABC transporter (866 aa)
Rv1827.1 | Rv1827 | Mycobacterium tuberculosis H37Rv hypothetical protein cfp17 (163 aa)
Rv2031c.1 | Rv2031c | Mycobacterium tuberculosis H37Rv heat shock protein hspX (145 aa)
Rv2094c.1 | Rv2094c | Mycobacterium tuberculosis H37Rv SEC-independent protein translocase membrane-bound protein tatA (84 aa)
Rv2127.1 | Rv2127 | Mycobacterium tuberculosis H37Rv L-asparagine permease ansP1 (490 aa)
Rv2140c.1 | Rv2140c | Mycobacterium tuberculosis H37Rv conserved hypothetical protein (177 aa)
Rv2147c.1 | Rv2147c | Mycobacterium tuberculosis H37Rv conserved hypothetical protein (242 aa)
Rv2151c.1 | Rv2151c | Mycobacterium tuberculosis H37Rv cell division protein ftsQ (315 aa)
Rv2187.1 | Rv2187 | Mycobacterium tuberculosis H37Rv long-chain fatty-acid-CoA ligase fadD15 (601 aa)
Rv2197c.1 | Rv2197c | Mycobacterium tuberculosis H37Rv conserved membrane protein (215 aa)
Rv2198c.1 | Rv2198c | Mycobacterium tuberculosis H37Rv membrane protein mmpS3 (300 aa)

Rv2204c.1 | Rv2204c | Mycobacterium tuberculosis H37Rv conserved hypothetical protein (119 aa)
Rv2213.1 | Rv2213 | Mycobacterium tuberculosis H37Rv aminopeptidase pepB (516 aa)
Rv2244.1 | Rv2244 | Mycobacterium tuberculosis H37Rv meromycolate extension acyl carrier protein acpM (116 aa)
Rv2338c.1 | Rv2338c | Mycobacterium tuberculosis H37Rv molybdopterin biosynthesis protein moeW (319 aa)
Rv2461c.1 | Rv2461c | Mycobacterium tuberculosis H37Rv ATP-dependent clp protease proteolytic subunit 1 clpP1 (201 aa)
Rv2536.1 | Rv2536 | Mycobacterium tuberculosis H37Rv conserved membrane protein (231 aa)
Rv2586c.1 | Rv2586c | Mycobacterium tuberculosis H37Rv protein-export membrane protein secF (443 aa)
Rv2625c.1 | Rv2625c | Mycobacterium tuberculosis H37Rv conserved alanine and leucine rich membrane protein (394 aa)
Rv2696c.1 | Rv2696c | Mycobacterium tuberculosis H37Rv conserved alanine, glycine and valine rich protein (260 aa)
Rv2744c.1 | Rv2744c | Mycobacterium tuberculosis H37Rv conserved alanine rich protein (271 aa)
Rv2986c.1 | Rv2986c | Mycobacterium tuberculosis H37Rv histone-like DNA-binding protein hupB (215 aa)
Rv2996c.1 | Rv2996c | Mycobacterium tuberculosis H37Rv D-3-phosphoglycerate dehydrogenase serA1 (529 aa)
Rv3127.1 | Rv3127 | Mycobacterium tuberculosis H37Rv conserved hypothetical protein (345 aa)
Rv3200c.1 | Rv3200c | Mycobacterium tuberculosis H37Rv transmembrane cation transporter (356 aa)
Rv3269.1 | Rv3269 | Mycobacterium tuberculosis H37Rv conserved hypothetical protein (94 aa)
Rv3273.1 | Rv3273 | Mycobacterium tuberculosis H37Rv transmembrane carbonic anhydrase (765 aa)
Rv3441c.1 | Rv3441c | Mycobacterium tuberculosis H37Rv phospho-sugar mutase mrsA (449 aa)
Rv3443c.1 | Rv3443c | Mycobacterium tuberculosis H37Rv 50S ribosomal protein L13 rplM (148 aa)
Rv3458c.1 | Rv3458c | Mycobacterium tuberculosis H37Rv 30S ribosomal protein S4 rpsD (202 aa)
Rv3462c.1 | Rv3462c | Mycobacterium tuberculosis H37Rv translation initiation factor IF-1 infA (74 aa)
Rv3604c.1 | Rv3604c | Mycobacterium tuberculosis H37Rv conserved alanine, arginine and proline rich membrane protein (398 aa)
Rv3814c.1 | Rv3814c | Mycobacterium tuberculosis H37Rv acyltransferase (262 aa)
Rv3817.1 | Rv3817 | Mycobacterium tuberculosis H37Rv phosphotransferase (252 aa)
Rv3849.1 | Rv3849 | Mycobacterium tuberculosis H37Rv conserved hypothetical protein (133 aa)
Rv3860.1 | Rv3860 | Mycobacterium tuberculosis H37Rv conserved hypothetical protein (391 aa)
Rv3868.1 | Rv3868 | Mycobacterium tuberculosis H37Rv conserved hypothetical protein (574 aa)
Rv3874.1 | Rv3874 | Mycobacterium tuberculosis H37Rv 10 kda culture filtrate antigen esxB (101 aa)
Rv3876.1 | Rv3876 | Mycobacterium tuberculosis H37Rv conserved alanine and proline rich protein (667 aa)
Rv3880c.1 | Rv3880c | Mycobacterium tuberculosis H37Rv conserved hypothetical protein (116 aa)
Rv3910.1 | Rv3910 | Mycobacterium tuberculosis H37Rv conserved membrane protein (1185 aa)
Rv3914.1 | Rv3914 | Mycobacterium tuberculosis H37Rv thioredoxin trxC (117 aa)

Table A.3

Online Phosphochip enrichment Whole Cell Lysate

Non-Phospho Elute	
Accession Number	**Protein Name**
O05299	ESAT-6-like protein esxK
O05300	ESAT-6-like protein esxL
O05793	Putative thiosulfate sulfurtransferase
O06153	Universal stress protein Rv1636/MT1672
O06186	Hypoxic response protein 1
O06189	Universal stress protein Rv2623/MT2698
O06327	30S ribosomal protein S13
O07438	Alanyl-tRNA synthetase
O07932	Putative ESAT-6-like protein 10
O33246	Prokaryotic ubiquitin-like protein Pup
O50463	2-oxoglutarate decarboxylase
O53275	Electron transfer flavoprotein subunit alpha
O53442	Putative acyl-[acyl-carrier-protein] desaturase desA2
O53624	Uncharacterized protein Rv0079/MT0086
O53946	ESX-5 secretion system protein EccE5
P09621	10 kDa chaperonin
P0A4V4	Antigen 85-C
P0A4W6	Meromycolate extension acyl carrier protein
P0A4X0	NADP-dependent alcohol dehydrogenase C
P0A4Z8	Aspartokinase
P0A500	ATP synthase subunit b-delta

P0A518	60 kDa chaperonin 1
P0A520	60 kDa chaperonin 2
P0A526	ATP-dependent Clp protease proteolytic subunit 1
P0A544	D-3-phosphoglycerate dehydrogenase
P0A558	Elongation factor Tu
P0A566	ESAT-6-like protein esxB
P0A570	ESAT-6-like protein esxN
P0A590	Glutamine synthetase 1
P0A5B7	Alpha-crystallin
P0A5B9	Chaperone protein dnaK
P0A5J4	Malate synthase G
P0A5J6	Malate dehydrogenase
P0A5N2	Antigen 84
P0A5P6	Heparin-binding hemagglutinin
P0A5S4	Serine/threonine-protein kinase pknB
P0A5V2	50S ribosomal protein L7/L12
P0A5V8	50S ribosomal protein L32
P0A5X0	30S ribosomal protein S10
P0A5X6	30S ribosomal protein S3
P0A608	Superoxide dismutase [Cu-Zn]
P0A616	Thioredoxin
P0A650	Probable diacyglycerol O-acyltransferase tgs1
P0A654	UPF0133 protein Rv3716c/MT3819
P0C5C2	Cyclopropane mycolic acid synthase 1
P0C5C4	35 kDa protein
P0CG95	Uncharacterized protein Rv0814c
P0CG96	Uncharacterized protein Rv3118
P0CG97	Uncharacterized protein MT0836
P0CG98	Uncharacterized protein MT3200
P15712	Phosphate-binding protein pstS 1
P30234	Alanine dehydrogenase
P41194	30S ribosomal protein S7
P60176	Adenosylhomocysteinase
P60442	50S ribosomal protein L3
P61181	50S ribosomal protein L22
P63429	Uncharacterized protein Rv0873/MT0896
P63456	3-oxoacyl-[acyl-carrier-protein] synthase 2
P63484	Uncharacterized oxidoreductase Rv2298/MT2355
P63673	ATP synthase subunit alpha
P63677	ATP synthase subunit beta
P63693	Uncharacterized protein Rv1488/MT1533.2
P63885	Ubiquinol-cytochrome c reductase cytochrome b subunit
P63937	Probable aldehyde dehydrogenase
P64178	Glyceraldehyde-3-phosphate dehydrogenase
P64301	Haloalkane dehalogenase 1
P64853	Uncharacterized protein Rv1480/MT1527
P64875	Putative nitroreductase Rv1558
P64897	Uncharacterized protein Rv1827/MT1875
P65065	Uncharacterized protein Rv3292/MT3391
P65149	Ketol-acid reductoisomerase
P65172	Uncharacterized oxidoreductase Rv1843c/MT1891
P65308	Putative lipoprotein lpqE
P65340	5-methyltetrahydropteroyltriglutamate--homocysteine methyltransferase
P65633	Dihydrolipoyllysine-residue succinyltransferase component of 2-oxoglutarate dehydrogenase complex
P65648	Protein lsr2
P65762	Probable peptidyl-prolyl cis-trans isomerase A
P66006	Probable soluble pyridine nucleotide transhydrogenase
P66315	50S ribosomal protein L9
P66574	30S ribosomal protein S5
P66639	30S ribosomal protein S9
P66701	DNA-directed RNA polymerase subunit alpha
P66734	Ribosome-recycling factor
P66779	Uncharacterized oxidoreductase Rv1543/MT1595
P66952	Probable thiol peroxidase
P67210	Probable diacyglycerol O-acyltransferase tgs2
P69230	30S ribosomal protein S18 1

P69440	Adenylate kinase
P71559	Succinyl-CoA ligase [ADP-forming] subunit beta
P77899	S-adenosylmethionine synthase
P95058	30S ribosomal protein S17
P95071	50S ribosomal protein L15
P95109	DNA-binding protein HU homolog
P95124	Uncharacterized oxidoreductase Rv2971/MT3049
P95143	Putative L-lactate dehydrogenase [cytochrome] 2
P95242	Putative ESAT-6-like protein 6
P95243	Putative ESAT-6-like protein 7
P96237	Probable bacterioferritin BfrB
P96363	ESAT-6-like protein esxJ
P96364	ESAT-6-like protein esxI
P96377	Enolase
P96825	Putative short-chain type dehydrogenase/reductase Rv0148
P96888	Putative thiosulfate sulfurtransferase sseA
Q08129	Catalase-peroxidase
Q10504	Pyruvate dehydrogenase E1 component
Q10530	Citrate synthase 1
Q50824	Putative acyl-[acyl-carrier-protein] desaturase desA1
Q79FX8	Hydroxymycolate synthase MmaA4
PhosphoElute	
Accession Number	**Protein Name**
O05793	Putative thiosulfate sulfurtransferase
O05800	Uncharacterized protein Rv3127/MT3212
O05851	Putative isochorismate synthase
O05871	Serine/threonine-protein kinase pknD
O06294	Isoniazid-inductible protein iniC
O06325	30S ribosomal protein S4
O33261	L-asparagine permease 1
O33357	Delta-aminolevulinic acid dehydratase
O53442	Putative acyl-[acyl-carrier-protein] desaturase desA2
O53657	Putative membrane protein mmpL3
O69733	ESX-1 secretion system protein EccA1
O69740	ESX-1 secretion-associated protein EspI
P09621	10 kDa chaperonin
P0A520	60 kDa chaperonin 2
P0A558	Elongation factor Tu
P0A5B7	Alpha-crystallin
P0A5B9	Chaperone protein dnaK
P0A5K8	Large-conductance mechanosensitive channel
P0A5S4	Serine/threonine-protein kinase pknB
P0A5V2	50S ribosomal protein L7/L12
P0A632	Indole-3-glycerol phosphate synthase
P0A650	Probable diacyglycerol O-acyltransferase tgs1
P0A680	DNA-directed RNA polymerase subunit beta
P0C5C4	35 kDa protein
P63345	Proteasome-associated ATPase
P63673	ATP synthase subunit alpha
P63693	Uncharacterized protein Rv1488/MT1533.2
P64097	Electron transfer flavoprotein subunit beta
P64207	GTP cyclohydrolase 1
P64897	Uncharacterized protein Rv1827/MT1875
P65025	Uncharacterized protein Rv2588c/MT2665
P65374	Putative membrane protein mmpL11
P65378	Putative membrane protein mmpS3
P65842	Uncharacterized RNA pseudouridine synthase Rv1711/MT1751.1
P66785	Protein translocase subunit secA 2
P66801	Uncharacterized protein Rv0505c/MT0526
P66842	Cell division protein ftsY homolog
P67582	Threonyl-tRNA synthetase
P69440	Adenylate kinase
P71544	Uncharacterized protein Rv0966c/MT0994
P71575	Uncharacterized protein Rv0007/MT0007
P71691	UPF0052 protein Rv1422/MT1465

P95140	Phthiodiolone/phenolphthiodiolone dimycocerosates ketoreductase
Q10389	Uncharacterized protein Rv2197c/MT2253
Q10788	Elongation factor Ts
Q50601	Probable glycine dehydrogenase [decarboxylating]
Q50634	Protein-export membrane protein secD
Q79FD7	Ribose-5-phosphate isomerase B

REFERENCES

1. Brennan PJ. Structure, function, and biogenesis of the cell wall of Mycobacterium tuberculosis. Tuberculosis 2003;83(1-3):91-97.
2. Yuan Y, Mead D, Schroeder BG, Zhu Y, Barry CE. The biosynthesis of mycolic acids in Mycobacterium tuberculosis. Enzymatic methyl(ene) transfer to acyl carrier protein bound meromycolic acid in vitro. J Biol Chem 1998;273(33):21282-90.
3. Yuan Y, Zhu Y, Crane DD, Barry CE. The effect of oxygenated mycolic acid composition on cell wall function and macrophage growth in Mycobacterium tuberculosis. Mol Microbiol 1998;29(6):1449-58.
4. Barry CE, Lee RE, Mdluli K, Sampson AE, Schroeder BG, Slayden RA, Yuan Y. Mycolic acids: structure, biosynthesis and physiological functions. Prog Lipid Res 1998;37(2-3):143-79.
5. Korf J, Stoltz A, Verschoor J, De Baetselier P, Grooten J. The Mycobacterium tuberculosis cell wall component mycolic acid elicits pathogen-associated host innate immune responses. Eur J Immunol 2005;35(3):890-900.
6. Takayama K, Wang C, Besra GS. Pathway to synthesis and processing of mycolic acids in Mycobacterium tuberculosis. Clin Microbiol Rev 2005;18(1):81-101.
7. Schaeffer ML, Agnihotri G, Volker C, Kallender H, Brennan PJ, Lonsdale JT. Purification and biochemical characterization of the Mycobacterium tuberculosis beta-ketoacyl-acyl carrier protein synthases KasA and KasB. J Biol Chem 2001;276(50):47029-37.
8. Kremer L, Dover LG, Carrère S, Nampoothiri KM, Lesjean S, Brown AK, Brennan PJ, Minnikin DE, Locht C, Besra GS. Mycolic acid biosynthesis and enzymic characterization of the beta-ketoacyl-ACP synthase A-condensing enzyme from Mycobacterium tuberculosis. Biochem J 2002;364(Pt 2):423-30.
9. Dubnau E, Lanéelle MA, Soares S, Bénichou A, Vaz T, Promé D, Promé JC, Daffé M, Quémard A. Mycobacterium bovis BCG genes involved in the biosynthesis of cyclopropyl keto- and hydroxy-mycolic acids. Mol Microbiol 1997;23(2):313-22.
10. Yuan Y, Barry CE. A common mechanism for the biosynthesis of methoxy and cyclopropyl mycolic acids in Mycobacterium tuberculosis. Proc Natl Acad Sci U S A 1996;93(23):12828-33.
11. Veyron-Churlet R, Guerrini O, Mourey L, Daffé M, Zerbib D. Protein-protein interactions within the Fatty Acid Synthase-II system of Mycobacterium tuberculosis are essential for mycobacterial viability. Mol Microbiol 2004;54(5):1161-72.
12. Veyron-Churlet R, Bigot S, Guerrini O, Verdoux S, Malaga W, Daffé M, Zerbib D. The biosynthesis of mycolic acids in Mycobacterium tuberculosis relies on multiple specialized elongation complexes interconnected by specific protein-protein interactions. J Mol Biol 2005;353(4):847-58.
13. Molle V, Brown AK, Besra GS, Cozzone AJ, Kremer L. The condensing activities of the Mycobacterium tuberculosis type II fatty acid synthase are differentially regulated by phosphorylation. J Biol Chem 2006;281(40):30094-103.

14. Molle V, Gulten G, Vilchèze C, Veyron-Churlet R, Zanella-Cléon I, Sacchettini JC, Jacobs WR, Kremer L. Phosphorylation of InhA inhibits mycolic acid biosynthesis and growth of Mycobacterium tuberculosis. Mol Microbiol 2010;78(6):1591-605.
15. Villén J, Gygi SP. The SCX/IMAC enrichment approach for global phosphorylation analysis by mass spectrometry. Nat Protoc 2008;3(10):1630-8.
16. Nisbet AD, Saundry RH, Moir AJG, Fothergill LA, Fothergill JE. THE COMPLETE AMINO-ACID-SEQUENCE OF HEN OVALBUMIN. European Journal of Biochemistry 1981;115(2):335-345.
17. Vilchèze C, Molle V, Carrère-Kremer S, Leiba J, Mourey L, Shenai S, Baronian G, Tufariello J, Hartman T, Veyron-Churlet R and others. Phosphorylation of KasB regulates virulence and acid-fastness in Mycobacterium tuberculosis. PLoS Pathog 2014;10(5):e1004115.

LIST OF ABBREVIATIONS

ACN	Acetonitrile
ADH	Aldehyde dehydrogenase
APAO	*N*-acetylpolyamine oxidase
BAL	Bronchoalveolar lavage
BCG	Bacillus-Calmette Guerin
C1INH	Plasma protease C1 inhibitor
CE	Capillary electrophoresis
CE	Collision energy
CR	Complement receptor
CuAO	Copper dependent amine oxidases
D0	Day 0 of anti-TB treatment; diagnosis
DAO	Diamine oxidase
DC	Dendritic cell
dcRT-MLPA	Dual-color reverse-transcriptase multiplex ligation-dependent probe amplification
DFS	Disease free survival
DH	Hydoxyacyl dehydrase
DMRM	Dynamic multiple reaction monitoring
EIC	Extracted ion chromatogram
ELISA	Enzyme-linked immunosorbent assay
ER	Enoyl reductase
ESI	Electrospray ionization
FA	Formic acid
FAS I	Fatty acid synthase I
FAS II	Fatty acid synthase II
GABA	γ-aminobutyric acid
Gal	Galactose
GalNAc	*N*-acetylgalactosamine

GC	Gas chromatography
HC	Household contact
HCA	Hexacosanoic acid
HFBA	Heptofluorobutyric acid
HIV	Human immunodeficiency virus
HMDB	Human metabolome database
HPLC	High performance liquid chromatography
IFN	Interferon
IGRA	Interferon-γ release assays
INH	Isoniazid
IS	Internal standard
KAS	Ketoacyl synthase
KR	Ketoacyl reductase
LAM	Lipoarabinomannan
LC	Liquid chromatography
M1	Month 1 of anti-TB treatment
M2	Month 2 of anti-TB treatment
M6	Month 6 of anti-TB treatment
m/z	Mass to charge ratio
MALDI	Matrix assisted laser desorption/ionization
MAMTs	Mycolic acid methyltransferases
ManLam	Mannose capped lipoarabinomannan
MDR	Multiple drug resistant
MR	Mannose receptor
MRM	Multiple reaction monitoring
MS	Mass spectrometry/Mass spectrometer
Mtb	*Mycobacterium tuberculosis*
NAA	Nucleic acid amplification
Neu5Ac	*N*-acetylneuraminic acid
NIST	National Institutes of Standards and Technology
NMR	Nuclear magnetic resonance

NPV	Negative predictive value
NTM	Non-tuberculous mycobacteria
OS	Overall survival
PBMC	Peripheral blood mononuclear cell
PET-CT	Positron emission tomography-computed tomography
PFS	Progression free survival
PPD	Purified protein derivative
PPV	Positive predictive value
PTE	Proportion of treatment effect explained
PZA	Pyrazinamide
QC	Quality control
QQQ	Triple quadrupole
Q-TOF	Quadrupole Time-of-Flight
RIF	Rifampicin
ROC	Receiver operating curve
SAA	Serum amyloid A
SELDI	Surface-enhanced laser desorption/ionization
SIM	Single ion monitoring
SLE	Systemic lupus erythematosus
SPE	Solid phase extraction
SRM	Single reaction monitoring
SSAT	Spermidine/spermine *N*-acetyltransferase
STE	Surrogate threshold effect
TB	Tuberculosis
TbAd	Tuberculosinyladenosine
TBSA	Tuberculostearic acid
TLR	Toll-like receptor
TMS	Trimethylsilyl
TNF	Tumor necrosis factor
TOF	Time-of-Flight
TST	Tuberculin skin test

VOC	Volatile organic compound
W2	Week 2 of anti-TB treatment
W8	Week 8 of anti-TB treatment